UNIVERSITY OF SOUTHAMPTON

BEST USE OF BIPOLAR TRANSISTORS IN THE RADIATION ENVIRONMENTS OF THE NUCLEAR POWER INDUSTRY

Richard Edward Sharp

Doctor of Philosophy

Faculty of Engineering and Applied Science

May 2003

UNIVERSITY OF SOUTHAMPTON

ABSTRACT

FACULTY OF ENGINEERING AND APPLIED SCIENCE

DEPARTMENT OF ELECTRONICS AND COMPUTER SCIENCE

Doctor of Philosophy

BEST USE OF BIPOLAR TRANSISTORS IN THE RADIATION ENVIRONMENTS OF THE NUCLEAR POWER INDUSTRY

by Richard Edward Sharp

The effects of exposure to high total doses of gamma radiation have been investigated for bipolar transistors. DC point measurements, current-voltage and capacitance-voltage techniques have been used to characterise the response of a number of commercially produced devices and to compare their radiation-induced changes in performance with those exhibited by a set of specially fabricated transistors with known geometry and process history. Irradiation was carried out with cobalt-60 sources at dose rates typical of the radiation environments found in nuclear power industry facilities and at total doses of up to 1 MGy.

Substantial changes in several of the measured parameters were found, particularly gain and saturation voltage. Leakage currents and breakdown voltages were less severely affected. Gain was noted, in some cases, to show a slight increase at high total doses, after the initial degradation. This has been linked to changes in surface conditions brought about by the irradiation. Significant differences were found between the response of devices biased during irradiation and those left unbiased. This has considerable implications for the use of bipolar transistors in equipment destined for applications in these environments and a series of recommendations for designers is presented.

Contents

List of tables

List of figures

1 Preface

The original inspiration for this work grew out of the author's experiences in the late 1980's when supporting BNFL staff in their efforts to obtain reliable electronic equipment for use in the radiation environments of the nuclear reprocessing and waste treatment plant operating at Sellafield. It was clear that no guidance was available for the designers of electronic circuits on how to use semiconductor components successfully at high total doses of gamma radiation. The little unclassified material that had been published either did not cover sufficiently high total doses or was derived from data obtained with different types of radiation, leading to quite different effects. It became clear that two strands were needed in the effort to meet the needs of the industry. The first strand was to generate the data from which to develop useful guidelines. The second was to create a forum in which the information could pass to the people who needed it; a forum that had a high enough profile to be easily identified and accessed; and a means by which users could interrogate the data to ask questions that had not been answered by the standard presentation of the information. Two projects in particular helped to address these needs. The first was the ENTOREL project, part of the EC-funded TELEMAN programme that grew out of the research needs identified following the Chernobyl incident in 1986. This project enabled high quality radiation effects data to be created and pooled into a pan-European database. The database was subsequently made available to organisations working in the nuclear industry throughout western Europe.

The second project was carried out within AEA Technology and compared the effects of gamma radiation produced by spent fuel with that emitted by cobalt-60. The main purpose of this project was to determine whether the much cheaper and easier to handle cobalt isotope could reliably replicate the effects suffered during operation of components in nuclear industry radiation environments. As a result of this project, a large quantity of data on basic types of component was created. However, the limited funding meant that not all the data were fully analysed.

From the outcome of these projects, coupled with the on-going parallel efforts to develop reliable plant-specific items, grew the idea to study in more depth the best

ways in which to use components in general, and bipolar transistors in particular, in the nuclear industry.

This work has taken some ten years to complete and, even so, a good number of questions remain. The relevance of the topic has risen and fallen during this period, as the reliability and safety of operations in the nuclear sector has undergone varying levels of scrutiny. At a time of renewed interest in the nuclear option, I hope that this work may contribute a little to ease the burden of designers striving to make their equipment contribute positively to this reliable and safe operation.

2 Acknowledgements

The United Kingdom Atomic Energy Authority (UKAEA) and AEA Technology plc have funded the bulk of the experimental activities forming the basis of the work described here. The test and measurement equipment and use of the irradiation facility were made available through this route. This help and assistance is gratefully acknowledged. Particular thanks go to David Garlick for his encouragement in the early stages of the work and to Lee Pater for his help with practical experimental aspects.

I would also like to thank my supervisor, Arthur Brunnschweiler, for his advice and encouragement; Kurt Lauridsen of the Risø National Laboratory for his help with the literature review; and many colleagues in AEA Technology, British Nuclear Fuels Ltd. and UKAEA for countless useful discussions.

Finally, I dedicate this work to my wife, Helen, for her support throughout.

3 Glossary and abbreviations

3.1 TERMS USED IN THE TEXT

absorbed dose: the energy imparted to matter by charged or uncharged ionising particles. The unit of measurement of absorbed dose is the gray, Gy.

AGR: advanced gas-cooled reactor, the second-generation type of commercial nuclear reactor built in the UK.

alpha radiation: highly energetic nuclei of helium atoms carrying a positive charge. The penetrating power of alpha particles is very low and external irradiation by alpha radiation is of little consequence for electronic components.

beta radiation: extremely energetic electrons. The energy and, hence, penetrating power varies considerably, depending on the parent radioisotope and passage through surrounding materials.

cobalt-60: a radioactive isotope of cobalt with a half-life of 5.27 years, emitting two gamma rays with energies of 1.17 and 1.33 MeV. Beta radiation is also emitted but is shielded by the encapsulation used to prevent radioactive material becoming deposited on other surfaces when the cobalt is used as an industrial, radiation source.

contamination: the presence of radioactive material on the surface of an item, rendering it hazardous to the touch and requiring special handling techniques.

COTS: commercial off the shelf, used to describe components that have been manufactured by a standard, high volume process flow, as opposed to, for example, radiation hardened components made in much smaller quantities.

dose rate: the rate of energy deposition in a sample as a result of exposure to radiation. The SI unit of measurement of dose rate is the gray per second, Gy/s.

equivalent dose: a quantity used to express on a common scale the risk to exposed persons from all types of ionising radiation. The unit of measurement of equivalent dose is the sievert, Sv.

gamma radiation: electromagnetic radiation, produced during the decay of most radioisotopes and originating from the nucleus of the atom. Gamma rays travel at the speed of light and can be very penetrating.

gray (Gy): the unit of measurement of absorbed dose, equivalent to 1 joule per kilogram or 6.242 x 10^{12} MeV per kilogram.

rad: the imperial equivalent of the gray where 1 rad ≡ 0.01 gray.

rem: the imperial equivalent of the sievert, where 1 rem ≡ 0.01 sievert.

sievert (Sv): the unit of measurement of dose equivalent, being equal to the absorbed dose to tissue in gray multiplied by appropriate weighting factors, depending on the type of radiation concerned.

total integrated dose: the sum of all the exposures to radiation experienced by a sample, calculated by integrating dose rate over time. This term is often shortened to total dose or TID. The SI unit of total integrated dose is the gray, Gy. Other terms used for this quantity are absorbed dose and total dose.

TVT: tenth value thickness, the thickness of material required in order to reduce the gamma radiation dose rate by one order of magnitude.

X-rays: relatively low energy electromagnetic radiation, originating from the decay of radioisotopes. X-rays originate from the inner electron shells of the atom.

3.2 NOTATION USED IN EQUATIONS

The following quantities have been used in equations throughout this work:

A_J	cross-sectional area of p-n junction
A_s	depleted area
C_B	bulk concentration
C_M	measured capacitance per unit area
C_{pl}	capacitance per unit area of the depletion region
C_s	capacitance per unit area of the surface layers
D	diffusion coefficient
D_B	minority carrier diffusion coefficient
D_n	diffusivity of electrons
D_p	diffusivity of holes
h_{FB}	common-base current gain
h_{FE}	common-emitter current gain
I	current
I_b	base current

I_B	base current
I_c	collector current
I_C	collector current
I_{cbo}	collector-base leakage current
I_{ceo}	collector-emitter leakage current
I_{diff}	diffusion current
I_e	emitter current
I_E	emitter current
I_r	reverse current
I_{rec}	recombination current
k	Boltzmann's constant
K	energy dependent lifetime damage coefficient
L	channel or diffusion length
L_n	diffusion length of electrons
L_p	diffusion length of holes
n_i	intrinsic carrier concentration
N_A	concentration of acceptors
N_D	concentration of donors
N_e	electron total dose
N_{st}	density of surface recombination-generation centres per unit area
N_t	density of traps
p	minority carrier concentration
p_B	minority carrier concentration in the base
p_{eq}	equilibrium minority carrier concentration
q	the charge on an electron, equivalent to 1.6×10^{-19} C
Q	charge
R_s	surface recombination rate
s_0	surface recombination velocity of a surface with no surface space-charge region
t_s	storage time
T	temperature
V	voltage
V_{BE}	base-emitter voltage
$V_{(br)cbo}$	collector-base breakdown voltage

$V_{(br)ceo}$	collector-emitter breakdown voltage
$V_{ce(sat)}$	collector-emitter saturation voltage
V_{EB}	emitter-base voltage
V_f	forward voltage drop
V_j	junction voltage
V_{rm}	reverse breakdown voltage
V_s	voltage across the depletion region
v_{th}	thermal velocity of carriers
V_z	zener voltage
W	depletion region width
W_B	base width
α	common-base current gain
α_T	transport factor
β	common-emitter current gain
β_F	forward gain
β_R	reverse gain
γ	emitter efficiency
ε_s	permittivity of silicon
Λ	common emitter gain-bandwidth product
Φ	neutron fluence
τ	lifetime
τ_F	total recombination rate constant or forward transit time
τ_n	minority carrier lifetime in the base
τ_p	minority carrier lifetime in an n-type semiconductor
τ_R	reverse transit time
τ_0	effective lifetime within a reverse-biased depletion region
σ	conductivity

4 Introduction

The nuclear power industry covers the complete range of activities from the mining of uranium ore, through fuel fabrication and use in a reactor to generate electricity, on to spent fuel and waste handling and ending with the decommissioning of nuclear facilities and long term waste storage or disposal. In some countries, such as the UK, France and Japan, most spent fuel is reprocessed to extract the more than 95% of unused uranium, enabling it to be recycled for the production of fresh fuel. This sequence is called the fuel cycle, the principal stages of which are illustrated in figure 4.1 (Anon, 2001).

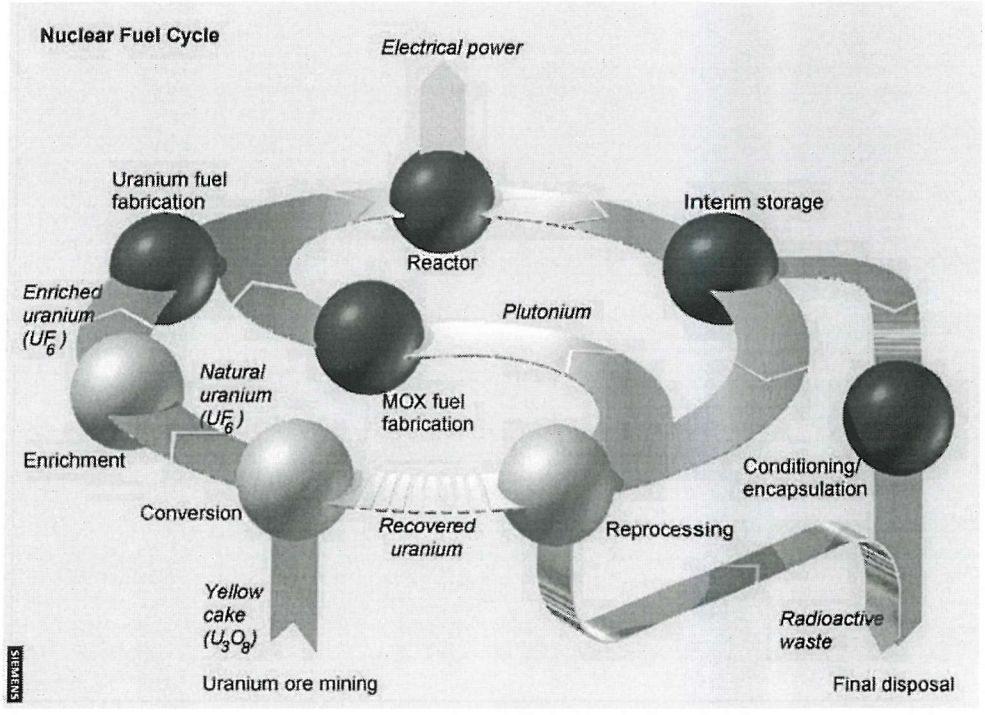

Figure 4.1: A pictorial representation of the nuclear fuel cycle.

Uranium is a radioactive element and many stages in the fuel cycle have associated with them sufficiently high ionising radiation levels as to preclude direct, manual operations. Protective measures are required in order to avoid adverse health effects on the personnel involved, as well as on the wider public. In these activities, mechanical aids are frequently used both to replace manual operations and to increase the capability or throughput of the process. Large, mechanical machines operate by means of either electrical or hydraulic power and, in both cases, electromechanical equipment is used to some extent. This equipment often incorporates control circuits,

sensors and transducers or signal processing functions, all requiring the use of electronic components. Unfortunately, some types of electronic component, especially semiconductor devices, can exhibit a sensitivity to radiation almost as great as that shown by humans. One of the more common semiconductor components used these applications is the bipolar transistor and it is certainly possible to use some types of this device to measure exposure to radiation.

Given that man-access to many nuclear facilities is difficult or impossible, the reliability of equipment deployed in a radiation environment is paramount. Features are often built in to facilitate remote maintenance or removal of the item to a lower radiation area, where hands-on repair may be possible. However, a long life or high degree of radiation tolerance in the first place is important in reducing operating costs and plant down-time. In order to predict the lifetime of a piece of equipment, a good understanding of the effects of radiation on the electronic components used therein is clearly important.

Whilst electronic circuits usually contain a number of different types of electronic component, bipolar transistors have been chosen for study in this work as they are particularly widespread and useful for a number of basic functions found in many types of circuitry. Passive components, including resistors and capacitors, have a relatively high degree of radiation tolerance and the degradation mechanisms involved are well understood. Semiconductor devices can be more sensitive to the damaging effects of ionising radiation and have attracted a reputation of poor reliability in such environments. Nevertheless, some types of device are extremely radiation tolerant and operate within the manufacturer's specification to incredibly high total doses. It is unfortunate that the parameters that govern radiation tolerance are usually unimportant, even unknown, to the manufacturer and a minor process change to improve yield may lead to a dramatic change in the response of the component to radiation.

A limited number of manufacturers offers devices with a guarantee of radiation tolerance. However, these devices are sold principally to customers in the military and space sectors, which have significantly different radiation tolerance requirements from the nuclear power industry. Typical total dose requirements are two or three orders of magnitude lower in these applications. Furthermore, the range of device types is limited (for example, no guaranteed radiation tolerant bipolar transistor is currently marketed), availability is usually very poor and prices several times higher than for

their standard equivalents. For these reasons, commercial off-the-shelf (COTS) components find widespread use, even in aerospace equipment, for which the radiation tolerant components that are available are targeted.

The nuclear power industry makes considerable use of COTS components and COTS equipment, often with minor modifications to improve its usability in remote applications or to aid the ease with which it can be decontaminated in order to facilitate hands-on maintenance or disposal. Equipment using relatively low-technology solutions is preferred as its inherent radiation tolerance tends to be greater than for that using state of the art, digital devices.

Nevertheless, there are applications that have a requirement for a degree of radiation tolerance greater than that that is achievable with COTS equipment. For these needs, special circuit designs are required and this is where knowledge of the effects of radiation on components is required. VLSI devices can degrade in various ways, leading either to a gradual deterioration in functional parameters or to a sudden, complete failure, depending on the device type and technology. Discrete devices are more predictable in that they nearly always show the gradual deterioration type of response to irradiation. This conveys several advantages when compared with heavily integrated devices. Firstly, assuming that the pattern of degradation with radiation exposure is known, the percentage of remaining life can easily be determined. Secondly, a circuit can be designed to operate with the degraded parameter values known to apply at the target total dose, ensuring that it will function up to this point. Finally, discrete circuitry can more easily be designed to be robust to physical, electrical and mechanical shocks. This can be important in some applications, such as crane-mounted sensor systems or mobile inspection devices.

In order for a radiation tolerant circuit design to be reliable and successful, it must be based upon an accurate prediction of the response of both the components and the circuit to radiation exposure. Type testing is one way in which this prediction can be made, although this can be costly and may be required for each different manufacturer's production lot. A more analytical method of predicting the effects of radiation on a given component in a radiation environment is desirable and forms the main motivation behind this work. This would enable designers more rapidly to develop new circuits and equipment, allowing the industry to profit from the associated economic benefits in a more timely manner.

5 Aims

The principal aims of this work are threefold:

1. to develop an understanding of the underlying effects of ionising radiation on the principal electronic characteristics of discrete electronic components, in particular silicon bipolar transistors;

2. to relate these effects to physical properties of the devices;

3. to develop a predictive methodology for assessing the likely effects of radiation exposure on a known type of bipolar transistor. This methodology must be useful to the designer or user of an item of equipment, rather than to the transistor manufacturer or component designer.

The driving force behind these aims is a desire to be able to design electronic equipment with a high degree of radiation tolerance without going through several rounds of prototype development, test and measurement. This traditional process is expensive and it can take a number of years before a product is brought to market. As reliability is such a critical aspect for equipment operating in an area where hands-on access is impossible, the performance of a new machine or sensor must be proven to a high degree of confidence, requiring extensive testing and verification. One cycle of manufacture, testing and analysis can take twelve months. A better understanding at the design stage of the response of a device to radiation exposure should help to reduce the number of development cycles, enabling better, more reliable products to be launched more rapidly.

6 Literature review

6.1 TRANSISTOR OPERATION

The theory of the operation of bipolar transistors has been described in great detail in a number of publications since its invention in 1947, including Bardeen (1948), Shockley (1949), Grove (1967), Sze (1985) and Ashburn (1988). For most purposes, the device may be considered essentially as two back-to-back, p-n diodes, connected in either p-n-p or n-p-n configuration. The central region is called the base and the other two regions are called the collector and emitter. Usually, the emitter is relatively heavily doped and the collector rather more lightly doped.

Under normal operating conditions, i.e. the active mode, the emitter-base junction is forward-biased and the collector-base junction is reverse-biased. The circuit symbols representing a pnp and a npn bipolar transistor under these conditions are shown in figure 6.1.

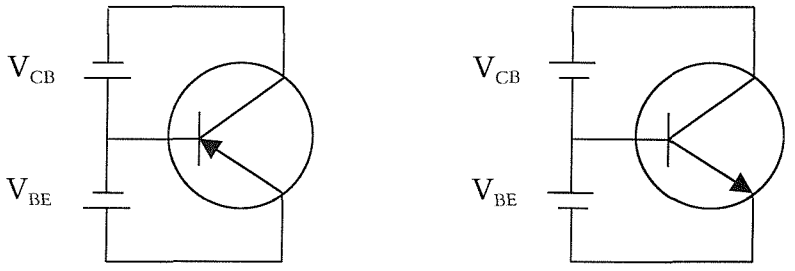

Figure 6.1: bias arrangements under normal operating conditions for a pnp transistor (left) and a npn transistor (right).

6.1.1 Basic theory

The relationship between current and voltage may readily be derived for an ideal transistor once a number of assumptions have been made:

- the device has uniform doping in each region
- there is low-level injection
- there are no recombination-generation currents in the depletion regions
- there are no series resistances in the device

Where the entire potential drop across the device occurs across the depletion region at a junction, the steady-state characteristics of the device, including the minority carrier distribution, are governed by the one-dimensional diffusion equation (all the equations in this section are based upon an NPN transistor and are taken mainly from Grove):

$$D_B\left(\frac{\partial^2 n}{\partial x^2}\right)-\left(\frac{n-n_{eq}}{\tau_n}\right)=0 \tag{6.1}$$

where D_B is the minority carrier diffusion coefficient, n_{eq} is the equilibrium minority carrier concentration and τ_n is the minority carrier lifetime (definitions of all the terms used in equations in this work are given in chapter 3). The intrinsic gain property of a bipolar transistor is determined primarily by the characteristics of the emitter-base junction. For the example of the base, this equation is subject to the boundary conditions:

$$n(0)=n_B e^{qV_{BE}/kT} \tag{6.2}$$

and

$$n(W_B)=0 \tag{6.3}$$

where n_B is the equilibrium minority carrier concentration within the base and W_B is the base width.

The first boundary condition states that the minority carrier concentration at the edge of the emitter-base junction region is increased above its equilibrium value due to the applied potential difference present at the base-emitter junction. The second boundary condition results from the fact that the base-collector junction is reverse-biased and so all the minority carriers will be swept into the collector. Hence, the minority carrier concentration will be zero at its edge. The solution to this equation is:

$$n(x)=n_B\left[1-\frac{\sinh\frac{x}{L_n}}{\sinh\frac{W_B}{L_n}}\right]+\left(n(0)-n_B\right)\left[\frac{\sinh\frac{W_B-x}{L_n}}{\sinh\frac{W_B}{L_n}}\right] \tag{6.4}$$

where L_n is the minority carrier diffusion length (defined below). For $|V_{EB}|>>kT/q$, this simplifies to:

$$n(x) = n(0)\left(\frac{\sinh\frac{W_B - x}{L_n}}{\sinh\frac{W_B}{L_n}}\right) \tag{6.5}$$

For narrow base devices ($W_B << L_n$), this approximates to a simple, straight-line solution. This condition is true for many modern, small-signal transistors, exhibiting negligible recombination in the base:

$$n(x) = n(0)\left(1 - \frac{x}{W_B}\right) \tag{6.6}$$

In all these cases, the minority carrier diffusion length for electrons, L_n, is defined as:

$$L_n = \sqrt{D_n \tau_n} \tag{6.7}$$

6.1.2 Recombination

In the presence of certain defects, charge carriers can recombine or be generated within the electrically active regions of a device. The relative magnitude of the recombination and generation currents depends on the defect density and the properties of the initial silicon, as well as external influences, such as radiation. We will now consider the effect this has on the operation of a bipolar transistor.

For wide base devices (i.e. where $W_B << L_n$ is not true), such as power devices, recombination in the base is non-negligible and is defined as the difference between the currents on either side of the base region.

$$I_{rec} = I_{ne} - I_{nc} \tag{6.8}$$

where I_{ne} is the minority carrier diffusion current at the emitter edge of the base and I_{nc} is the minority carrier diffusion current at the collector edge of the base. The recombination current in the base contributes to the base current.

Using equation 6.5 and the following generalised expression for the diffusion current

$$I = qAD_B \frac{dn}{dx} \tag{6.9}$$

yields expressions for the diffusion currents at either edge of the base:

$$I_{ne} = qAD_B\left(\frac{dn(x)}{dx}\right)_{x=0} = \frac{-qAD_B n_B}{L_n}\coth\left(\frac{W_B}{L_n}\right)e^{qV_{BE}/kT} \qquad (6.10)$$

and

$$I_{nc} = qAD_B\left(\frac{dn(x)}{dx}\right)_{x=W_B} = \frac{-qAD_B n_B}{L_n \sinh\left(\frac{W_B}{L_n}\right)}e^{qV_{BE}/kT} \qquad (6.11)$$

By applying the two expressions derived for the minority carrier currents above, the recombination current is therefore given by:

$$I_{rec} = -\frac{qAD_B n_B}{L_n \sinh\left(\frac{W_B}{L_n}\right)}\left(\cosh\left(\frac{W_B}{L_n}\right)-1\right)e^{qV_{BE}/kT} \qquad (6.12)$$

This equation indicates that the recombination current in the neutral base is a function of the base width, as would intuitively be expected. It also predicts a dependence according to $exp(qV_{BE}/kT)$.

In silicon transistors, however, there is often more recombination in the emitter-base depletion region. The degree of recombination here depends on the density and energy level of the traps present in the depletion region. The most effective traps have energies at the centre of the band gap and so the worst case condition is to assume that all the traps lie here. Ashburn (1980) shows that, under these conditions, the recombination current can be defined by:

$$I_{rec} = \frac{1}{2}qAW_B\sigma v_{th}N_t n_i e^{qV_{BE}/2kT} \qquad (6.13)$$

Thus, for strong recombination, a dependence according to $exp(qV_{BE}/2kT)$ is predicted, together with an increase with the density of traps (N_t) and the capture cross-section (σ). This might be expected to be the case for a heavily irradiated device if the irradiation were to introduce a high concentration of recombination traps in the base region.

6.1.3 Other parameters

A range of other parameters is worth defining here.

The emitter efficiency, γ, is defined as the ratio of the diffusion current in the base to the total emitter current:

$$\gamma \equiv \frac{I_{diff,B}}{I_E} = \frac{I_{diff,B}}{I_{diff,B} + I_{diff,E} + I_{rec}} \tag{6.14}$$

where $I_{diff,B}$ and $I_{diff,E}$ are the diffusion currents in the base and emitter, respectively. It can be seen that an efficient transistor is one in which the recombination current and the diffusion current in the emitter are small with respect to the diffusion current in the base. Hence, the emitter doping must be high compared with the base doping. Both Ashburn and Grove show that the equation for the forward diffusion current can be given as:

$$I_{diff} = -qD\frac{n_i^2}{C_B L_n} e^{q|V_{BE}|/kT} A_J \tag{6.15}$$

(where n_i is the intrinsic carrier concentration, C_B the bulk concentration, L_n the diffusion length and A_J the cross-sectional area of the junction). Similarly, the equation for the recombination current is:

$$I_{rec} = -\frac{1}{2} q \frac{n_i}{\tau} W e^{q|V_{BE}|/2kT} A_J \tag{6.16}$$

Grove develops equation 6.14, using equations 6.15 and 6.16, to show:

$$\gamma = \frac{1}{1 + \frac{N_{AB} W_B}{D_{nB}} \left(\frac{D_{pE}}{N_{DE} W_E} + \frac{W_{EB}/\tau_0}{2 n_i e^{qV_{EB}/2kT}} \right)} \tag{6.17}$$

or, simplified:

$$\gamma = \frac{1}{1 + \frac{B}{E} + \frac{1}{2}\sqrt{\frac{qBA_J}{I_{diff,B}} R}} \tag{6.18}$$

where:

$$B \equiv \frac{N_{DB} W_B}{D_{pB}} \tag{6.19}$$

$$E \equiv \frac{N_{AE} W_E}{D_{nE}} \tag{6.20}$$

$$R \equiv \frac{W_{EB}}{\tau_0} \tag{6.21}$$

B is the base factor and depends on the number of impurities in the base region. E is the emitter factor and depends on the number of impurities in the emitter region. R is the recombination factor and indicates the recombination rate in the emitter-base depletion region. As lifetime is known to be reduced by particle irradiation, this factor is expected to increase significantly as a transistor is exposed to gamma radiation.
From the definition of emitter efficiency given by equation 6.14, the current carried by minority carriers into the base is γI_E. The fraction of this current reaching the collector-base depletion region, i.e. traversing the base region, is the transport factor and is defined by:

$$\alpha_T \equiv \frac{I_{e,C}}{I_{e,B}} \tag{6.22}$$

where $I_{e,C}$ is the electron current reaching the collector and $I_{e,B}$ is the electron current injected into the base. An efficient base is one in which the two currents are nearly equal, i.e. when the base is narrow. From equation 6.5, this can be shown to lead to:

$$\alpha_T \equiv \frac{1}{\cosh \frac{W_B}{L_{nB}}} \tag{6.23}$$

where L_{nB} is the diffusion length of minority carriers in the base region. For "good" transistors, the base width is much smaller than this diffusion length. Thus:

$$\alpha_T \cong 1 - \frac{1}{2}\left(\frac{W_B}{L_{nB}}\right)^2 \tag{6.24}$$

6.1.4 Surface effects

Surface effects are also known to be important for many types of transistor but the analysis above does not consider these. Surface recombination modifies the final term of equation 6.21, R, (Grove (1967)) according to:

$$R \equiv \frac{W_{EB}}{\tau_0} + s_0 \frac{A_s}{A_J} \tag{6.25}$$

where A_s is the depleted surface area and s_0, the surface recombination velocity is defined as:

$$s_0 = \sigma v_{th} N_{st} \tag{6.26}$$

The area of the depleted surface region is normally small and limited mostly to the dimensions of the base at the surface. Hence, the second term of equation 6.25 can normally be neglected. Under conditions of charge imbalance in or over the oxide surface of a device, the depleted region can be extended. Whilst this larger depleted area in itself does not affect the injection of carriers in to the base, it can create favourable conditions for the recombination of carriers, both at the surface and within the bulk of the depleted region. This leads to an increase in base current while leaving the collector current unchanged, i.e. the gain falls.

Reddi (1967) derives an expression for the surface recombination rate as follows:

$$R_s = \frac{s_0 n_i^2 A_s \left(1 - e^{qV_{BE}/kT}\right)}{C_B} \tag{6.27}$$

This equation indicates that the surface recombination rate has a dependence according to $exp(qV_{BE}/kT)$. Following a derivation based on the centre of the band-gap, the corresponding surface recombination current is shown by Reddi to have a dependence according to $exp(qV_{BE}/2kT)$. This is in contrast to the bulk recombination current in the low-level injection regime, which shows a $exp(qV_{BE}/kT)$ dependence, but the same as the bulk recombination current under high-level injection conditions. Both Grove and Reddi compare the surface recombination velocity with the minority carrier lifetime. Grove gives an expression for the lifetime during low-level injection:

$$\tau = \frac{1}{\sigma \upsilon_{th} N_t} \tag{6.28}$$

Comparing this with equation 6.26, it is clear that the inverse of surface recombination velocity is analogous to lifetime during bulk recombination.

6.1.5 Gain

Two terms are defined in order to indicate the usefulness of a transistor as an amplifier. These are the common-base current gain, α, and the common-emitter current gain, β. These are defined as follows:

$$\alpha \equiv h_{FB} \equiv \frac{I_C}{I_B} = \gamma \alpha_T + \frac{I_{CBO}}{I_E} \tag{6.29}$$

If the reverse-biased collector-base leakage current, I_{CBO}, is negligible (which may not be true for irradiated devices), this can be simplified to:

$$\alpha = \gamma\alpha_T \tag{6.30}$$

Similarly:

$$\beta \equiv h_{FE} \equiv \frac{I_C}{I_B} = \left(\frac{\gamma\alpha_T}{1-\gamma\alpha_T}\right)\left(1+\frac{I_{CBO}}{\gamma\alpha_T I_B}\right) \tag{6.31}$$

and, for negligible I_{CBO}:

$$\beta = \left(\frac{\gamma\alpha_T}{1-\gamma\alpha_T}\right) \tag{6.32}$$

For a good transistor, the transport factor and the emitter efficiency are nearly unity. Thus, combining with equations 6.17, 6.24, for a transistor with high common-emitter gain, we have:

$$\frac{1}{\beta} \approx 1-\gamma\alpha_T \approx \frac{1}{2}\left(\frac{W_B}{L_{nB}}\right)^2 + \left(\frac{N_{AB}W_B}{D_{nB}}\frac{D_{pE}}{N_{DE}W_E}\right) + \left(\frac{N_{AB}W_B}{D_{nB}}\frac{W_{EB}/\tau_0}{2n_i e^{qV_{EB}/2kT}}\right) \tag{6.33}$$

The first term in this equation arises from recombination in the base, the second from injection into the emitter and the third from recombination in the emitter-base space-charge region. Any radiation-induced variations in the lifetime would be expected to affect both the first and the third terms and thus reduce the gain in a linear fashion. Hence, the determination of the variation in lifetime with total dose is important in the context of this work. Again, surface effects and conductivity modulation at high currents are omitted from this equation.

One further term of interest is derived empirically by Miller (1955), relating breakdown voltage and gain:

$$BV_{CEO} = BV_{CBO}\sqrt[n]{(1-\alpha)} \approx \frac{BV_{CBO}}{\sqrt[n]{\beta}} \tag{6.34}$$

where n takes values between 3 and 6. This indicates that the collector-emitter breakdown voltage is inversely proportional to the common emitter current gain of the device.

6.2 GUMMEL PLOTS

6.2.1 Outline

The Gummel plot is an effective mechanism for analysing many operational characteristics of a bipolar transistor and consists of a graph of the variation in base and collector current on a logarithmic scale with base-emitter voltage on a linear scale. A Gummel plot for an ideal transistor is shown in figure 6.2. The slope of both curves is constant and equal to q/kT. Changes in the slope of either curve indicate deviations from the ideal; for example, recombination in the emitter-base depletion region or high-level injection effects.

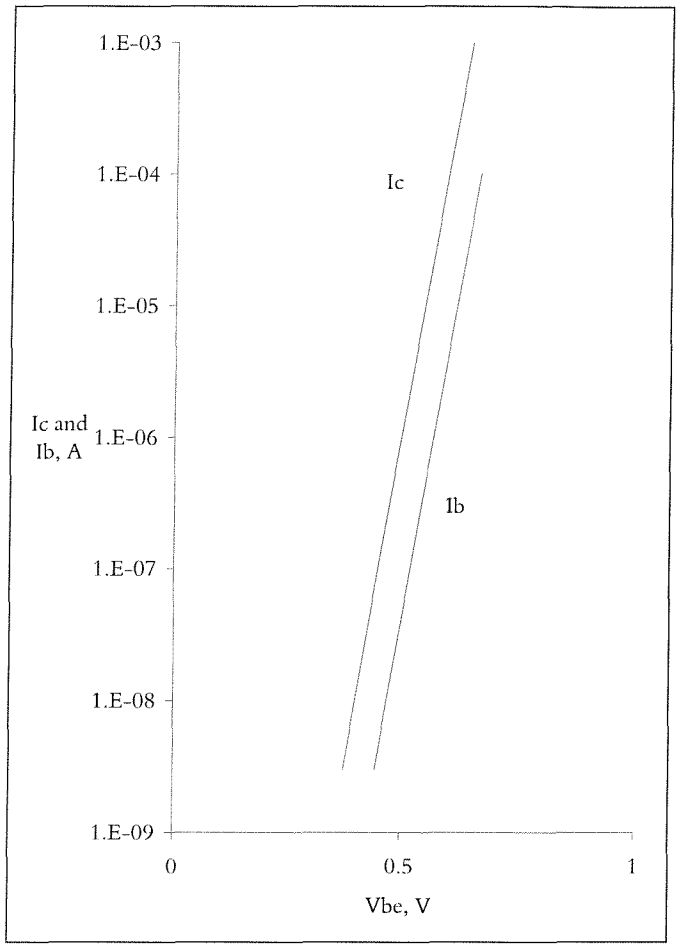

Figure 6.2: a Gummel plot for an ideal bipolar transistor.

A Gummel plot for a real device will deviate from the ideal, although the curves for some modern types of device are remarkably close to it. Typically, a transistor will exhibit some level of recombination in the depletion region and non-zero collector and emitter resistances, leading to non-linearities in the plot. This is illustrated below in figure 6.3 for a 'real' device, showing some of these deviations from the ideal.

Ashburn (1998) expands on Sah (1957) with an analysis similar to that earlier in this chapter, to show that the reduced slope in the base current curve at low voltages is due to recombination in the emitter-base depletion region. The slope changes from a q/kT dependency to a q/mkT shape, with m, the ideality factor, lying between 1 and 2, as shown in equation 6.16 above. For strong recombination where space-charge recombination dominates, this equation predicts an ideality factor of 2. The practical value for a given transistor depends on the physical nature of the traps involved, increasing with trap density and decreasing with distance from the centre of the band.

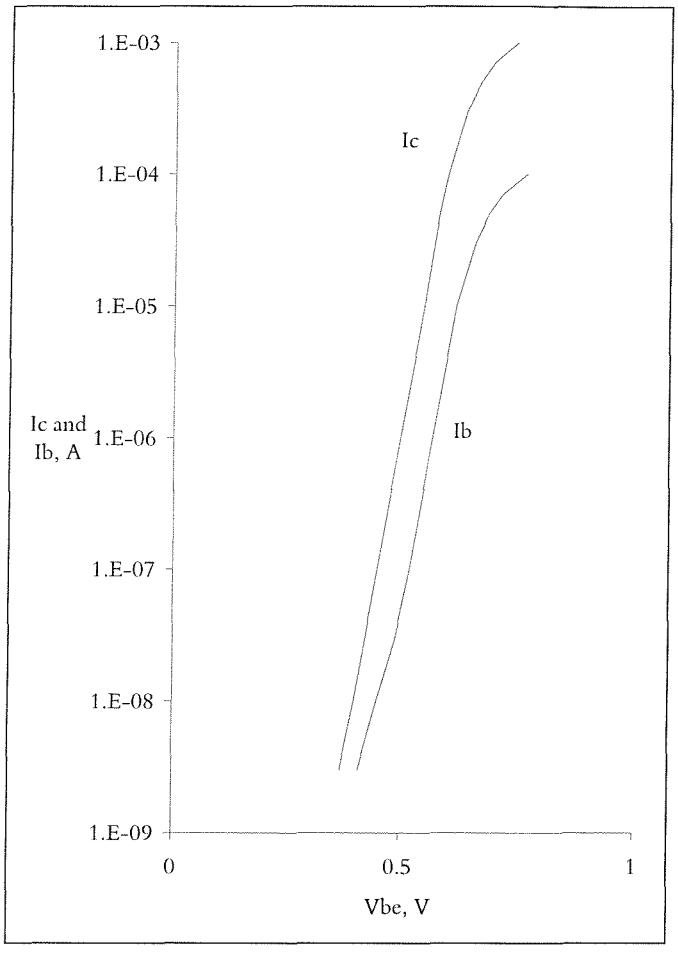

Figure 6.3: a Gummel plot for a 'real' device.

The q/kT dependence is an indication of diffusion current being the predominant mechanism over this range of current. As the dependence changes to q/mkT, then this shows the growing domination of recombination in the emitter-base depletion region over the operation of the device. The total current in the base is given by:

$$I_B = I_{diff,BE} + I_{rec} \tag{6.35}$$

By applying equations 6.15 and 6.16, this can be expressed as:

$$I_B = I_1 e^{qV_{BE}/kT} + I_2 e^{qV_{BE}/mkT} \tag{6.36}$$

A Gummel plot reveals the value of the ideality factor, m, and how it changes over the range of V_{BE} of interest. Repeating this as the device is subjected to increasing total doses of radiation will show how rapidly the effect of recombination grows under this influence.

The second deviation from the ideal may be seen at the high voltage end of the collector current curve. At high currents, the injected electron concentration in the base becomes comparable with or exceeds the doping concentration. In this case, the hole concentration must also increase in order to maintain charge neutrality. This is referred to as high-level injection or conductivity modulation.

Equation 6.15 shows that the collector current is inversely proportional to the base doping concentration. Hence, the rate of increase in collector current will fall as the high-level injection region is entered. Hall (1956) shows that, under these conditions, the collector current varies as:

$$I_C = I' e^{qV_{BE}/2kT} \tag{6.37}$$

and so the slope of the collector current curve in the Gummel plot reduces, as shown in figure 6.3. This is important for power devices, which have a relatively low base doping level. However, for small-signal devices, the transition is not so clear and series resistances also play a role, leading to a gradual change in the slope.

6.2.2 The Ebers-Moll model

The Ebers-Moll model is a simple, large signal model that describes the DC behaviour of a bipolar transistor. Both junctions are modelled as an ideal diode and a current source in an anti-parallel configuration.Two equations are used to define the currents flowing in the diodes:

$$I_F = I_{Esat}\left(e^{qV_{BE}/kT} - 1\right) \tag{6.38}$$

$$I_R = I_{Csat}\left(e^{qV_{BC}/kT} - 1\right) \tag{6.39}$$

where I_{Esat} and I_{Csat} are the saturation currents flowing in the emitter and collector, respectively. A third equation links these saturation currents to the common base current gain in either direction:

$$\alpha_F I_{Esat} = \alpha_R I_{Csat} = I_S \tag{6.40}$$

Consequently, three parameters are required fully to describe a transistor according to this model: α_F, α_R and I_S. Using these parameters, the terminal currents can be described very simply:

$$I_C = \alpha_F I_F - I_R \tag{6.41}$$

$$I_E = \alpha_R I_R - I_F \tag{6.42}$$

$$I_B = (1-\alpha_F)I_F + (1-\alpha_R)I_R \tag{6.43}$$

This model provides the expected exponential relationship between base-emitter voltage and current, as shown on the Gummel plot, as well as the transistor action resulting from the very narrow base. The model can be simplified in the case of operation out of saturation. It should be noted that the Ebers-Moll model does not include recombination in the emitter-base region.

6.2.3 The Gummel-Poon model

The Ebers-Moll model can be extended into the AC regime by adding features. One version of this that also improves on the modelling of DC parameters is the Gummel-Poon model. This model has the advantage of including high-level injection effects, basewidth modulation and variations in the forward transit time with collector current.

In order better to facilitate the modelling of, for example, recombination, the common component of the emitter and collector currents is identified separately:

$$I_{CT} = \frac{I_S}{Q_B}\left[\left(e^{qV_{B'E'}/kT} - 1\right) - \left(e^{qV_{B'C'}/kT} - 1\right)\right] \tag{6.44}$$

where Q_B is the majority carrier charge in the base, normalised to the zero-bias value. At zero bias, this parameter has the value unity. When bias is applied to the collector and emitter, additional components of majority carrier charge are introduced and these combine to alter the value of Q_B. By taking Q_B to be positive, the derivation of the normalised majority carrier charge in the base yields the equation:

$$Q_B = \frac{Q_1}{2} + \left[\left(\frac{Q_1}{2}\right)^2 + Q_2\right]^{1/2} \tag{6.45}$$

where

$$Q_1 = \left[1 - \frac{V_{B'C'}}{V_{AF}} - \frac{V_{B'E'}}{V_{AR}}\right]^{-1} \tag{6.46}$$

and

$$Q_2 = \frac{BI_S}{I_{KF}}\left(e^{qV_{B'E'}/kT} - 1\right) + \frac{I_S}{I_{KR}}\left(e^{qV_{B'C'}/kT} - 1\right) \tag{6.47}$$

For a practical transistor, a plot of the collector current against collector-emitter voltage yields a straight line at high values of bias. As the bias voltage approaches zero, the slope of the curve increases so that the collector current cuts off at zero bias. However, if the high bias curve is extrapolated back along the voltage axis, this gives an intercept known as the Early voltage (V_{AF}), illustrated in figure 6.4.

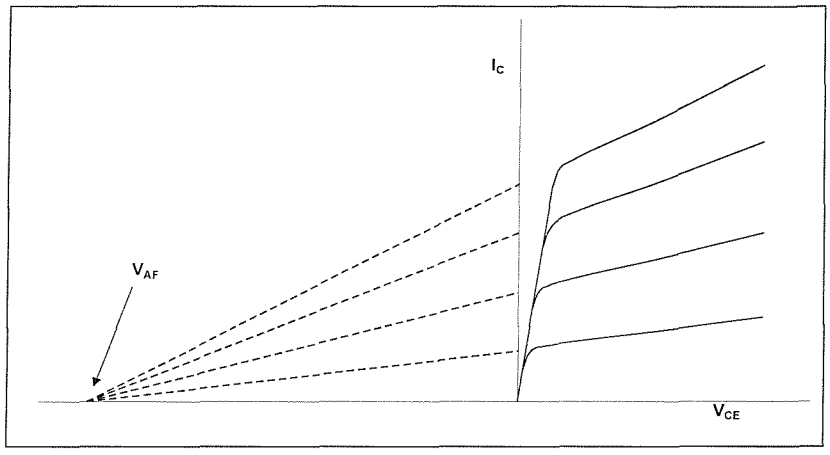

Figure 6.4: definition of the Early voltage.

The same value is obtained whatever value of base-emitter voltage is applied and it models base narrowing effects due to the depletion region encroaching into the base. The term V_{AR} in equation 6.46 is the equivalent reverse Early voltage, applying in the case of a reverse biased emitter-base junction. I_{KF} is the forward knee current, defining the onset of high-level injection, i.e. where the slope of the curves on the Gummel plot changes from a q/kT dependence to a q/mkT dependence. I_{KR} is the equivalent reverse knee current. The parameter B is used to model base widening effects at high current density. Various analytical expressions have been used for this parameter but it may be assumed to be unity for many purposes.

Furthermore, it may be noted that, in the Gummel-Poon model, the condition for the onset of high-level injection is:

$$Q_2 >> \frac{Q_1^{\,2}}{4} \tag{6.48}$$

6.3 RECOMBINATION LIFETIME

Recombination in the base has already been shown to play a significant role in determining the characteristics of a real device. It is to be expected, therefore, that knowledge of the recombination lifetime and the way in which it changes with irradiation, would yield some insights into the radiation response of a device. The key lies in finding a suitable way in which to measure it.

For the case of a simple p-n junction (where the conductivity of the p-type material is much greater than that of the n-type material), the charge storage model defines the charge stored in the base region as the integral of the linear minority charge carrier density over the entire junction. Consequently, the current flowing through the junction is defined as:

$$I = \frac{dQ}{dt} + \frac{Q}{\tau_p} \tag{6.49}$$

where τ_p is the minority charge carrier lifetime. The second term in this equation represents the recombination rate in the base region (i.e. the n-type material).

A real junction is not quite as simple as this and the minority charge carrier lifetime is replaced by an effective lifetime, adjusted for charge carriers drifting to a contact before recombination occurs. Kuno (1964) solves equation 6.49 to obtain the following expression for the storage, or transit, time:

$$t_s = \tau_F \left[\ln\left(1 + \frac{I_F}{I_R}\right) - \ln\left(1 + \frac{\tau_R}{\tau_F}\right) \right] \tag{6.50}$$

This solution is valid only for the time during which the excess charge is being removed, i.e. t_s in figure 6.5. During this time, a nearly constant reverse current flows and the junction voltage does not change significantly.

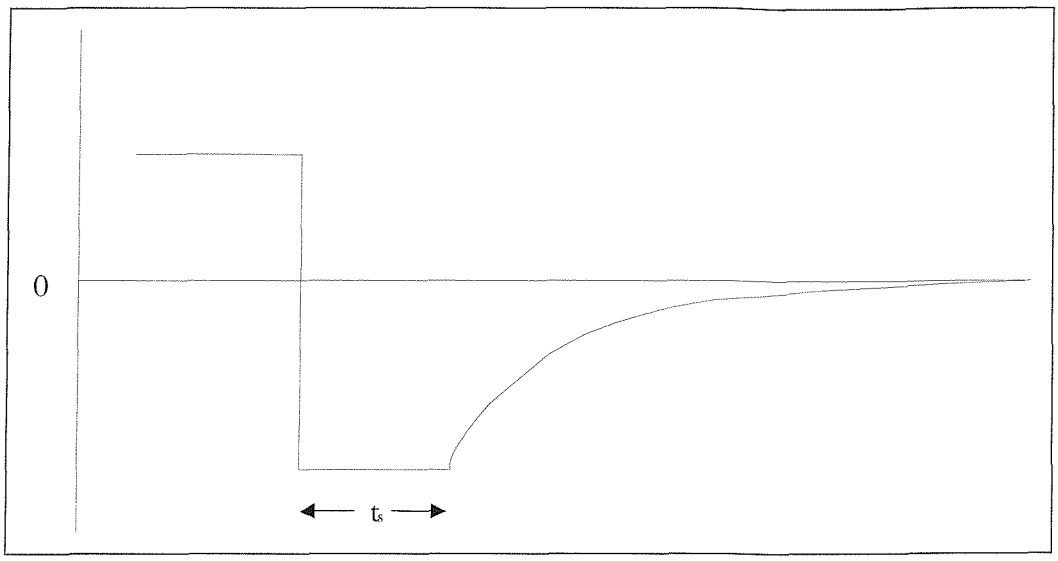

Figure 6.5: the current switching characteristics of a p-n junction.

A plot of the storage time against the first logarithmic term will give a straight line with a slope of τ_F, the total recombination rate constant, and an intercept of the second logarithmic term. If $\tau_F >> \tau_R$ then the right hand term disappears and the expression simplifies to:

$$t_s = \tau_F \ln\left(1+\frac{I_F}{I_R}\right) \tag{6.51}$$

For a bipolar transistor, the picture is more complex because minority charge carriers are stored in the base. This stored charge and its decay lifetime determine the AC behaviour of the transistor. By using the charge control model of the transistor, we can consider the stored charge in the forward biased, active region as:

$$Q_F = I_c \tau_F \tag{6.52}$$

while the stored charge in the reverse biased mode is:

$$Q_R = I_c \tau_R \tag{6.53}$$

When a transistor is saturated, both junctions are forward biased and injecting charge into the base. Hence, the charge may greatly exceed that required to support the collector current. Under these circumstances, in order to turn off the collector current, this excess charge must first be removed. There is thus a corresponding storage delay before the collector voltage can start to rise. During this storage delay time, the base current may go negative while the excess charge is removed. In fact, this is beneficial as it serves to reduce the delay time. The shape of the current

transient is very similar to that for the simple junction, shown in figure 6.5. The base current may be written as follows:

$$I_b = \frac{I_c}{\beta} - \frac{Q_s}{\tau_s} - \frac{dQ_s}{dt} \tag{6.54}$$

where Q_s is the excess charge, β the current gain and τ_s the effective time constant for the decay of the charge, given by:

$$\tau_s = \frac{\tau_F \beta_F (1+\beta_R) + \beta_F \beta_R \tau_R}{\beta_F + \beta_R + 1} \tag{6.55}$$

To determine the storage time, we find the initial value of Q_s in equation 6.54 by setting the base current to its initial value, I_F, and neglecting the derivative term. Integrating this expression then gives the decay of charge with a constant reverse base current ($-I_R$). Setting Q_s to zero to find the delay time then gives:

$$t_{sd} = \tau_s \left[\ln\left(1 + \frac{I_F}{I_R}\right) - \ln\left(1 + \frac{I_{bo}}{I_R}\right) \right] \tag{6.56}$$

where I_{bo} is the base current at saturation point on the collector. As I_R is constant during the transit time period, a plot of t_{sd} against the first logarithmic term then gives a slope of τ_s and an intercept of the second logarithmic term.

Substituting this value of τ_s into equation 6.55 and assuming that $\tau_F << \tau_R$, gives a simple expression for the lifetime:

$$\tau_s = \frac{\beta_F \beta_R \tau_R}{\beta_F + \beta_R + 1} \tag{6.57}$$

and, hence:

$$\tau_R = \frac{\tau_s (\beta_F + \beta_R + 1)}{\beta_F \beta_R} \tag{6.58}$$

6.4 RADIATION EFFECTS

Several workers, particularly Messenger (1958, 1965(1) and 1973), have investigated the effect of radiation on lifetime in bipolar transistors. However, the overwhelming majority of these studies have been limited to neutron radiation effects alone. Neutron radiation is known to cause far more displacement or bulk damage than ionisation damage, whereas gamma radiation causes many times more ionisation damage than

displacement damage. Thus, the neutron radiation effects studies are only loosely applicable to gamma radiation.

For the case of neutron radiation, it has been verified that the density of radiation-induced recombination centres is directly proportional to the neutron fluence (i.e. the total number of neutrons incident per unit area on the device). Messenger has also demonstrated that the minority carrier lifetime is a function of the radiation dose according to:

$$\frac{1}{\tau} = \frac{1}{\tau_0} + \frac{\Phi}{K} \tag{6.59}$$

where K is an energy dependent lifetime damage constant. Messenger goes on to show that the gain of a transistor is affected by neutron irradiation according to:

$$\frac{1}{\beta} = \frac{1}{\beta_0} + \frac{\Phi}{\omega_T K} \tag{6.60}$$

where:

$$\omega_T = 2\Pi\Lambda \tag{6.61}$$

and Λ represents the common emitter gain-bandwidth product. This derivation makes two assumptions:

- the gain is at least 3
- surface recombination does not change with total dose.

It is noted that this relation applies to both emitter-base field recombination and to bulk recombination.

Reddi (1967) illustrates three examples of transistor and their response to radiation, based upon an increase in charge density within or surrounding the surface oxide layer. A transistor with a low base surface doping concentration will show a rapid degradation of h_{FE} with total dose, reaching a minimum and then recovering back to the pre-irradiation level as total dose increases. A transistor with a medium level of base doping shows a gain response that starts to fall at a slightly higher total dose, reaches a minimum and then recovers but only to a level somewhat below that before irradiation. A transistor with a higher base doping level will show a monotonic fall in gain, albeit starting at a higher total dose than in either of the two other cases. The fall in gain is due to an increase in the base current. The rise in base current with surface

depletion is due to increased surface recombination, as well as bulk recombination in the surface depletion region. The bulk recombination increases monotonically with surface depletion and saturates at the point of surface inversion. Surface recombination, on the other hand, reaches a peak when the surface approaches a near-intrinsic condition. The combination can lead to a non-monotonic decrease in gain. Reddi presents experimental data that indicate that at surface doping concentrations of less than 3 x 10^{18} atoms/cm^3, surface inversion near the emitter-base junction has little effect on gain, while, if the doping concentration exceeds 4 x 10^{18} atoms/cm^3 then severe degradation of gain can be expected.

Grove (1967) presents data from electron irradiation experiments showing how the measured lifetime decreases with total dose. Assuming that the incident radiation creates recombination centres uniformly throughout the device, he derives the following expression for the concentration of recombination centres after irradiation:

$$N_t = N_{t0} + KN_e \tag{6.62}$$

where N_{t0} is the pre-irradiation concentration, K is the probability of an individual unit of radiation (e.g. a neutron or gamma ray) creating a recombination centre and N_e is the total dose. Using equation 6.28, this leads to:

$$\tau = \frac{\tau_0}{1+\left(\frac{KN_e}{N_{t0}}\right)} \tag{6.63}$$

which shows that the lifetime decreases from its original value in an inversely proportional manner with total dose.

Poch (1968) and Hart (1978) have separated the change in gain as a result of irradiation into two components:

$$\Delta\frac{1}{\beta} = \frac{1}{\beta} - \frac{1}{\beta_0} \tag{6.64}$$

Empirically, by the use of, for example, Gummel plots, it has been shown that the change in gain is due to a change in the base current, rather than the collector current. Hart shows that this equation then becomes:

$$\Delta\frac{1}{\beta} = \frac{\Delta I_B}{I_C} = \frac{1}{I_C}\left(\Delta I_{"bulk"} + \Delta I_{"surface"}\right) \tag{6.65}$$

Surface effects are relatively unimportant for neutron radiation and so the second term has traditionally been neglected in many papers. However, for gamma radiation, both terms are important and, in fact, the surface term may be the first to cause a noticeable reduction in gain for many transistors. Poch modifies equation 6.64 to divide the change in gain into bulk and surface terms:

$$\Delta\frac{1}{\beta} = \Delta\frac{1}{\beta_B} + \Delta\frac{1}{\beta_S} \tag{6.66}$$

and then develops this in a similar manner to that of Messenger:

$$\Delta\frac{1}{\beta} = K_B\Phi + K_S\Phi^n \tag{6.67}$$

where K_B is a bulk damage constant, K_S a surface damage constant and Φ the total dose. The value of n is quoted as lying between 0.4 and 1, depending on the device structure and processing history. The values of the damage constants are shown to be dependent on the collector current, following a predominantly logarithmic relation. Poch goes on to suggest that gamma radiation, such as produced by the cobalt-60 isotope, causes purely surface recombination-type damage with bulk damage from Compton electrons being insignificant. However, it should be remembered that he was dealing with radiation damage in the context of military systems and satellites, where the total doses are relatively low compared with those found in nuclear applications. Empirical data obtained for a much wider range of total dose indicates that this suggestion does appear to apply for the low to moderate total dose regime but that bulk damage starts to make a significant contribution at higher total doses. This bulk damage can therefore become of importance for systems operating in the nuclear industry.

Radiation effects can be manifested in two ways that further affect the parameters defined above. Firstly, a channel can be created due to ionisation of the surface region. This can also be seen for some types of passivation layer, causing low impedance paths to appear across critical regions of the device. Secondly, a conductive path can be created between the pins of a packaged device due to effects on the material of the case or encapsulation. Whilst the parameters of the device itself are not affected directly by this phenomenon, the effect on the circuit may give this impression and be just as harmful.

Recent published studies have concentrated on the use of digital components in applications such as space and military systems, particularly in the USA. As a result, this work has been based primarily on MOS technologies and devices. A detailed understanding of the role of different types of defect in the relationship between MOS transistors and irradiation has been developed (such as Ma (1989)) but it has not proved possible readily to transfer this to bipolar technologies.

6.5 CAPACITANCE-VOLTAGE PLOTS

Different dopant species and concentrations across the three main regions of a bipolar transistor lead to the establishment of electric fields within the device. The presence of passivation and other surface layers can further complicate the picture if charge is accumulated within these layers or at their surfaces. A small external voltage can be applied to compensate for the internal electric field.

A simple p-n junction can be regarded as a parallel-plate capacitor with the plates separated by a distance equal to the depletion layer width. For a junction in reverse bias, it may be assumed that all the charge transferred to the semiconductor as a result of changing the applied bias appears as a change in the charge contained within the depletion region. Capacitance per unit area is defined as the rate of change in the charge per unit area with voltage:

$$C = \frac{dQ}{dV} \tag{6.68}$$

Applying Poisson's equation, it may be seen that this gives:

$$C = \frac{K_s \varepsilon_0}{W} \tag{6.69}$$

where K_s is the dielectric constant of the silicon in the depletion region, W is the width of the depletion region and ε_0 is the permittivity of free space. Grove shows that for a one-sided step junction, corresponding to a typical base-emitter junction in a bipolar transistor, equation 6.69 may be developed to yield:

$$C = \sqrt{\frac{qK_s \varepsilon_0 N_B}{2(V_R + \phi_B)}} \tag{6.70}$$

where V_R is the applied reverse bias and ϕ_B is the built-in voltage of the junction capacitor. This equation can be rearranged to give:

$$\frac{1}{C^2} = \frac{2}{qK_s\varepsilon_0 N_B}(V_R + \phi_B) \tag{6.71}$$

Hence, by plotting $1/C^2$ against the applied voltage, the distribution of doping concentration is revealed. If the doping concentration is constant throughout the depletion region then the plot will be a straight line. The intercept on the voltage axis is the built-in voltage. In this case, the doping concentration is the sum of the doping concentration introduced intentionally when fabricating the device and the concentration of acceptor or donor-like impurities also present in the material. In the case of an irradiated transistor, the concentration of defects introduced by irradiation must be added to this. Consequently, by measuring the change in doping concentration with irradiation, the radiation-induced defect concentration can be determined.

7 Current state of knowledge

7.1 THE INTERACTION OF RADIATION WITH MATTER

The interaction of particle radiation, i.e. neutrons, protons and ions, with matter is complex. As such types of radiation form only a very small percentage of the total radiation environment associated with the nuclear power facilities relevant to this work, they will not be considered further here.

The slowing down and stopping of beta radiation, or electrons, in matter is governed almost entirely by multiple scattering, giving an effect resembling diffusion. Beta radiation of a given energy has a defined range in matter and shielding to protect vulnerable components is a viable option in some circumstances.

7.1.1 Gamma radiation absorption mechanisms

There are four main processes by which electromagnetic radiation (X-rays and gamma radiation) can be absorbed by a material: photoelectric absorption and Rayleigh (coherent) scattering, which dominate at low energies; Compton (incoherent) scattering, which is most important at energies in the range from 0.2 to 5 MeV; and pair production, which dominates at high energies. Photonuclear reactions can occur in certain circumstances but are not considered here as very high energy gamma rays are required and these are not usually found in the environments of relevance. Figure 7.1 illustrates the relative importance of the three main mechanisms with increasing photon energy (Sharp 1994). By way of comparison, figure 7.2 from the same source illustrates the typical gamma radiation energy spectrum emitted by spent fuel.

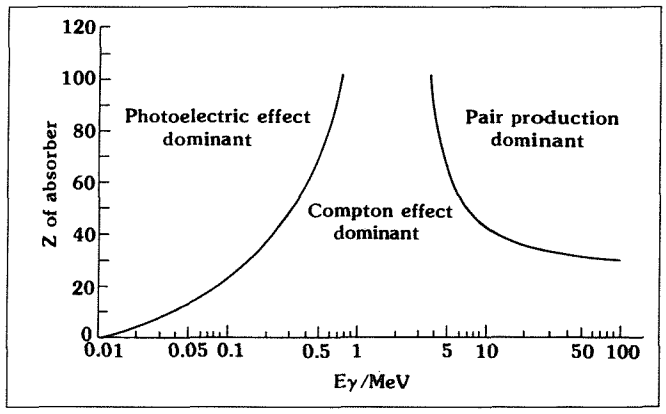

Figure 7.1: the three main interaction mechanisms of gamma radiation with matter.

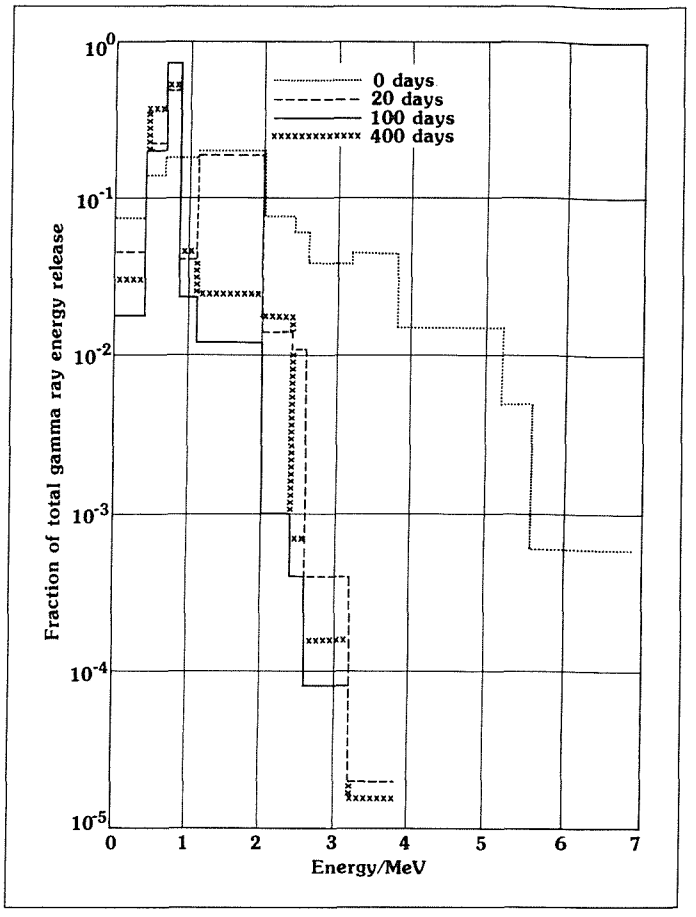

Figure 7.2: the energy spectrum of gamma radiation emitted by spent fuel at various times after discharge from a reactor.

This figure shows that the radiation emitted by the spent fuel (in this case, from an AGR reactor) covers a wide range of energy from zero to several MeV. This is indicative of the many different radioactive isotopes present in spent fuel, each with its own individual, characteristic emission that, summed together, give a broad, overlapping spectrum with more than one peak. Being a mixture of isotopes, there is also a variety of half lives and so the spectrum changes with time not only in amplitude but also in form. Isotopes emitting high energy radiation tend to have the shorter half lives and so the mean energy decreases with time, as can be seen by comparing the curves for different decay periods in the above figure. One benefit of storing used fuel elements in a pond at the reactor for a short period prior to transport is clearly demonstrated.

The photoelectric process involves the absorption of a photon by an atom, causing the ejection of an electron from the innermost electronic shell of the atom. This is accompanied by characteristic X-rays or Auger electrons in the case of light atoms. The photon energy, $h\nu$, must be greater than the electron binding energy, β, and the

difference is carried by the photoelectron as kinetic energy. Absorption is most likely when $h\nu$ is roughly equal to β.

The Compton effect involves the scattering of photons by atomic electrons that can be regarded as free and should be treated relativistically. The electron acquires some energy from the photon and the paths of both are altered. High energy photons tend to scatter in the forward direction and transfer more of their energy to the electron. This is the dominant absorption process for spent fuel gamma radiation. At lower energies the assumption of free electrons breaks down and we have to consider coherent Rayleigh scattering that, again, is very peaked in the forward direction, especially at the upper end of the energy range.

Pair production occurs only with photons with energy greater than 1.022 MeV and involves the annihilation of the photon and the production of an electron and a positron (this energy is the rest mass of the two particles). In order to absorb recoil momentum, this has to take place in the presence of a third body and generally an atomic nucleus is most likely.

Gamma radiation does not have a well-defined range over which it is absorbed in materials. Rather, it is continuously and gradually absorbed, resulting in a steadily lower intensity with depth into the material. The equation governing this absorption has an exponential form:

$$I_{(t)} = I_{(o)} e^{-(\frac{\mu}{\rho})t} \tag{7.1}$$

where $I_{(o)}$ is the incident dose rate, $I_{(t)}$ is the dose rate at depth t, measured in kg/m^2, and μ/ρ is the mass absorption coefficient for the material. The mass absorption coefficient is a function of density and so the dose rate decreases as the radiation penetrates the absorbing medium.

Figure 7.3 illustrates the reduction in dose rate of 1 MeV gamma radiation passing through a lead block. It should further be noted that the mass absorption coefficient is also a function of the radiation energy and figure 7.4 shows a similar curve for 200 keV gamma radiation in order to illustrate this dependence.

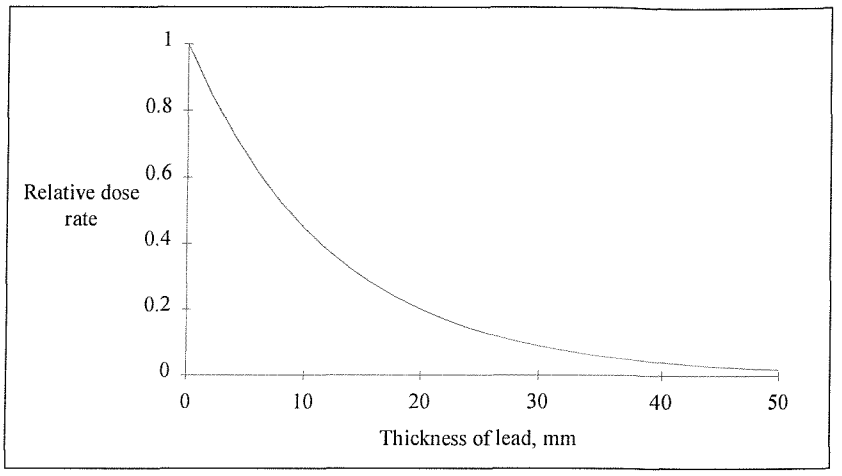

Figure 7.3: the effect of lead shielding on 1 MeV gamma radiation.

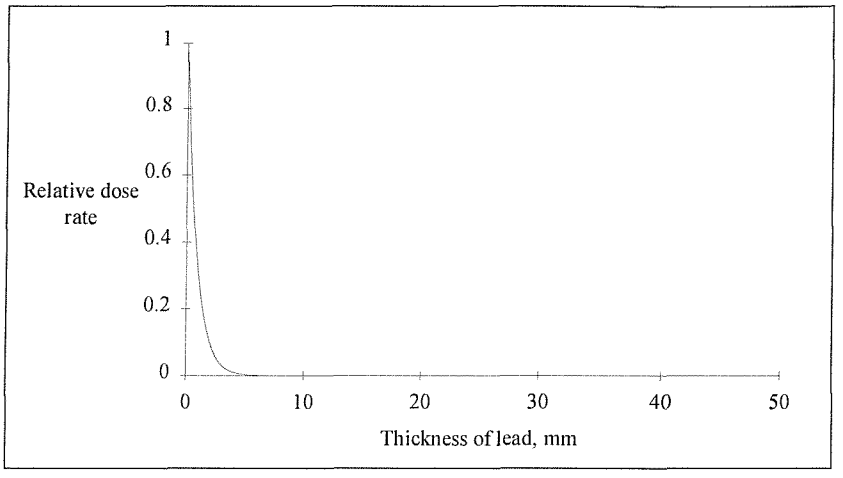

Figure 7.4: the effect of lead shielding on 200 keV gamma radiation.

A figure of merit often used in shielding calculations is the tenth-value thickness or TVT. This indicates the thickness of material required in order to reduce the radiation dose rate by one order of magnitude for gamma radiation of a given energy. Some values of TVT for various materials and radiation energies are shown in table 7.1.

Energy (MeV)	Lead	Iron	Aluminium
0.1	0.4	8	50
0.2	2	20	70
1.0	29	49	139
1.5	39	60	170

Table 7.1: Tenth value thickness figures in mm for various materials and radiation energy values.

7.1.2 Electrical effects

All types of radiation can be considered to interact with matter in three basic ways: ionisation, displacement and heating. The first of these covers effects such as charge separation and chemical bond breakage via the creation of electron-hole pairs, while the second refers to the movement of an atom away from the site it occupied prior to irradiation, i.e. atomic displacement. The relative importance of these two effects depends on the nature of the radiation and the type of material with which it interacts. It is also possible for one type of interaction to give rise to the other as a secondary effect. Consequently, it is often difficult to predict how a particular type and absorbed dose of radiation will affect the electrical or mechanical properties of a sample of material, let alone the properties of a finished component manufactured from it. The third effect, heating, occurs with all materials but is especially important for metals, as these contain delocalised electrons that cannot undergo ionisation in the manner described above.

7.1.2.1 Ionisation effects

The term ionisation covers a broad range of phenomena in which sufficient energy is transferred to an electron to enable it to leave its parent atom. This leaves a positive charge, or hole, on the atom and, in many materials, this charge is mobile so that the electron-hole pair may recombine or drift apart, producing conductivity in the material. This is of particular importance to the performance of electronic devices. In organic materials, a different outcome is possible in which the removal of an electron can cause a chemical bond to break. The subsequent remaking of these bonds in different configurations can result in quite different properties of the irradiated material.

Ionisation effects are normally associated with gamma radiation and charged particles, particularly electrons, whether from beta radiation or generated in a secondary manner by the photoelectric or Compton processes. Secondary electrons and holes are created along the length of the particle track and these may subsequently recombine, become trapped at defects or traps or, if an electric field is present, collected at external electrodes.

As already discussed, although the primary mechanisms by which photons and charged particles interact with matter are different, the net result in both cases is the creation of free carriers. Thus, in practice, it is often found that similar doses of gamma and beta

radiation produce identical effects in bulk materials. A significant difference between the two types of radiation is their range in matter: electromagnetic radiation is generally more penetrating than charged particles. Moreover, charged particles of a particular energy often have a very well defined range, whereas the intensity of electromagnetic radiation decays exponentially with distance, as shown above. For thin samples, this is not a problem as energy is deposited almost uniformly throughout the width of the sample. For thick samples this is not the case and significant differences are then found between similar doses of gamma and beta radiation or even between identical doses of beta radiation from electrons with different energies.
One example of an ionisation effect is the transport and subsequent trapping of mobile charges in thin film oxide dielectrics operated under high applied voltage fields. The presence of such an undesirable charge sheet in thin oxide films can completely disrupt the operation of metal-oxide-semiconductor (MOS) devices, unless the charge is dispersed in some way. Charge trapping also occurs in the oxide regions of bipolar devices (i.e. usually near the surface passivation layer) and this phenomenon is responsible for some of the degradation observed in these devices.

7.1.2.2 Displacement effects

In a displacement interaction, an atom is moved from its original position. This displacement may be a direct result of the collision of a particle or it may be a secondary process. In either case, the creation of such defects in a crystalline solid has a direct effect on the conduction of electrons and a variety of properties may be changed. Displacement damage may also be called dislocation or bulk damage.
All forms of radiation are capable of producing atomic displacements but the precise nature of the damage is often dependent on the particular type and energy involved. In the case of silicon, beta and gamma radiation tend to produce point defects (Frenkel defects, the association of a displaced atom and the vacancy in the lattice where it was originally situated) that typically consist of one or two atoms and contain, at most, 10 atoms (Corbett 1966). In the case of gamma radiation, bulk damage is normally caused by a secondary electron created by the photoelectric or Compton mechanisms or pair production. This is because the probability of a gamma ray displacing an atom directly is very small (Kahn 1959, Vavilov 1965). Point defects and clusters give rise to qualitatively similar changes in electrical and transport properties and if it is necessary

to separate the two then careful analysis must be made of the changes themselves and their introduction rates.

The colliding particle can transfer only a fraction of its energy to the atomic lattice it enters. For neutrons, this fraction is around 0.133, while for electrons it is only 0.000078, the difference being related to the ratio of the masses of the particles involved and assuming simple, Newtonian mechanics (Kaye and Laby 1986). Therefore, a 1 MeV neutron can produce recoil silicon atoms with a maximum energy of 133 keV, while a 1 MeV electron can produce recoil atoms with a maximum energy of only 78 eV. Consequently, the pattern of damage resulting will vary with the type of radiation. Lattice defects will be produced when the recoil atoms acquire an energy greater than the displacement energy threshold for the crystal lattice. For silicon, this threshold is between 15 and 30 eV, depending on the type and energy of the radiation (Vavilov 1965). An electron energy of at least 0.145 MeV is required for displacement damage to occur (Rappaport and Loferski 1955). The maximum energy of a Compton electron produced as a result of cobalt-60 irradiation is about 0.95 MeV (Corbett 1966). Thus, many electron-hole pairs and lattice defects can result from the absorption of each gamma ray. A number of other types of defect are also produced by irradiation but the mechanisms for their production are less clear.

7.2 SUMMARY OF KNOWN RADIATION EFFECTS ON SEMICONDUCTOR ELECTRONIC COMPONENTS

Ionising radiation has been known for more than 50 years to cause deleterious effects on semiconductor devices. The first recorded incidence of radiation affecting the operation of electronic equipment followed the STARFISH nuclear explosion in 1962. This explosion led directly to operational problems with several satellites in earth orbit, including the failure of TELSTAR 1 in November 1962. Subsequently, many types of event attributable to man's actions (nuclear explosions, accidents at nuclear facilities and deliberate misuse of radioactive sources), as well as natural events (solar coronal mass ejections and high altitude air flights), have caused temporary disruption or failure of electronic systems. This section examines the extent of the effects arising from these events, viewed from three perspectives: the microscopic or semiconductor level, the device level and from the point of view of a piece of equipment using such devices.

7.2.1 Semiconductor level

The fundamental effects of the interaction of radiation with matter have been studied for several decades, almost since the dawn of the transistor era. Military applications for modern electronics have meant that radiation effects on semiconductors were the subject of extensive study as soon as devices were developed. At the semiconductor level, this work took the form of identifying changes in basic properties associated with exposure to ionising radiation. Principal among these are carrier lifetime, mobility and material resistivity. The very early work concentrated on particle radiation effects, especially neutrons. Subsequently, an understanding of the effects of ionising, electromagnetic radiation, i.e. gamma radiation, was also developed.

Carrier lifetime is affected by the density of defects in the structure of the semiconductor lattice. Certain defects lead to the recombination of electrons and holes, hence their name of recombination centres. A greater density of recombination centres reduces the time for which a carrier can move before encountering one, hence reducing its lifetime. The interaction of ionising radiation with silicon leads to the creation of a variety of defects, resulting from the way in which the energy given up by the radiation during its passage through the material is absorbed. A common example is the V-O defect, consisting of a vacancy in the lattice associated with an off-site, substitutional oxygen atom, sometimes identified as the A-centre. This defect has a neutral charge state but can trap an additional electron, acting as a recombination centre. V-O complexes are the main oxygen-related defect formed when radiation interacts with silicon (Corbett (1961) and Ewels (1997)), especially for silicon manufactured by the Czochralski method, which is particularly rich in oxygen (Lindström (2000)).

Carrier mobility is closely linked to carrier lifetime and is a measure of the ease with which a hole or electron can travel through the silicon lattice. As the number of defects acting as recombination centres increases, the progress of the carrier is impeded and its mobility is said to decrease.

The overall defect density, combined with the doping density put in place during the manufacture of the silicon, defines the resistivity of the material. As the defect density increases, the resistivity of the material also rises. With gamma radiation, this effect does not become significant until rather high total integrated doses have been applied. Changes in lifetime and mobility are observed well before the onset of an increase in the resistivity. However, for equipment destined for use in the higher radiation

environments of the nuclear industry, it is conceivable that this effect could lead to, for example, an unacceptable increase in power consumption for some systems.

7.2.2 Device level

For the designer of a sensor or electronic module that is required to tolerate a given total dose of radiation, the important factors are changes in operating parameters of the devices he wishes to employ. It is these changes that will dictate which components he may use for a particular application and the way in which he can use them. For bipolar transistors, a number of the most important parameters show considerable sensitivity to radiation, particularly gain, leakage current and saturation voltage. MOS devices are even more sensitive and movements in the operating point of MOSFETs, giving threshold voltage shifts of several volts, can lead to their failure after total integrated doses of just a few gray. This means that electronic equipment using these devices can be as sensitive to radiation as is the human body (Clarke, 2001).

The most important parameter for many transistor designs is the common emitter current gain, often termed β. For many types of transistor, this parameter shows a rapid decline with increasing total integrated dose, with the rate of fall reducing until the gain reaches a more or less stable value at less than 10% of its initial level. This effect has been demonstrated many times, for example by Messenger (1986) and Holmes-Siedle (1993). Sharp (1993(2)) illustrates this for two different sources of radiation, as shown in figure 7.5.

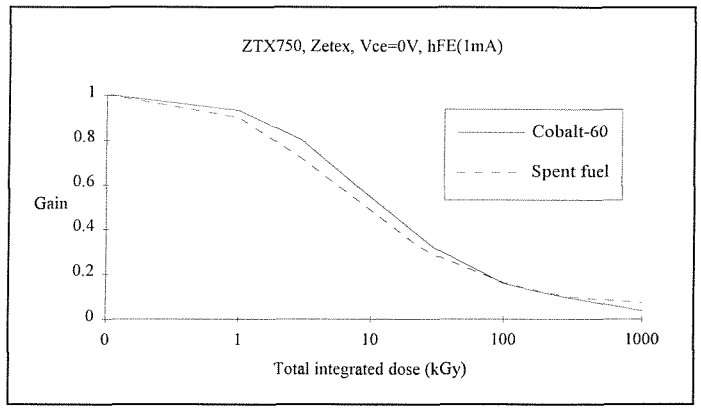

Figure 7.5: change in gain with total dose for ZTX750 transistors.

The shape of the curve varies from one type of device to another and this can be seen by comparing the previous figure with figure 7.6, showing data for BC549C npn transistors, from the same paper by Sharp (1993(2)).

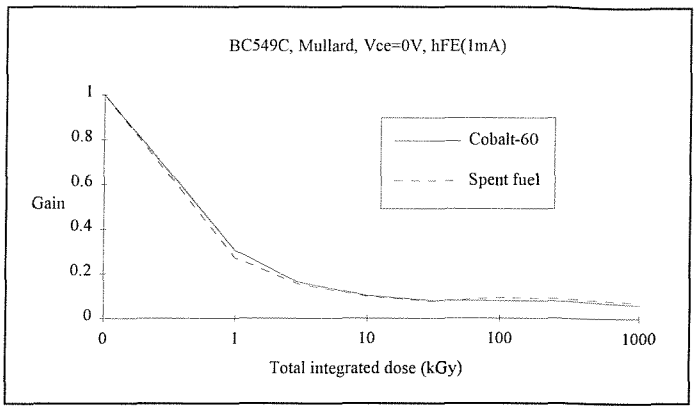

Figure 7.6: change in gain with total dose for BC549C transistors.

Whilst figures 7.5 and 7.6 illustrate that the shape of the gain degradation curve varies from one type of device to another, they also indicate that it is consistent for devices of the same device type. In fact, this is really true only for devices from the same manufacturer and the same production batch. It is quite commonly found that devices from different manufacturers, batches, lots or fabrication lines, whilst overtly of the same design, can show surprisingly large differences in their radiation response. Poch (1968) has shown that even variations within devices from the same manufacturer can be significant. Figure 7.7 illustrates this, being for five sets of 2N2102 transistors from one day's production.

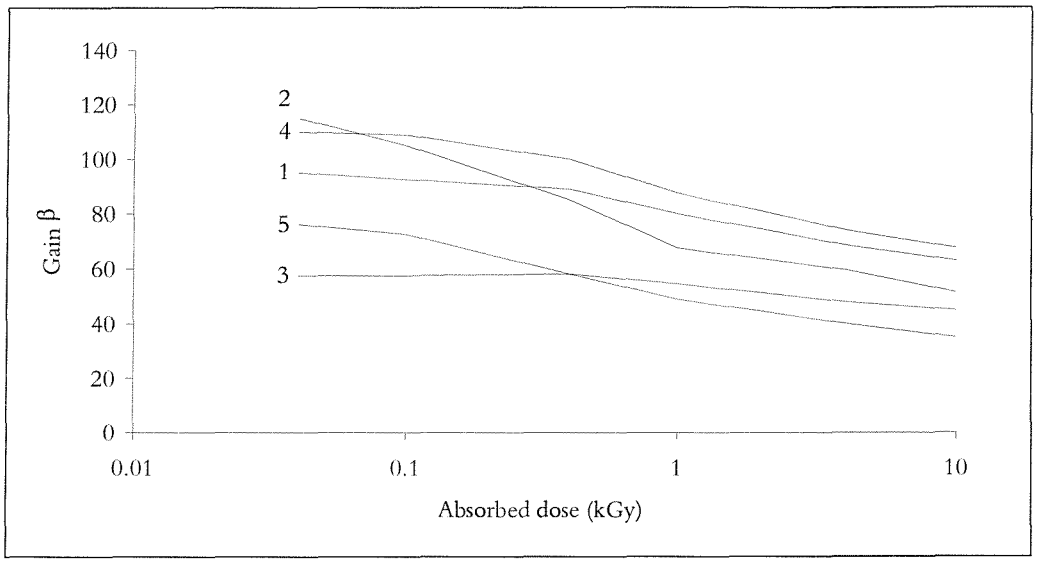

Figure 7.7: change in gain (Ic = 10 mA) with total dose for five production lots manufactured on the same day and in the same facility (from Poch (1968)).

An increase in leakage current of several orders of magnitude was a serious problem in the early days of the transistor, when devices were encapsulated in metal cans, backfilled with a low pressure of inert gas. Irradiation with neutrons ionised a

proportion of the gas molecules, which then became attracted to the biased regions of the unpassivated device, acting as a low resistance path across its surface (Blair, 1963). The advent of surface passivation cured this problem but other effects of radiation that also lead to an increase in leakage current, particularly across the collector-emitter junction, then became apparent. Figure 7.8 illustrates the change in collector-emitter leakage current for two types of device (Pater, 1995).

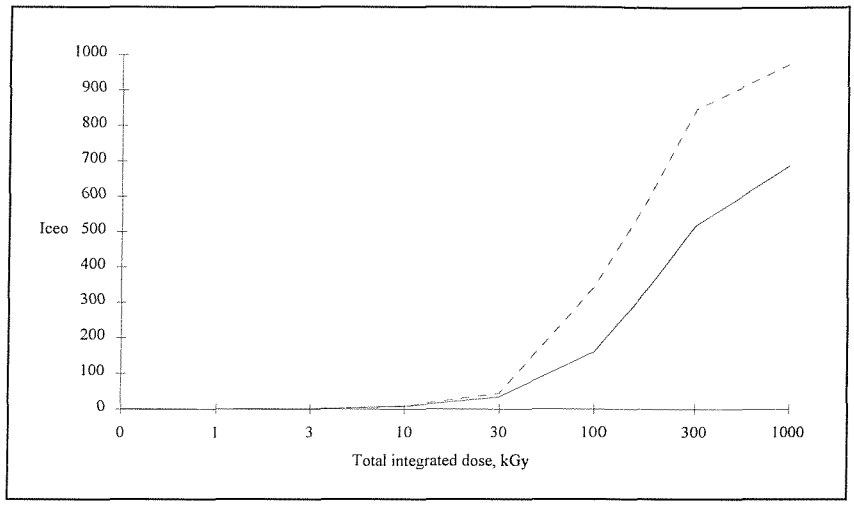

Figure 7.8: change in collector-emitter leakage current with total dose for BC549C (solid trace) and BC849C (dashed trace) transistors, manufactured by Philips.

The other important design parameter that can show significant changes with radiation is saturation voltage. Modern bipolar transistors often have datasheet values of saturation voltage well below 0.1 V. With irradiation to a total dose of 1 MGy, it is possible for this to increase several-fold, as shown in figure 7.9, also taken from Pater (1995).

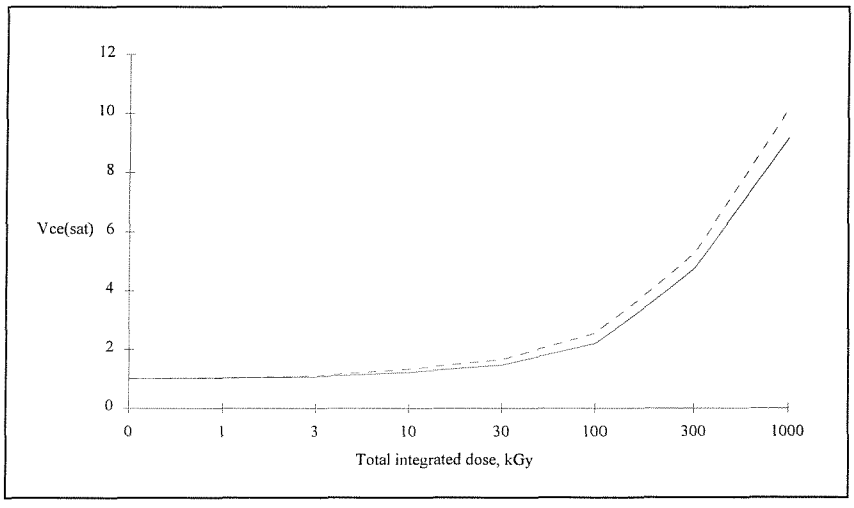

Figure 7.9: change in saturation voltage with total dose for MPSA92 (solid trace) and FMMTA92 (dashed trace) transistors, manufactured by Zetex.

Whilst increasing saturation voltage is linked to falling gain, this does not explain why some devices show a large change in saturation voltage and others a small change, even when the radiation-induced change in gain is similar. This effect remains poorly understood by the radiation effects community.

Other device parameters are also affected by radiation but, in most cases, do not have a marked impact on the circuit design process. Reasons for this include the effect being small, the parameter being important only for certain circuit configurations and the change resulting in an improvement in the parameter. An example of the latter case is collector-emitter breakdown voltage. At high total integrated doses, the resistivity of the silicon starts to be affected, resulting in a slight increase. This is manifested as an increase in the breakdown voltage between the collector and emitter terminals. Figure 7.10 provides an example of this effect.

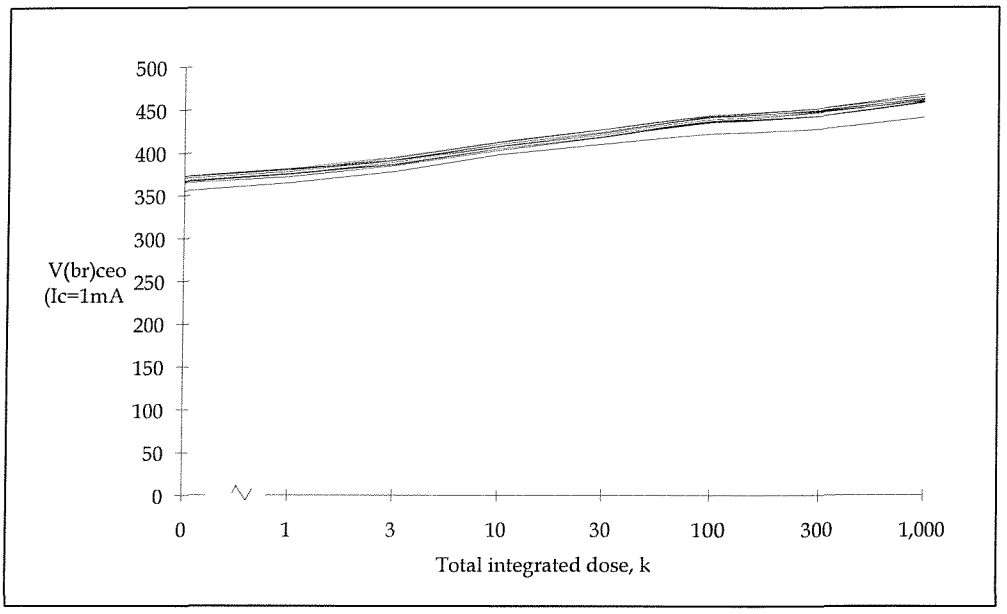

Figure 7.10: change in collector-emitter breakdown voltage with total dose (in kGy) for FMMTA42 transistors, manufactured by Zetex (DS1501).

7.2.3 Equipment level

From the point of view of the user of a piece of electronic equipment, the effects of radiation appear as changes in power consumption, a reduction in functionality or a fall in the reliability of the system. All of these are undesirable but may also occur simply as a result of age and degradation mechanisms other than irradiation. The aim of the equipment designer is to increase the level of radiation tolerance of the system

to the point at which other degradation mechanisms become as important. Going beyond this point yields no benefit.

For the plant operator, the maintenance of electrical and electronic systems to ensure their functionality is a very important part of his role. In order to achieve this effectively, the reliability of the equipment must be known to some accuracy. He does not want to replace the item more often than necessary, as this increases costs and plant downtime. On the other hand, he does want to replace items sufficiently frequently that the majority of their lifetime is used but before the rising edge of the bathtub failure curve begins to introduce unplanned maintenance outages. Having confidence in the degree of radiation tolerance quoted for a given item is important in planning the maintenance associated with it. This applies equally to items installed in the plant, as well as to tools for carrying out the maintenance and to inspection systems used in unplanned breakdowns or for periodic assessments of plant condition.

The mode of failure due to radiation effects is often such that a warning of impending failure is given. For example, a region of saturated, white pixels may appear on the image of a closed-circuit television camera a few days before the picture disappears altogether (Sharp, 1995). Alternatively, the distance readings reported by an optical metrology system may indicate that the concrete cell wall opposite is retreating with time, pointing to a reduction in amplitude of the received signal due to loss of gain in a phototransistor.

These examples show that an indication of the mode of failure is as important to the plant operator as knowledge of the expected total dose to failure itself. Often, conditions in-cell are different from those assumed by the plant designer, who may have drawn up his parameters ten years earlier. Changes in the use to which a plant is put are not uncommon over the years and so the radiation levels inside a facility may increase or decrease as time goes by. The operator may not be aware of this directly and so an early warning sign from the equipment is often a valuable aid.

7.3 ASPECTS SPECIFIC TO NUCLEAR POWER INDUSTRY ENVIRONMENTS

The majority of research into radiation effects on semiconductor devices is carried out for near-to-market purposes. The end users come from a small number of fields, principally the military, aerospace, nuclear, medical physics and industrial sectors. Each

of these has a slightly different radiation environment and this influences the research that is undertaken. The principal differences between the various radiation conditions relate to the species of radiation, dose rate and total integrated dose. Table 7.2 summarises these differences for the five areas. The predominant types of radiation are listed in order of importance in terms of their effects on electronic systems. Neutron radiation is indicated by an 'n'; beta and electron radiation by a 'β', gamma radiation by a 'γ'; alpha radiation by an 'α'; protons by a 'p'; and X-rays by an 'X'.

	Types of radiation	Dose rate	Total dose
Military	n, X, γ	H	L
Aerospace	β, p	L – M	M
Nuclear	γ, β, X, n, α	L – H	H
Medical physics	X, γ, β	L – M	L
Industrial	γ, X	L – M	L – M

Table 7.2: the radiation environments associated with the five principal sectors using electronic components under irradiation.

The three largest market sectors are military, space and nuclear power. Traditionally, most of the research into radiation effects on semiconductors has been funded by military programmes in the USA, although space applications have become more prominent during the past decade or so. This table illustrates the fact that the nuclear power industry is unique with its requirement for knowledge of high total dose effects on electronics. Furthermore, the majority of applications involve exposure to radiation at dose rates much lower than those found in military situations and higher than those found in space. Hence, the data that have been generated by most of the large research programmes to date is largely applicable only with great care to applications in the nuclear sector. They cannot be used reliably there without an understanding of the influence of the different test conditions compared with the conditions in service. Typical patterns of work in fuel handling, reprocessing and waste handling plant in the nuclear sector involve using equipment during the working day and then leaving it unused overnight. Depending on the operator and working practices in the plant, the equipment may remain in the radiation environment overnight or may be moved to a lower dose rate region in order to reduce the dose uptake. Equipment associated with

operating reactors tends to be exposed to a relatively stable radiation environment, apart from tools used for fuel loading and unloading which have a very low duty cycle.

7.4 THE INFLUENCE OF PACKAGE STYLE AND PRE-TREATMENT

There have been several studies reported that have considered the influence of package style and treatment processes, such as burn-in, on the radiation effects observed later in the life of a component, including those by Clark (1995), Barnes (1997) and Wall (1998 and 1999). These effects appear to be particularly pronounced at very low dose rates, such as those seen in geostationary or interplanetary space orbits. The work showed that devices irradiated at very low dose rates, i.e. in the region of 20 μGy/hr, can show a much greater rate of change in some parameters than when irradiated at a dose rate of 500 μGy/hr or above. These effects seem to be related to the thermal budget received by the device during the packaging and testing phases of its manufacture and were especially apparent for devices in ceramic packages rather than metal or plastic encapsulation.

Work carried out by the author of this work and reported by Wall (1998 and 1999) indicates that, for the dose rates likely to be encountered in the majority of post-reactor plant in the nuclear industry, package style and the thermal history of the devices during fabrication and packaging are unlikely to be significant factors in their later response to radiation in these environments. As a result of this, these aspects were not examined for the work reported here.

7.5 ENHANCED LOW DOSE RATE EFFECTS

Over the past five years, several teams have reported much higher than expected rates of damage in devices irradiated at very low dose rates, i.e. comparable with the dose rates found in space. The accepted international test procedures (in particular those published by the US Department of Defense (anon (1991)) and the European Space Agency (anon (1995))) specify that radiation testing be carried out at higher dose rates in order to reduce the test duration to manageable levels. Experimental results at these very low dose rates (e.g. Fleetwood (1995) and Wall (1999)) has shown that damage can be several times worse than predicted from the higher dose rate data. As these dose rates are much lower than those typically found in nuclear power industry plant, this

effect is unlikely to be a factor in determining the life of electronic systems in these applications and so has not been examined in this work. In fact, this effect may well be more relevant to office or laboratory equipment located in the background radiation environments of those regions with specific geological features yielding higher than average concentrations of radon gas in the atmosphere, whether or not the equipment is associated with a nuclear facility.

7.6 TECHNIQUES FOR COPING WITH RADIATION EFFECTS

The first stage in dealing with a potential radiation effects problem is to determine all relevant aspects of the operating environment. This includes all the factors identified above as having an influence on the total dose effects. The second stage is to define the limits of operation of the equipment, materials or components, i.e. what is meant by failure?

The response of most materials and electronic components to radiation does not involve a sudden change from full functionality to complete failure, rather a gradual degradation of many parameters takes place. It is often not a simple matter to decide where on the curve of degradation to place the failure point. Indeed, for most materials, an arbitrary limit of 25% or 50% is often used (Schönbacher (1989)).

Conversely, for integrated devices, electronic circuits and pieces of equipment, a combination of the gradual degradation of a number of components does often lead to a sudden failure, without warning. In this case, it is up to the designer to allow for a degree of degradation in individual component parameter values appropriate to the total dose radiation tolerance required, in a similar manner to designing to worst case datasheet values, as opposed to typical values.

Often, it is not possible to determine the radiation tolerance of a circuit or piece of equipment from the design data. Indeed, the inherent variability of radiation tolerance for semiconductor components means that COTS devices invariably require radiation testing, even if several manufacturer's lots of the same device type have already been characterised. From these data, it may then be possible to assess the probable radiation tolerance of the complete circuit. However, the component test data may still be insufficient to give a suitably accurate assessment and, in this case, radiation testing of the system can prove necessary.

Once the environment and limits of operation of the equipment have been identified, it is then possible to decide what measures to take in order to ensure that that equipment continues to function as required. If this involves the use of radiation test data then these must be examined carefully to determine the relevance of the test conditions under which the data were generated to the conditions in the application. If there are any disparities then the effect of these must be assessed and allowed for. This applies for both organic materials and electronic components. For higher levels of total dose, i.e. above 10 kGy, or for operations extending over several years, it is better to avoid polymers containing halogens. These may be present as part of the base polymer, for example as in PVC, or as additives, often as bromine for fire resistance. This measure will prevent radiolytic corrosive substances attacking exposed component leads and other parts of the equipment.

The modelling of total dose effects is becoming established as a useful technique for predicting the response of an electronic circuit to radiation, as may be seen in Sharp (1993). If the basic response data are available for the components of interest then simulators, such as the various SPICE programs, are able to translate this into the response of the circuit. However, this approach still requires extensive radiation testing in order to generate the component data. The next step is to develop a fundamental understanding of the influence of radiation damage on the device physics so that component data may be extrapolated to other components or to other irradiation conditions without the need to carry out further testing. This area is rather less well advanced and is addressed by the current work.

8 Advances sought by this work

Current practice within the nuclear power industry has several implications for the use of electronic components in general and bipolar transistors in particular. A common approach is to regard electronic equipment as inherently unreliable within radiation environments due to radiation-induced degradation of the parameters of components, leading to the failure of the equipment in an unpredictable manner and at an inconvenient time with regard to the operations being carried out in the facility. The usual remedy applied to deal with this issue is to exclude electronic equipment from the active area. Exceptions are made where the equipment is required for safety purposes or offers significant benefits for the staff in an operational sense. However, in the latter case, further constraints are normally placed upon the equipment; for example, including features such as extended fasteners and special connectors to permit remote maintenance or custom cases or racking for the equipment to reduce the accumulation of radioactive contamination that would complicate repairs or disposal.

Certain types of electronic equipment are used in radioactive facilities, where the performance of the equipment has been demonstrated to be acceptable and where the modifications to ease its installation, use, repair and disposal have been completed. Examples include closed-circuit television and robotic inspection systems. The degree of reliability demanded by operators at present has permitted only the more basic types of circuit and device to be used because it is not currently possible to predict the performance of a circuit without extensive radiation type-testing. This is costly and not attractive to manufacturers for relatively small sales volumes.

It is clear that any new techniques to enable the reliability of electronic equipment demonstrably to be improved will be welcomed by the nuclear industry. Not only will they improve the efficiency of operations but they should also permit the cost of the equipment to be reduced as a result of the diminished requirement for radiation testing.

The first aim of the current work is to establish the baseline performance of bipolar transistors in the radiation environments found within the nuclear industry. Some aspects of this topic have been addressed previously but only for certain, specific

projects or applications. This work aims to extend the coverage to include the entire range of conditions found, enabling the findings to be applied to a broad spectrum of applications and activities.

Secondly, the work aims to relate the radiation-induced effects observed to physical properties of the devices. This will not directly help the circuit designer using bipolar devices but should enable a deeper understanding of the mechanisms to be gained.

This understanding will then contribute to the third aim, the development of predictive techniques to estimate the likely effects of radiation on a new type of device or circuit in order to improve reliability and extend the lifetime of equipment.

These techniques must be useful to the circuit designer or plant operator, i.e. should not address the fabrication of devices. The justification for this is that the volumes of devices used by the nuclear power industry are very small in comparison to those for standard commercial markets. The military market is considerably larger than the nuclear market and even that sector is finding it ever more difficult to identify component manufacturers who will entertain the production of special versions of devices for hostile environments, even with a healthy price premium. The probability of finding component manufacturers who would produce special versions for the nuclear industry is correspondingly smaller. Hence, any defensive practices required to enable the deployment of equipment into nuclear facilities must be taken by the circuit designer or the user of the equipment.

Possible techniques could include the following suggestions:

- circuit design practices
- component pre-treatment
- PCB layout arrangements
- the selection of certain types of packaging materials
- redundancy
- bias arrangements
- positioning of equipment
- duty-cycle considerations

These options will be discussed more fully in later sections.

9 Experimental techniques

9.1 CHOICE OF TEST SAMPLES

The preliminary experimental stages (phase 1) used commercially available bipolar transistors, some small-signal devices and some medium power devices. These were taken from a range of manufacturers and used for their low price and convenience. All were discrete devices, in standard plastic or metal packages. Care was taken to ensure that each batch of devices that was irradiated together originated from the same manufacturer's date code. This did not provide wafer or even, in some cases, lot traceability but was the best that could be done for commercial grade devices.
The phase 2 experiments were carried out on devices fabricated with the SUMC mask set by the University of Southampton Microelectronics facility. These devices were specially designed to present a variety of geometries on one chip, particularly with regard to perimeter to area ratio, and have been used on a number of projects by other researchers at the University. 28-pin DIL headers were used with eight different devices being bonded out in each package, as shown in figure 9.1. Each device had a different geometry, giving the full range in each package.

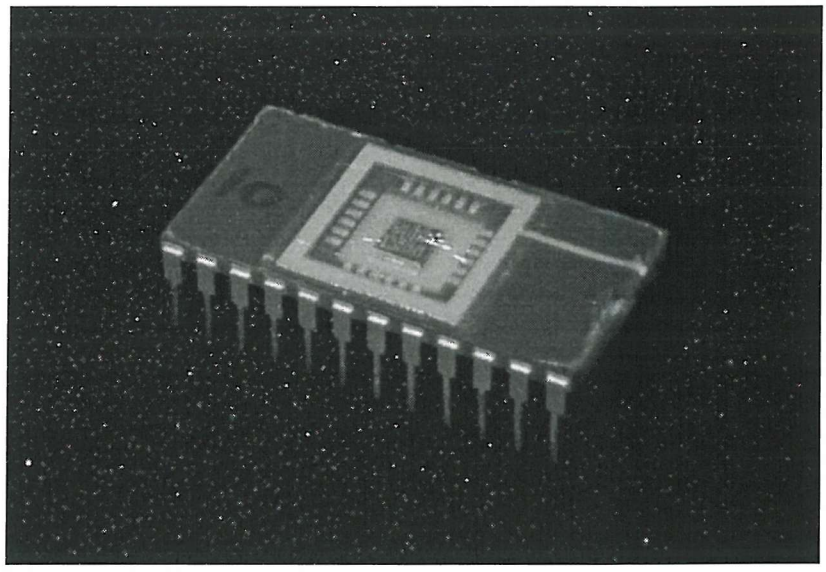

Figure 9.1: SU device package number 10.

9.2 DESCRIPTION OF THE IRRADIATION FACILITY

The majority of the irradiations described in this work were carried out in concrete, shielded cells, each fitted with four cobalt-60 sources. The cells were located at AEA

Technology's Harwell site in Oxfordshire. Three different cells were used, although the internal geometry and facilities were nearly identical. Cobalt-60 emits gamma radiation with two characteristic energies, 1.173 and 1.332 MeV. The beta radiation also emitted by cobalt-60 was shielded by the aluminium and steel encapsulation used to prevent the transfer of radioactive material from the sources themselves. Figure 9.2 illustrates the arrangement of the sources in one of the cells. Four, identical sources were used, disposed in a square array. The arrangement and capabilities of the facility have been described elsewhere by the author (Sharp (2000)).

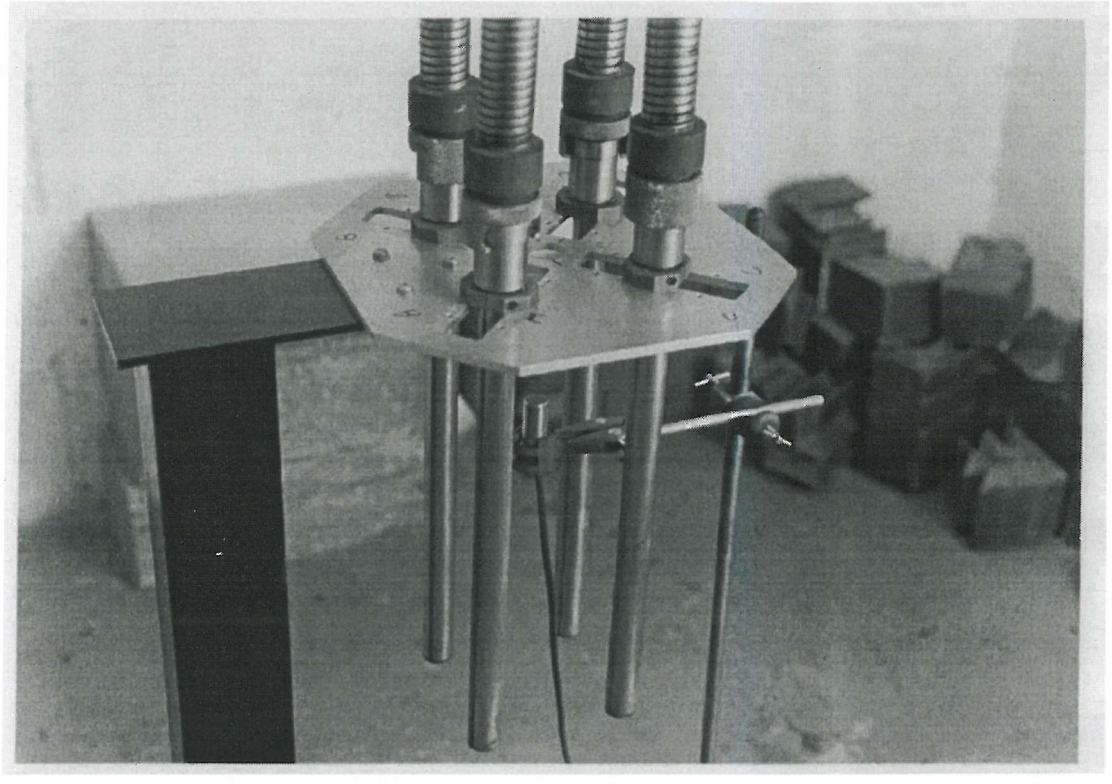

Figure 9.2: cobalt cell 4 at AEA Technology's Harwell site.

The separation of the sources could be varied, according to the size of sample and the dose rate required. For high dose rate irradiations, the sample was placed in the centre of the array. For lower dose rates, samples were placed outside the array and, in some cases, had shielding interposed in order to reduce the dose rate further than could be achieved within the geometrical constraints of the cell structure.

A small number of irradiations was carried out in the former spent fuel pond, also located at Harwell. This facility closed in 1991 and so was used for only a few of the early experiments.

9.3 DESCRIPTION OF THE MEASURING EQUIPMENT

DC parameters of the test samples were measured with a Hewlett Packard HP4142B parameter analyser. This is a computer-controlled, industrial standard instrument, very commonly used in the study of radiation effects on semiconductor components. It can measure DC current and voltage down to femtoamp and millivolt levels, under both continuous and pulsed conditions. Four-point, Kelvin probe measurement fixtures are employed and the system self calibrates itself at frequent intervals during use. The test software was written in HP BASIC and verified against measurements made with other equipment or results from previously verified software. A sample test program listing is included at appendix A.

A Keighley 590 C-V measuring instrument was used for the capacitance-voltage measurements. This instrument is computer-controlled in the same manner as the HP4142. Again, custom test software using HP BASIC was written and this was verified by making measurements on fixed value capacitors with a known C-V response.

The DLTS measurements were made with a Boonton DL4600 machine, fitted with a Boonton S4910 capacitance meter. This equipment was located at the University of Southampton and proved very unreliable, despite several repairs by the manufacturer. Some results were obtained but, after a few months, this measuring technique was not pursued further.

A variety of other, standard laboratory test equipment was used, including oscilloscopes, digital multimeters and power supplies. All the test equipment used for this work (except the DLTS machine) fell within the scope of the calibration and maintenance regime employed by AEA Technology's Radiation Testing Service and forming part of the certified ISO 9001 QA system. This is a strict policy, requiring the calibration of each instrument at least once each year, followed by a comparison of the test results against previous data to check for any long-term drift or instability in the instrument.

9.4 RADIATION TESTING STANDARDS

There are two international standards that are used for the radiation testing of electronic components. ESA basic specification no. SCC-22900 (Anon, 1995) covers the testing of components for use in the space programmes of the European Space

Agency. It specifies dose rates and total dose intervals that are appropriate for these applications but that are uncommon in the nuclear sector. However, the principals of sample handling, labelling, biasing during irradiation and time intervals between irradiation and measurement are all applicable.

Mil-Std-883 method 1019.4 (Anon, 1991) is an American standard used for both military and space programmes. It is similar to the ESA specification and suffers the same shortcomings in terms of applicability to nuclear applications.

Over a period of nearly fifteen years, AEA Technology has developed its own procedures for radiation testing for nuclear applications. These procedures form work instructions within the QA system and are more attuned to the requirements of users in this field than are the two standards referred to above. Two of these work instructions are described more fully in the next section.

9.5 RADIATION TESTING PROCEDURE USED FOR THIS WORK

Most of the irradiations carried out for this work were effected according to the AEA Technology procedure AEAT/GP/26/4/17 (Smith, 1996). Those irradiations carried out prior to May 1996, when the procedure came into effect, followed a broadly similar pattern of work, although this was not documented in the same manner. The procedure describes how samples are to be handled and identified and how records are to be kept, as well as covering the calibration of test and measuring equipment and the control of sub-contractors.

Under the procedure come a number of work instructions, providing detailed instructions on how to carry out a specific activity. Two of these are relevant to this work. The first covers the irradiation of samples in a cobalt-60 cell (Pater, 1996 (1)), detailing the methods for labelling and packaging samples, dosimetry and record keeping. Important points include:

- the labelling of each test sample in such a manner that the legibility of the label is not affected by irradiation
- the packaging and handling of samples in order to avoid damage other than that caused by irradiation
- use of an approved and calibrated system of dosimetry with an accuracy of ± 10% or better

- the mounting of test samples in the irradiation facility so that they are secure and remain in a position at which the dose rate is known and does not vary significantly over the volume of the sample
- the use of an approved method of calculating the total dose received by a sample during a given exposure to radiation
- the records that are to be kept for each irradiation

The second work instruction covers the testing of bipolar transistors using the HP4142B system (Pater, 1996 (2)), detailing how to identify individual test records and how to handle test samples. This procedure ensures that test data produced by the ATE are uniquely identified and can be related to the corresponding irradiation.

9.6 QUALITY ASSURANCE PROCEDURES

AEA Technology is certified to ISO 9001:1994. All the irradiations and measurements forming part of this work were carried out according to the requirements of this certification, including but not limited to the recording of data, calibration of equipment and sample handling procedures. Adherence to the standards is checked by a programme of monitoring and audits, both internal and by an independent certifying body.

9.7 THE EXPECTED INFLUENCE OF THE CHOSEN TEST PROCEDURE ON THE RESULTS

There are several factors associated with radiation testing that can affect the outcome of an experiment. The most obvious of these, perhaps, concern the type of radiation and the total dose. However, dose rate, biasing conditions and measurement techniques can also influence the results and different approaches are taken for different applications. The most important rule is to ensure that the test conditions either match those of the application or can be related directly to them. The relation should be direct and clear, perhaps from an accepted relationship between two variables or based upon established practice or empirical data.

The justification for the type of radiation, total doses and dose rates chosen for this work has already been made. The ranges used correspond to those found in the nuclear power industry. These conditions are different from those found in space and

military environments and are also different from the recommended test procedures for these two sectors. This can be expected to result in slightly different post-irradiation data than would be obtained when testing for either of these application groups. In particular, the total doses used here are much higher than found in any application outside the nuclear sector, leading to greater degradation than is normally encountered in, e.g. space systems.

The majority of the measurement techniques used here are standard industrial practice, using commercial test equipment. The one exception concerns the reverse storage time measurements, for which a custom test rig was built as this could be effected for a much lower cost than the commercial equivalent.

Bias conditions during irradiation can have an affect on the measured post-irradiation characteristics. The two relevant international standards call for 'worst-case' bias conditions to be applied in the absence of clear directions from the application. It is not always clear what the worst-case conditions are until the experiment has been carried out so some assumptions have to be made. For this work, a typical bias arrangement for a bipolar transistor used in an amplifying circuit has been used, coupled with tests at zero bias, corresponding to periods when the equipment is not in use and has been switched off but remains within the radiation environment. This situation might be experienced during periods of maintenance in nearby parts of the plant; during other phases of a multi-phase activity within the one radioactive facility; or simply overnight, where single-shift operation is applied.

10 Phase 1 experiments

10.1 OVERVIEW

The first phase of experiments was conceived with the aim of developing the measurement techniques that would be used on test samples of known characteristics. At this stage, it was not known whether the various techniques available would be useful or applicable to the work and this provided a means of selecting those that would be used later. Accordingly, commercially available devices were used as test vehicles for their ready availability and low cost.

10.2 DESCRIPTION OF THE TEST SAMPLES

The range of device types and the tests that were carried out on them are shown in table 10.1 (this table excludes those bipolar transistors for which only Gummel plot and dc point measurements were made as these are listed in their corresponding sections below).

	Reference	Reverse storage time	DLTS	Gummel plot	DC
1N4148	DS1317	Y			Y
1N5624	DS1339				Y
BAT85	DS1332				Y
OA202	DS1334				Y
TIP31A			Y		
TIP41C	DS1465 DS1466	Y	Y	Y	Y
TIP42C	DS1467	Y		Y	Y
ZTX450	DS1463	Y	Y	Y	Y
ZTX550	DS1464			Y	Y

Table 10.1: choice of device types for the phase 1 experiments.

10.3 IRRADIATION PROCEDURE

Many separate irradiation runs were required in order to generate the volume of test data included in this section. These were carried out over a period of some five years, using the spent fuel pond and two cobalt cells. The testing procedures described in chapter 9 were used for these samples. All the diodes and bipolar transistors were irradiated with their leads shorted together by wrapping tightly in metal foil, i.e. no bias voltage was applied. The control devices were kept either in a similar condition or mounted in a piece of conductive foam during the time that the other devices were being irradiated. All the devices were kept either wrapped in foil or mounted in conductive foam during the periods between the end of the measurements and the start of the next stage of irradiation. In most cases, these latter periods were between minutes and a few hours. In some cases, however, the period reached a few days, principally to bridge weekends or public holidays.

10.4 REVERSE STORAGE TIME MEASUREMENTS

The recombination lifetime in the base is a key parameter of the characteristics of a p-n junction. It determines the voltage drop in forward conduction and the recovery time for a device switched abruptly from forward to reverse conduction. Precise control of the carrier lifetime during reverse transients is especially important for high power semiconductors, such as GTO thyristors and IGBTs. While less important for the efficient operation of small-signal transistors, a knowledge of the magnitude and nature of the change in recombination lifetime brought about by exposure to radiation should enable the development of an understanding of how radiation tolerance can be improved.

In an attempt to develop this understanding, measurements of the reverse storage time were carried out using the circuit shown in figure 10.1. The recombination lifetime is a difficult parameter to measure directly and so this indirect method was chosen. The input signal was a square wave of magnitude approximately 2 V. The repeat frequency was varied to suit the reverse transient observed for a given device type.

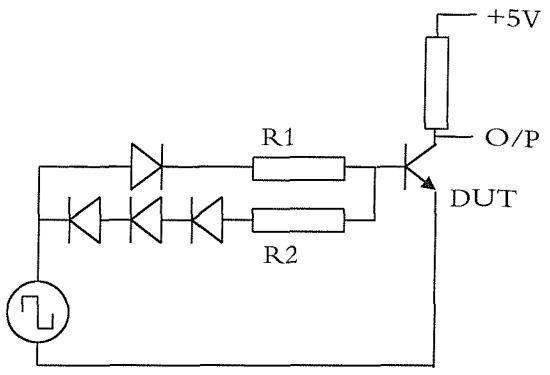

Figure 10.1: test circuit for the reverse storage time measurements.

Measurements were made with ZTX450, TIP41C and TIP42C transistors. The results were mixed. The first results from the ZTX450 devices were well behaved and approximately in line with those expected. One unirradiated device and one device irradiated to a total dose of 10 kGy were examined and gave the results shown in figure 10.2.

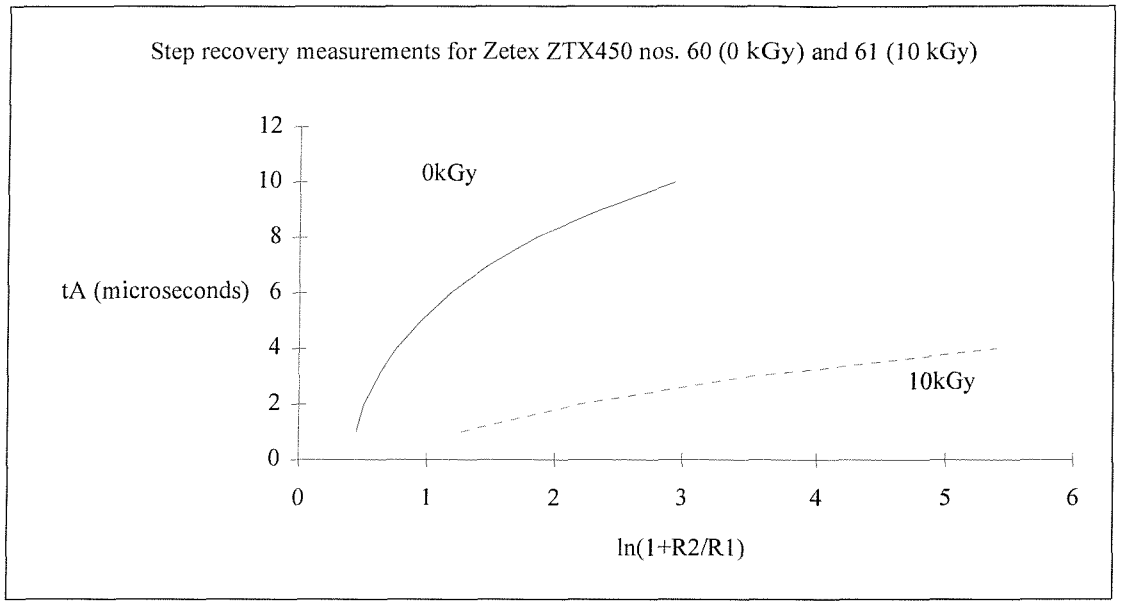

Figure 10.2: step recovery measurements for two ZTX450 devices, one unirradiated and one irradiated to a total dose of 10 kGy.

The reverse storage time can be seen to have decreased by a factor of between 3 and 5 between the two devices. However, pre-irradiation measurements were not available for the irradiated device. Although the two devices had the same date code, they did not necessarily exhibit the same reverse storage time characteristics prior to irradiation. Thus, how much of the difference in lifetime between the two devices was due to irradiation and how much to pre-existing variations in characteristics could not be determined. It can also be seen that the pre-irradiation curve is not the straight line

predicted by the theory. This could be due to errors in measuring the small values of either storage time or *ln(1+R2/R1)* or to one of the assumptions made in the analysis in chapter 6 not being entirely correct for these devices. For example, the transistor may not have been fully saturating or reverse current flowing during the storage time may not have been constant.

Using equations 6.45 to 6.47, we can determine the effective time constant for the decay of charge from the slope of the curves in figure 10.2. This is straightforward for the post-irradiation case as the curve is nearly a straight line. The values obtained are shown in table 10.2.

	0 kGy	10 kGy
Slope	3.4	0.71
Intercept	1.0	0.30

Table 10.2: measured values of slope and intercept for the curves in figure 10.2.

Making the assumption that the forward and reverse values of β are the same and equal to 108 before irradiation and 50 after irradiation to a total dose of 10 kGy, this gives values for the reverse storage time of:

$$\tau_R = 64nS \qquad \textit{before irradiation}$$

$$\tau_R = 29nS \qquad \textit{after } 10kGy$$

However, the best position for the slope of the curve through the pre-irradiation data is debatable. The above figures assume that all the measurement points are included. If the points at the lower values of storage time are assumed to have a higher degree of uncertainly associated with them because of their small magnitude then the slope reduces somewhat, bringing the pre-irradiation value of the lifetime, τ_R, down slightly. Overall, we can conclude that irradiation has reduced the lifetime by approximately half.

Further measurements, at successive stages of total dose on the same device, were made with the TIP devices. The results of these measurements were less satisfactory, showing only a very small change, if any, in lifetime for total doses up to 10 kGy. Figures 10.3 and 10.4 illustrate this for the TIP41C and TIP42C devices, respectively.

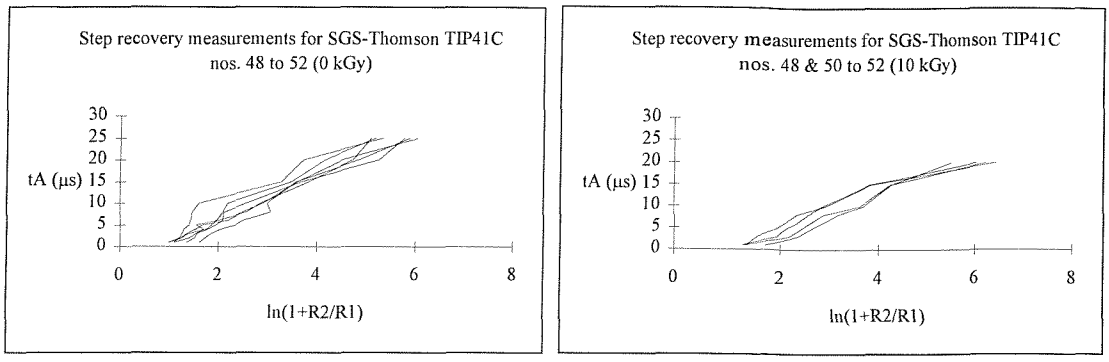

Figure 10.3: step recovery measurements for TIP41C transistors before and after irradiation to a total dose of 10 kGy.

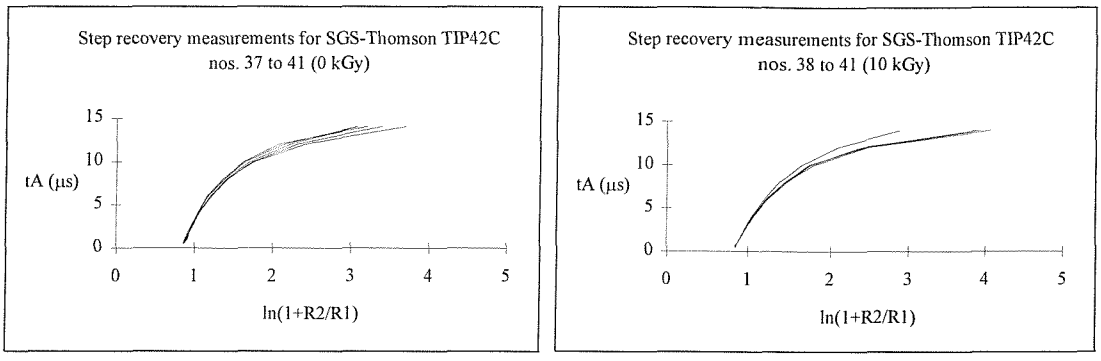

Figure 10.4: step recovery measurements for TIP42C transistors before and after irradiation to a total dose of 10 kGy.

The apparently small change in reverse storage time contrasts with the two-thirds reduction in gain after a total dose of 10 kGy measured on the same devices at the same stages of irradiation (DS1466 and DS1467), reinforcing the impression of a problem with the measurement technique.

No further measurements using this technique were made during the first phase of this work.

10.5 DLTS

Deep level transient spectroscopy has become a routine tool for the identification and measurement of electron and hole traps in semiconductor devices. The technique was originally developed in the mid-1970's (Lang, 1974) and various different versions have subsequently been proposed (Blood, 1992). However, the basic principle remains the same throughout.

DLTS is normally applied to a Schottky diode but may be used with care on any p-n junction. The principle behind the technique is that a capacitance transient is

produced when the junction is switched from reverse bias to zero bias. The transient results from the thermal emission of carriers from traps in the more highly doped region of the junction. The time constant of the transient is peculiar to the type of trap and DLTS utilises this feature to identify characteristic temperatures and number densities for each trap. From these data, an Arrhenius plot can be drawn to identify the energy level of each trap.

Lang showed that DLTS offers some advantages over more traditional techniques, such as thermally stimulated currents (TSC), including independence of the direction and rate of temperature scan and a much improved signal-to-noise ratio due to the shorter time constants which may be applied.

Some DLTS measurements have been made on irradiated devices for this work but poor reliability of the equipment meant that few useful results were obtained. Several repairs by the manufacturer were not able to correct the problems. Those results that were obtained showed that relatively low doses of radiation caused noticeable peaks in the DLTS trace, implying that well-defined traps do exist. For example, figure 10.5 shows a plot for a TIP41C medium power, npn bipolar transistor after irradiation to a total integrated dose of 10 kGy. Comparison with data published by Moll (2000) indicates that both the peaks at around 130K and at 230K are due to a double vacancy defect (leading to both acceptor and donor levels, with the two acceptor levels being seen here). There is evidence of a third peak at around 200K, which could actually be a diminution of the higher double vacancy peak as a result of the presence of a more complex defect, a combination of an interstitial cluster of individual defects combined with an interstitial oxygen atom. This forms a hole trap, i.e. a donor level, which would tend to compensate for the DLTS signal of the double vacancy electron trap. However, insufficient results were obtained to enable any meaningful analysis to be carried out. Due to the equipment problems, this measurement technique was not pursued further.

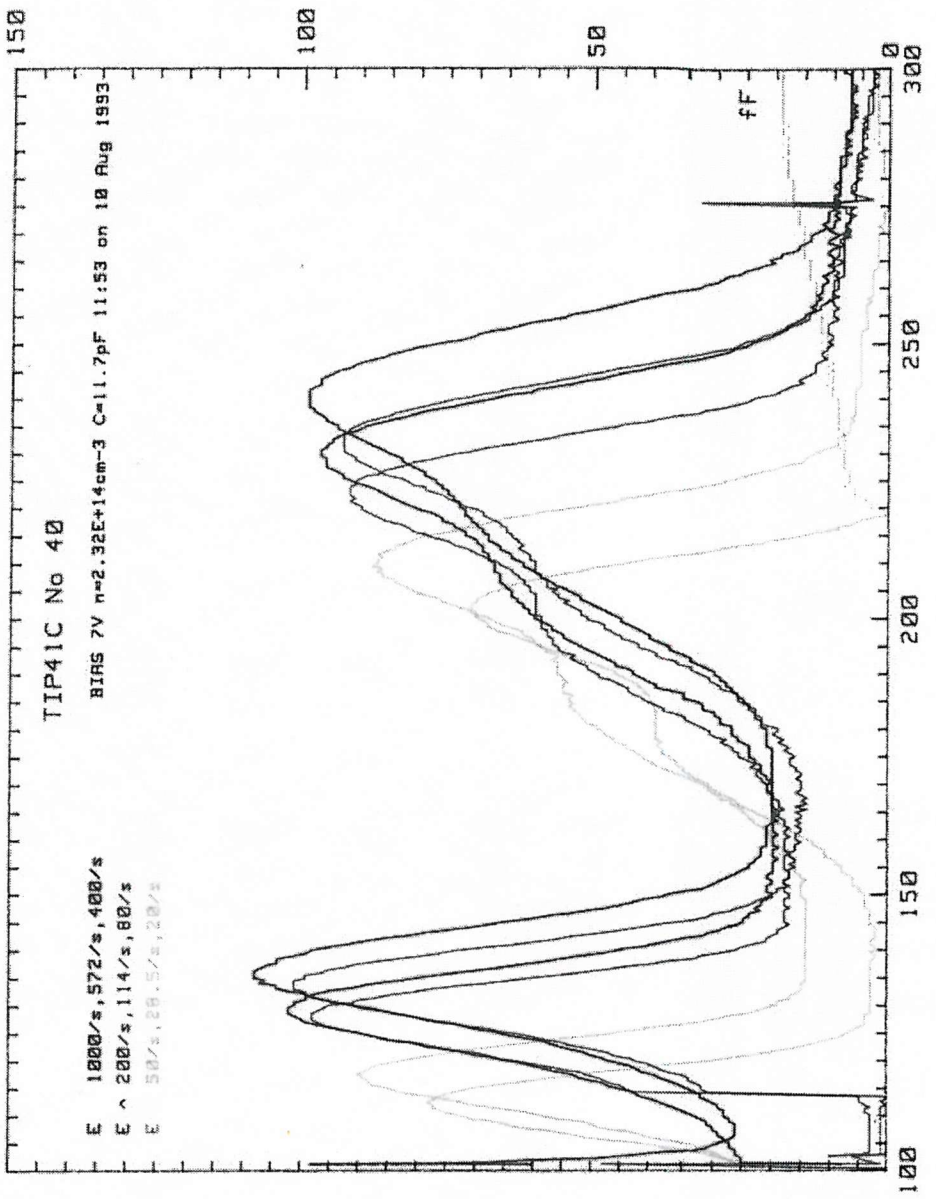

Figure 10.5. DLTS plot for a TIP41C transistor irradiated to a total dose of 10 kGy.

10.6 GUMMEL PLOT AND DC POINT MEASUREMENTS

Test routines and software already existed for making dc point measurements of some device parameters, including gain, saturation voltage and collector-emitter leakage current, using the HP4142B test equipment described in section 9.3. These routines were used to examine the effects of radiation on a range of two and three-terminal devices in order to gain a first level understanding of the effects of high total doses on a range of operating parameters. The types of device studied included signal, power and zener diodes and small-signal and medium power bipolar transistors.

10.6.1 Diodes

The dc characteristics of most types of silicon diode change little with total dose until very high values have been accumulated. Over the range of total dose of interest to the nuclear industry (up to 1 MGy), forward and reverse voltage drops typically show changes of less than 5%. Figure 10.6 illustrates this for a set of eighteen 1N4148 signal diodes manufactured by Philips.

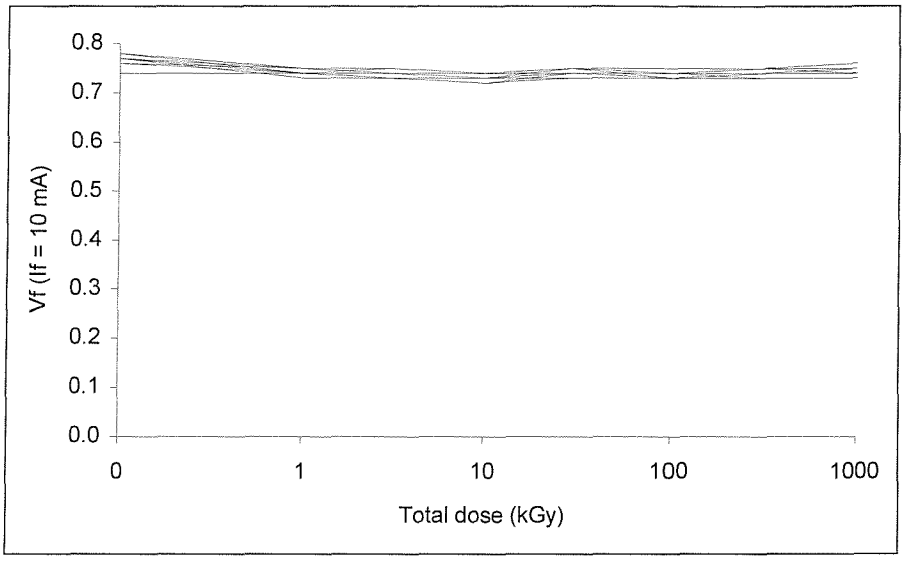

Figure 10.6: change in forward voltage drop with total dose for 1N4148 diodes (DS1317).

Even for total doses of a few hundreds of kilogray, the reverse breakdown voltage usually remains constant, although can start to rise noticeably in rare instances. This increase is usually of no concern for circuits using the diodes but indicates the growth of displacement damage in the device as a result of irradiation, even with electromagnetic radiation in the form of gamma rays. Figure 10.7 shows the response

of reverse breakdown voltage to total dose in the case of eighteen BAT85 diodes, also manufactured by Philips.

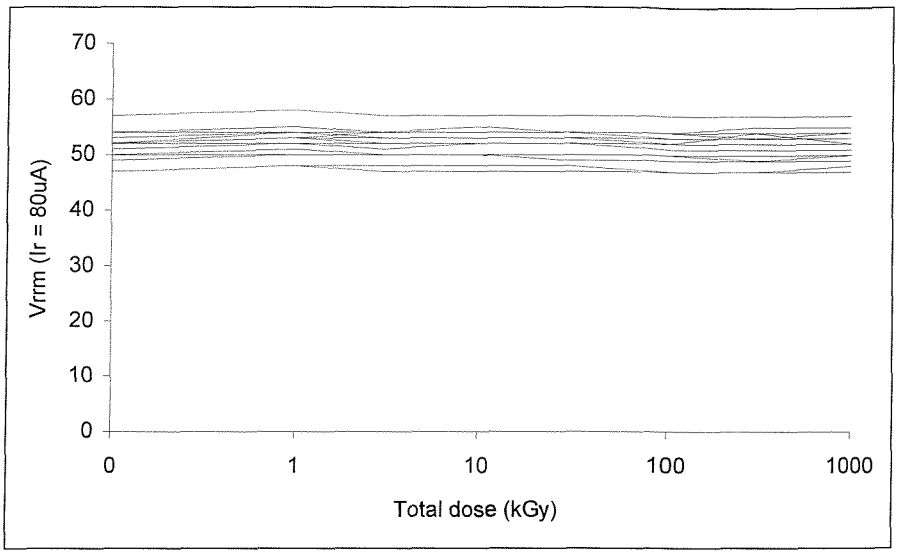

Figure 10.7: change in reverse breakdown voltage with total dose for BAT85 diodes (DS1332).

The one parameter that can show large changes is leakage current. Indeed, some types of diode are manufactured especially to enhance this effect for use as radiation detectors. Even so, for most commercial devices, the leakage current does not change significantly with total dose up to 1 MGy. The change in leakage current measured for OA202 small-signal diodes from Philips and for 1N5624 power diodes from Harris is shown in figures 10.8 and 10.9.

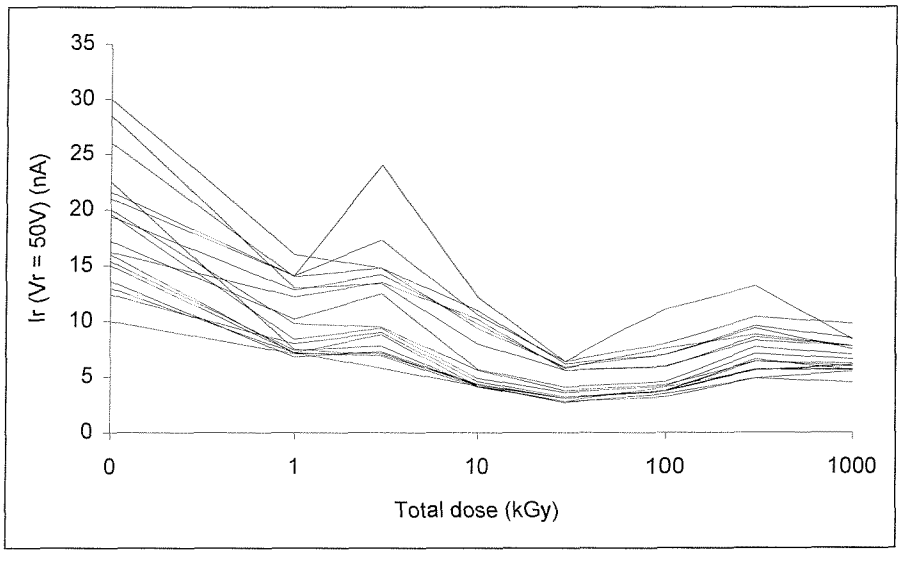

Figure 10.8: change in reverse leakage current with total dose for OA202 small-signal diodes (DS1334).

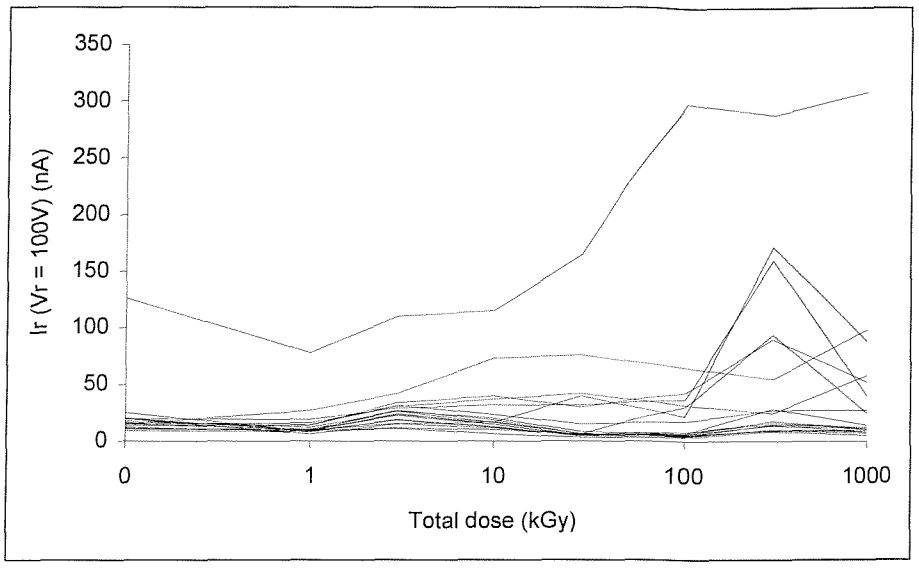

Figure 10.9: change in reverse leakage current with total dose for 1N5624 power diodes (DS1339)

In both cases, sets of eighteen diodes were tested. A change is observable for the small-signal diodes (a slight reduction, in fact) but it is not significant enough to affect the operation of a circuit using the diode. The figure for the power diodes shows a good deal more variation from one device to another and a broadly increasing trend. Increases of between two and six times can be seen, although some examples show no increase at all. Again, most circuits using these devices would not be affected significantly by changes of this order.

10.6.2 Bipolar transistors

The test software used for the initial measurements was capable of measuring gain, saturation voltage, collector-emitter leakage current and collector-emitter breakdown voltage. Over a period of time, the scope of these routines was expanded to include a wider range of parameters, encompassing leakage current and breakdown voltage between four combinations of terminal and Gummel plot measurements. Test fixtures were available for all types of small-signal transistors in conventional packages and for many types of medium power devices. The basic test routine described in chapter 9 was used to assess the effects of radiation on a large number of types of commercially-available device. The device type numbers and manufacturers are listed in table 10.3.

Type number	Manufacturer	Ref.	Type number	Manufacturer	Ref.
2N2907A	Motorola	DS1487	BCW72	Philips	DS1507
		DS1491	BCY70	Semelab	DS1379
2N3704	Motorola	DS1402	BCY70	SGS-Thomson	DS1400
2N3906	Motorola	DS1401	BCY72	Motorola	DS1488
BC108	Philips	DS1399			DS1492
BC108	SGS-Thomson	DS1493	BF550	Philips	DS1476
		DS1522	BF822	Philips	DS1477
BC109	Mullard	DS1376	BFY50	Semelab	DS1380
BC109C	Philips	DS1372	FMMTA42	Zetex	DS1479
BC109C	Semelab	DS1377			DS1501
		DS1485	FMMTA92	Zetex	DS1478
		DS1489			DS1503
BC179	Motorola	DS1375	FMMT491	Zetex	DS1506
BC547B	Philips	DS1496	FMMT591	Zetex	DS1508
BC549	N/K	DS1373	MPSA42	Zetex	DS1498
BC549	Mullard	DS1378	MPSA92	Zetex	DS1499
BC549	ITT	DS1486	TIP32A	SGS-Thomson	DS1434
		DS1490			- 1436
BC549C	Philips	DS1494	TIP41C	SGS-Thomson	DS1465
BC557B	Philips	DS1497			- 1466
BC559	Motorola	DS1374	TIP42C	SGS-Thomson	DS1431
BC559	Mullard	DS1381			- 1433
BC559C	N/K	DS1495			DS1437
BC849C	Philips	DS1475			- 1439
BC849C	Philips	DS1500			DS1467
BC859C	Philips	DS1474	ZTX450	Zetex	DS1463
		DS1502	ZTX550	Zetex	DS1464
BCW70	Philips	DS1509			

Table 10.3: types of bipolar transistor for which DC point measurements were made.

Examples of the changes in parameter values observed as a result of these measurements are shown in the following figures and accord well with the generally accepted result of irradiation detailed in the literature and described in chapter 7. The most dramatic changes were seen in gain. Every type of bipolar transistor tested exhibited a fall of many tens of per cent in gain with increasing total dose. This effect is illustrated in figure 10.10 for a set of eighteen BC109 transistors manufactured by Mullard that were exposed to gamma radiation from a cobalt-60 source. The precise shape of the curve varies from one type of device to another, as can be seen from a comparison of figure 10.10 with figure 10.11, the latter showing the response of a set of fifteen FMMTA92 transistors produced by Zetex to the same experiment as those in figure 10.10.

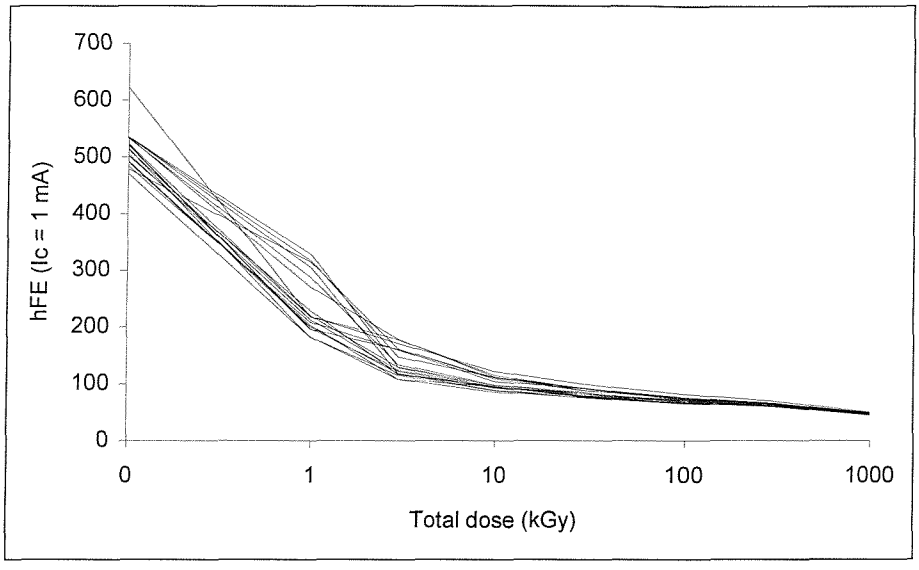

Figure 10.10: change in gain with total dose for BC109 transistors (DS1376).

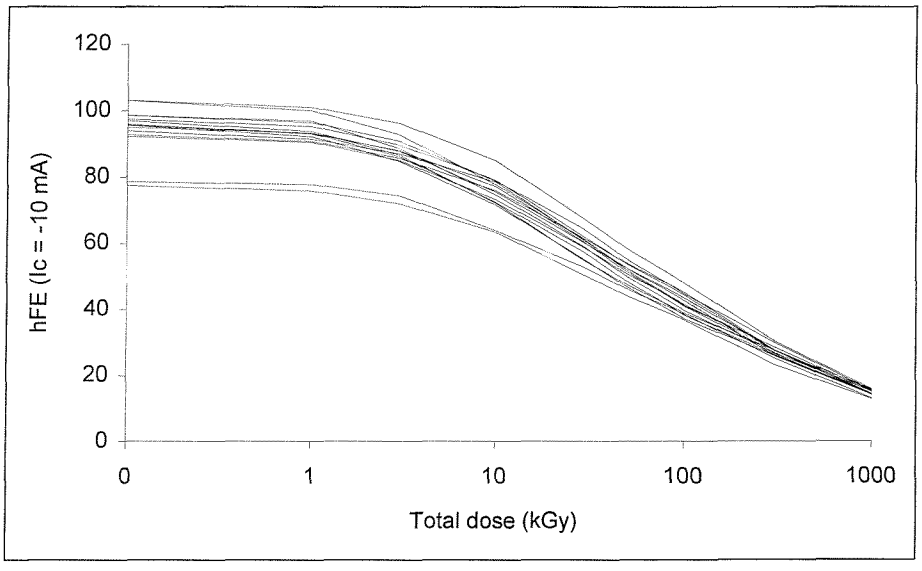

Figure 10.11: change in gain with total dose for FMMTA92 transistors (DS1478).

The consistency between the devices in each of the groups tested is indicative of their common origin. In fact, the results from this stage of the work bore out the findings from the literature that quite different response curves can be exhibited by devices of nominally the same type when they are manufactured in a different manner, be it by a different fabrication plant or even from a different source of silicon. For example, figures 10.12 and 10.13 show the gain degradation curve for two different batches of BC549 transistors manufactured by Mullard and ITT, respectively.

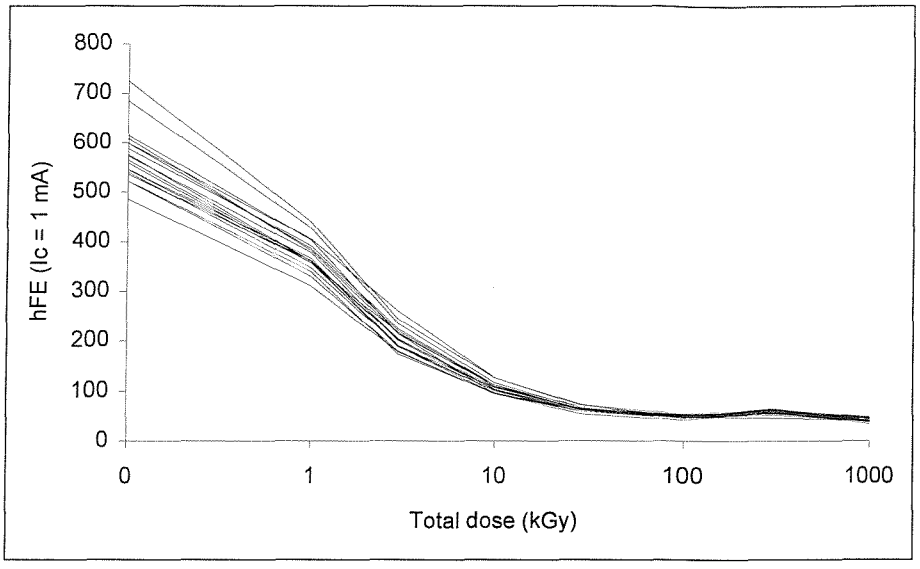

Figure 10.12: change in gain with total dose for BC549 transistors by Mullard (DS1378).

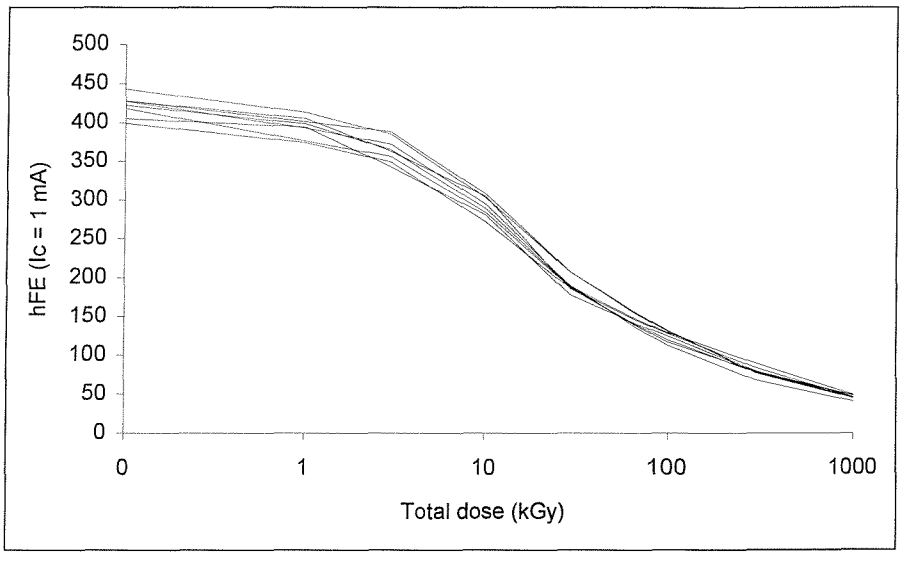

Figure 10.13: change in gain with total dose for BC549 transistors by ITT (DS1490).

Saturation voltage also showed clear changes in many cases, generally rising monotonically and showing increases of up to 300%, as illustrated in figure 10.14 for BC859C transistors, manufactured by Philips.

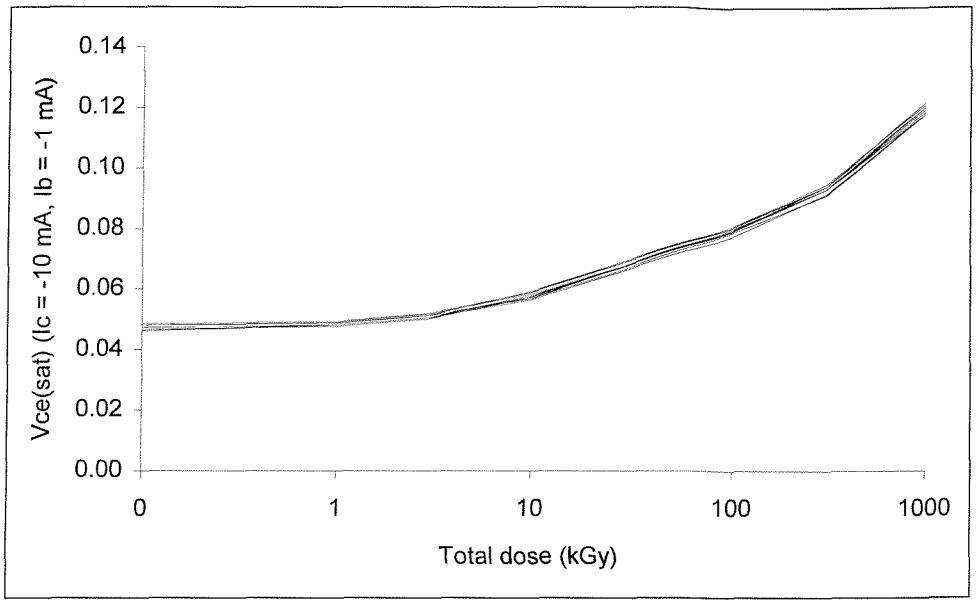

Figure 10.14: change in saturation voltage with total dose for ten BC859C transistors (DS1502).

Breakdown voltage responded to radiation in much the same manner for bipolar transistors as for the diodes discussed in the previous section. Small increases were seen for many types at the upper end of the total dose range, although a small number of cases was found where the increase was much greater. Figure 10.15 shows this for BCW72 transistors, manufactured by Philips (the upper limit of measurement in this case was 100V).

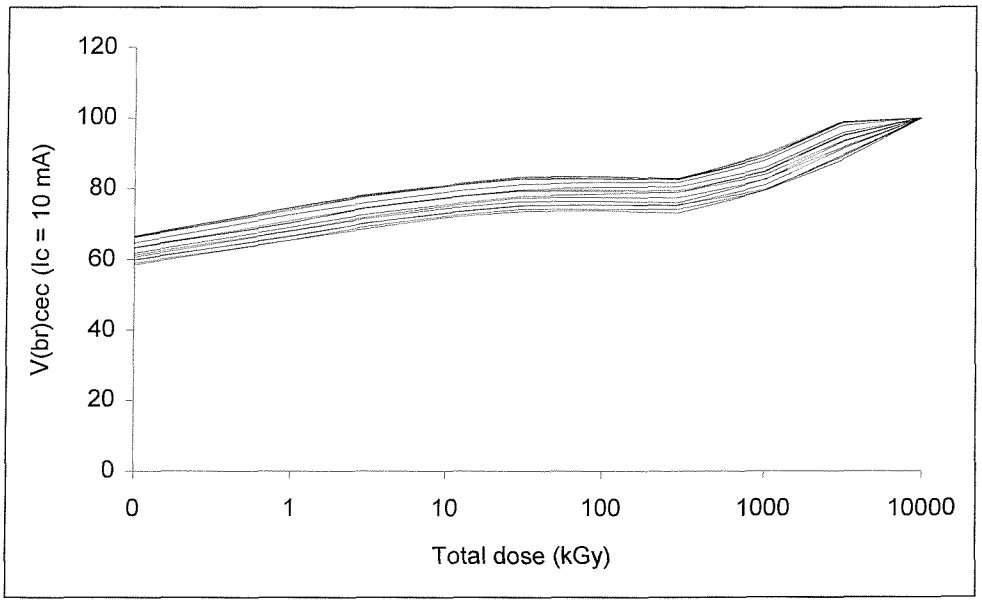

Figure 10.15: change in collector-emitter breakdown voltage with total dose for ten BCW72 transistors (DS1507).

Collector-emitter leakage currents almost always increase with total dose and this was borne out by the measurements made for this work. The rate of increase varies with the type of device and may be nearly linear or closer to an exponential curve. Figure 10.16 illustrates the change in collector-emitter leakage current for BC849C transistors, manufactured by Philips. This device is a modern, passivated device of commercial design, encapsulated in a SOT23 surface mount package and benefiting from all the experience of the industry in producing stable, reliable devices.

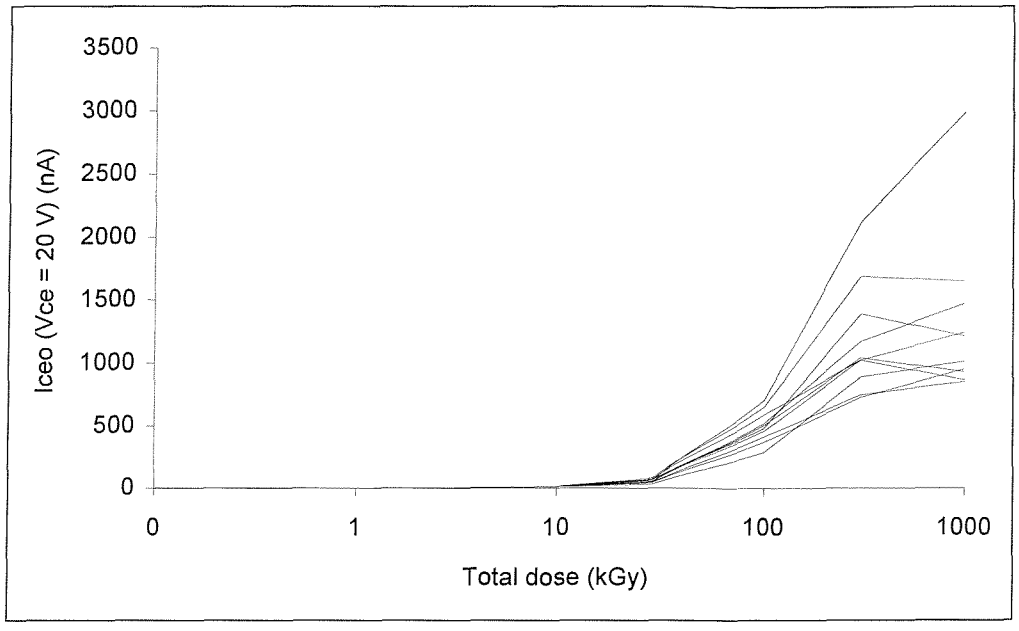

Figure 10.16: change in collector-emitter leakage current with total dose for BC849C transistors (DS1500).

Gummel plot measurements were added to the test software during this phase of the work. The first part of this involved establishing the best test conditions for the types of device of interest and obtaining a useful quantity of data within an acceptably short period of time. The HP4142B instrument was extremely effective in achieving this, with all the data required for the plots shown in this section being recorded, using the final version of the software, in just a few seconds. Manual methods would have taken many minutes for each device, during which time annealing of radiation damage would have been clear, leading to distortion of the results.

The basic shape of the Gummel plots obtained for the COTS devices matched well with the plot for a theoretically 'ideal' transistor. This was encouraging and confirmed that the measuring system was working well and as expected. Repeat measurements also confirmed that the measurements themselves were not leading to changes in the

shape of the curve for successive sets of readings. This meant that no significant thermal annealing was being introduced to the irradiated devices by virtue of making the measurements. Keeping the maximum measurement time short and minimising the maximum measurement current were essential factors in this.

The shape of the Gummel plot was expected to change with irradiation, particularly in the case of the base current curve. This can be seen in figure 10.17, showing the Gummel plot for sets of ZTX550 transistors, manufactured by Zetex, before irradiation and after a total integrated dose of 1 MGy.

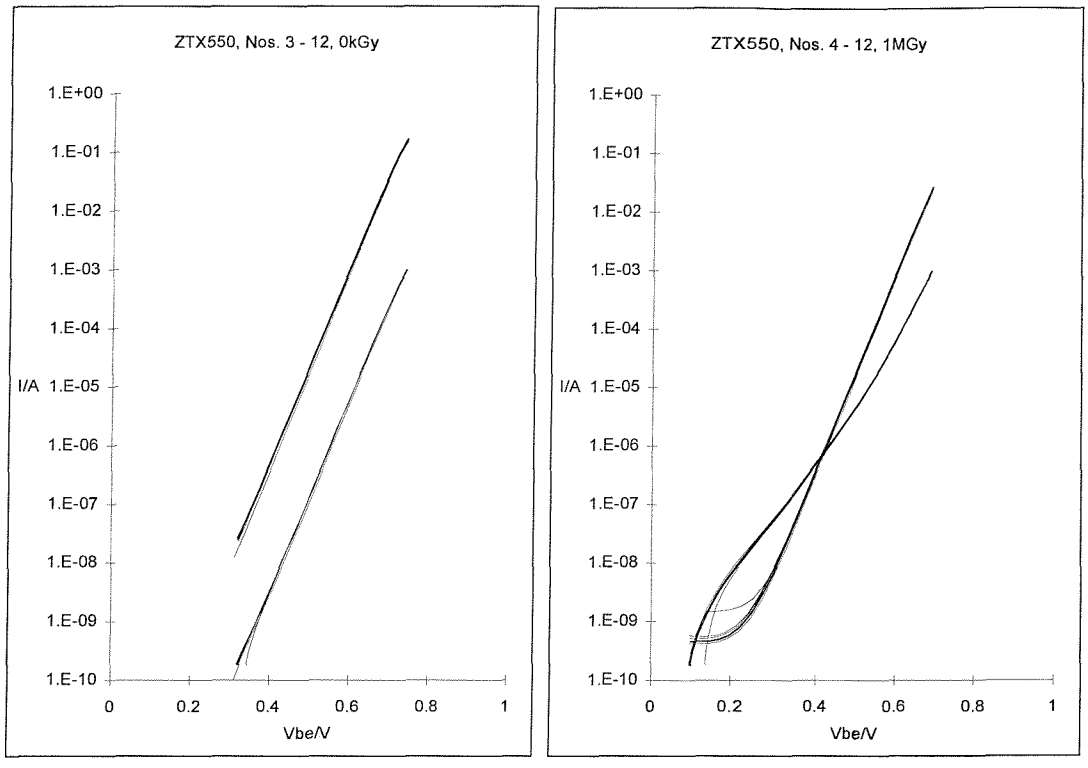

Figure 10.17: Gummel plots before and after irradiation to a total dose of 1 MGy.

Three regions can be observed in the base current curve. At high voltages, the curve is the same as before irradiation, indicating no change in the terminal resistances. The curve can be seen to rise significantly at medium base-emitter voltages, indicative of recombination in the emitter-base depletion region. This recombination is due to deep level traps being activated or produced in the base-emitter region, as described in chapter 6. The energy levels of the traps are typically near the centre of the band-gap and act in a similar manner to donor and acceptor levels. This aids the transfer of electrons and holes between the conduction and valence bands. The slope of the base current curve at medium voltages decreases with increasing total dose and this would

be expected to happen with increasing trap density. Thus, it can be seen that the number of recombination centres is increasing with total dose. At low voltages, the curve drops off rapidly as the collector-emitter leakage current regime is entered. The curves for the nine irradiated transistors remain well aligned even after irradiation, showing that these devices very probably originated from the same production batch and, possibly, even the same wafer. The changes in gain measured during the point value tests are shown clearly in the Gummel plots, with the greatest loss being at low current.

The changes in the Gummel plot evolve gradually with total dose, with most device types showing a similar pattern of development. Figures 10.18 to 10.22 show a sequence of plots at successive total integrated doses for TIP41C transistors, manufactured by SGS-Thomson. These illustrate the continued development of radiation-induced changes as the total dose increases, mirroring the degradation observed, for example, in the gain plots.

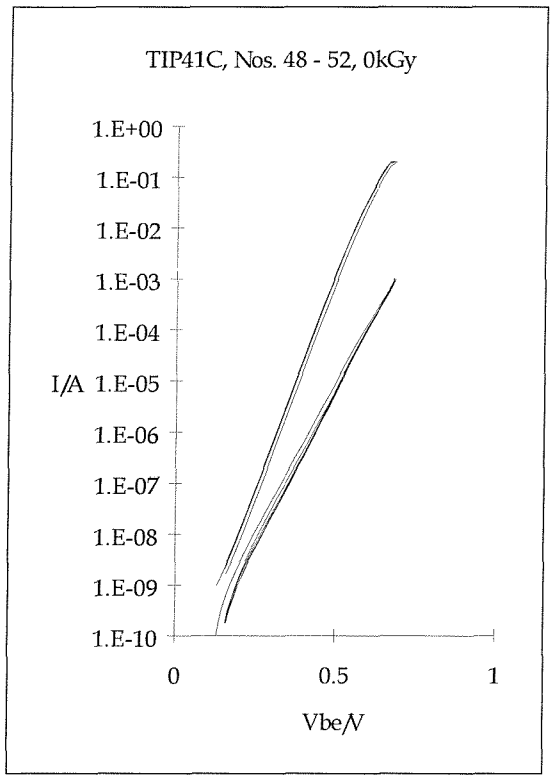

Figure 10.18: Gummel plots for TIP41C transistors before irradiation.

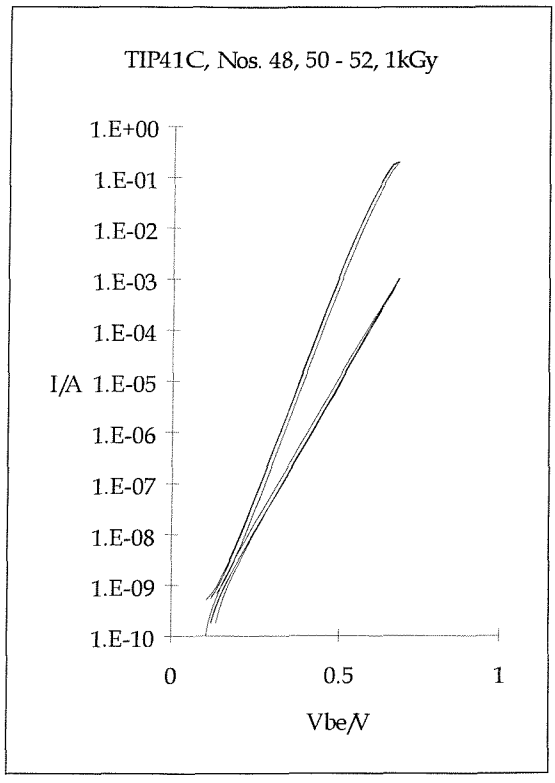

Figure 10.19: Gummel plots for TIP41C transistors after 1 kGy.

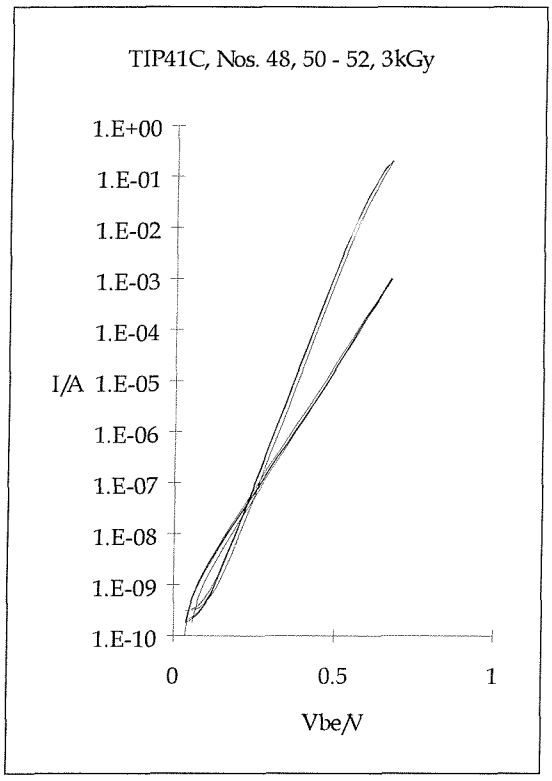

Figure 10.20: Gummel plots for TIP41C transistors after 3 kGy.

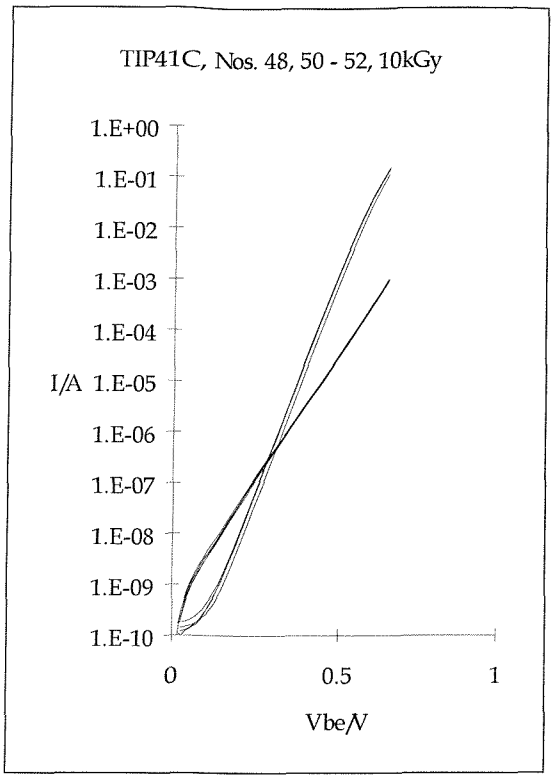

Figure 10.21: Gummel plots for TIP41C transistors after 10 kGy.

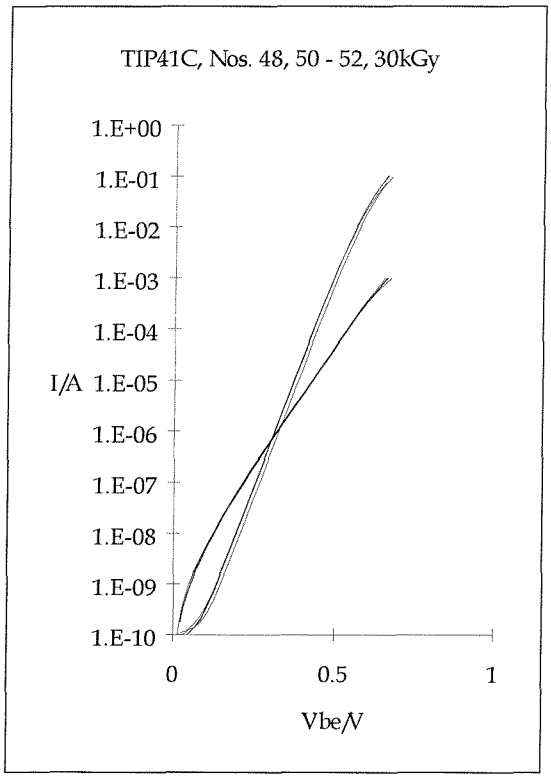

Figure 10.22: Gummel plots for TIP41C transistors after 30 kGy.

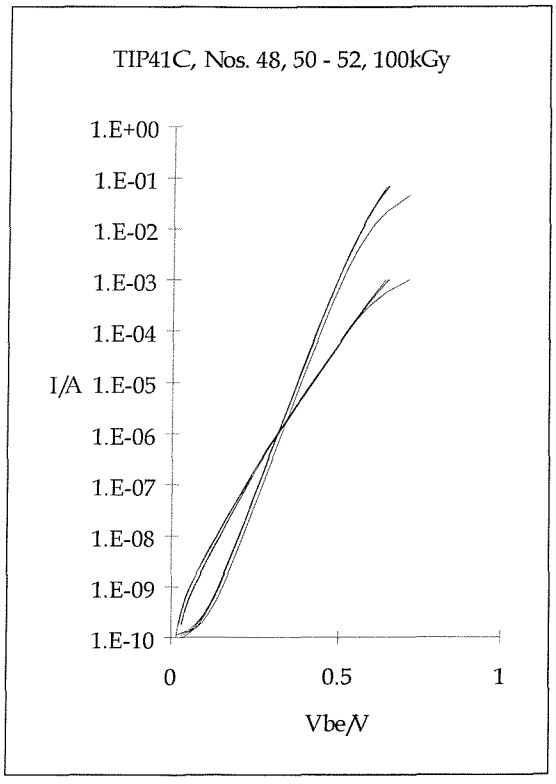

Figure 10.23: Gummel plots for TIP41C transistors after 100 kGy.

11 Review of phase 1 results

11.1 SUITABILITY OF MEASUREMENT TECHNIQUES

Three measurement techniques were used in the first phase of the work: lifetime, DLTS and dc readings. Many of the lifetime measurements proved unsatisfactory in that the expected changes in minority carrier lifetime were observed in only some of the test samples. It was not clear why these changes were not seen for the other types of device. Furthermore, the measurement of storage times of less than 1 microsecond proved to be beyond the capability of the available instrumentation. For those devices that did show a measurable change in lifetime, it fell below this measurement limit after a relatively modest total dose. Whilst storage times as long at 30 microseconds appeared to have been measured in some cases, these did not change with irradiation, indicating that either the wrong reading was being taken or that the test rig was not set up correctly for those types of transistor. Furthermore, the calculated values of lifetime were considerably shorter than expected, even before irradiation, being a few tens of nanoamps rather than microamps. The reasons for this were not clear.

Despite these set-backs, it was decided that lifetime measurements remained an important contributor to understanding the degradation of electrical parameters with irradiation and so they should be continued. Other measurement techniques were investigated but none was identified that could be used for packaged devices. A number of other measurements could be carried out but only on bare devices or specially fabricated test samples. Neither of these routes was open for this work and so the same technique was retained, despite its limitations.

The DLTS measurements were also unsatisfactory but the cause was clear in this instance. Reliability problems with the instrumentation were certainly the reason for the poor results. The anticipated time for a repair to be effected and the cost thereof meant that this technique was not pursued. The implications of this were that the nature of the defects apparently introduced by irradiation could not be explored so easily. The activation energies yielded by DLTS can be used to identify the physical manifestation of the defects present in a sample that can then be related to the likely interaction mechanisms of radiation with the material. The abandonment of this

technique meant that such interpretation would have to be based upon data gleaned from other measurements, for example the Gummel plot data.

The main success of the first phase of this work was the dc measurements. The software for both the point readings and the Gummel plots worked extremely effectively, provided the proper experimental procedures were followed, and yielded much useful data. Refinements to the voltages and currents at which various parameters were measured were made during the course of the tests and the final version of the test software allowed some of these to be varied at the beginning of a test run, according to the manufacturer's individual datasheet values. The readings obtained from both categories of device included in the tests (diodes and bipolar transistors) were clear and good confidence was gained from the high degree of correspondence between the pre-irradiation measurements and the quoted datasheet values. Sensitivity down to millivolt and picoamp levels was achieved for many parameters, allowing very precise readings to be taken. This enabled the precise comparison of results obtained, both before and after irradiation and at different stages of total dose. The test software developed for these measurements was used throughout the remainder of the experimental phase of this work.

11.2 REVIEW OF RESULTS

The irradiation procedures used during this first phase worked well, with results for the control devices remaining constant within the limits of error. No devices appeared to have sustained damage due to inappropriate handling, electrostatic discharge or from the measurement process itself. The relevance of irradiation with no bias applied to the devices was questioned and so plans for the second phase of the work were extended to include provision for irradiating some devices with bias applied. This situation was thought likely to be more relevant to applications of working equipment in the nuclear power industry, although the most appropriate bias conditions to use were not immediately obvious.

The majority of the lifetime measurements proved unsatisfactory. This was partly due to the limitations of the test equipment, with lifetimes of one microsecond or less not easily being measured. There were also unresolved difficulties with some types of device where the measured lifetime appeared not to change with irradiation, despite other parameters exhibiting significant shifts in value. Extending the range of the

measurement equipment to below one microsecond would have entailed expenditure outside the available budget and so this was accepted as a limiting factor on the usability of the technique. Despite these problems, encouraging results were obtained on some devices and showed that minority carrier lifetime did appear to be reduced significantly by irradiation, perhaps by 50% after a total dose of 10 kGy in the case of ZTX450 transistors.

It was regrettable that the DLTS equipment was not operational as this could have provided useful data at the sub-device level. One run was carried out successfully and indicated that traps were indeed present in an irradiated device and that these traps had clearly defined characteristic temperatures. However, it did not prove possible to continue the measurements and so this technique was abandoned.

The routine and procedures for Gummel plot and dc point measurements worked extremely well and were used to gather data on many types of device. Much of these data were used to gain a broad understanding of how radiation affects the electronic properties of semiconductor components, including both diodes and bipolar transistors. Other types of device, such as MOSFETs, light-emitting diodes, photodiodes, operational amplifiers, comparators and a selection of other linear integrated circuits, were also studied but have not been included in this work. This exercise served to place the results for bipolar transistors into context, both in terms of the magnitude of the effects observed and in terms of their location relative to other components in a practical circuit for a real piece of equipment.

The range of measurements made with the ATE was increased during the testing and the final range covered the parameters listed in table 11.1. This version of the software was also used for the second phase of the work.

Broadly speaking, the data obtained agreed well with those in the literature. Diodes showed only a slight response to total dose, probably corresponding to changes in resistivity. A wide range of bipolar transistors was examined. Several parameters showed large shifts, especially gain and saturation voltage. Breakdown voltages moved very little in most cases, while leakage currents showed a range of response, depending on the device type.

The Gummel plots showed well the changes in the base current curves with total dose. At low base-emitter voltages, the increase in base current was significant, leading to the changes in leakage current and gain observed in the point measurements.

Parameter	Symbol
Emitter-base leakage current	I_{ebo}
Collector-base leakage current	I_{cbo}
Collector-emitter leakage current	I_{ceo}
Base-emitter leakage current	I_{beo}
Saturation voltage	$V_{ce(sat)}$
Gain	h_{FE}
Emitter-base breakdown voltage	BV_{ebo}
Collector-base breakdown voltage	BV_{cbo}
Collector-emitter breakdown voltage	BV_{ceo}
Base-emitter breakdown voltage	BV_{beo}

Table 11.1: Parameters measured with the ATE and their abbreviations

In summary, the first phase of the work enabled the basic experimental procedures and ATE software to be developed, trialled and optimised so that data were obtained reliably, repeatably, without adversely affecting the test samples and in acceptably short test times. It also provided results that allowed an appreciation of the range and magnitude of radiation effects on electronic components to be gained, enabling the second phase to concentrate on the parameters of interest for addressing the second and third aims of the work, i.e. relating the observed effects to physical properties of the device and developing a methodology to predict the likely effects of radiation on a given bipolar transistor.

11.3 COMMENTS ON THE DEVICE TYPES

All the devices used for the first phase of the work were COTS types. The benefits of this approach included their ready availability, low cost and high reliability/quality. The principal disadvantage was a lack of knowledge of the device structure and geometry, together with the processing history. Some information on a few of the types of transistor was obtained from manufacturers but it was not sufficient to enable an examination of the sensitivity of the radiation effects to device geometry to be carried out. Furthermore, the lack of processing information became particularly relevant as the work progressed, when several papers were published concerning the effect of thermal treatments, such as burn-in, on the degree of radiation damage (e.g. Clark, 1995, and Barnes, 1997), as mentioned in chapter 7. Whilst a definitive

relationship between thermal treatment and radiation response remains elusive, an assurance of the consistency in application of such processes is important when making comparative measurements on batches of apparently similar devices irradiated under varying conditions. One reason for using a different set of test samples in the second phase of this work was to obtain such an assurance.

12 Phase 2 experiments

12.1 OVERVIEW

The purpose of the phase 2 experiments was to extend the range of data to cover the principal parameters of interest, to probe further the likely physical manifestations of the effects of ionising radiation on bipolar transistors and to enable predictive tools for the radiation effects to be developed.

12.2 DESCRIPTION OF THE TEST SAMPLES

The bulk of the phase 2 experiments were carried out on the batch of ten devices manufactured by Southampton University and described in chapter 9 above (hereafter referred to as the SU devices). Nine of these devices were allocated to be exposed to radiation, with the tenth remaining unexposed in order to act as a control sample for the measurements. Of the eight transistors bonded out in each package, only six functioned reliably on all ten devices and so measurements were confined to these alone. The collector contact was common for all the devices in a given package. All the devices were arranged vertically on the wafer. Table 12.1 lists the principal differentiating features of these devices, as measured by hand from a plot of the die structure.

Transistor type	Device number on die	Base area (μm^2)	Base perimeter (μm)	Emitter area (μm^2)	Emitter perimeter (μm)
1	1	26,800	670	6,800	1,600
2	4	21,200	630	8,000	1,750
3	5	21,200	630	4,100	1,300
4	6	2,400	200	750	110
5	7	5,900	320	1,500	160
6	8	10,900	420	3,000	360

Table 12.1: principal features of the six transistors on each SU device.

Notes to table 12.1:

- transistor types 1 and 2 have an emitter structure consisting of twenty-four large, square pads.
- transistor type 3 has an emitter structure consisting of twenty-four small, square pads.
- transistor type 6 has an emitter structure consisting of a rectangular pad of the given dimensions, surrounded by eleven small, square pads.

An excerpt from the plot of the die layout is appended herewith.

Additional measurements were made on a range of BC108 transistors. The type numbers of these devices are listed in table 12.2. Measurements were made on these devices in order to investigate a) further lifetime measurements; b) capacitance-voltage measurement techniques for application to the SU devices; and c) more detailed measurements for comparison with those obtained from the SU devices.

Type number	Manufacturer	Reference
BC108	Philips	DS1399
BC108	SGS-Thomson	DS1493, DS1522

Table 12.2: COTS devices used during phase 2.

The reasons for using the COTS devices in this phase of the work were the same as for their use in the first phase: availability, low cost and quality. Further batches of SU devices would have taken several months to fabricate and were more expensive than commercial devices costing just a few pence. The COTS devices were all small-signal, npn bipolar transistors, contained in standard TO-8 metal can packages.

12.3 IRRADIATION PROCEDURE

12.3.1 The SU devices

The SU devices were irradiated all together, in one run during December 1998 and January 1999. The timings of the individual stages are shown in table 12.3. The general irradiation procedure described earlier was followed for these devices. Nine of the SU devices were mounted on an irradiation board such that each device in each of six of the packages (2 to 7 inclusive) was under bias. All the devices in the other three packages (8, 9 and 10) had their pins shorted together. The devices were transported

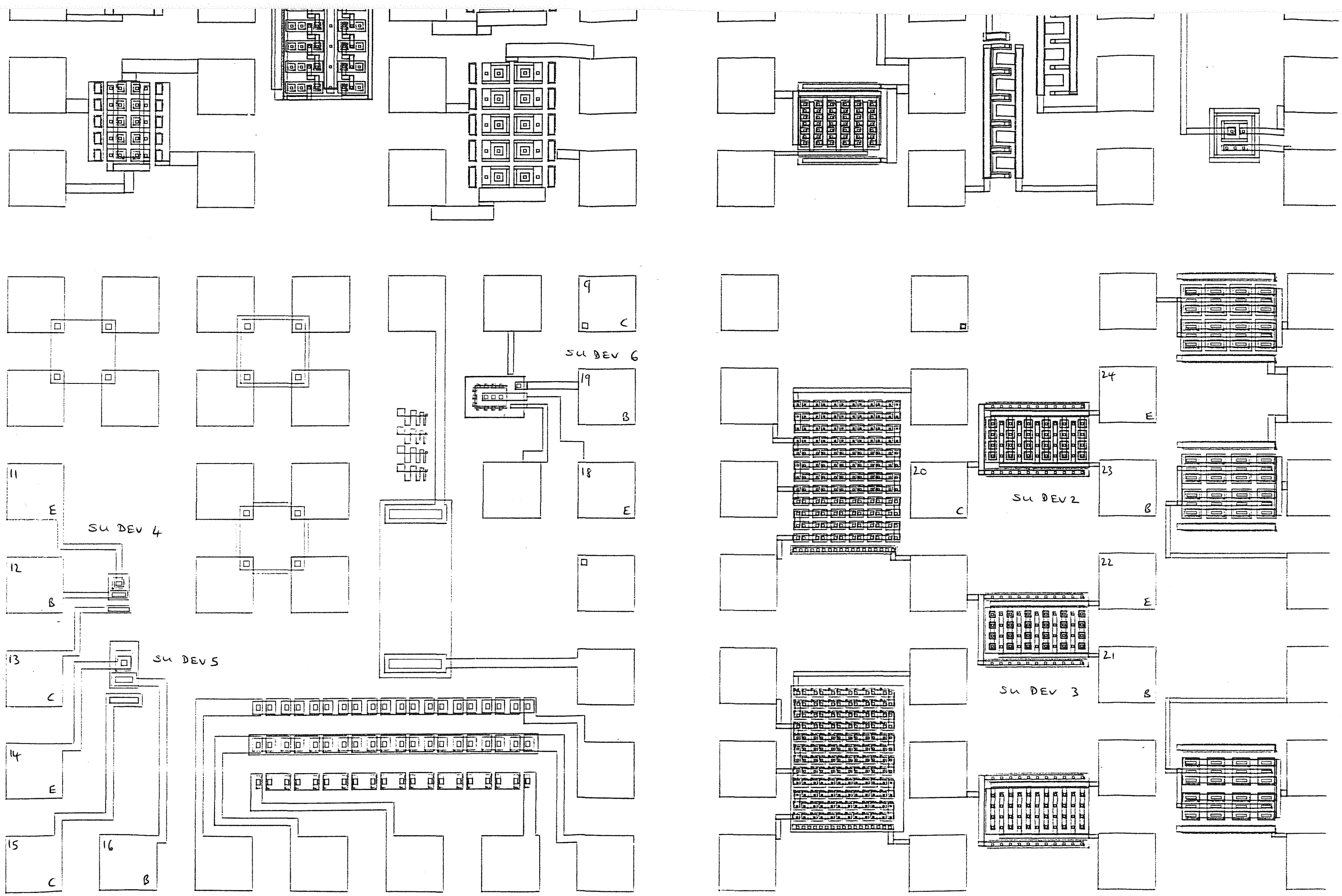

360 B1

BAEWCWM1

between the irradiation cell and the test laboratory on the irradiation board, being removed only when measurements were being made. A bias voltage of +10 V dc was applied once the board was mounted in the irradiation position.

Sample number	Time in	Date in	Time out	Date out	Irradiation time hh:mm:ss	Position	Dose rate (kGy/hr)	Total dose (kGy)
R898	08:31:00	22/12/98	08:42:01	22/12/98	0:11:01	4/ABCD/T1/2	5.29	1.0
R898	12:44:00	22/12/98	13:06:22	22/12/98	0:22:22	4/ABCD/T1/2	5.29	2.0
R898	09:18:00	29/12/98	10:37:17	29/12/98	1:19:17	4/ABCD/T1/2	5.28	7.0
R898	08:18:00	30/12/98	12:05:14	30/12/98	3:47:14	4/ABCD/T1/2	5.27	20
R898	17:54:00	04/01/99	07:57:00	5/1/99	14:03:00	4/ABCD/T1/2	5.26	74
R898	17:11:00	11/01/99	07:54:00	13/1/99	38:43:00	4/ABCD/T1/2	5.25	203
R898	17:53:00	13/01/99	10:37:00	18/1/99	112:44:00	4/ABCD/T1/2	5.24	591
R898	11:02:00	18/01/99	11:06:16	18/1/99	0:04:16	4/ABCD/T1/2	5.24	0.40
R898	11:14:00	18/01/99	11:17:00	18/1/99	0:03:00	4/ABCD/T1/2	5.24	0.29
R898	11:35:00	18/01/99	07:53:02	19/1/99	20:18:02	4/ABCD/T1/2	5.24	106

Table 12.3: Stage timings for the SU device irradiation.

Two bias circuits were used, according to the circuit diagrams shown in figures 12.1 and 12.2. Table 12.4 shows which transistors were biased according to which bias circuit. This gave a theoretical standing current consumption, with no devices mounted on the board, of 74 mA. The measured value was 63 mA, i.e. reasonably close and within the limits of error associated with the resistor values and the measuring instrument. With all nine devices mounted on the board, the current consumption rose to 147 mA prior to irradiation.

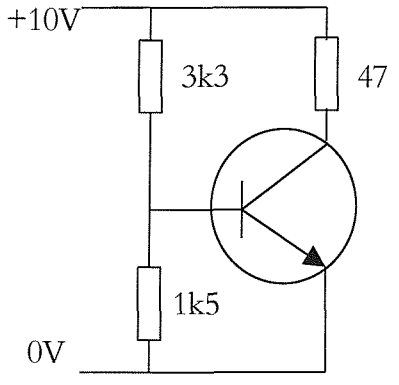

Figure 12.1: Bias arrangement 1 on the irradiation board.

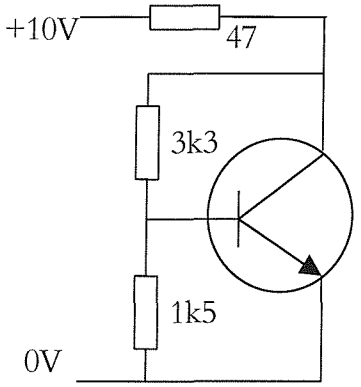

Figure 12.2: Bias arrangement 2 on the irradiation board.

Transistor number	Package number	Bias arrangement
1	2 – 7	2
2	2 – 7	2
3	2, 3, 5, 6, 7	2
3	4	1
4	2, 3, 4	1
4	5, 6, 7	2
5	2, 3, 4	1
5	5, 6, 7	2
6	2, 3, 4	1
6	5, 6, 7	2

Table 12.4: Bias arrangements applied to the SU transistors.

Records of the current consumption of the populated board were made throughout the irradiation stages and are shown in figure 12.3. A small decline in the current consumption at the higher values of total dose can be observed, although this amounts to no more than 8 mA difference from the pre-irradiation value.

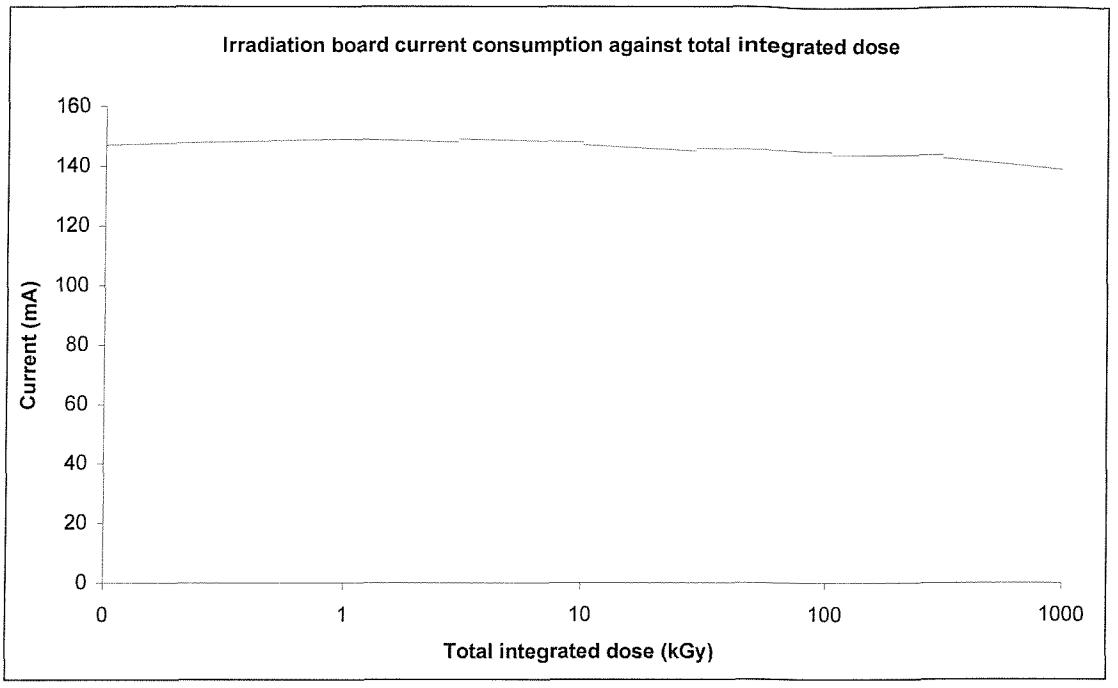

Figure 12.3: Current consumption for the irradiation board during irradiation.

The control device was stored in conductive foam during the irradiation stages, i.e. with no bias applied. Initially, it was thought that this would have but a negligible influence on the results. However, once the extent of the variation between apparently identical devices was realised, further measurements were made to ensure that this difference in bias conditions did not contribute to the changes observed. The control device was biased in the same board for a period of seven days, corresponding to the total time for which the irradiated devices were biased (column 6 of table 12.3). Measurements were made at the same intervals as for the irradiated devices and the results compared. Within the limits of error of the measurements, no significant differences between any of the sets of results were observed. This showed that the act of applying a bias voltage to the devices for a period of almost 200 hours did not, in itself, lead to the degradation of any of the measured parameters.

12.3.2 The BC108 transistors

In contrast with the SU devices, the BC108 devices manufactured by SGS-Thomson were irradiated later, during early 2001. Details of the timings for these irradiations are shown in table 12.5.

Sample number	Time in	Date in	Time out	Date out	Irradiation time hh:mm:ss	Position	Dose rate (kGy/hr)	Total dose (kGy)
M137	09:07:15	28/03/01	09:16:00	28/03/01	0:08:45	5/ABCD/1	6.80	1.0
M137	11:49:00	28/03/01	12:06:32	28/03/01	0:17:32	5/ABCD/1	6.80	2.0
M137	13:34:30	28/03/01	14:36:12	28/03/01	1:01:42	5/ABCD/1	6.80	7.0
M137	08:56:00	06/04/01	11:53:00	06/04/01	2:57:00	5/ABCD/1	6.77	20
M137	09:11:00	11/04/01	13:53:00	11/04/01	4:42:00	5/ABCD/1	6.76	32
M137	13:58:00	11/04/01	15:18:00	11/04/01	1:20:00	5/ABCD/1	6.76	9.0
M137	09:04:00	12/04/01	13:25:00	12/04/01	4:21:00	5/ABCD/1	6.76	29
M137	08:30:00	18/04/01	13:58:30	19/04/01	29:28:30	5/ABCD/1	6.74	199
M137	08:05:00	20/04/01	11:21:58	24/04/01	99:16:58	5/ABCD/1	6.74	669
M137	12:18:24	24/04/01	16:57:51	24/04/01	4:39:27	5/ABCD/1	6.73	31

Table 12.5: Stage timings for the BC108 irradiation (DS1522).

These transistors were irradiated unpowered, with the devices wrapped tightly in metal foil to ensure that all the leads were shorted together. The control device was not irradiated but stored in conductive foam during the periods when the other devices were being exposed to radiation. Once a stage of irradiation was completed, the devices were removed from the cell, transported to the test laboratory, removed from the foil and placed in conductive foam while electrical testing was carried out. After the electrical testing, they were again wrapped in foil and returned to the cell. The case of each device was inscribed with a unique serial number prior to the tests in order to ensure its reliable identification throughout the tests.

12.4 GUMMEL PLOT MEASUREMENTS

Gummel plot measurements were made with very little change to the test software from the phase 1 tests. This software proved reliable and robust and gave good results with short measurement times. The results presented in this section have been grouped by device type. In the case of the SU devices, each graph shows the results for an individual device across all the stages of irradiation, i.e. one figure shows the data for an individual device taken after each stage of irradiation. There is one graph for each of the ten devices of each type, grouped together to permit easy comparison. The data for the control (unirradiated) device are also included in order to demonstrate the consistency of the measurement process.

In the case of the COTS devices, the results for all devices of a given type are shown on the same graph. Most of these graphs exhibit a gradual, monotonic shift in the development of the curves and so the plots for only some of the radiation stages have been included. The plots for the intermediate stages simply show a mid-way point between those for the adjacent stages.

12.4.1 SU device 1

Figures 12.4 to 12.13 show the Gummel plots for devices of type 1 in each of the ten packages, with one plot for each package.

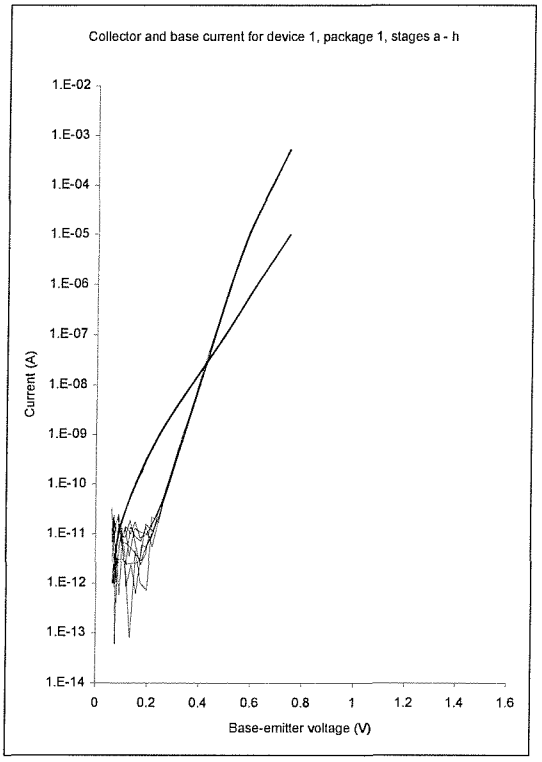

Figure 12.4: Gummel plots for device 1 in package 1.

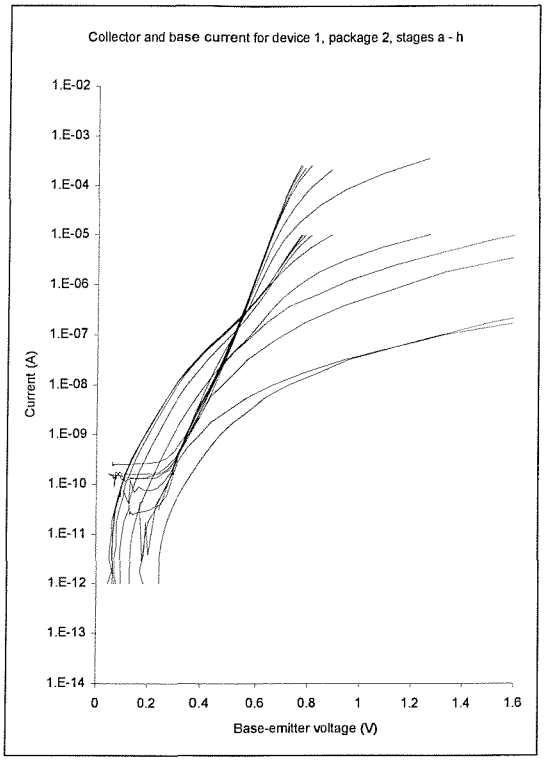

Figure 12.5: Gummel plots for device 1 in package 2.

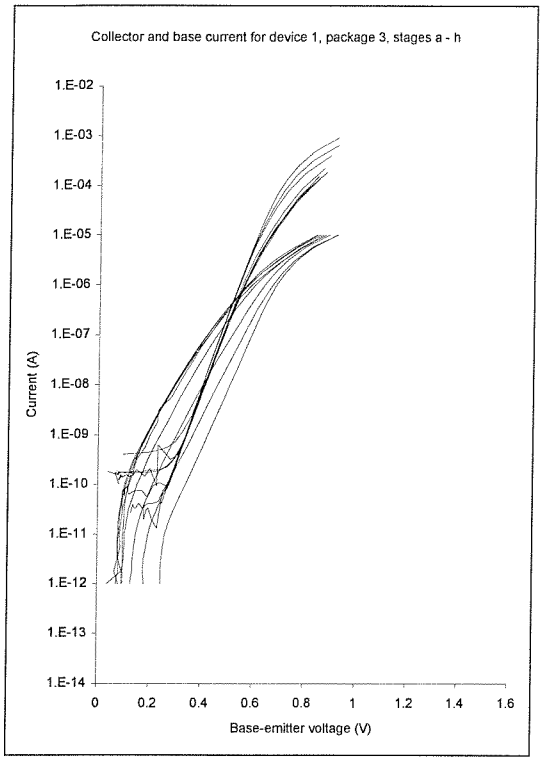

Figure 12.6: Gummel plots for device 1 in package 3.

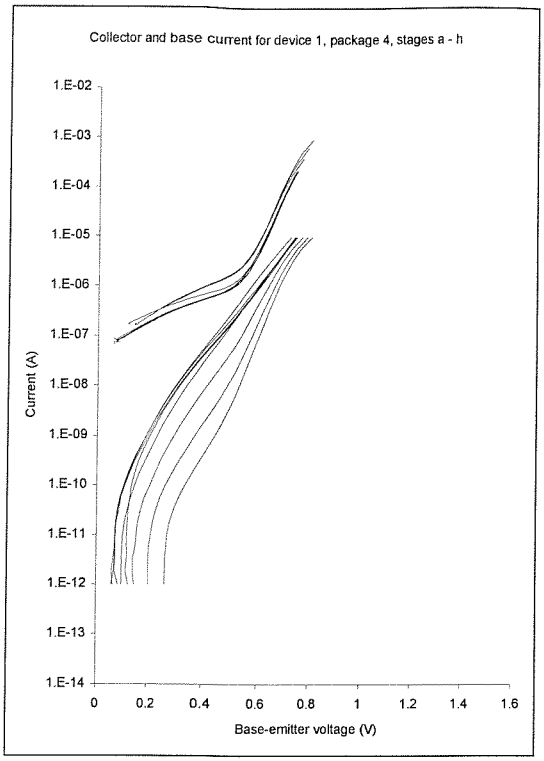

Figure 12.7: Gummel plots for device 1 in package 4.

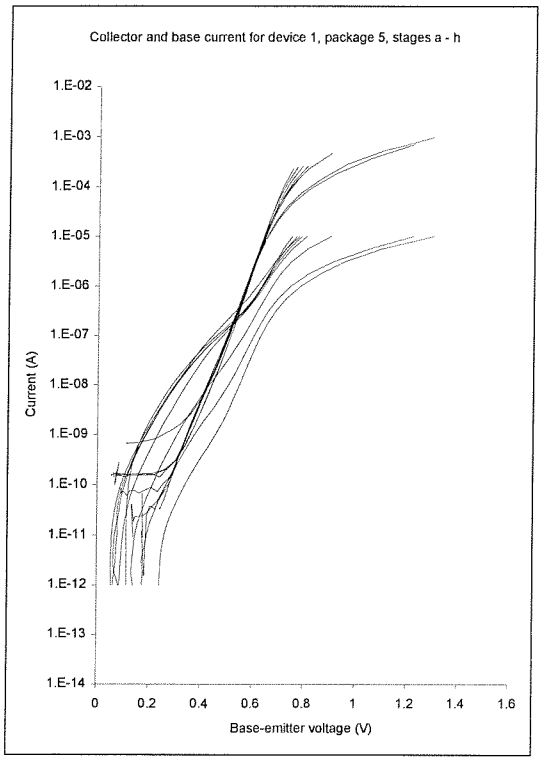

Figure 12.8: Gummel plots for device 1 in package 5.

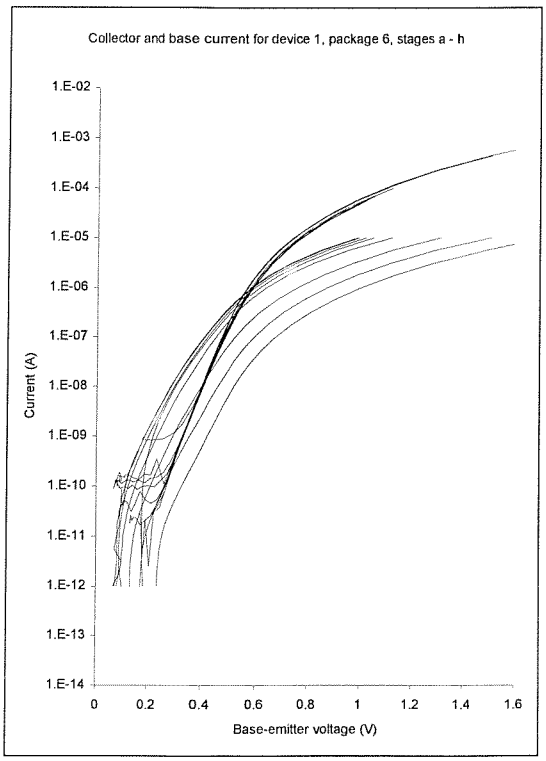

Figure 12.9: Gummel plots for device 1 in package 6.

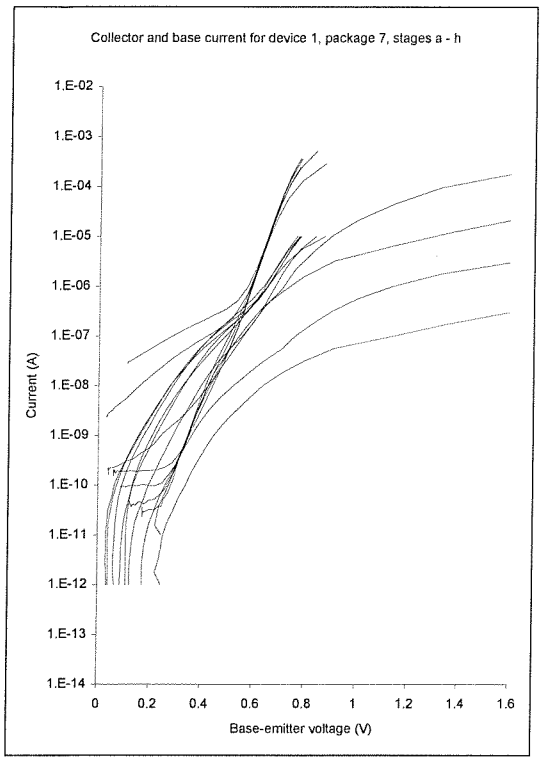

Figure 12.10: Gummel plots for device 1 in package 7.

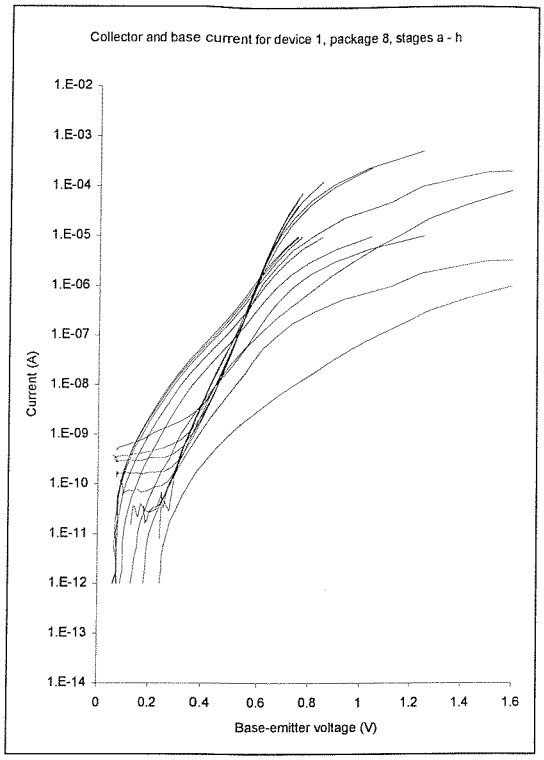

Figure 12.11: Gummel plots for device 1 in package 8.

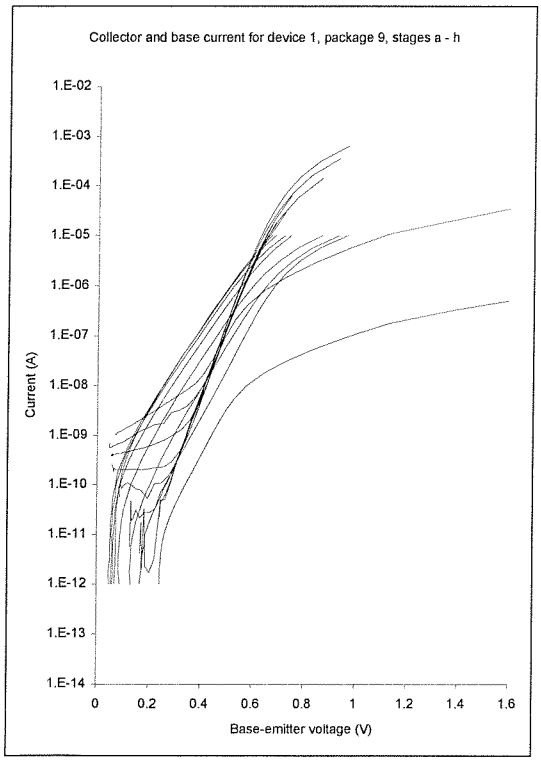

Figure 12.12: Gummel plots for device 1 in package 9.

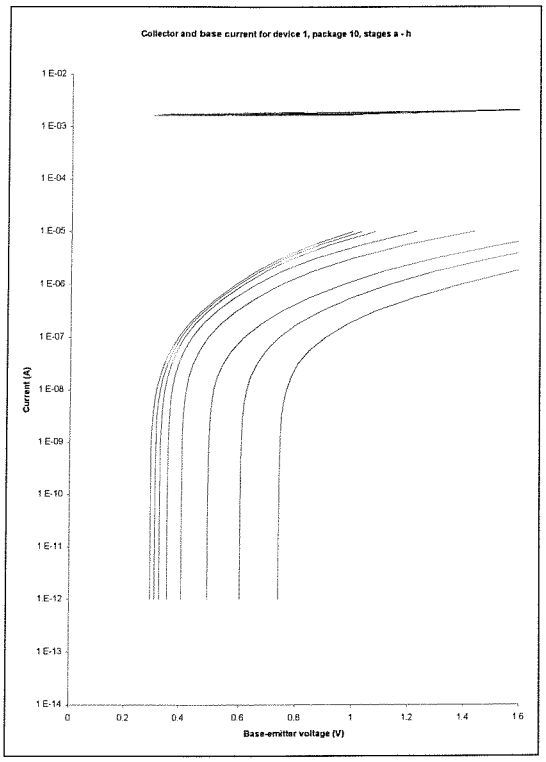

Figure 12.13: Gummel plots for device 1 in package 10.

Figure 12.4 shows clearly that the measurement process is consistent and that the results for a given device are repeatable. Each control device was electrically tested at the same time as the irradiated devices and shows a very good agreement across the eight sets of readings. There are differences at currents below 10 pA but this is at the limit of the instrument and was expected. It can be noted that the base current curves cross the collector current curves at a base-emitter voltage of approximately 0.4 V before irradiation.

Most of the other figures show a steadily rising set of curves for the base current and a broadly unchanging set of curves for the collector current. Some changes in the shape of the collector current curves can be seen at higher currents, especially in figures 12.5 and 12.8, possibly indicating an increase in terminal resistance or the onset of conductivity modulation, although a mechanism for either of these effects in this case is unclear. Also obvious in some figures, e.g. 12.10, 12.11 and 12.12, is the increase in collector leakage current at the higher stages of irradiation. This is reflected in the point data readings later in this chapter.

One clear point to emerge is the variation in the shape of the curves across the nine devices irradiated. Although nominally of the same type, fabricated at the same time, all on the same wafer and packaged in the same manner, there is very little consistency in the form of the plots. The variability exhibited here makes it difficult to draw conclusions based on the response of these devices to radiation and rules out the possibility of a meaningful statistical analysis.

12.4.2 SU device 2

Figures 12.14 to 12.23 show the Gummel plots for devices of type 2 in each of the ten packages.

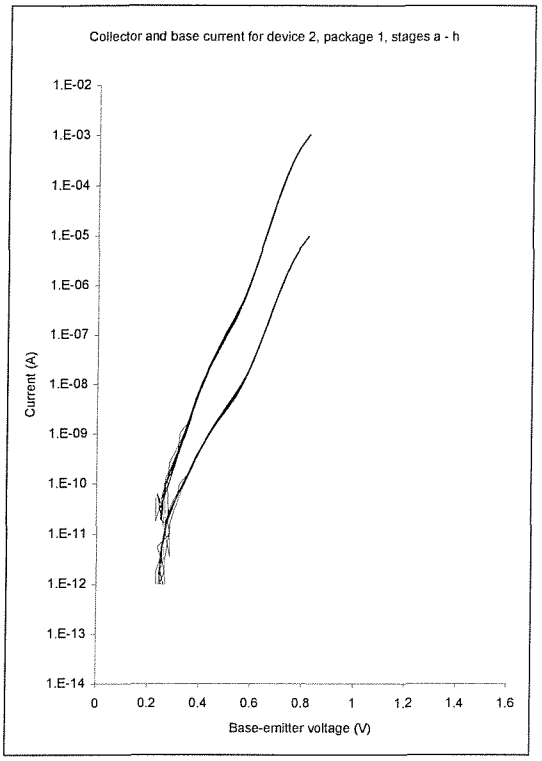

Figure 12.14: Gummel plots for device 2 in package 1.

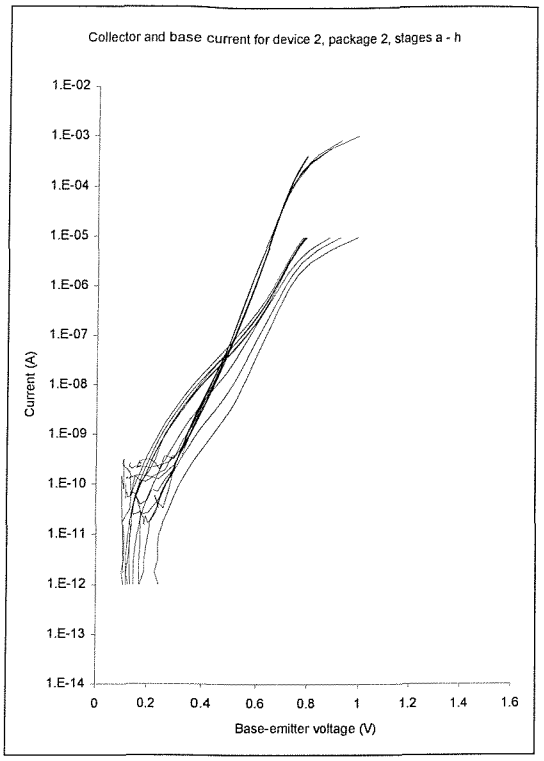

Figure 12.15: Gummel plots for device 2 in package 2.

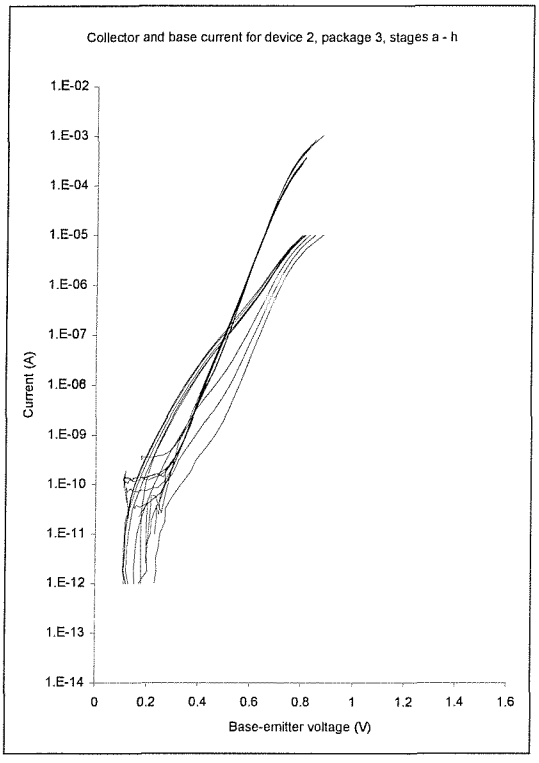

Figure 12.16: Gummel plots for device 2 in package 3.

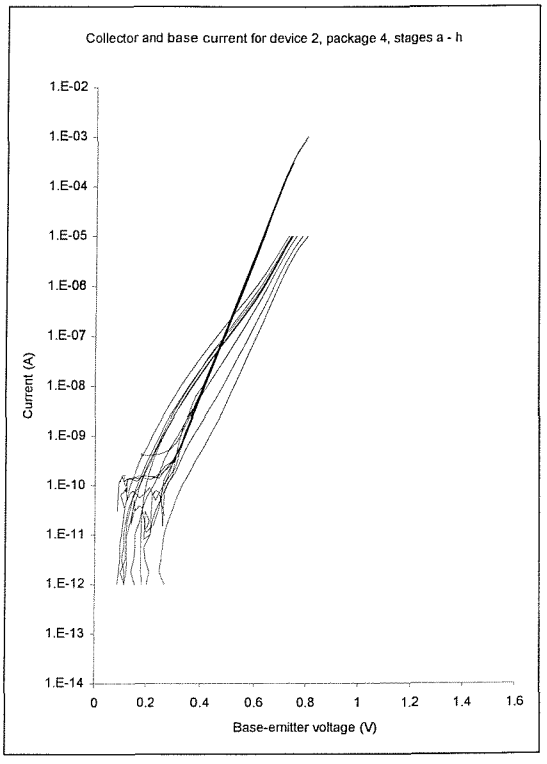

Figure 12.17: Gummel plots for device 2 in package 4.

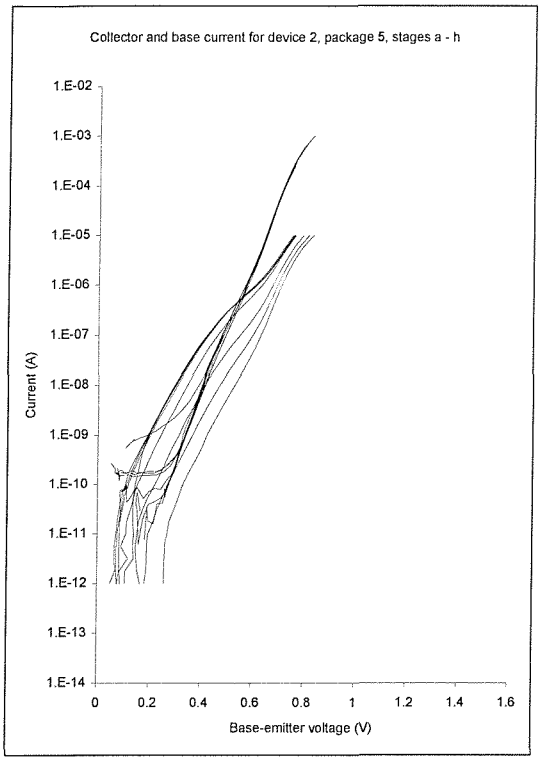

Figure 12.18: Gummel plots for device 2 in package 5.

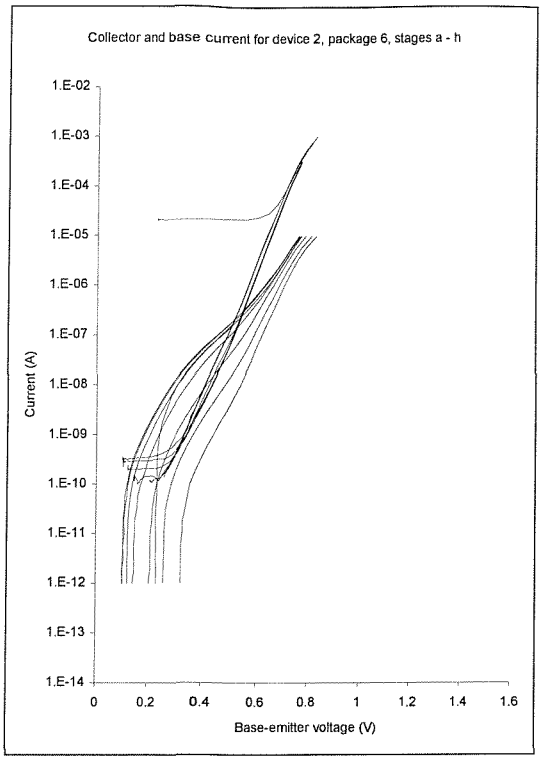

Figure 12.19: Gummel plots for device 2 in package 6.

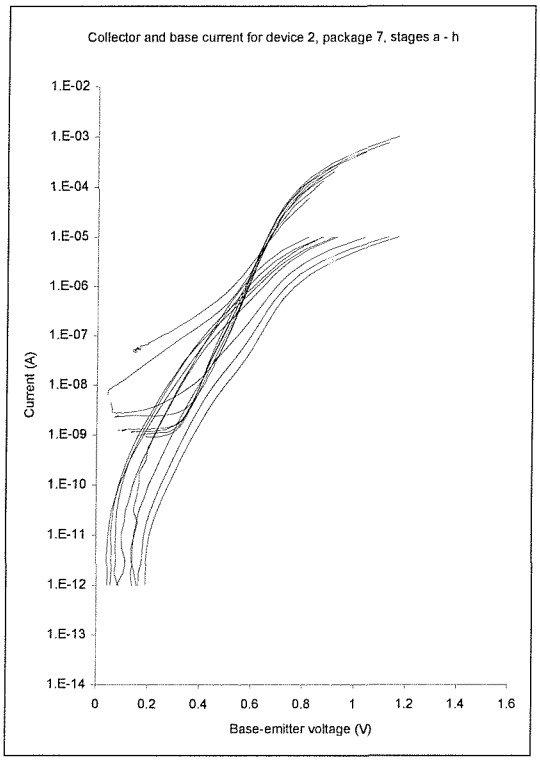

Figure 12.20: Gummel plots for device 2 in package 7.

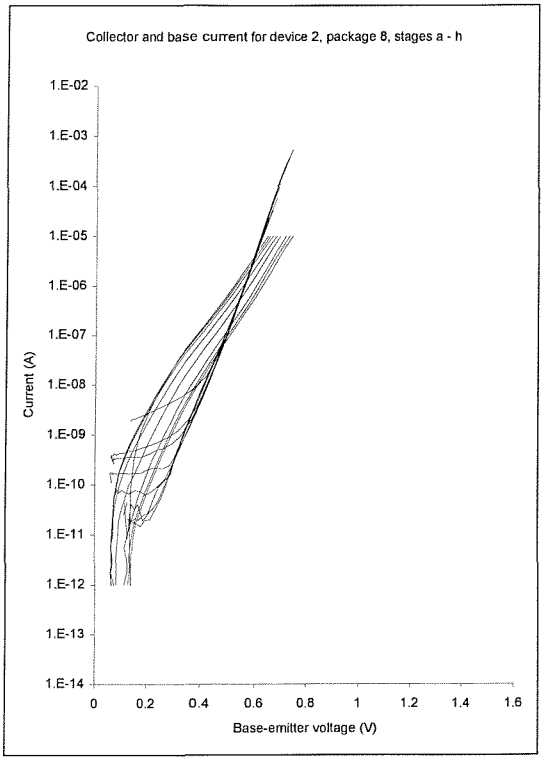

Figure 12.21: Gummel plots for device 2 in package 8.

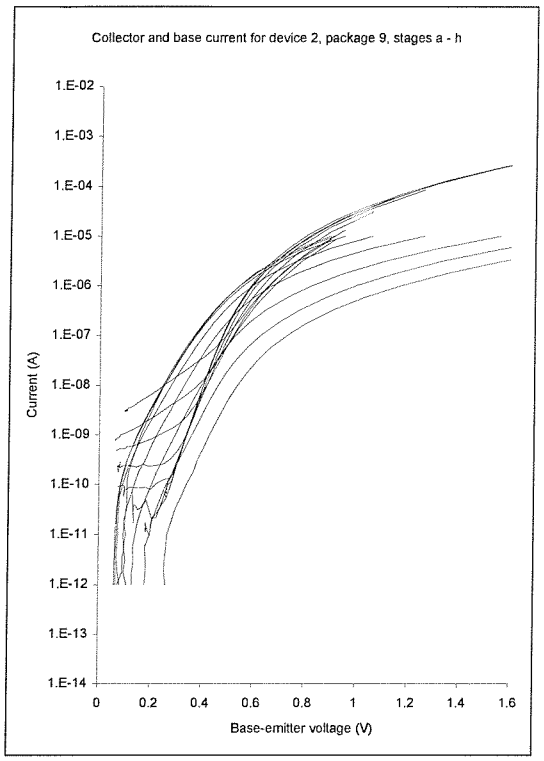

Figure 12.22: Gummel plots for device 2 in package 9.

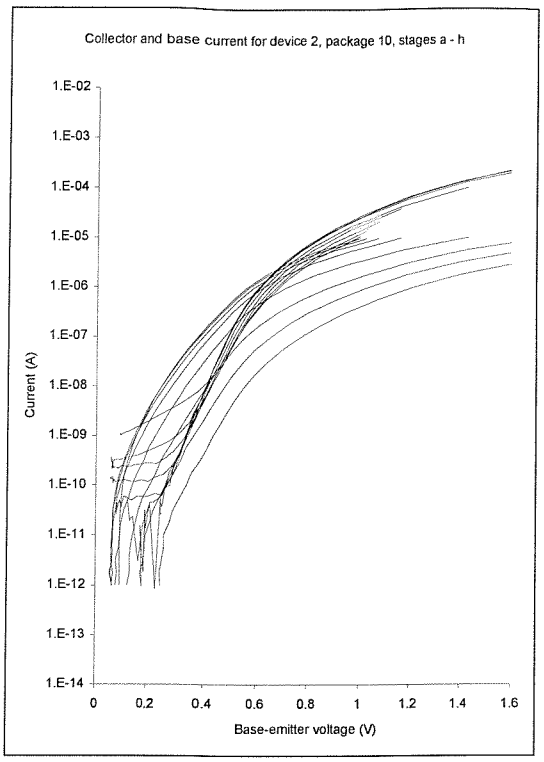

Figure 12.23: Gummel plots for device 2 in package 10.

The plots for the second device type again vary considerably with respect to each other. Shifts in the base current curves with total dose are observable, along with the development of high level effects in the collector current, especially in figures 12.22 and 12.23. Rising collector leakage current with total dose can also be seen in many of these figures.

Overall, there is a better degree of consistency between the nine irradiated devices, especially for packages 2 to 8, than was the case for the devices of type 1. The devices in packages 9 and 10 show very different results. This better degree of consistency permits a tentative inference that there is a slightly lower degree of shift in base current compared with that observed for the devices of type 1. The base current and collector current curves do not cross at all before irradiation (except for the device in package 8), in contrast with those for type 1, although a distinct kink can be made out.

12.4.3 SU device 3

Figures 12.24 to 12.29 show the Gummel plots for devices of type 3 in six of the ten packages.

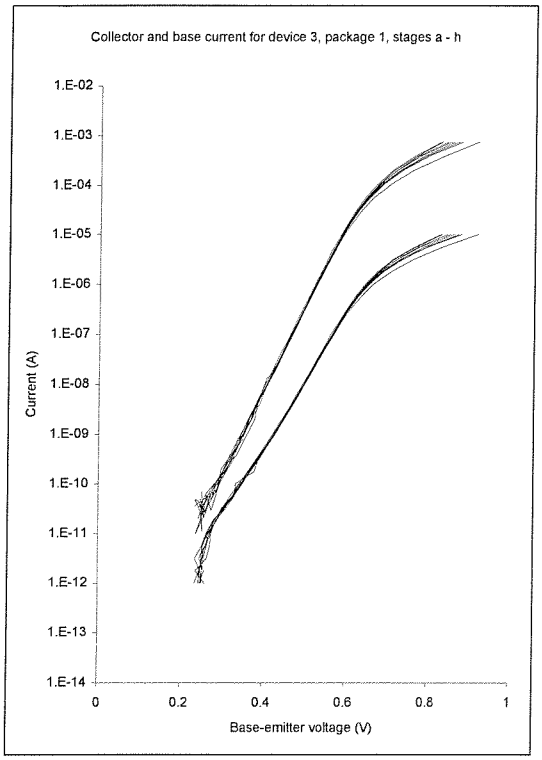

Figure 12.24: Gummel plots for device 3 in package 1.

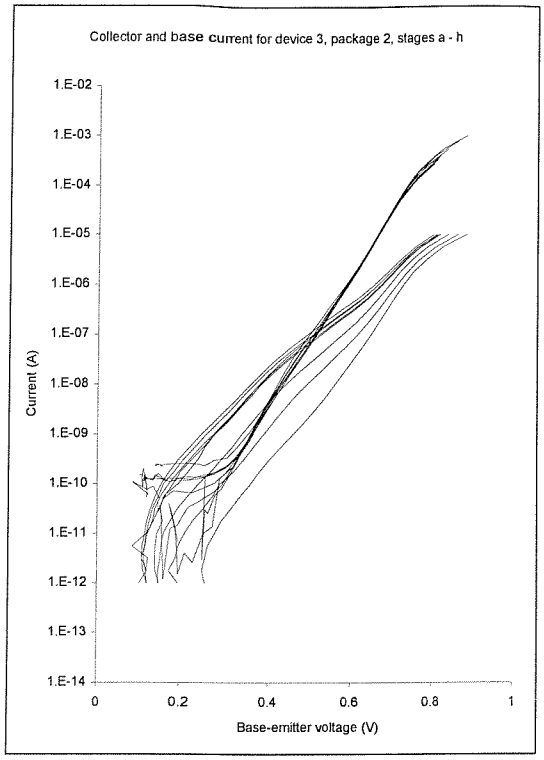

Figure 12.25: Gummel plots for device 3 in package 2.

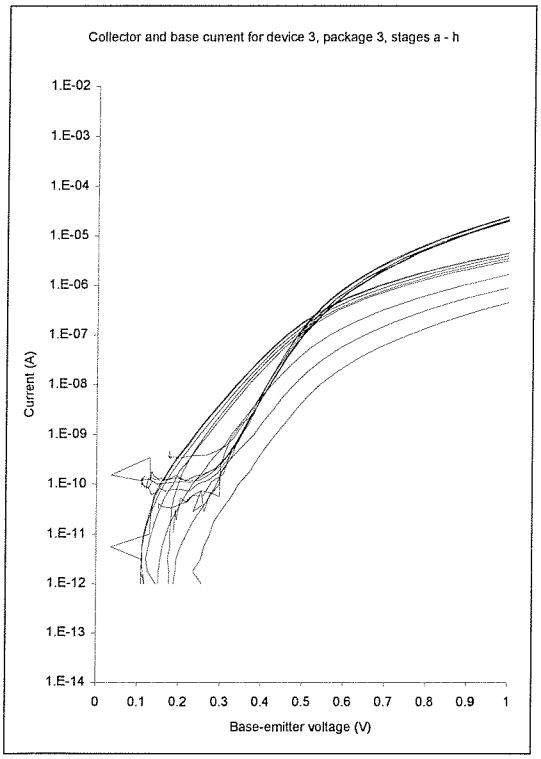

Figure 12.26: Gummel plots for device 3 in package 3.

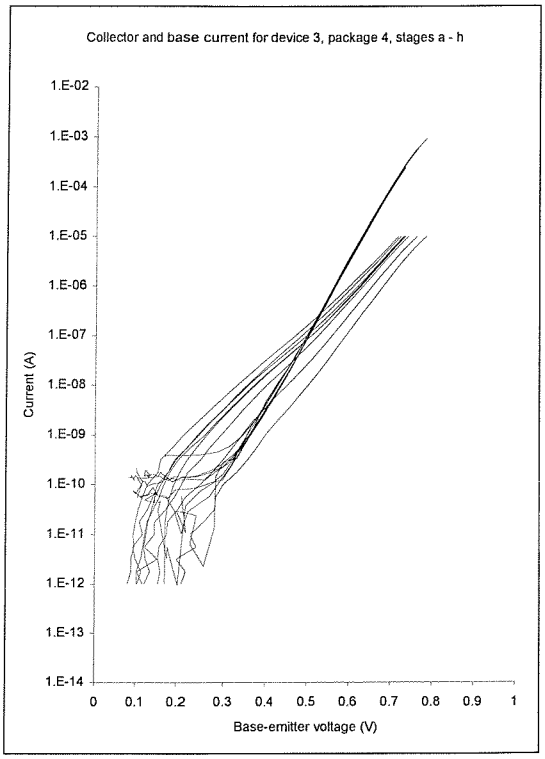

Figure 12.27: Gummel plots for device 3 in package 4.

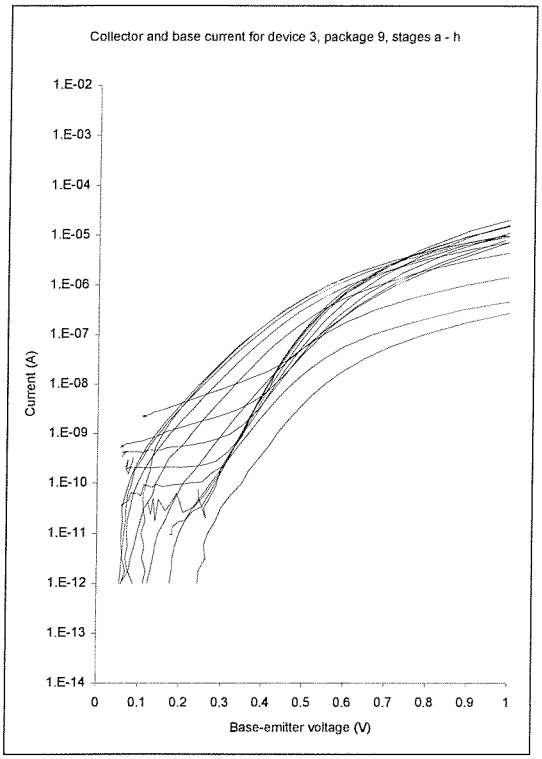

Figure 12.28: Gummel plots for device 3 in package 9.

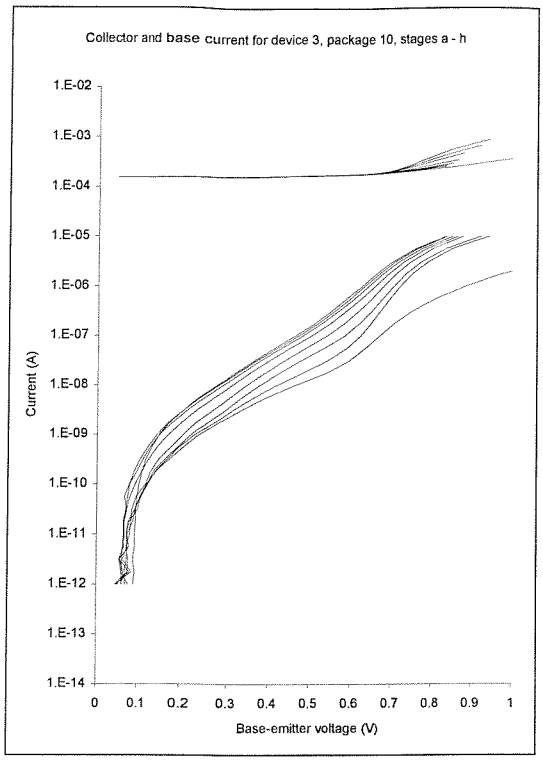

Figure 12.29: Gummel plots for device 3 in package 10.

The results for the devices of type 3 are similar to those for type 2. Divergence of both the collector and base current curves at high currents is observable for the control device, indicating that some ageing mechanism was at work even without irradiation. However, the effect was small compared with that brought about by the irradiation. The collector and base current curves do not cross before irradiation, as for the devices of type 2.

12.4.4 SU device 4

Figures 12.30 to 12.35 show the Gummel plots for devices of type 4 in six of the ten packages.

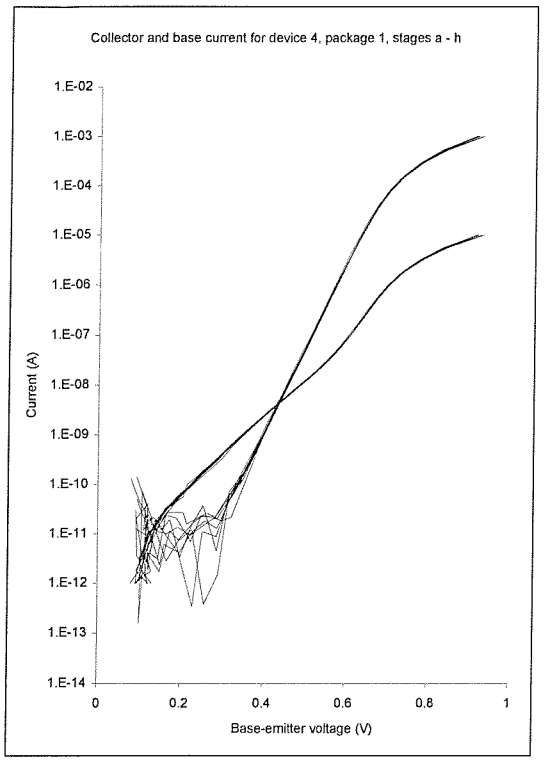

Figure 12.30: Gummel plots for device 4 in package 1.

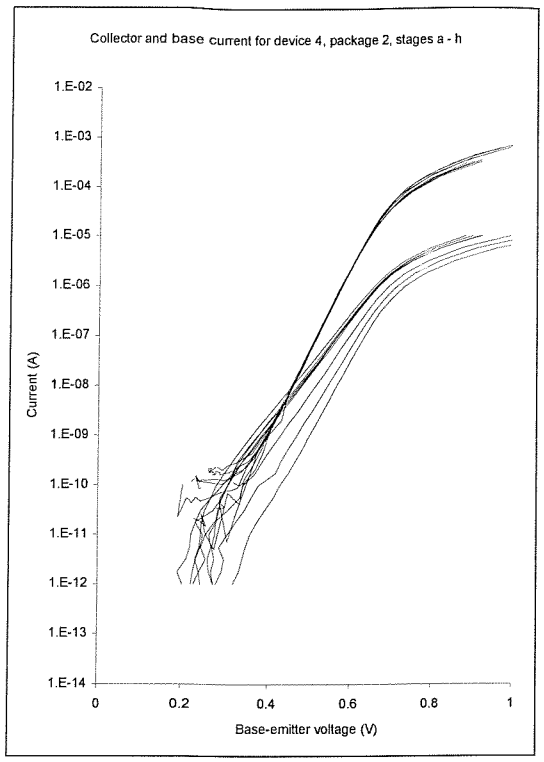

Figure 12.31: Gummel plots for device 4 in package 2.

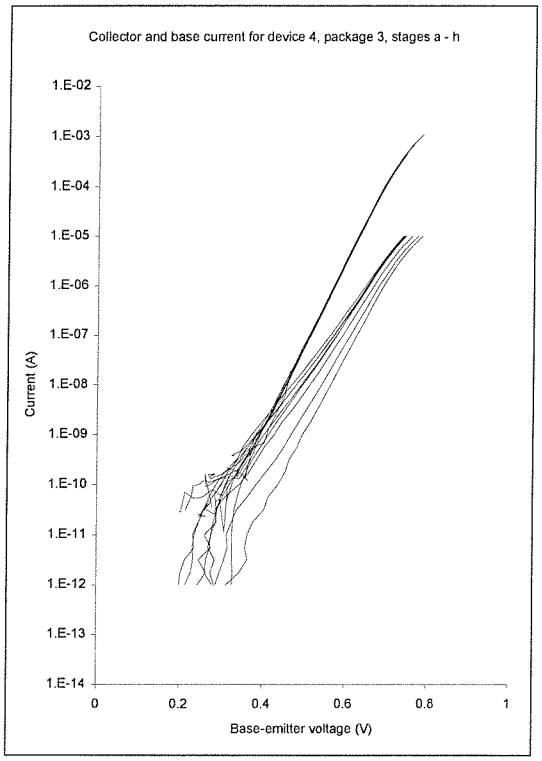

Figure 12.32: Gummel plots for device 4 in package 3.

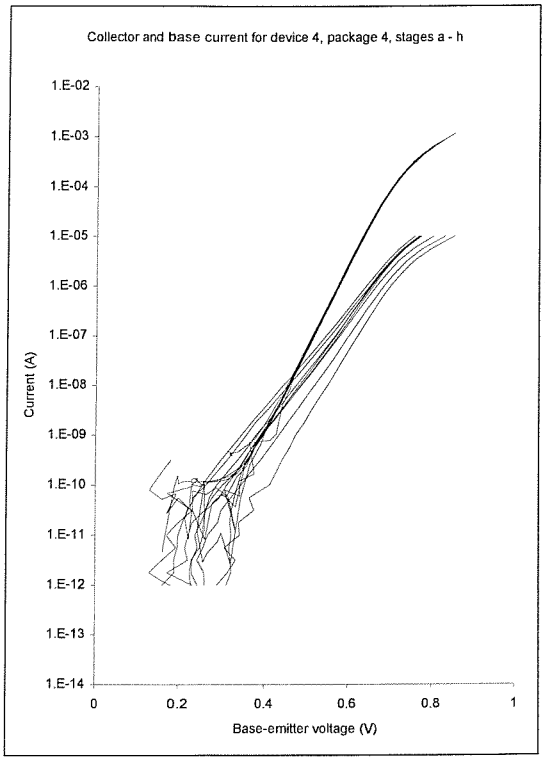

Figure 12.33: Gummel plots for device 4 in package 4.

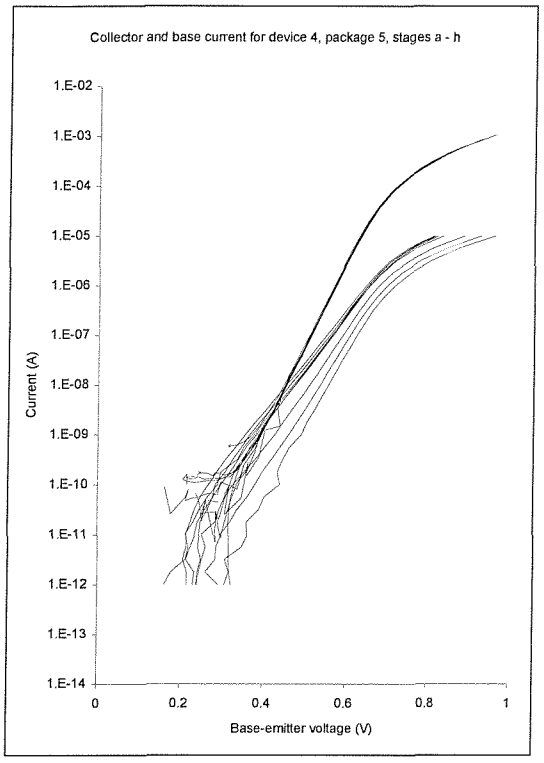

Figure 12.34: Gummel plots for device 4 in package 5.

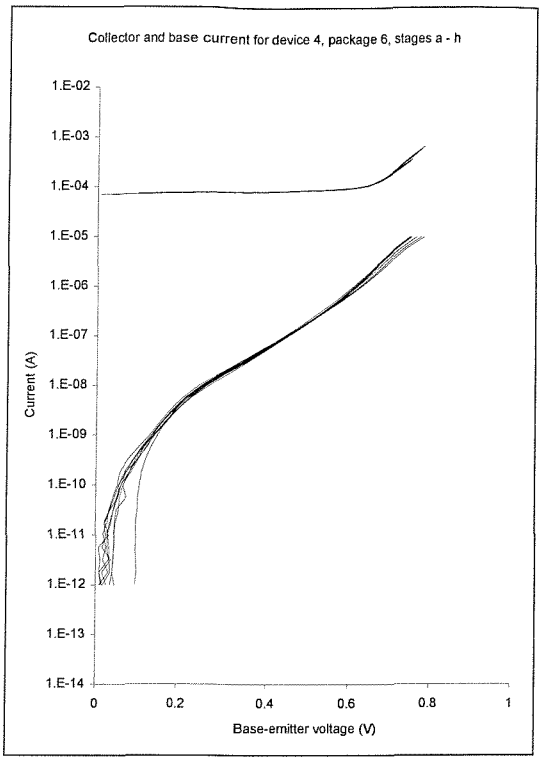

Figure 12.35: Gummel plots for device 4 in package 6.

The type 4 devices show a different range of response from the three previous types. The base and collector current curves cross at around 0.4 V for the control device but not for all of the others. High level injection effects are not observable for any of these devices. Shifts in the base current curves do occur with irradiation, except for the device in package 6, shown in figure 12.35. However, the collector leakage current for this device indicates that it was not functioning at all well throughout the tests and therefore little confidence can be placed in these data. (Figure 12.62 further illustrates this point.) The overall magnitude of the shift in the base current curves was comparable with that for devices of types 2 and 3.

12.4.5 SU device 5

Figures 12.36 to 12.41 show the Gummel plots for devices of type 5 in six of the ten packages.

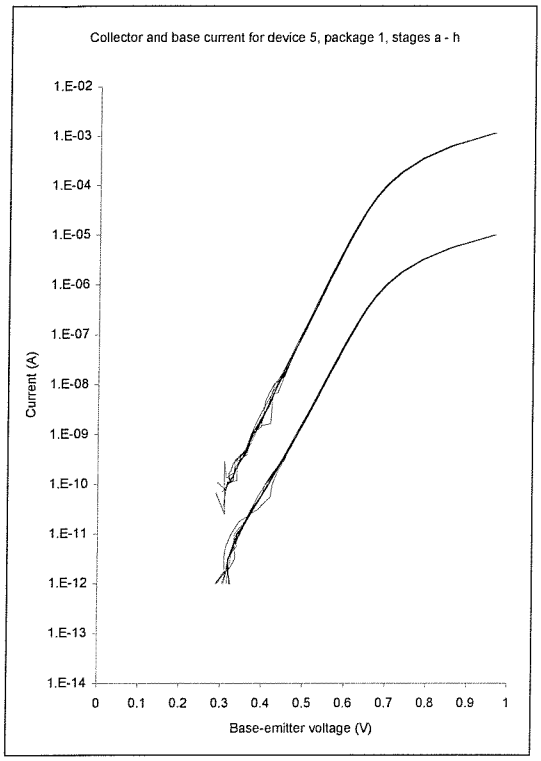

Figure 12.36: Gummel plots for device 5 in package 1.

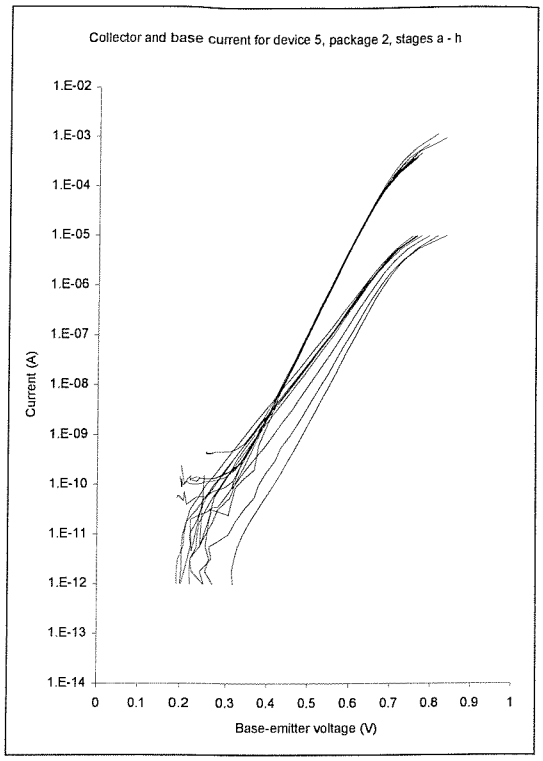

Figure 12.37: Gummel plots for device 5 in package 2.

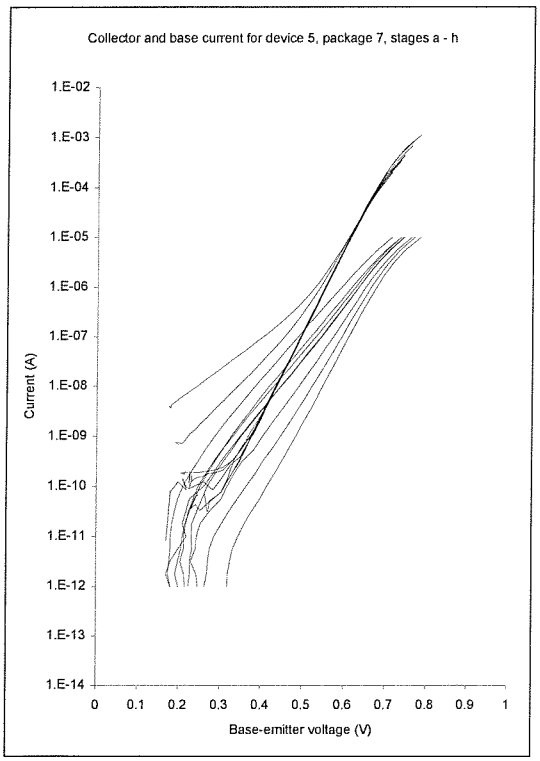

Figure 12.38: Gummel plots for device 5 in package 7.

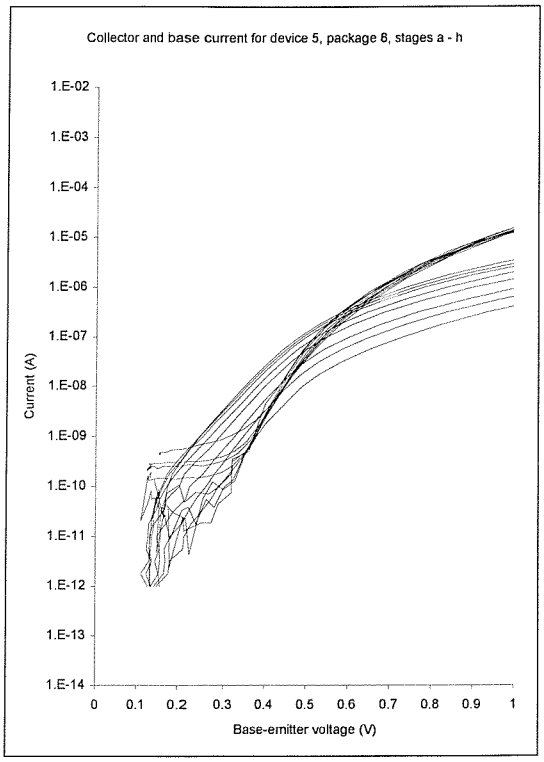

Figure 12.39: Gummel plots for device 5 in package 8.

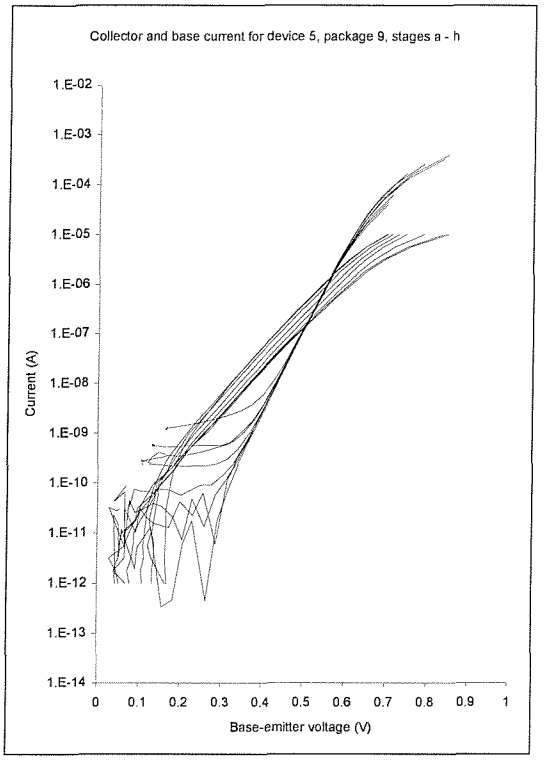

Figure 12.40: Gummel plots for device 5 in package 9.

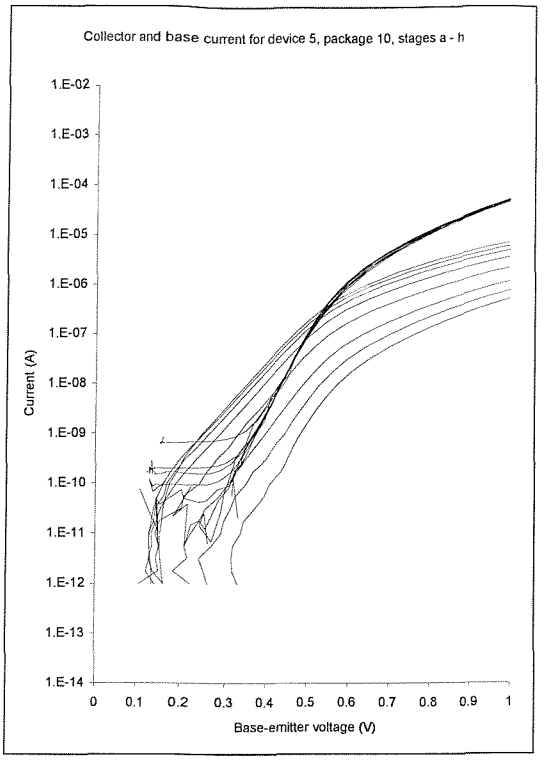

Figure 12.41: Gummel plots for device 5 in package 10.

The type 5 devices again show no crossing of the collector and base current curves before irradiation. There is a broader range of shapes in the plots across the ten devices of the same type than observed for devices of types 1 to 4. High level injection effects may be observable for two of the devices (figures 12.37 and 12.40) but the magnitude is small. The device in package 3 (not shown) had an operating region rather different from that of all the others, with the base-emitter voltage not falling below 0.5V. The average shift in the base current curves with total dose is the least of all across devices of types 1 to 5.

12.4.6 SU device 6

Figures 12.42 to 12.47 show the Gummel plots for devices of type 6 in six of the ten packages.

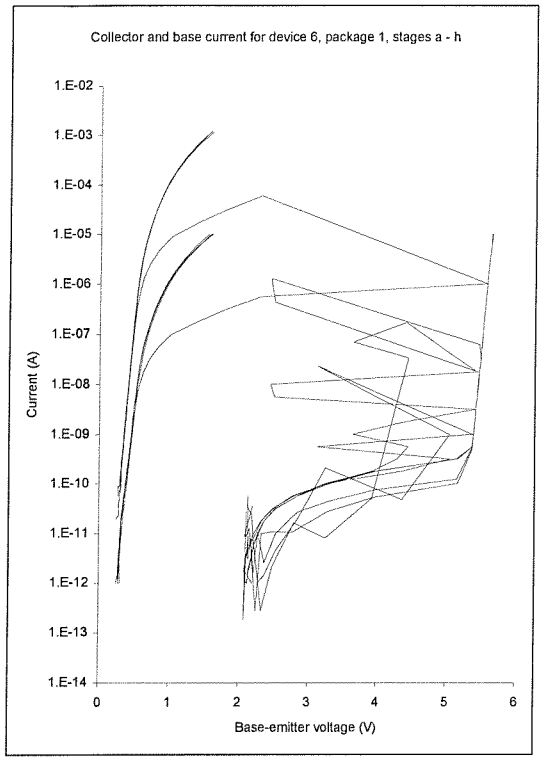

Figure 12.42: Gummel plots for device 6 in package 1.

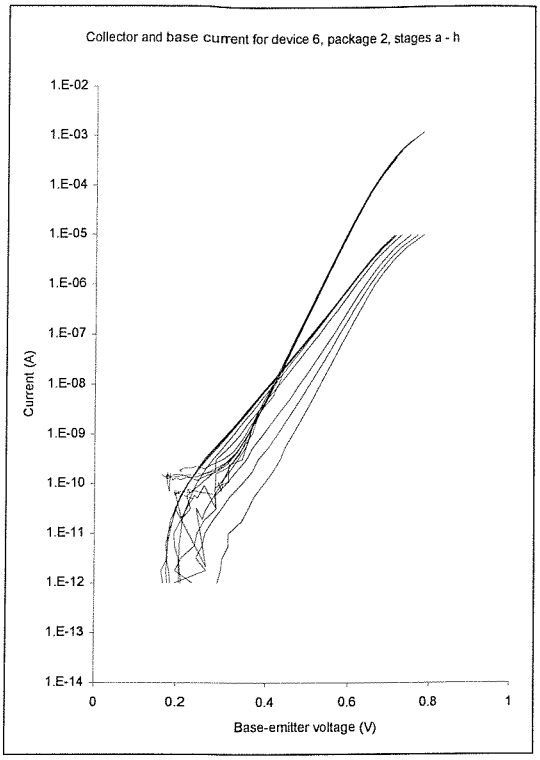

Figure 12.43: Gummel plots for device 6 in package 2.

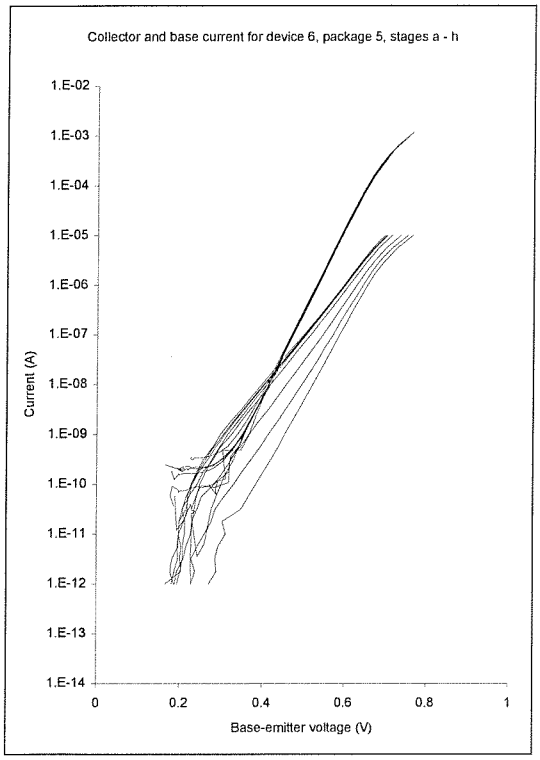

Figure 12.44: Gummel plots for device 6 in package 5.

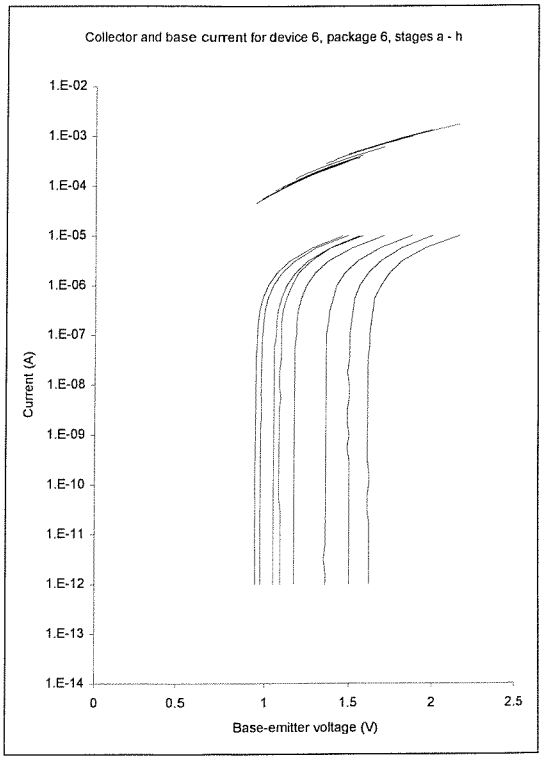

Figure 12.45: Gummel plots for device 6 in package 6.

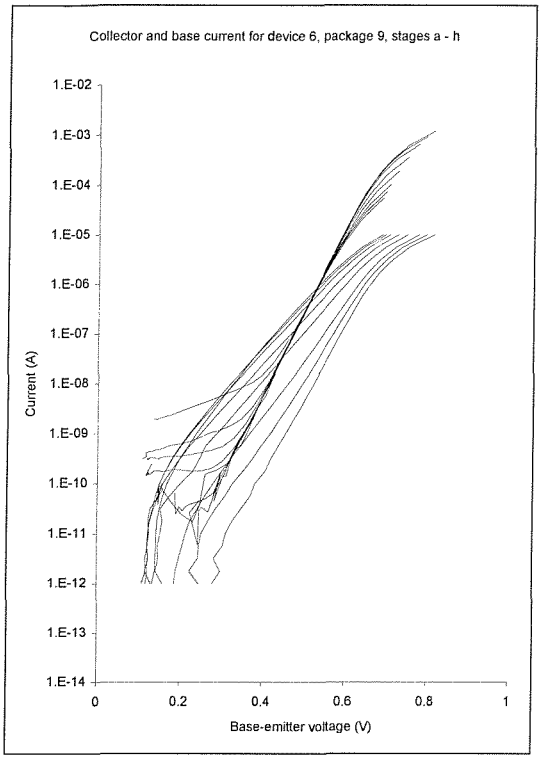

Figure 12.46: Gummel plots for device 6 in package 9.

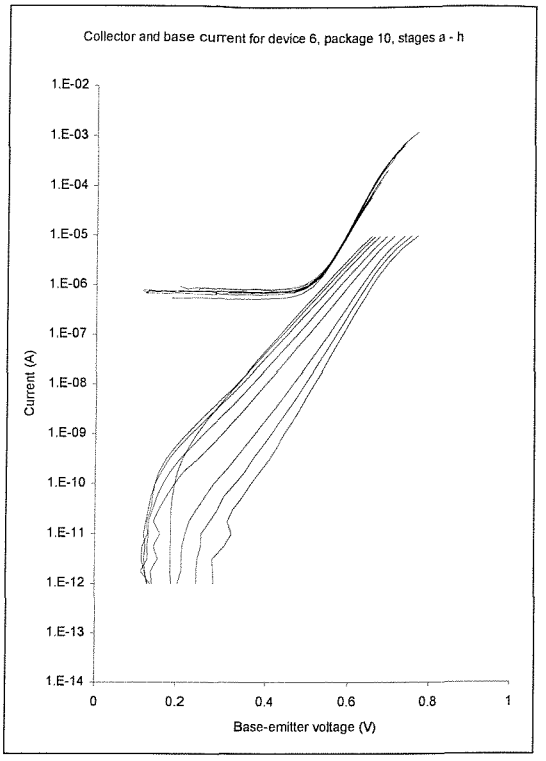

Figure 12.47: Gummel plots for device 6 in package 10.

The devices of type 6 continue the trend of extreme variability across the ten examples nominally of the same type. The control device, in particular, showed some large variations and wildly unpredictable readings on some measurements. The other devices also showed different effects.

The device in package 6 (figure 12.45) shows a similar behaviour to the type 5 device in package 3 with the base-emitter voltage not falling below a certain, high value, 1 V in this case.

The shifts in the base current curves are the least of all the device types. High level injection type effects are visible only for the device in package 9 (figure 12.46).

12.4.7 The BC108 transistors

The Gummel plots for the BC108 devices have been arranged differently from those for the SU devices, in that the set of devices behaved sufficiently similarly to enable all the data at a given stage of irradiation to be viewed together. There was a clear, steady progression in the trend observed and so data are presented here only for alternate stages.

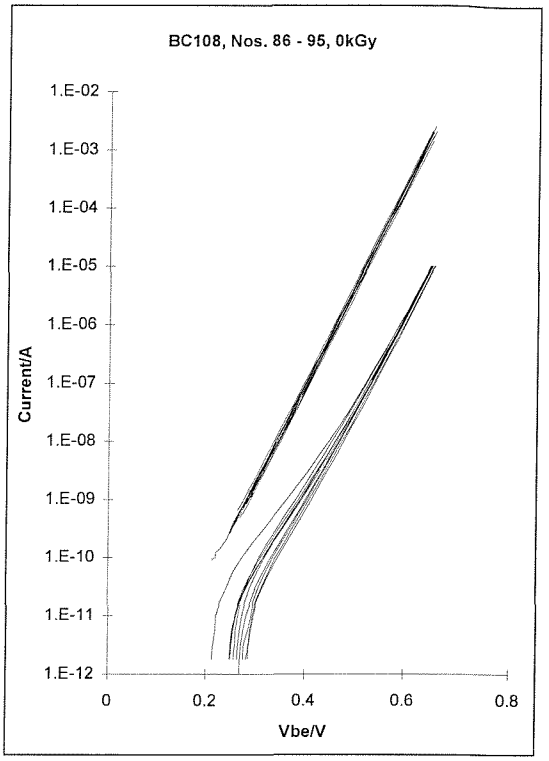

Figure 12.48: Gummel plot for BC108 devices before irradiation (DS1522).

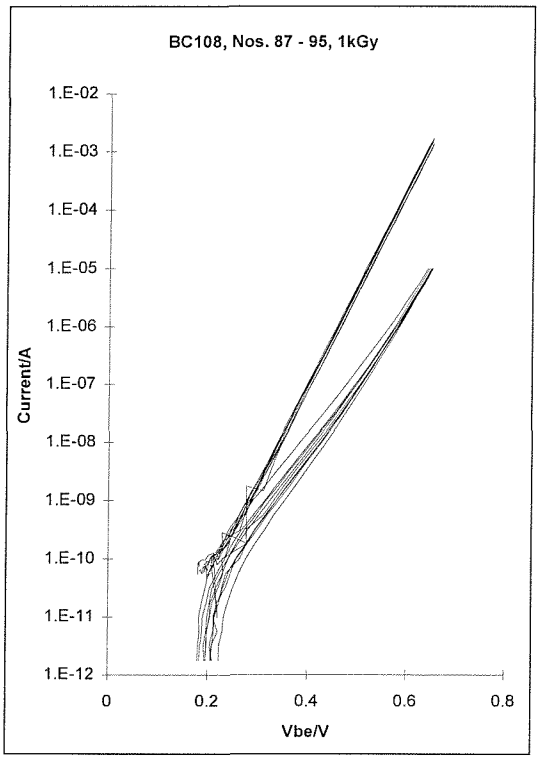

Figure 12.49: Gummel plots for BC108 devices after 1 kGy.

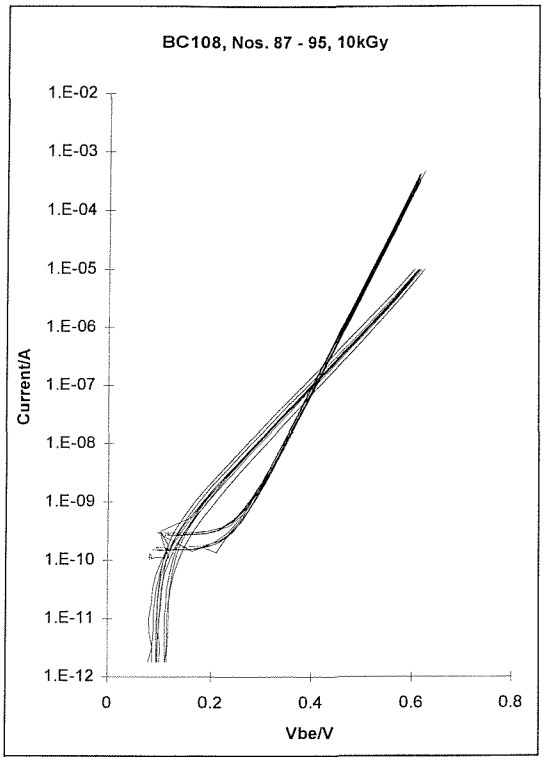

Figure 12.50: Gummel plots for BC108 devices after 10 kGy.

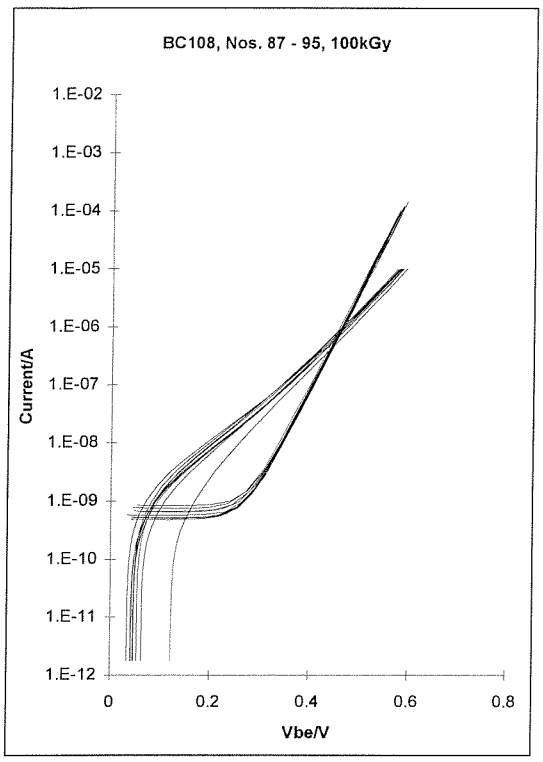

Figure 12.51: Gummel plots for BC108 devices after 100 kGy.

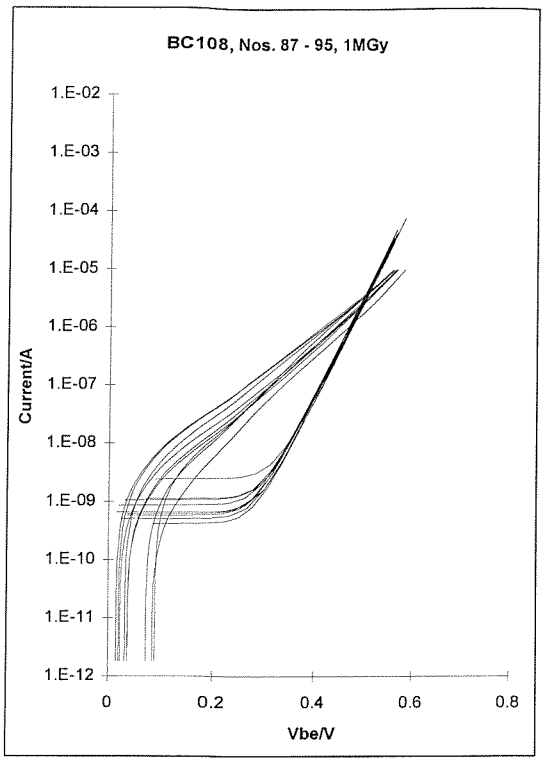

Figure 12.52: Gummel plots for BC108 devices after 1 MGy.

The Gummel plots for the BC108 devices are much better-behaved than those for the SU devices are. As the readings for the nine devices were all in close agreement, it is possible to plot the data for all the devices at a given stage on the same graph, making the consistency across the batch clear.

The collector and base current curves do not cross before irradiation. There is a significant shift in the base current curves with total dose and a slight increase in the range of base current values across the sample set. High level injection type effects are not observable for any of the devices at any stage of irradiation.

In order to facilitate an easy comparison between the BC108 and SU devices, figure 12.53 illustrates the BC108 data in the same manner as that for the SU devices, i.e. all the data for BC108 device number 87 at each stage of irradiation are shown on the same plot. The series of shifted base current curves is clearly displayed in this figure, together with an almost invariant set of collector current curves. The only change observable in the collector current curves is at low voltage, where the current, i.e. a leakage current, rises slightly with total dose. This may be compared with figure 12.63, showing the change in collector-base leakage current for these devices.

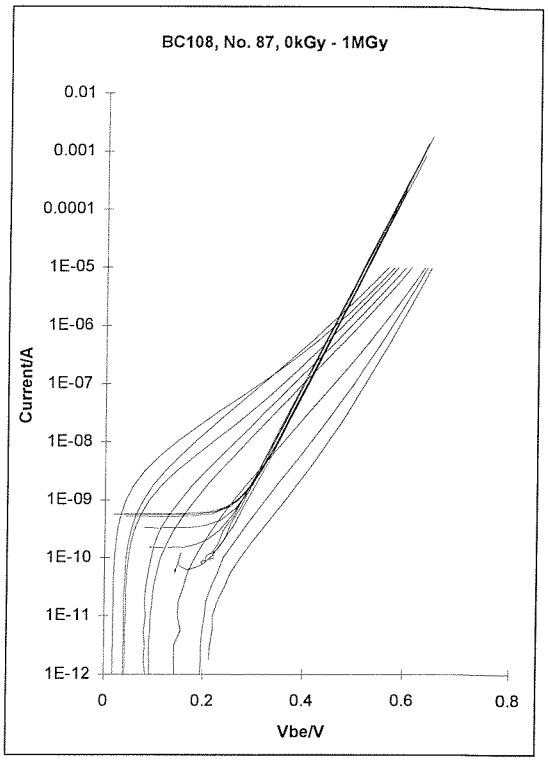

Figure 12.53: Gummel plot for BC108 device number 87 at all stages of irradiation.

The progressive shift in the base current characteristic with each stage of irradiation is clear. The only curve not to follow this pattern is that for 1 MGy. This is the highest current curve for high values of base-emitter voltage, as expected, but crosses the 300 kGy curve at approximately 0.35 V, i.e. at a base current of just above 100 nA, remaining between the 300 and 100 kGy curves over the rest of the base-emitter voltage range. Given that the collector current remains invariable over this range, this would correspond to a slight increase in gain for this device at that total dose.
The collector current curves are almost exactly the same at each stage of irradiation, apart from the collector leakage current. This shows a small but clear increase with total dose, as observed for some of the SU devices.

12.5 DC POINT DATA MEASUREMENTS

As for the Gummel plot measurement, the software used for the point data measurements in the first phase of the work proved very reliable and was used again for this phase, although minor modifications were made in order to allow for slightly different voltage and/or current conditions for specific parameters. This was carried out according to the definitions given in the associated manufacturer's data sheet for

the COTS devices and to guidelines provided by Southampton University for the SU devices. Essentially, the latter consisted of a maximum voltage of 10 V and a maximum current of a few tens of milliamps.

12.5.1 Emitter-base leakage current

This parameter was measured at an emitter-base voltage of 3 V, with the collector open-circuit.

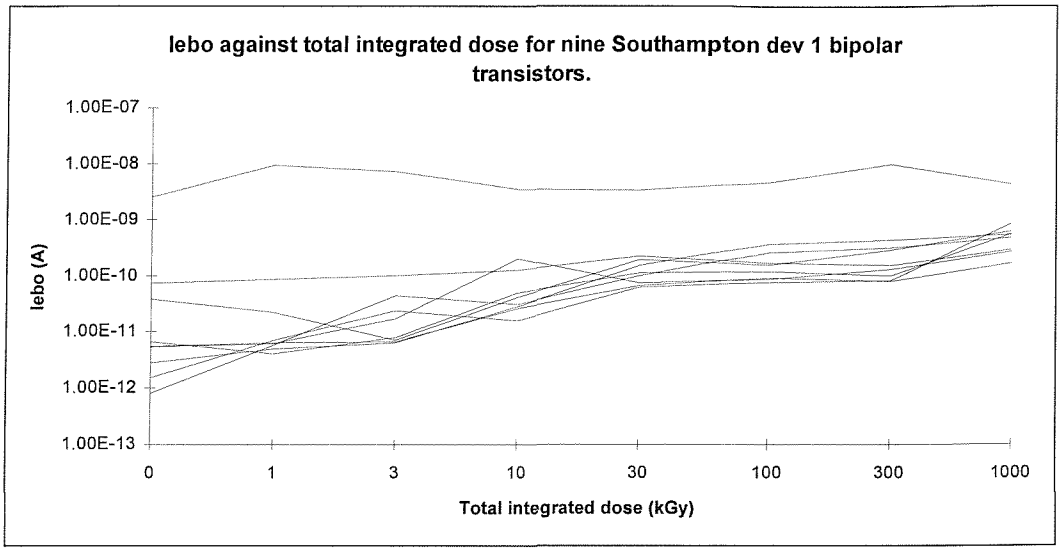

Figure 12.54: Change in Iebo against total dose for SU device 1.

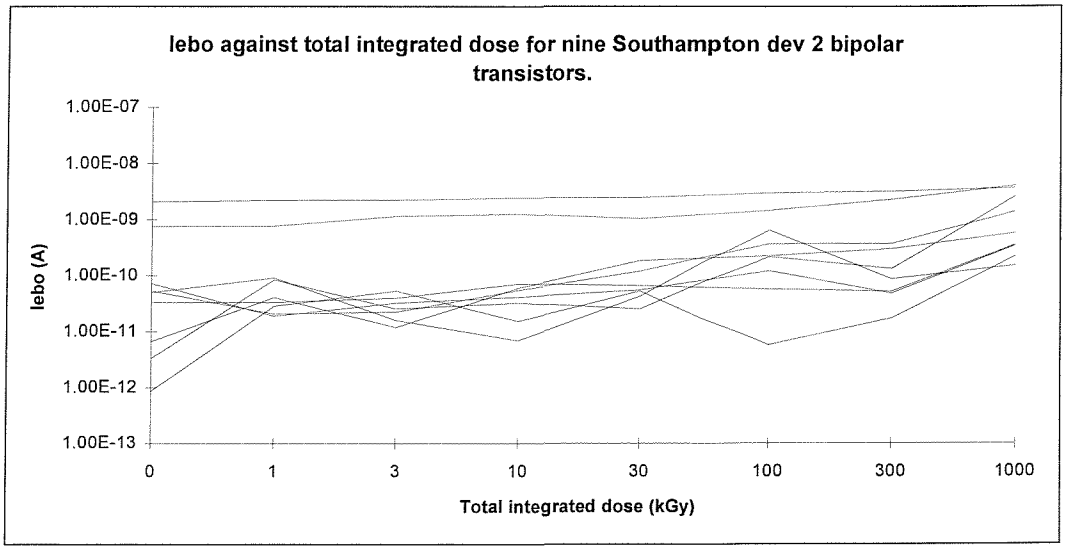

Figure 12.55: Change in Iebo against total dose for SU device 2.

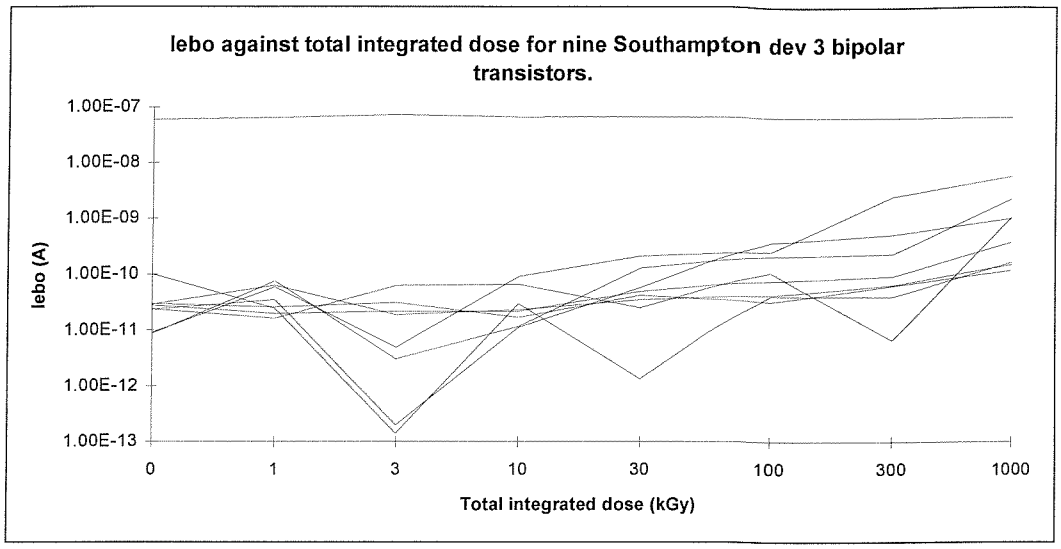

Figure 12.56: Change in Iebo against total dose for SU device 3.

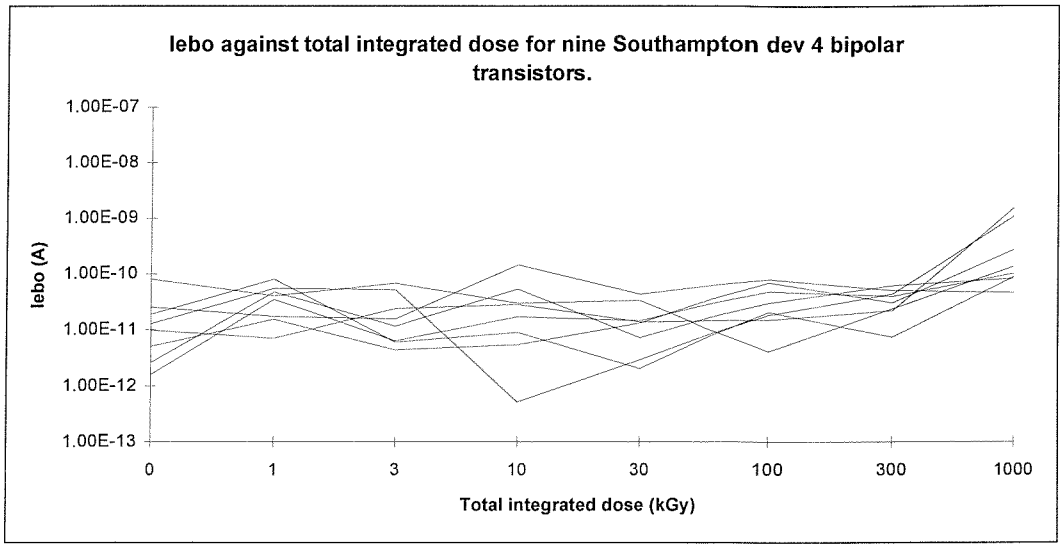

Figure 12.57: Change in Iebo against total dose for SU device 4.

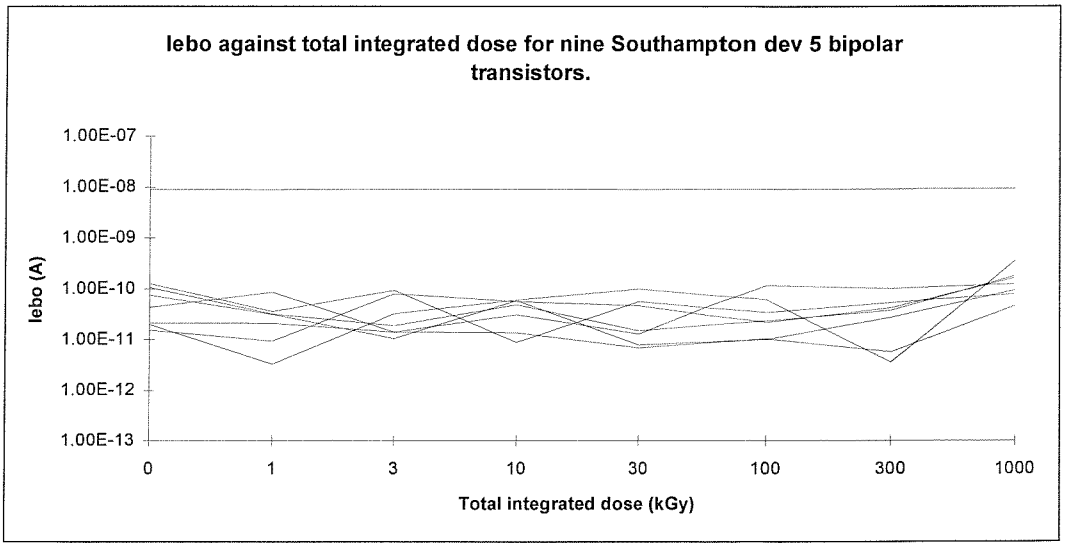

Figure 12.58: Change in Iebo against total dose for SU device 5.

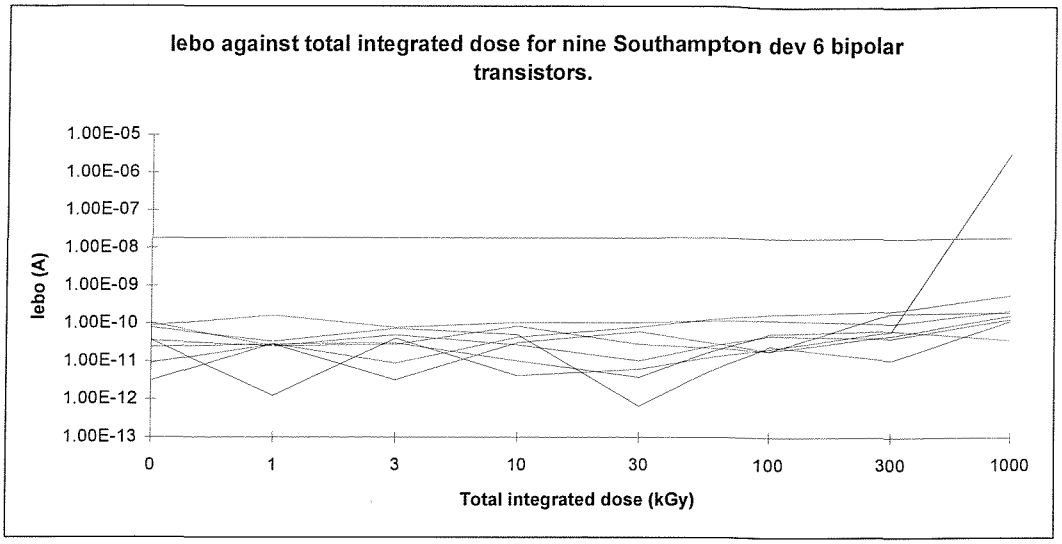

Figure 12.59: Change in Iebo against total dose for SU device 6.

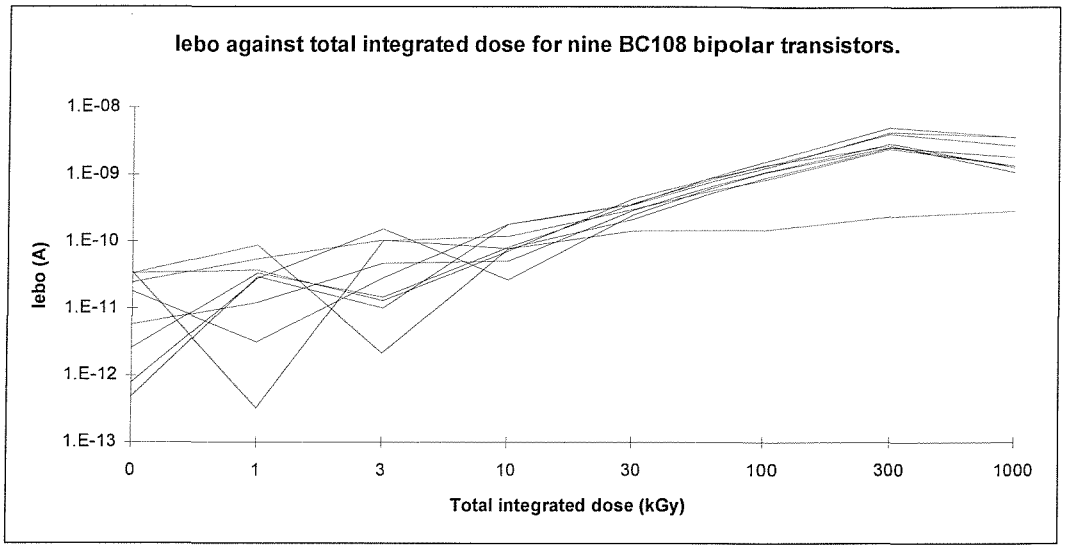

Figure 12.60: Change in Iebo against total dose for BC108 (DS1522).

Despite the very large differences between the Gummel plots for SU devices of a given type, the emitter-base leakage current results show rather closer agreement. Four of the six types have one or two devices with much higher values than the others, indicating a low resistance path somewhere in the structure of these individual devices. Leakage current results for these devices barely change with total dose, showing that this is likely to be due to current flowing around the junction rather than across it, as the latter would be expected to change with irradiation. The majority of the devices exhibit a slightly rising tendency with total dose, increasing by one or two orders of magnitude after a total dose of 1 MGy.

The BC108 devices show a similar, increasing trend, although the magnitude of the increase is rather larger at between two and three orders of magnitude, peaking at a

few nanoamps from a pre-irradiation value of between a few picoamps and a few tens of picoamps.

12.5.2 Collector-base leakage current

This parameter was measured with a collector-base voltage of 20 V, with the emitter open-circuit. The results for the SU devices were similar to those obtained for emitter-base leakage current and so only two examples are shown here.

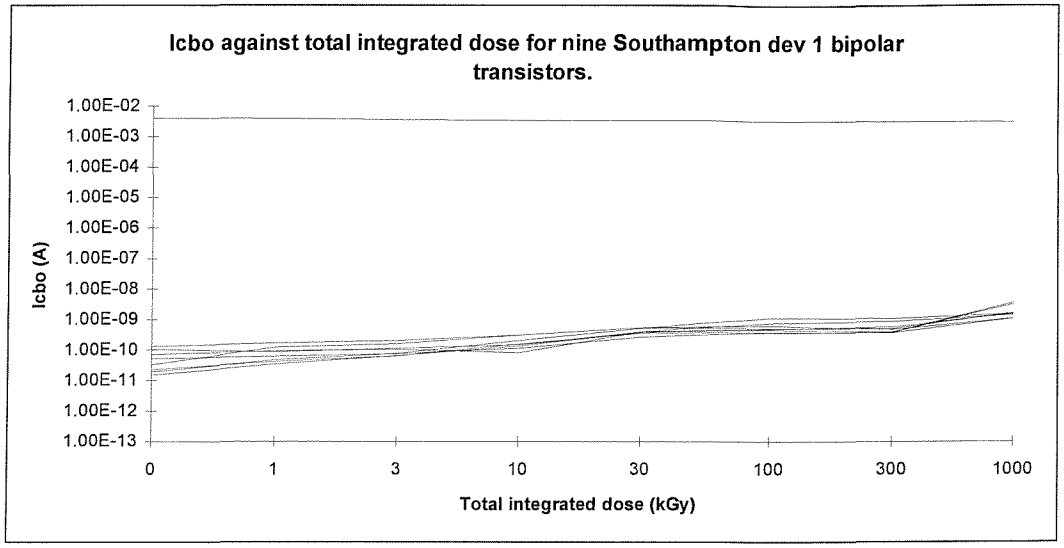

Figure 12.61: Change in Icbo against total dose for SU device 1.

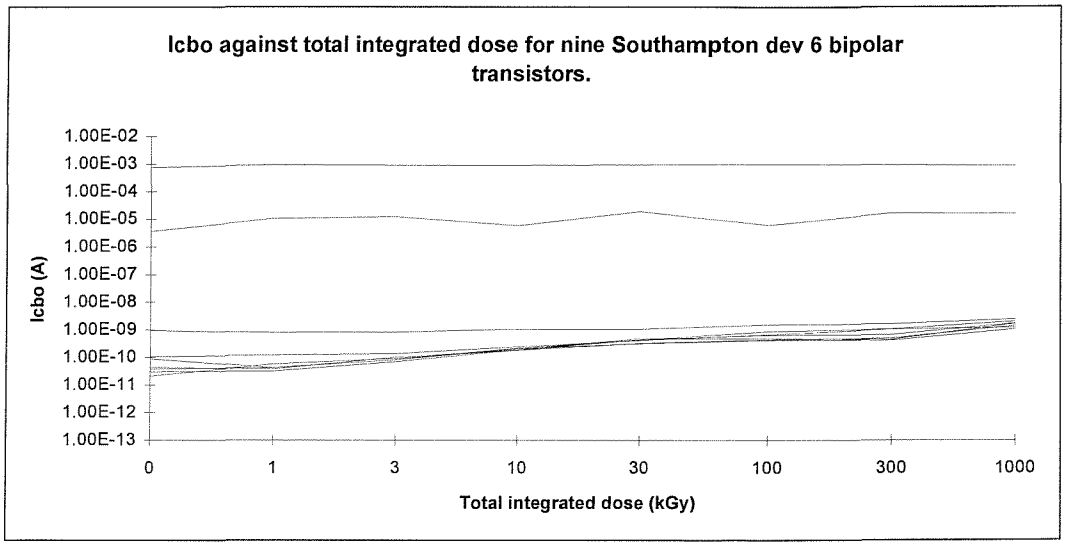

Figure 12.62: Change in Icbo against total dose for SU device 6.

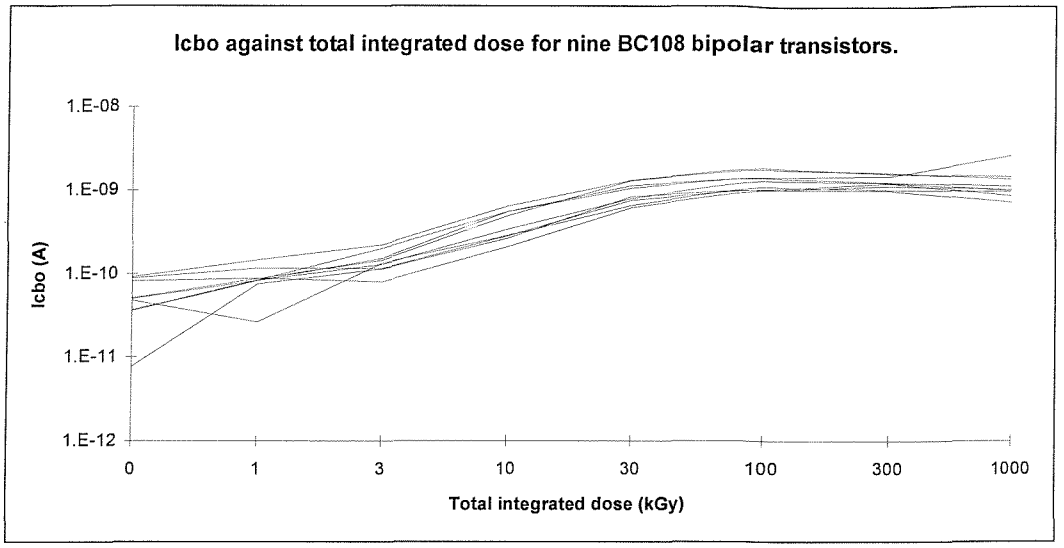

Figure 12.63: Change in Icbo against total dose for BC108 (DS1522).

The majority of the SU devices show a gradually increasing pattern with total dose. Again, occasional devices show an abnormally high and constant value across the range of total dose. The BC108 devices also show an increasing trend, this time of a similar magnitude to that of the SU devices, i.e. between one and two orders of magnitude. Nevertheless, the magnitude of collector-base leakage current remains small, justifying the assumption made in the derivation of equation 6.32 from equation 6.31.

12.5.3 Collector-emitter leakage current

This parameter was measured with a collector-emitter voltage of 20 V, with the base open circuit.

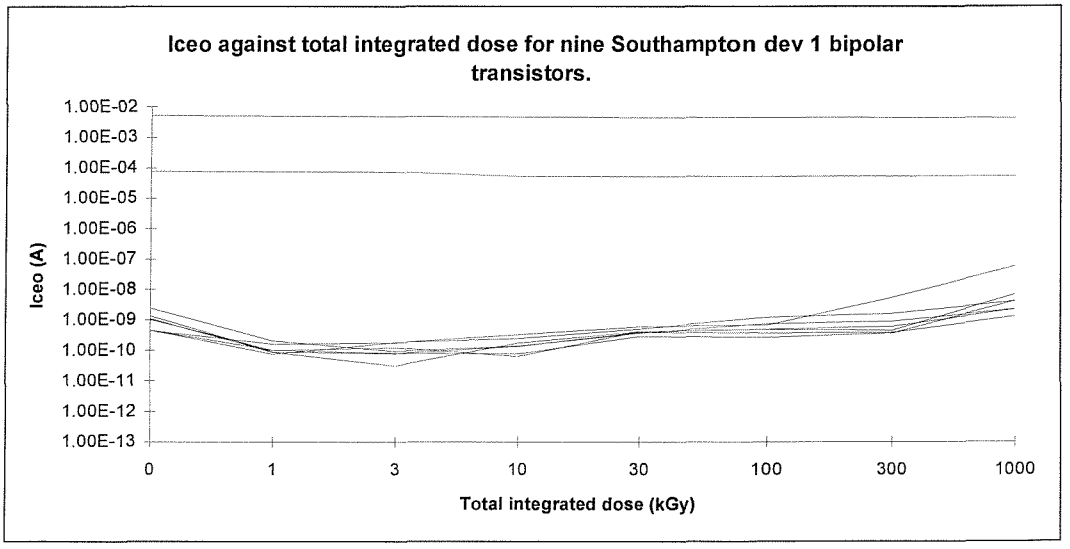

Figure 12.64: Change in Iceo against total dose for SU device 1.

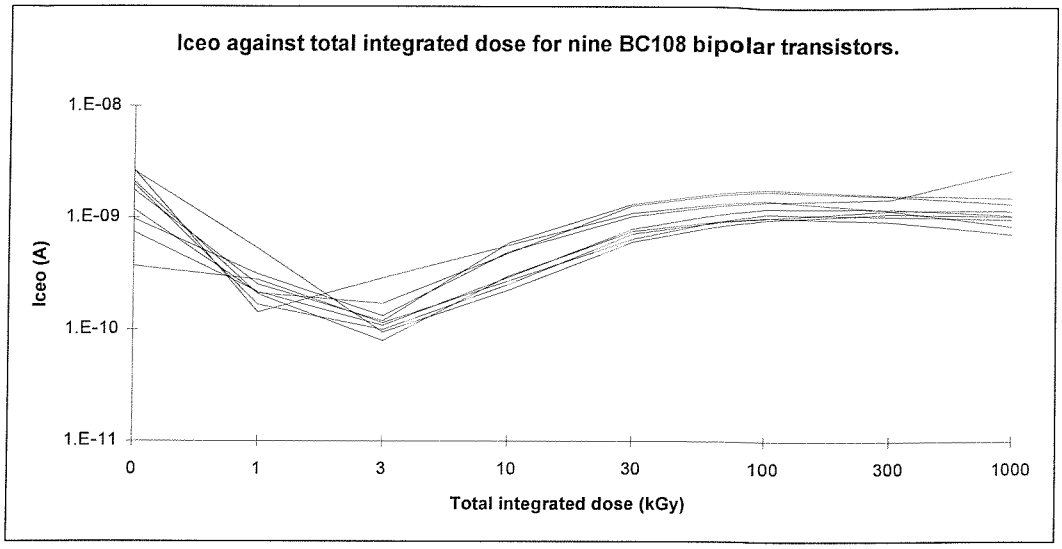

Figure 12.65: Change in Iceo against total dose for BC108 (DS1522).

All the SU devices showed similar results, with a small reduction in collector-emitter leakage current after the first two stages of total dose, followed by a very gradual increase up to 300 kGy. Finally, a more significant increase was observed after the final stage of irradiation, taking the final value of leakage current above the pre-irradiation value. Figure 12.64 is typical of the results for all six types of SU device.

The BC108 devices showed a similar pattern, with a decrease over the first two stages and then an increase at higher values of total dose. One difference was observed after the final stage, where the leakage current was observed the fall slightly for the BC108s, rather than increase further, as occurred for the SU devices.

12.5.4 Saturation voltage

This parameter was measured with a base current of 1 mA and a collector current of 10 mA. The base current was measured with a pulsed signal in order to avoid overheating the device. A pulse width of 1 millisecond was the minimum available with the test equipment and this was used for all the measurements.

It proved difficult to achieve these conditions for many of the SU devices. The data that were obtained show much higher values of saturation voltage than were expected, bearing out the unusual properties exhibited in the Gummel plots. Figure 12.66, for the devices of type 2, is typical.

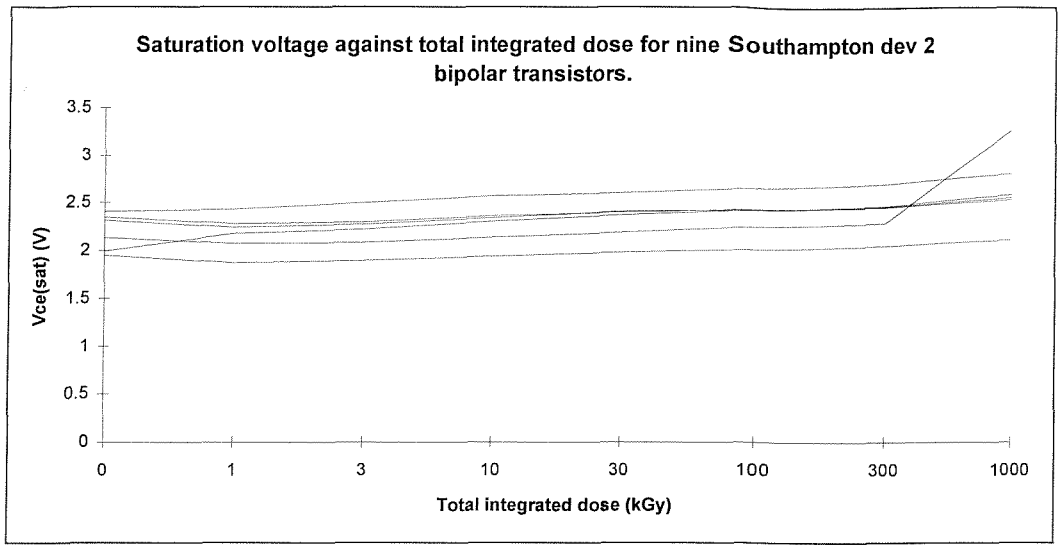

Figure 12.66: Change in saturation voltage against total dose for SU device 2.

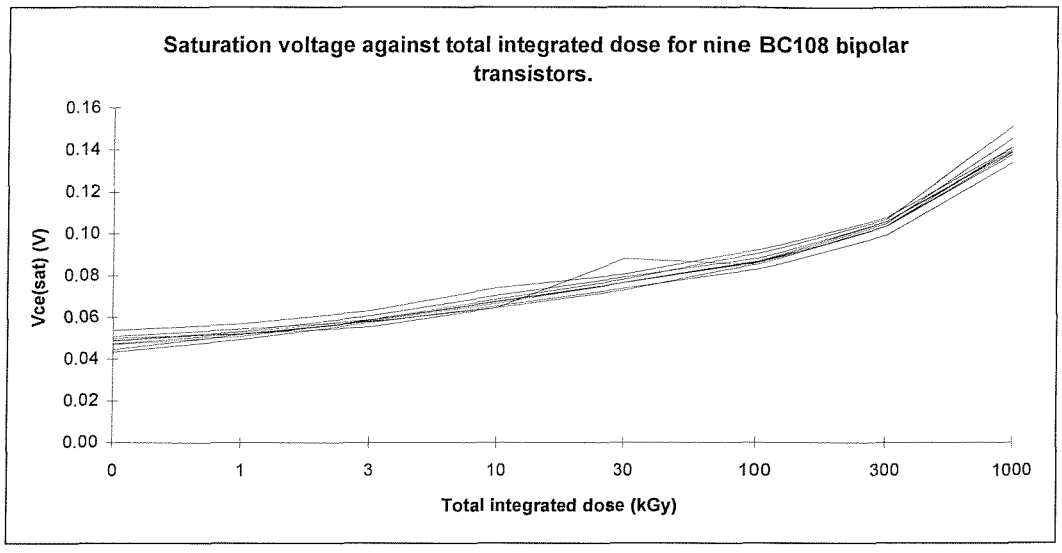

Figure 12.67: Change in saturation voltage against total dose for BC108 (DS1522).

The BC108 data are much better-behaved (figure 12.67). The initial values of saturation voltage are low, considerably below the designer's rule of thumb value of 0.1V. With increasing total dose, the value rises inexorably, reaching a value some three times the pre-irradiation value after a total dose of 1 MGy.

12.5.5 Gain

Gain was measured at four values of collector current (0.01, 0.1, 1 and 10 mA) for each of the SU devices. In every case, the shapes of the curves at the four different currents were very similar. All four curves are shown here for device 1 in order to illustrate this point. In the interests of saving space, this is not repeated for the other

five SU devices, except where there are specific features of interest or significant differences.

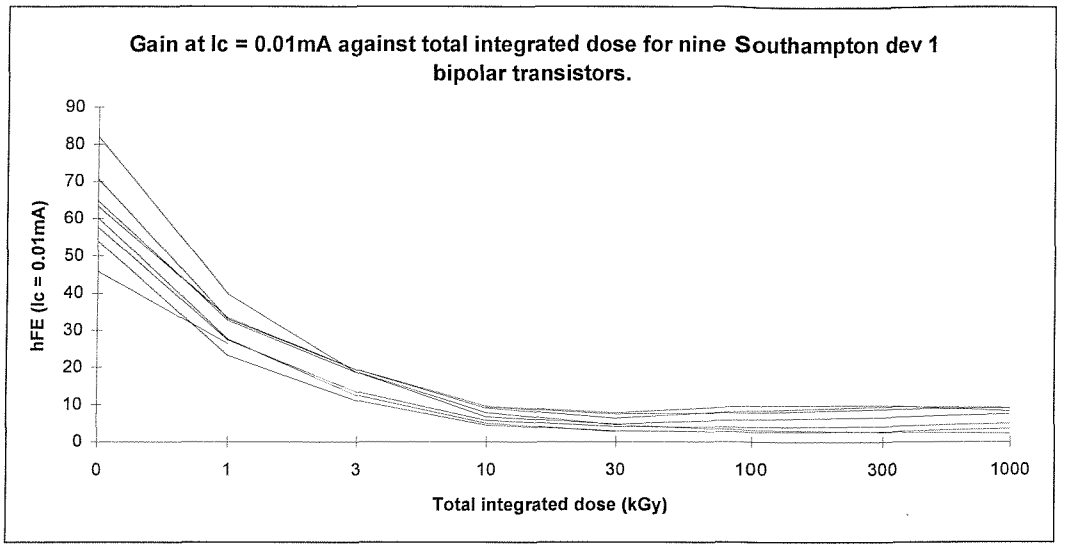

Figure12.68: Change in gain (Ic = 0.01 mA) against total dose for SU device 1.

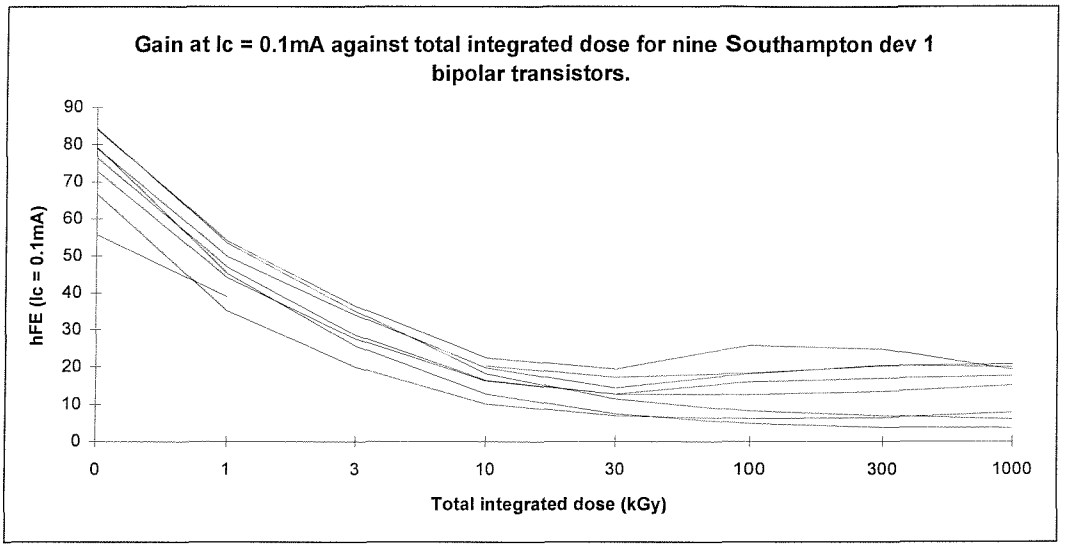

Figure 12.69: Change in gain (Ic = 0.1 mA) against total dose for SU device 1.

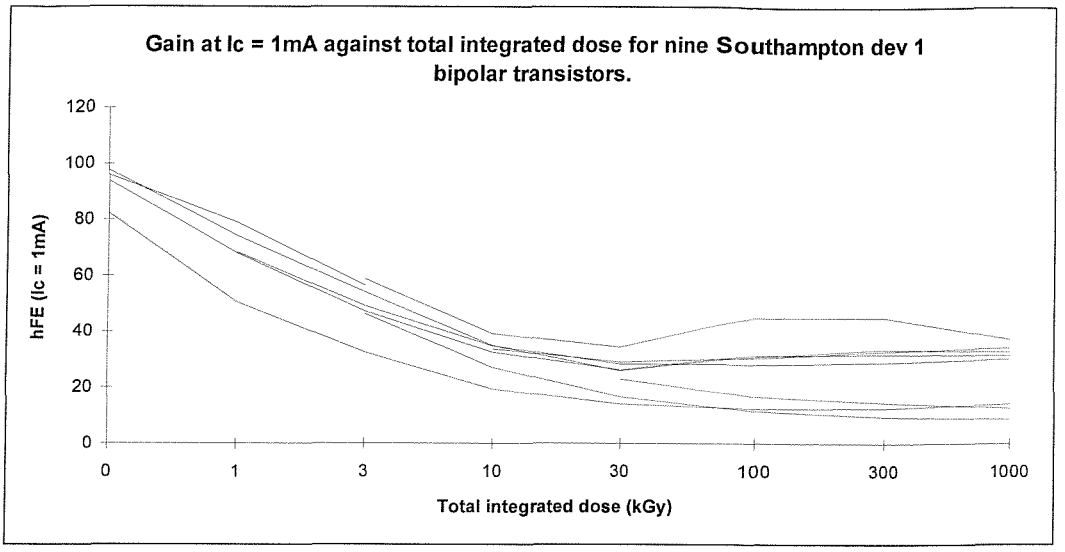

Figure 12.70: Change in gain (Ic = 1 mA) against total dose for SU device 1.

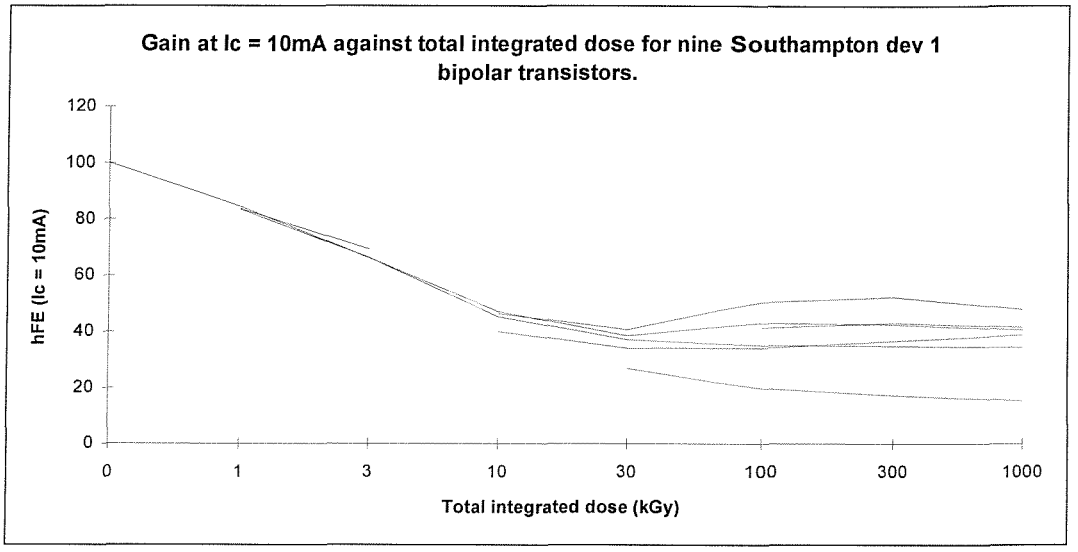

Figure 12.71: Change in gain (Ic = 10 mA) against total dose for SU device 1.

It can be seen that there is a nearly full set of curves at a collector current of 0.01 mA but rather fewer at 1 mA and even fewer at 10 mA. This is because it proved difficult to obtain the higher currents from all the devices, especially before irradiation. As the base current curves moved with increasing total dose, the situation improved in this respect, enabling the current targets to be achieved, albeit as the gain itself fell. This change in the base current curves can be seen clearly in the Gummel plots in section 12.4 above.

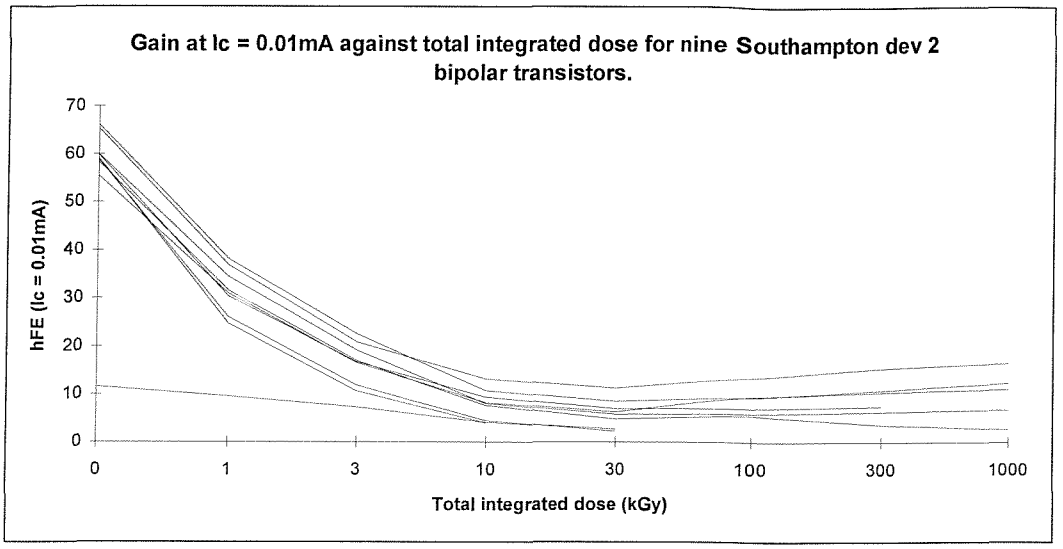

Figure 12.72: Change in gain (Ic = 0.01 mA) against total dose for SU device 2.

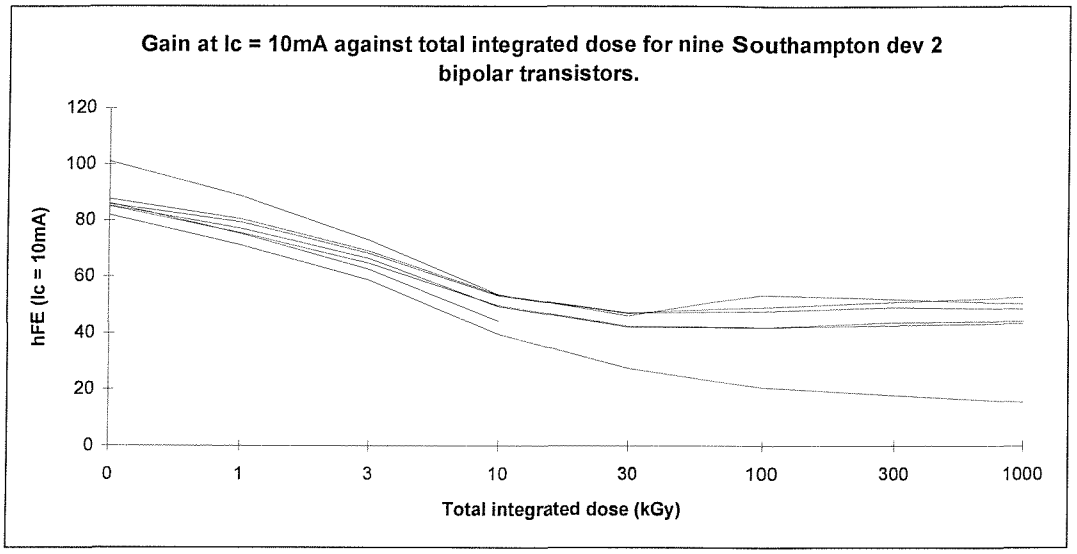

Figure 12.73: Change in gain (Ic = 10 mA) against total dose for SU device 2.

Some differences are apparent between the graphs for SU devices of types 1 and 2. At a collector current of 0.01 mA the curves decrease, as per the devices of type 1, but then rise noticeably at total doses in the range from 100 kGy to 1 MGy. At 10 mA, more devices were able to deliver the required current before irradiation. These separated into two distinct groups at the higher total doses, with the gain for one group continuing to fall with total dose while, for the other group, the gain fell and then rose in the same manner as for the lower current values.

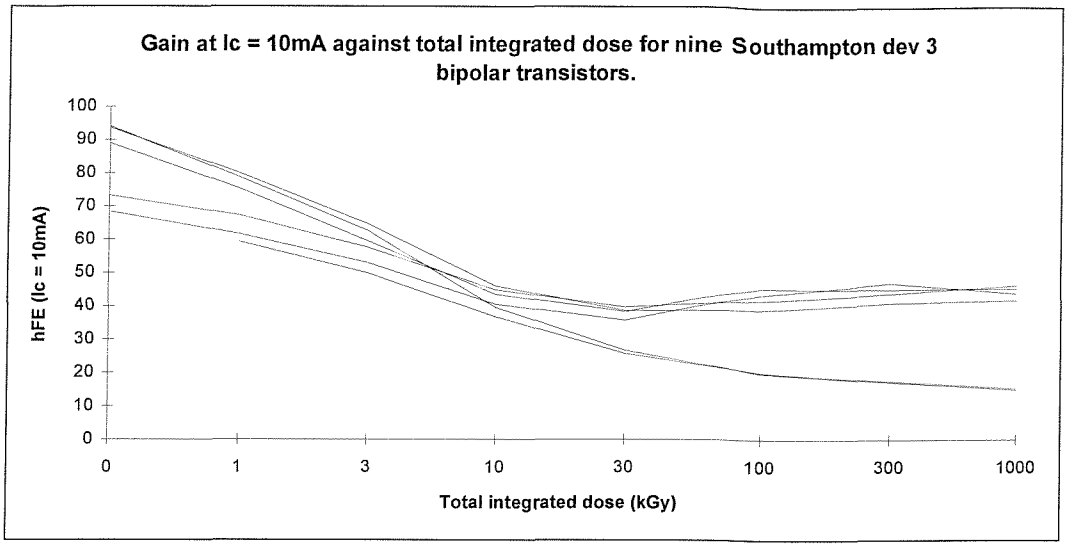

Figure 12.74: Change in gain (Ic = 10 mA) against total dose for SU device 3.

The type 3 devices showed curves very similar to those for types 1 and 2. At a collector current of 10 mA, the separation into two groups can again be seen.

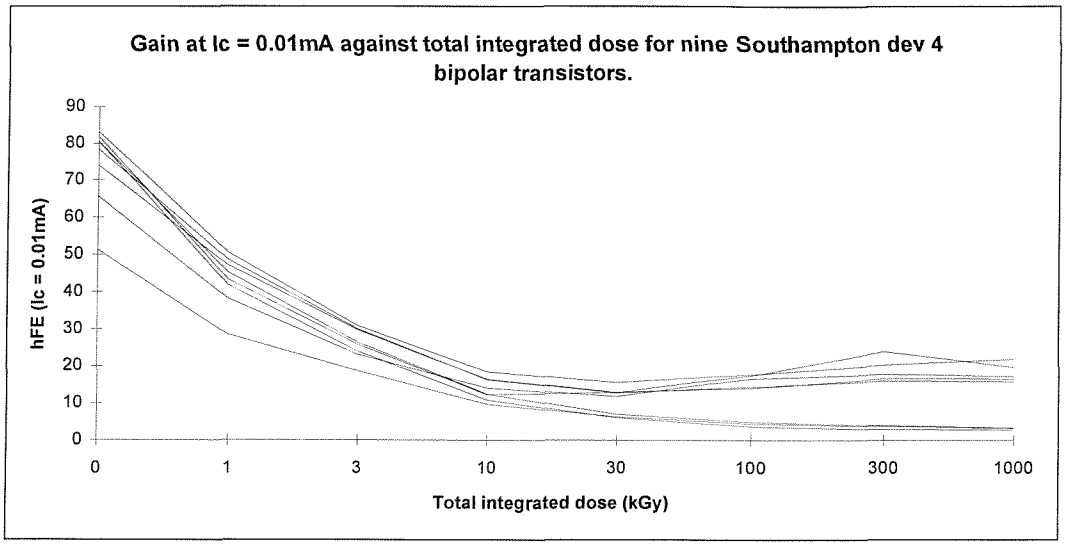

Figure 12.75: Change in gain (Ic = 0.01 mA) against total dose for SU device 4.

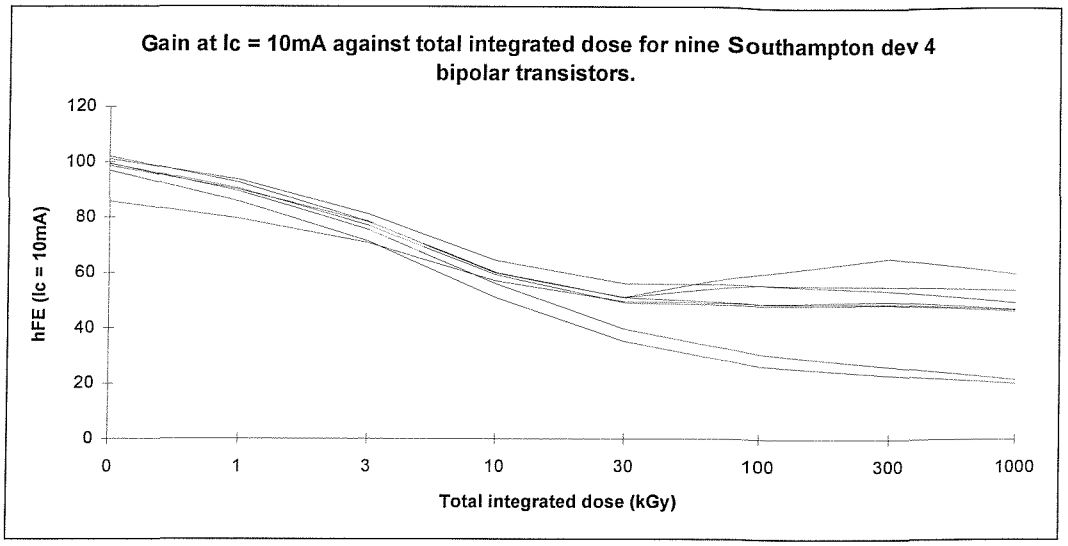

Figure 12.76: Change in gain (Ic = 10 mA) against total dose for SU device 4.

The type 4 devices presented results similar to those of the previous three types. In this case, the separation into two groups at the higher total doses was apparent across the whole range of collector current values.

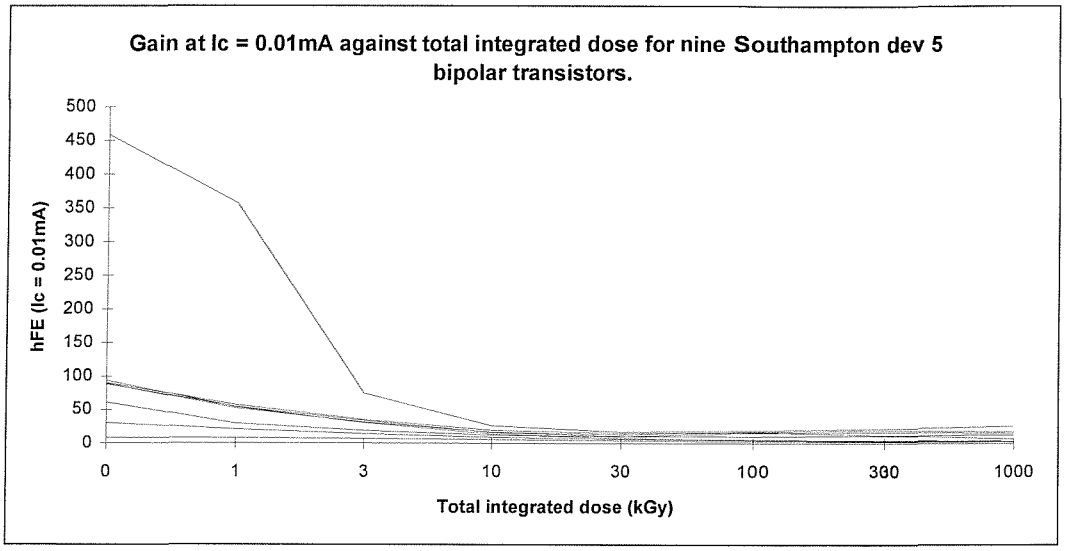

Figure 12.77: Change in gain (Ic = 0.01 mA) against total dose for SU device 5.

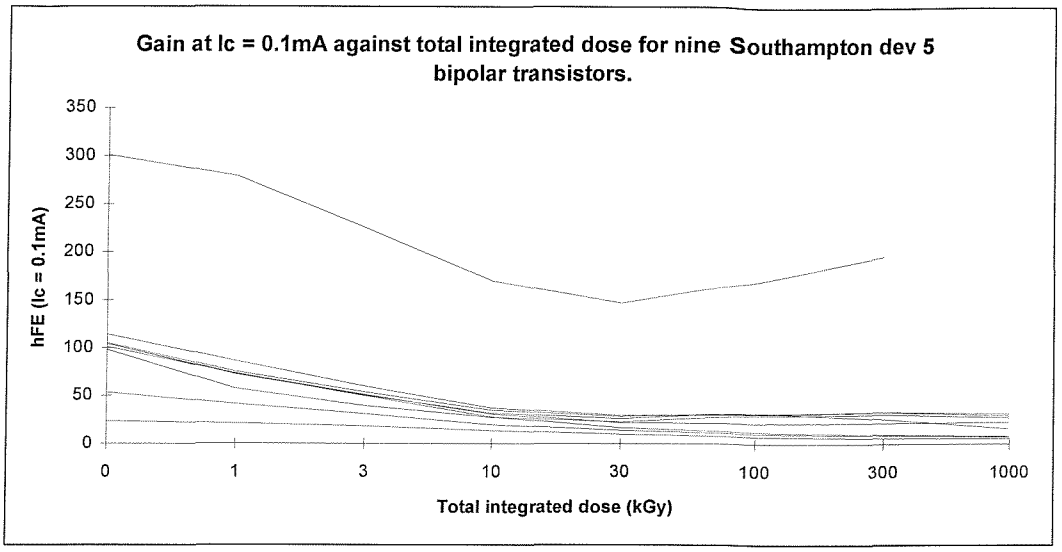

Figure 12.78: Change in gain (Ic = 0.1 mA) against total dose for SU device 5.

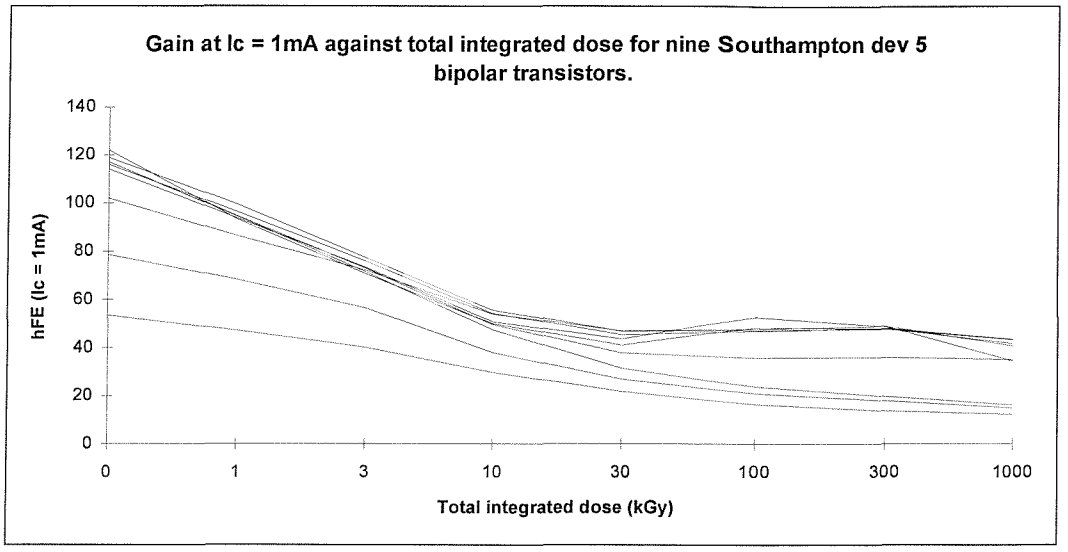

Figure 12.79: Change in gain (Ic = 1 mA) against total dose for SU device 5.

The devices of type 5 exhibited a rather different pattern of values for gain, compared with types 1 to 4. One device showed a much higher value than all the others before irradiation, when measured at a collector current of 0.01 or 0.1 mA. This was not the case at 1 or 10 mA, although the mean gain was higher for these devices than for any others. At the higher stages of total dose, the pattern became similar to that seen for the other types of device.

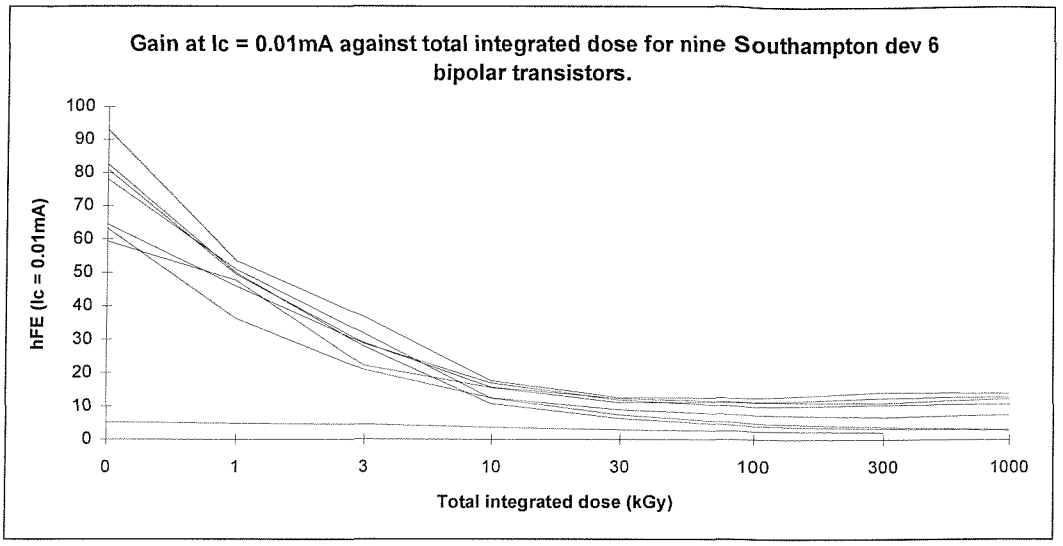

Figure 12.80: Change in gain (Ic = 0.01 mA) against total dose for SU device 6.

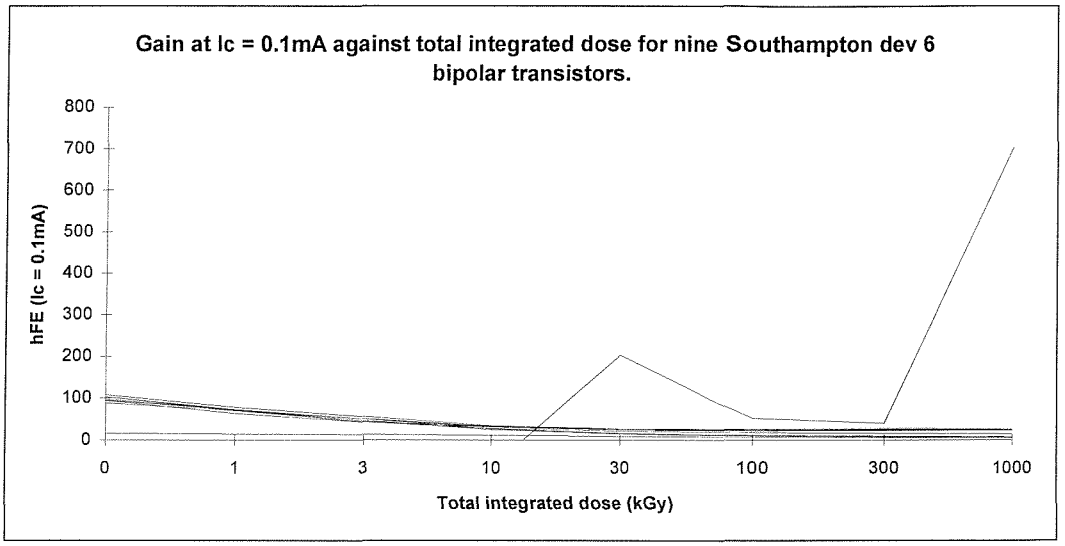

Figure 12.81: Change in gain (Ic = 0.1 mA) against total dose for SU device 6.

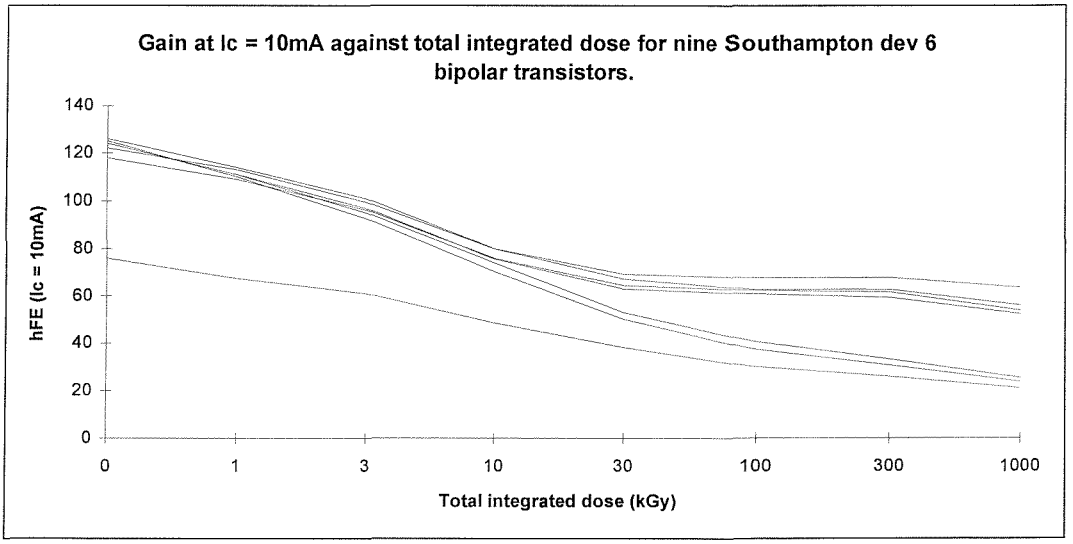

Figure 12.82: Change in gain (Ic = 10 mA) against total dose for SU device 6.

The response to radiation of gain for the type 6 devices proved to be rather different from that for the other types. At collector currents of 0.01 and 0.1 mA, one device started with a very low value of gain and this barely changed with irradiation, indicating that the device was not functioning properly at all. The curve for this same device can be seen as the lowest trace on the graph at 10 mA (figure 12.82), where it does not appear to be behaving in an unexpected manner. The other devices showed results similar to those for the previous types.

At 0.1 mA, most of the devices again followed the previous trends, although one was exceptional, apparently indicating a value of gain that increased considerably as total dose increased. However, this device also returned negative values of gain at each of the first four stages of total dose, when measured at this collector current. It also returned incomplete and/or negative values at collector currents of 0.01 and 10 mA, although the data at 1 mA were similar to those for the other devices.

The graph at 10 mA is similar to that for the devices of types 2, 3 and 4.

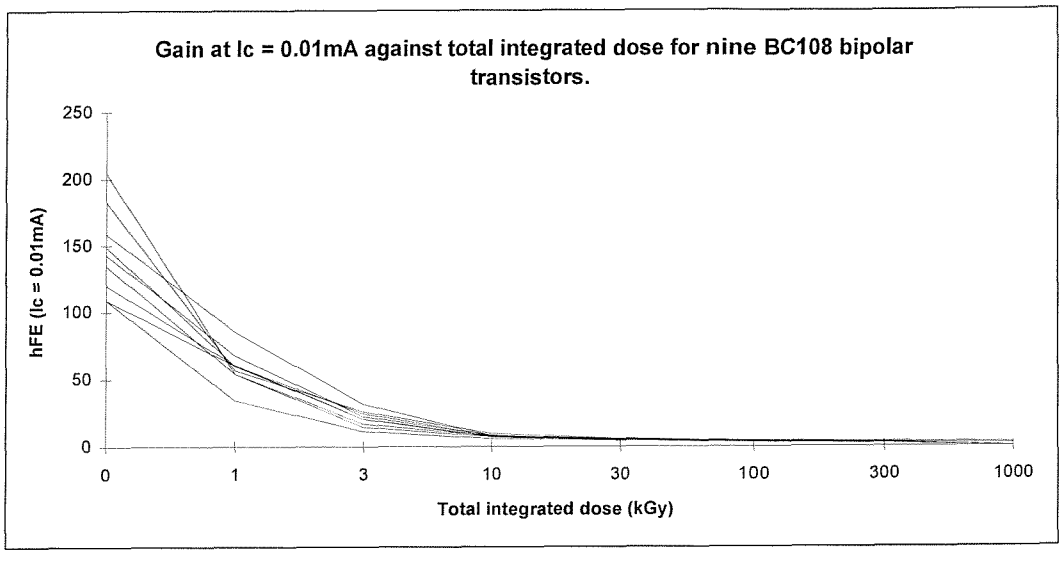

Figure 12.83: Change in gain (Ic = 0.01 mA) against total dose for BC108 (DS1522).

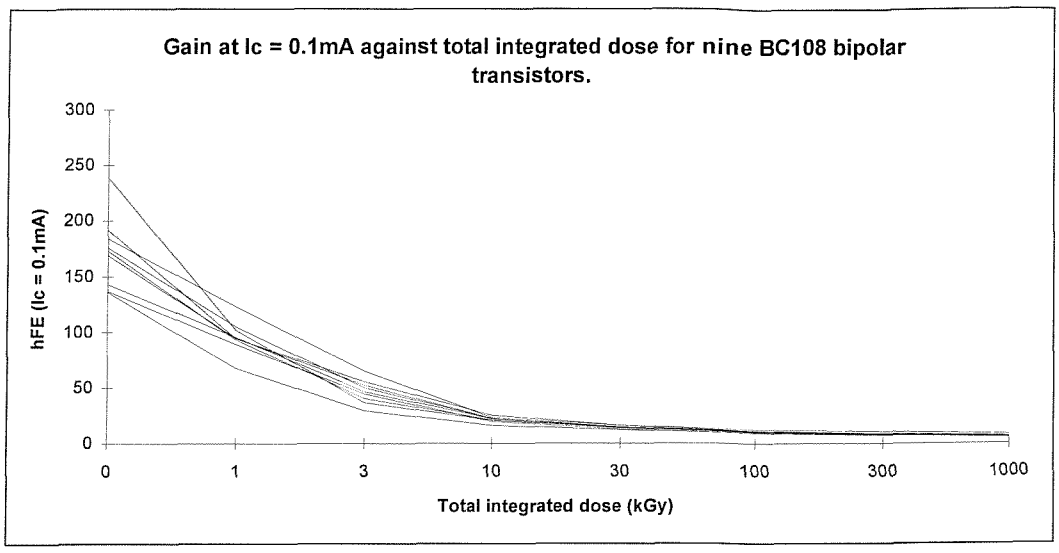

Figure 12.84: Change in gain (Ic = 0.1 mA) against total dose for BC108 (DS1522).

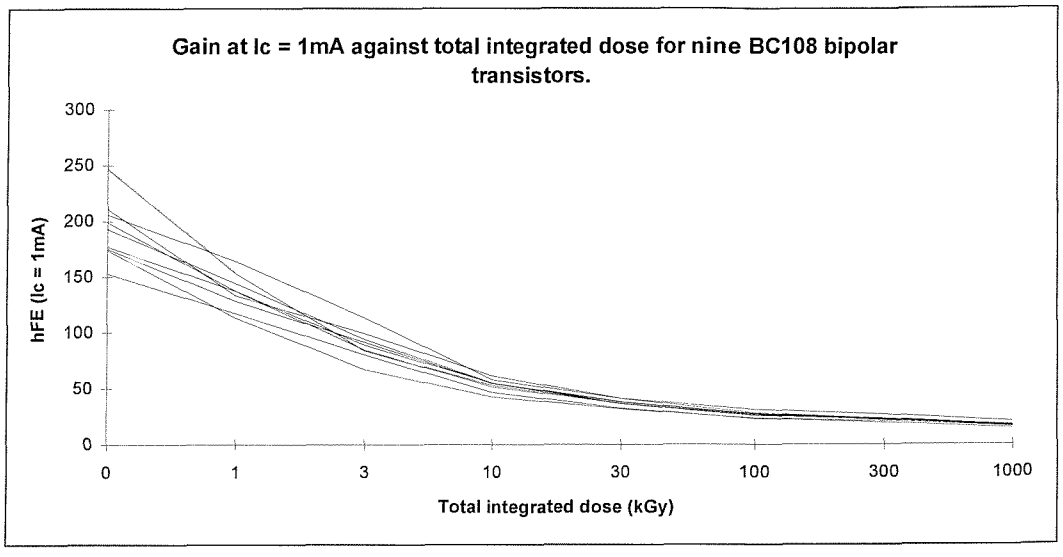

Figure 12.85: Change in gain (Ic = 1 mA) against total dose for BC108 (DS1522).

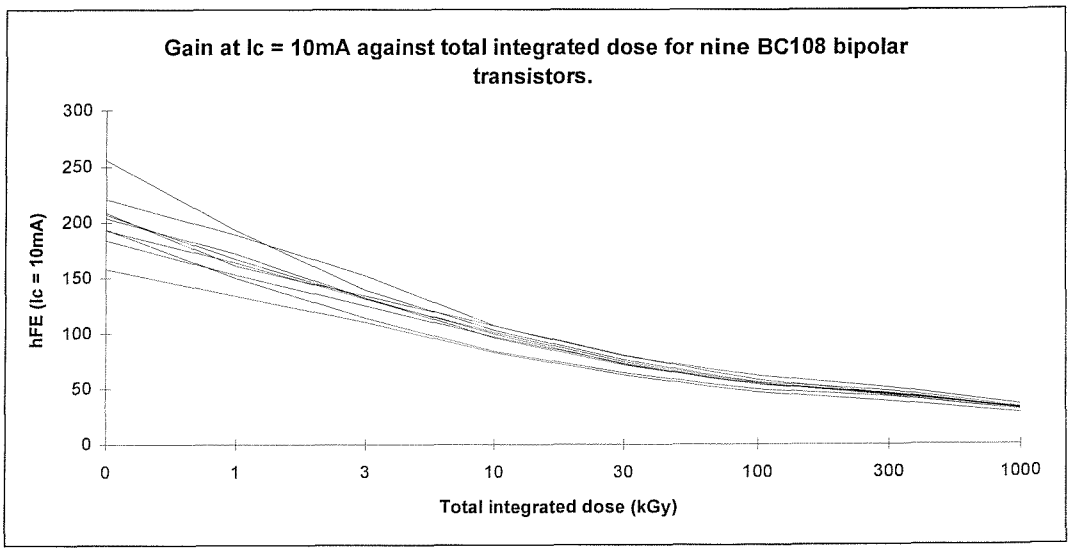

Figure 12.86: Change in gain (Ic = 10 mA) against total dose for BC108 (DS1522).

The graphs for the BC108 devices all show a monotonic decrease of gain with total dose. This is relatively unusual as many previous results, as shown above, include a slight rise at around 100 to 300 kGy. The graphs at all four values of collector current are substantially similar in shape, with a moderately higher rate of degradation at the lower values of current.

12.5.6 Emitter-base breakdown voltage

This parameter was measured with an emitter-base current of 0.01 mA, with the collector open circuit.

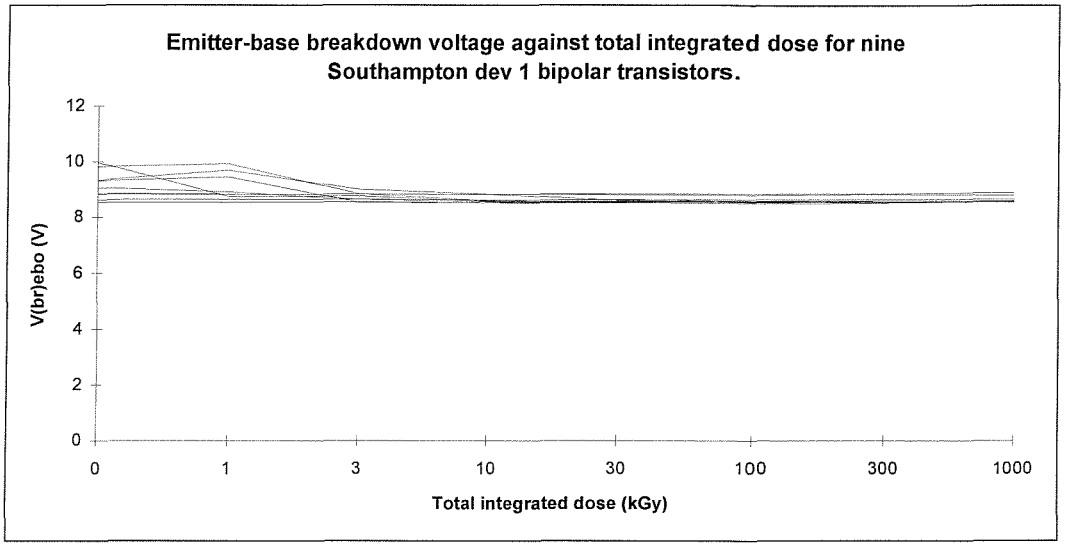

Figure 12.87: Change in V(BR)ebo against total dose for SU device 1.

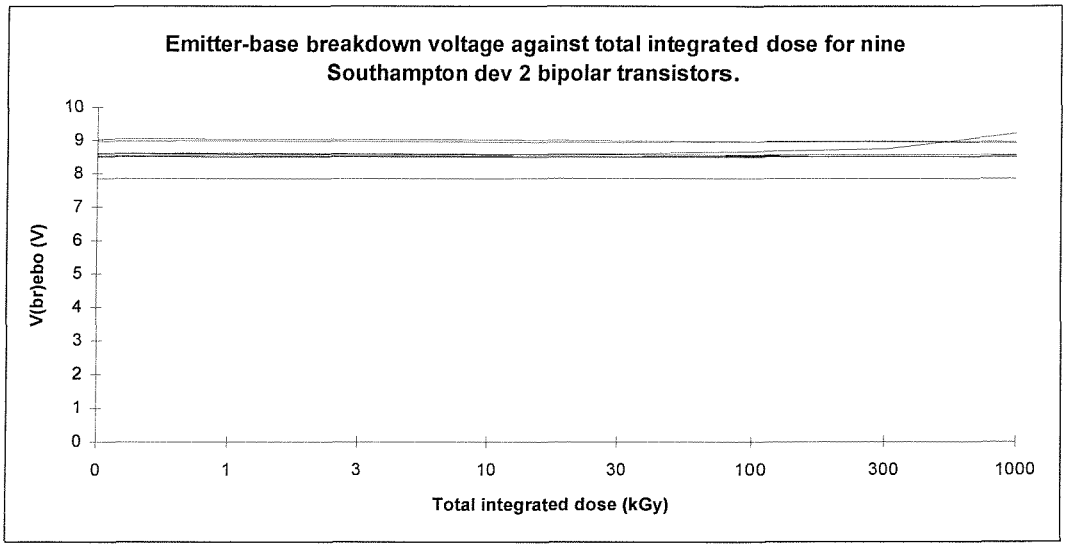

Figure 12.88: Change in V(BR)ebo against total dose for SU device 2.

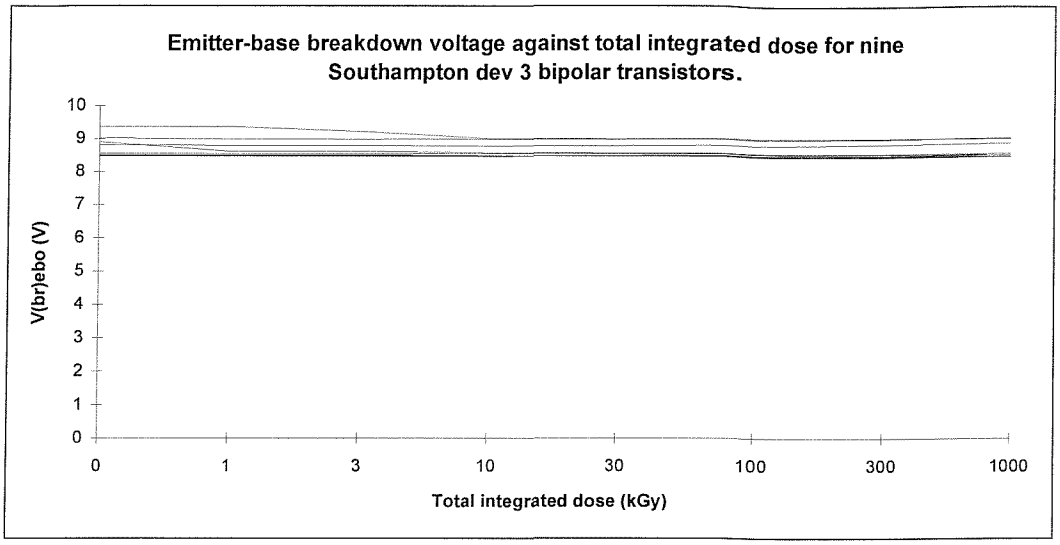

Figure 12.89: Change in V(BR)ebo against total dose for SU device 3.

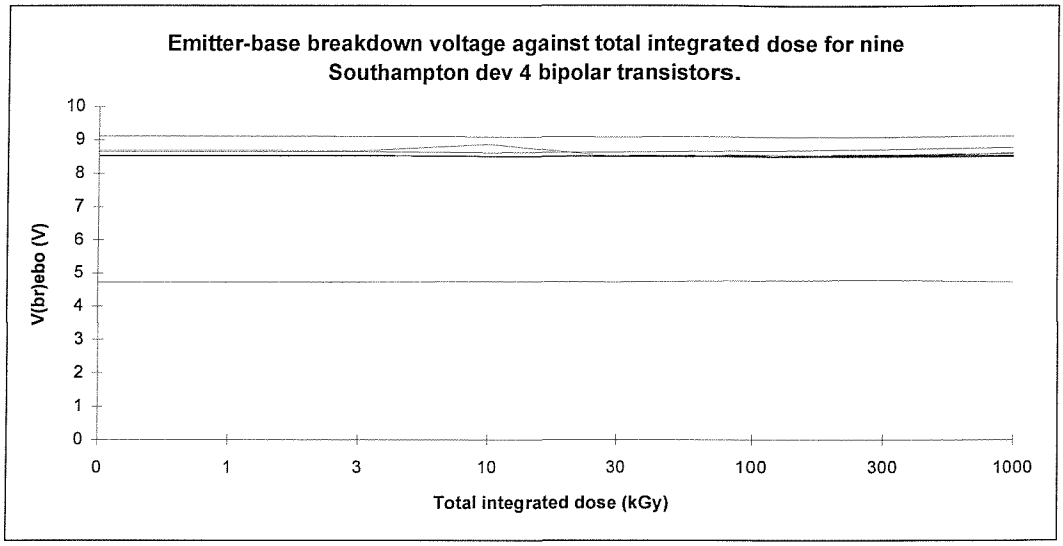

Figure 12.90: Change in V(BR)ebo against total dose for SU device 4.

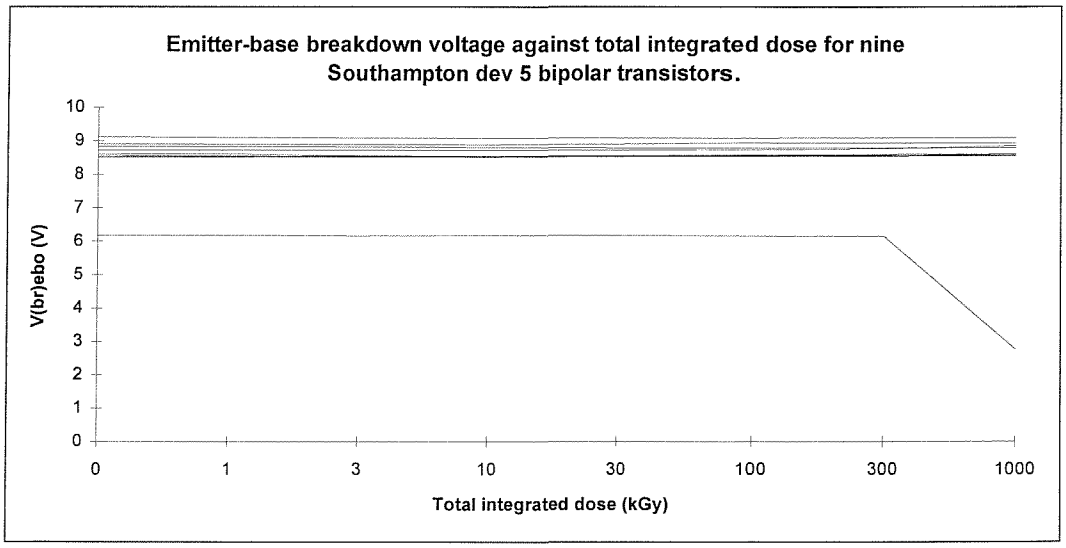

Figure 12.91: Change in V(BR)ebo against total dose for SU device 5.

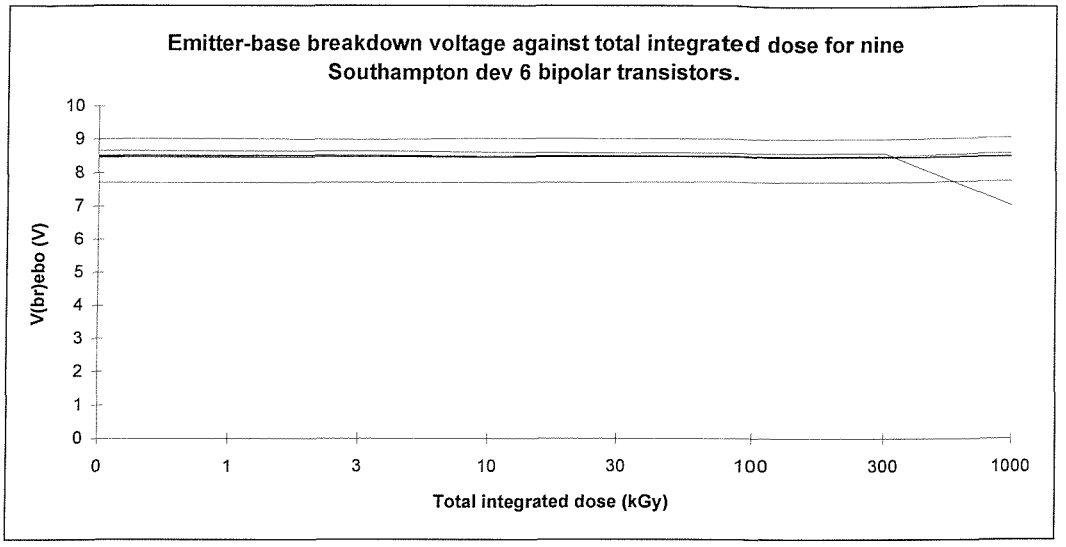

Figure 12.92: Change in V(BR)ebo against total dose for SU device 6.

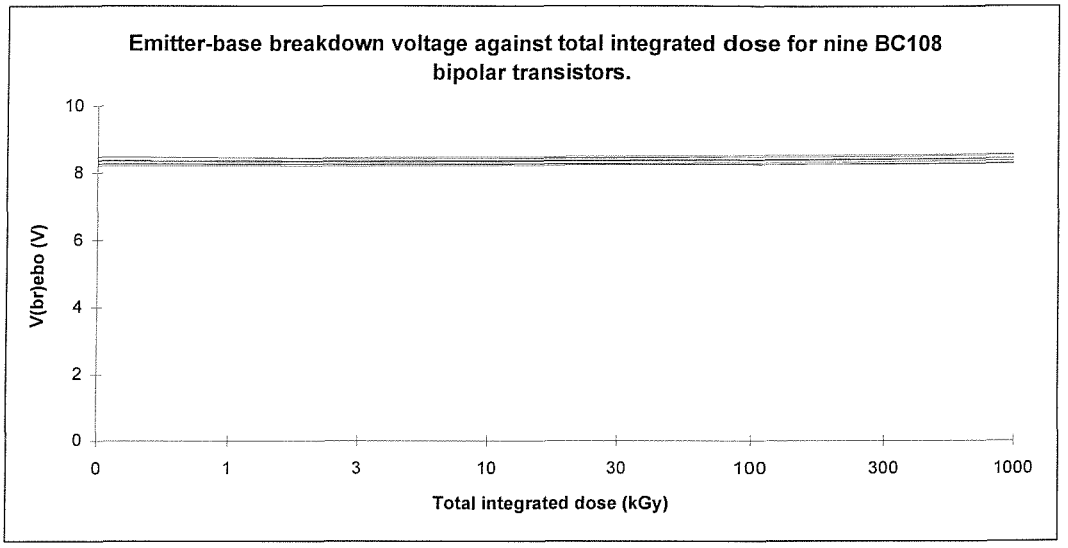

Figure 12.93: Change in V(BR)ebo against total dose for BC108 (DS1522).

Emitter-base breakdown voltage remained essentially unchanged with total dose for all the SU devices and for the BC108 transistors. A small number of exceptions was identified, with one device of types 5 and 6 in package number 6 showing a decrease after a total dose of 1 MGy and a different device showing an increase after 1 MGy. Furthermore, most of the devices of type 1 showed some variability over the first three stages of total dose, before settling down to a stable response.

12.5.7 Collector-base breakdown voltage

This parameter was measured with a collector-base current of 0.01 mA, with the emitter open circuit.

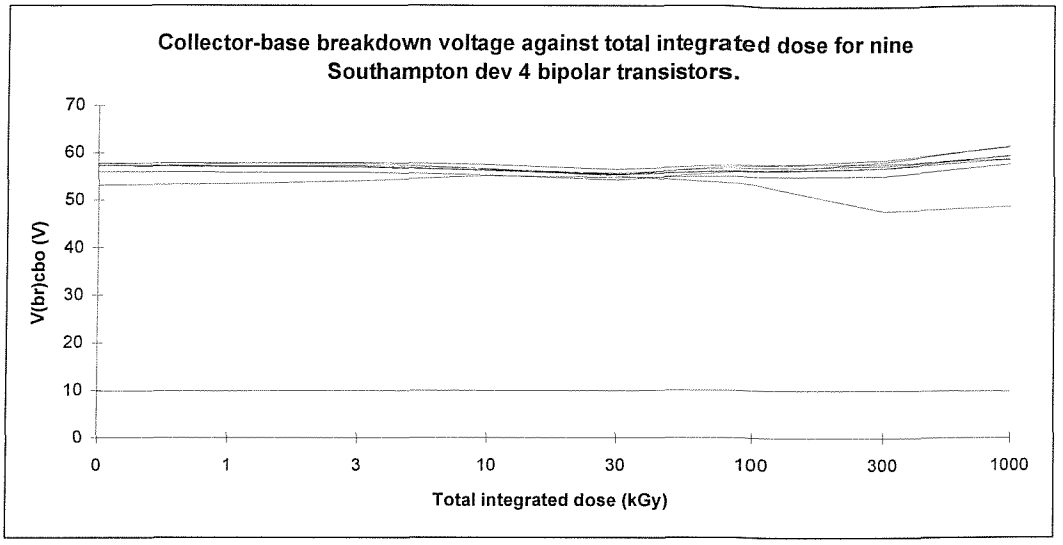

Figure 12.94: Change in V(BR)cbo against total dose for SU device 4.

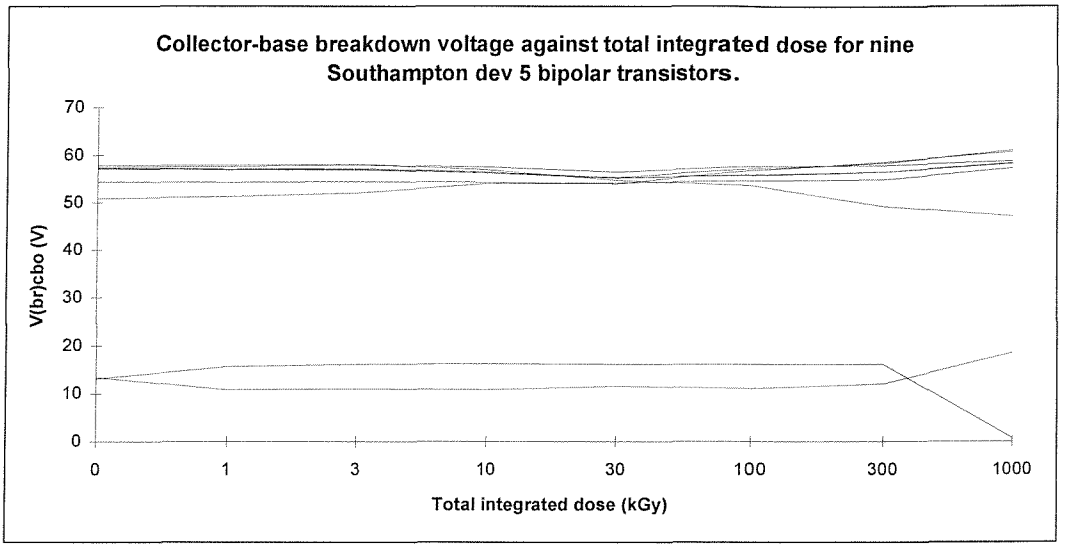

Figure 12.95: Change in V(BR)cbo against total dose for SU device 5.

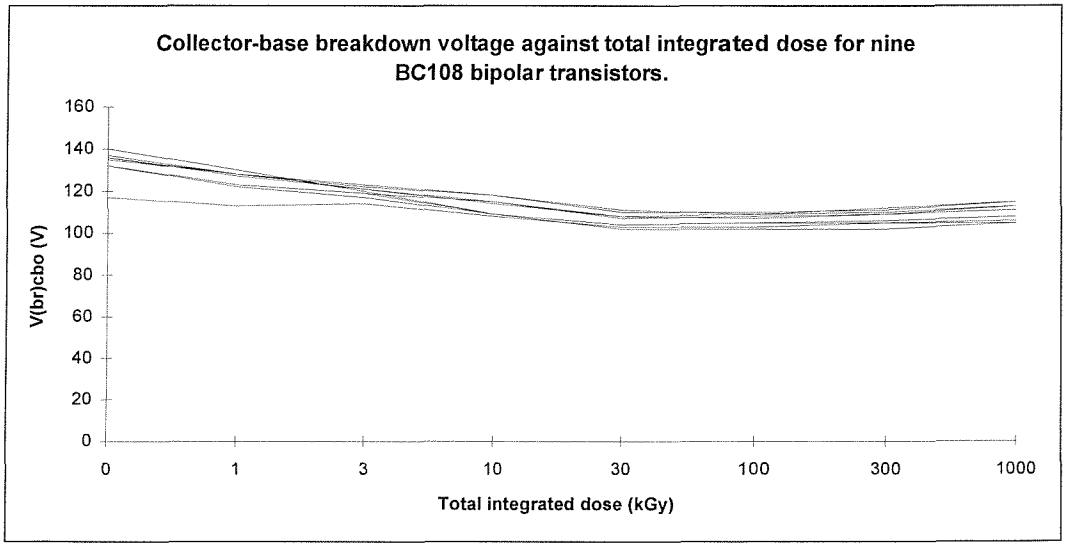

Figure 12.96: Change in V(BR)cbo against total dose for BC108 (DS1522).

Collector-base breakdown voltage also exhibited a broadly stable trend with total dose. The SU devices showed a slight increase at 300 kGy and 1 MGy, although this was only of the order of 5%. In each case, one or two devices showed unusual values, indicating inconsistency in the structure across the batch. The response was similar for all the types of SU device and so only two graphs are shown here.

The BC108 devices showed a declining trend as total dose increased, reaching a stable plateau after some 30 kGy, at around 85% of the pre-irradiation values.

12.5.8 Collector-emitter breakdown voltage

This parameter was measured with a collector-emitter current of 10 mA, with the base open circuit.

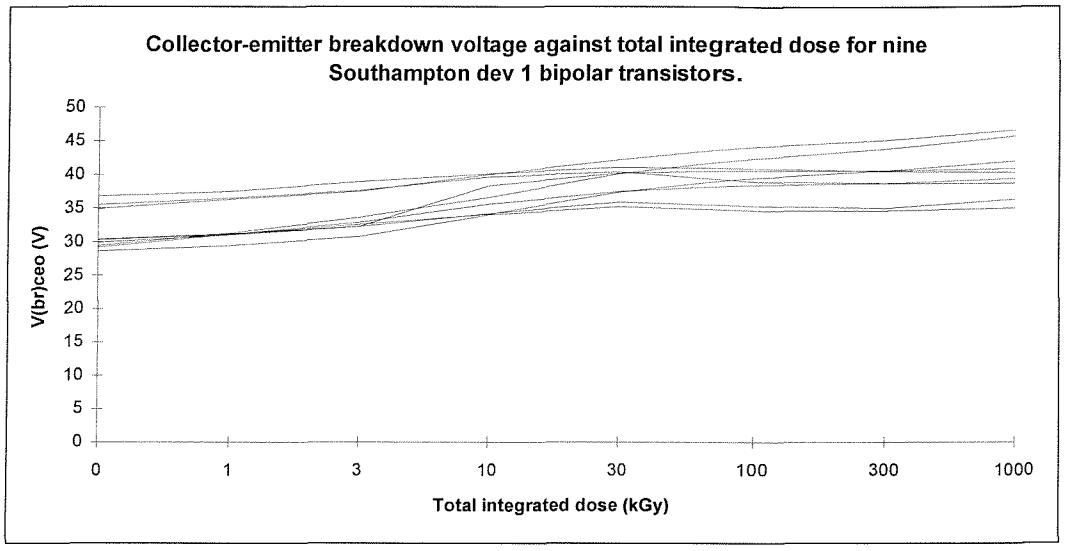

Figure 12.97: Change in V(BR)ceo against total dose for SU device 1.

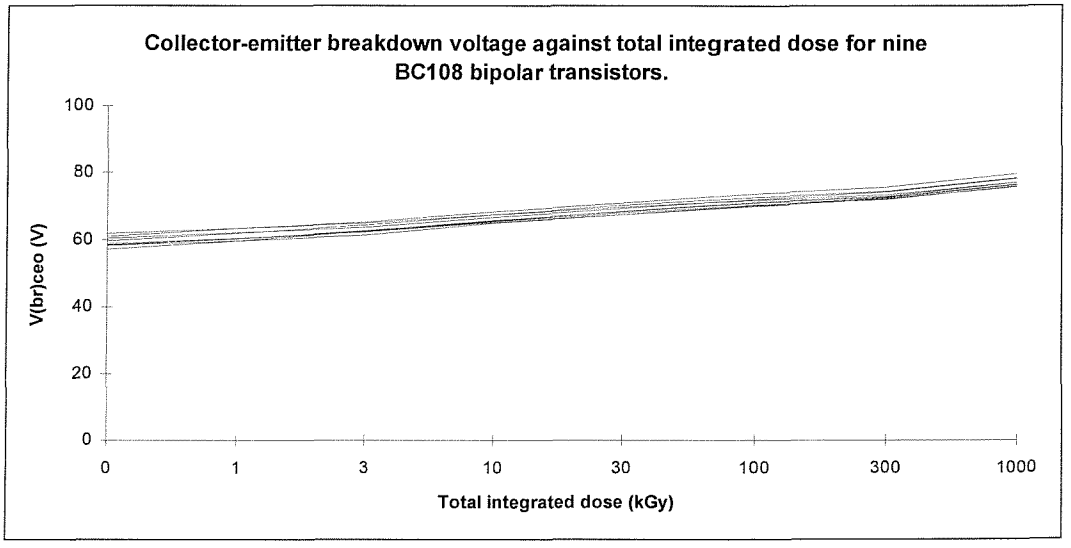

Figure 12.98: Change in V(BR)ceo against total dose for BC108 (DS1522).

The response of collector-emitter breakdown voltage to irradiation was very similar for all the SU devices and so only the graph for type 1 is shown here. The range of pre-irradiation values was from 25 to 40V. A gradual increase is observed, rising by around one third after a total dose of 1 MGy.

The same trend is seen for the BC108 devices, although the data here are grouped together more tightly than for the SU devices.

12.5.9 Base-emitter breakdown voltage

This parameter (the forward voltage drop) was measured with a base-emitter current of 0.01 mA, with the collector open circuit.

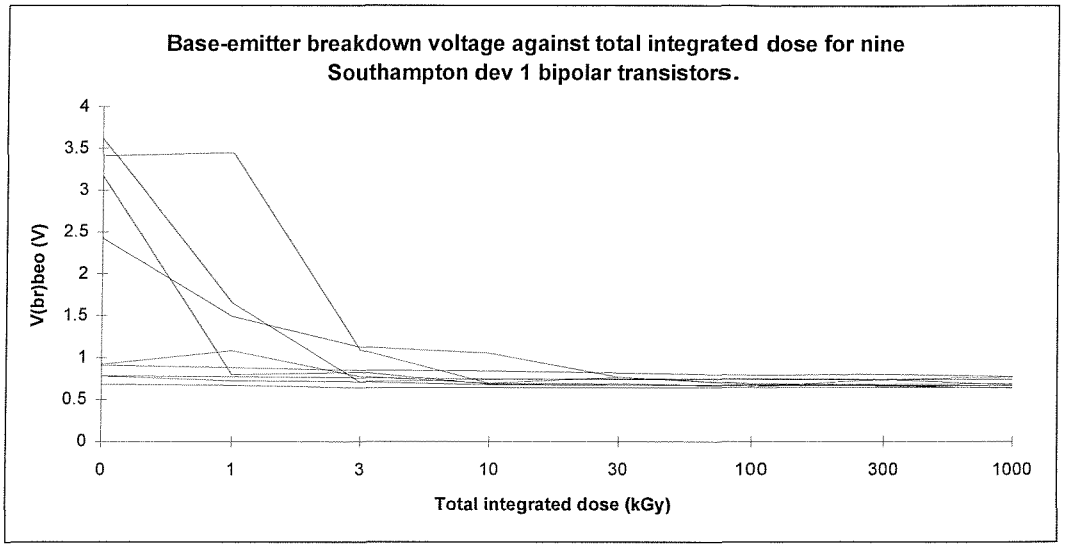

Figure 12.99: Change in V(BR)beo against total dose for SU device 1.

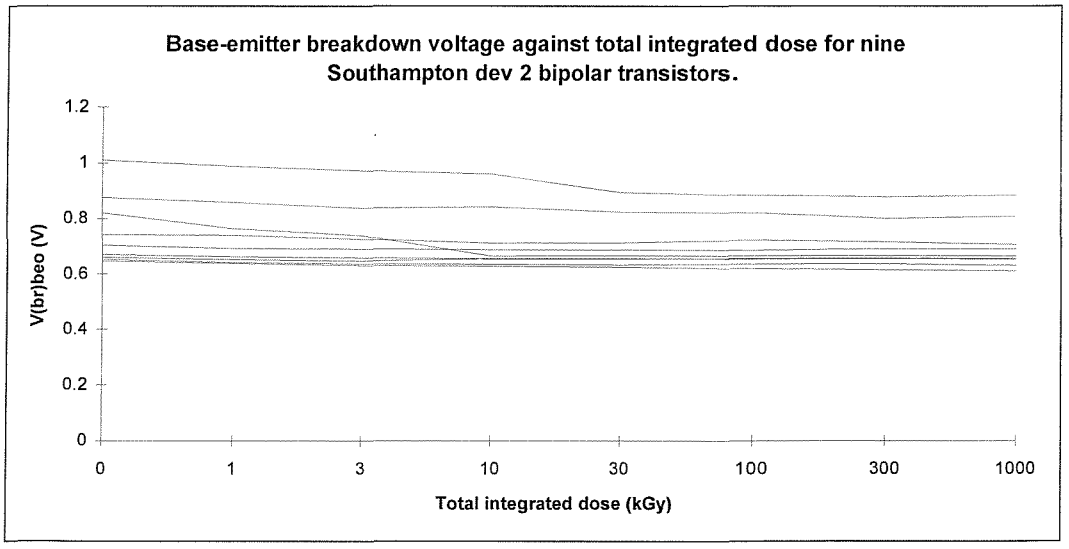

Figure 12.100: Change in V(BR)beo against total dose for SU device 2.

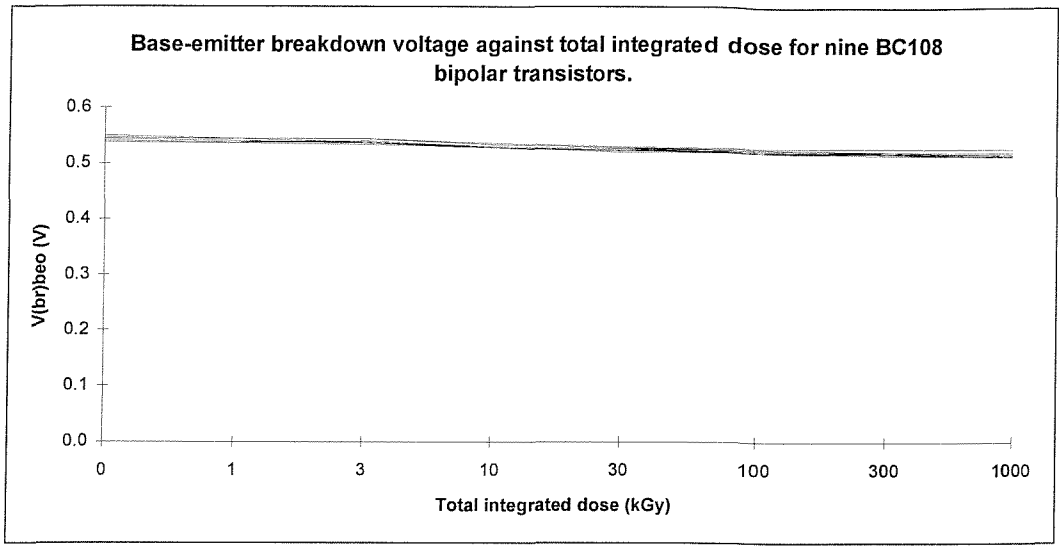

Figure 12.101: Change in V(BR)beo against total dose for BC108 (DS1522).

The forward voltage drop shows a wider degree of variability between the different types of SU device than does any of the other voltage measurements. Most of the devices have a value before irradiation of between 0.7 and 1.0 V, although some are as high as 3.5 V. The response of many of the devices to irradiation is very small but some of the higher values show a sharp reduction during the early stages of total dose. The devices of type 1 illustrate this most clearly, as can be seen in figure 12.99. The graphs for the devices of types 3 to 6 show no additional information to those included for types 1 and 2 above.

Figure 12.101 shows that values for the BC108 devices all start at around 0.55 V, falling slightly to 0.5 V after a total dose of 1 MGy.

12.6 C-V DATA

The phase 1 tests did not include C-V measurements as the equipment was not available at that time. Once it became possible to characterise the C-V response of devices then this technique was added to the portfolio of measurements made on the test samples. The instrumentation has been described above and was used initially for tests on the SU devices manufactured for this study and subsequently on a batch of COTS transistors for comparison purposes.

Relatively little information on the change in C-V characteristics of bipolar transistors with irradiation is available in the literature, despite there being a great deal of material relating to the investigation of traps in MOS capacitors and devices. Hence, the experimental set-up and measurement conditions were developed specifically for this

work over a number of iterations by use of fixed capacitors and COTS bipolar transistors. The optimum combination of voltage, sweep rate and number of measurement points was developed for these devices, ensuring that the process of taking the readings did not damage the test samples, produced the required data and did not take too long a time. The final version of the test software enabled some 120 readings over a bias voltage range from –1 to +5 V to be taken in approximately one minute. This was carried out at the two frequencies of applied voltage available from the instrumentation, 100 kHz and 1 MHz. It was not clear at the outset whether taking data at the two frequencies would prove useful or would show any differences. However, as the instrumentation was capable of making the measurements and the time penalty was not too onerous, both were included in the test regime. The data at the two frequencies eventually proved to be similar and so the majority of the plots presented here are at just 100 kHz.

Quasistatic C-V measurements, useful for investigating interface traps, were not possible with the instrumentation available. However, interface states are likely to affect the properties of bipolar transistors only in the low to moderate total dose region, as described above, and so this was not thought to be a significant impediment to the work.

12.6.1 SU devices

Figures 12.102 to 12.105 show the collector-base and emitter-base C-V plots at 100 kHz and 1 MHz, respectively, for device 1 in package number 1, over a voltage range from 0 to 5 volts, i.e. in the reverse bias regime. All further C-V graphs in this section cover only this range of voltage. The SU 1 device for which results are shown was in the control package and so the eight sets of curves taken at the same time as the other devices were irradiated (i.e. over a period of one month) would be expected to be nearly identical. It is clear from the figures that this is the case for this device, giving confidence in the repeatability of the instrumentation, software and measurement technique.

The parasitic capacitance of these devices was not measured directly but can be estimated from the known characteristics of the process. The oxide thickness was close to 0.5 microns. The capacitance was dominated by the large contact pads, some 120 microns square. This gives a value very close to one picofarad per pad.

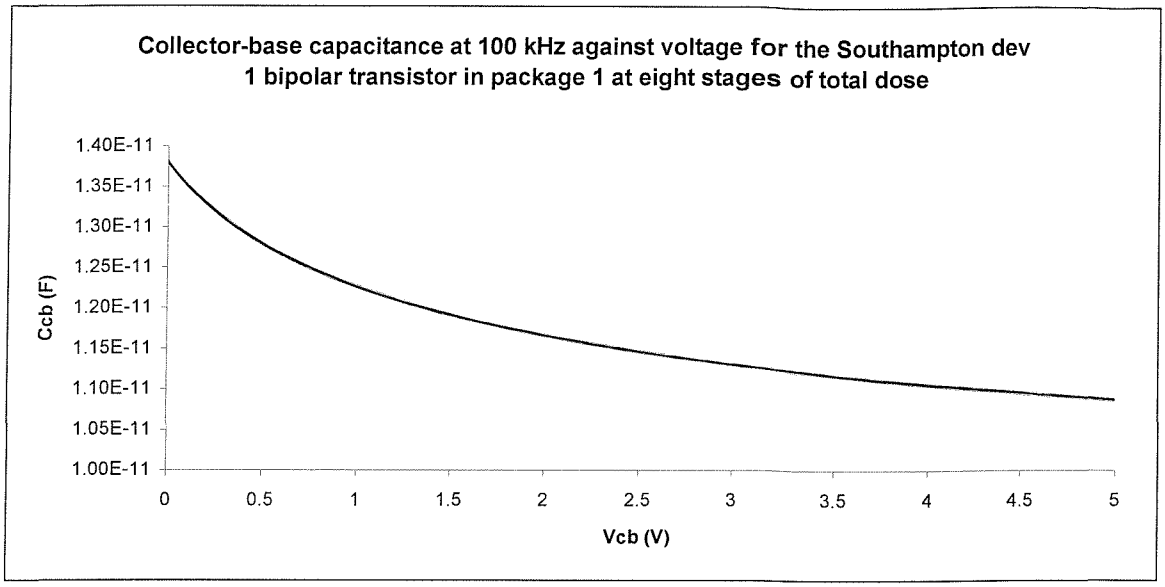

Figure 12.102: collector-base C-V plot at 100 kHz for SU device 1 in package 1.

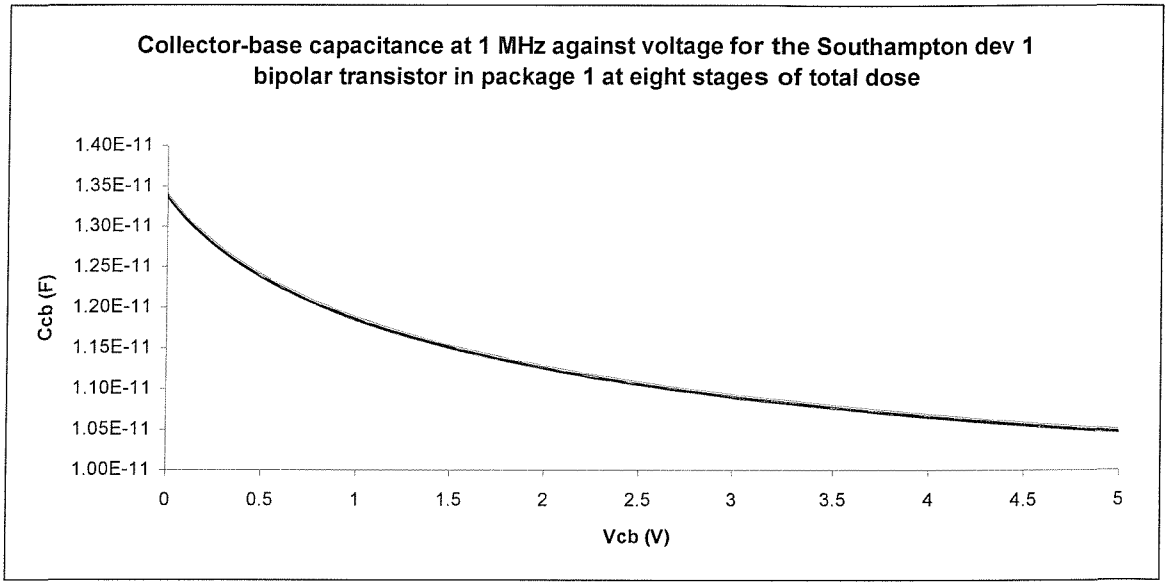

Figure 12.103: collector-base C-V plot at 1 MHz for SU device 1 in package 1.

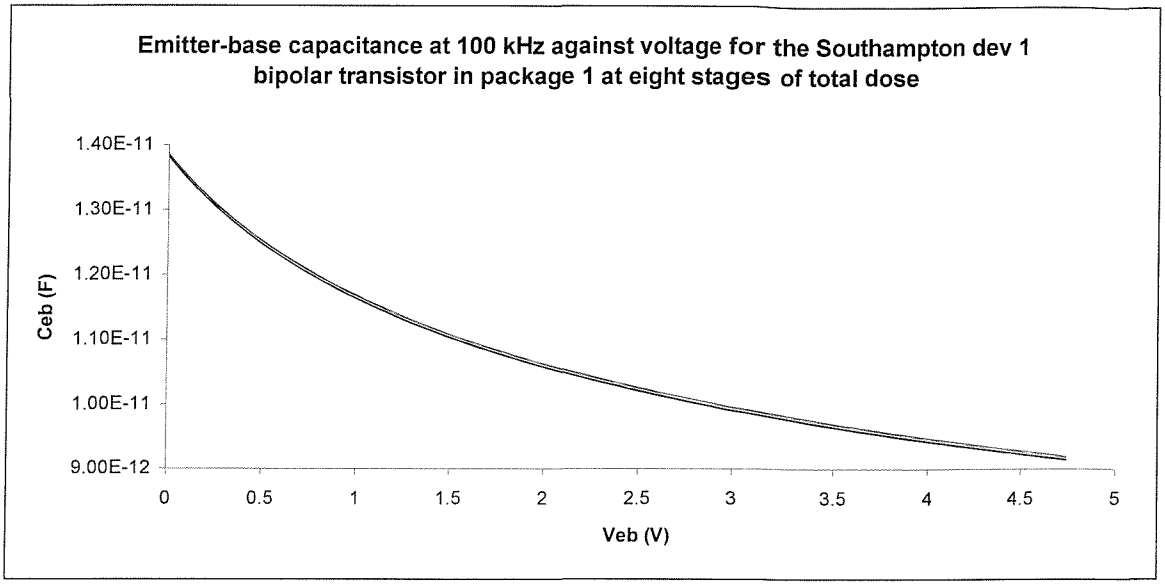

Figure 12.104: emitter-base C-V plot at 1 MHz for SU device 1 in package 1.

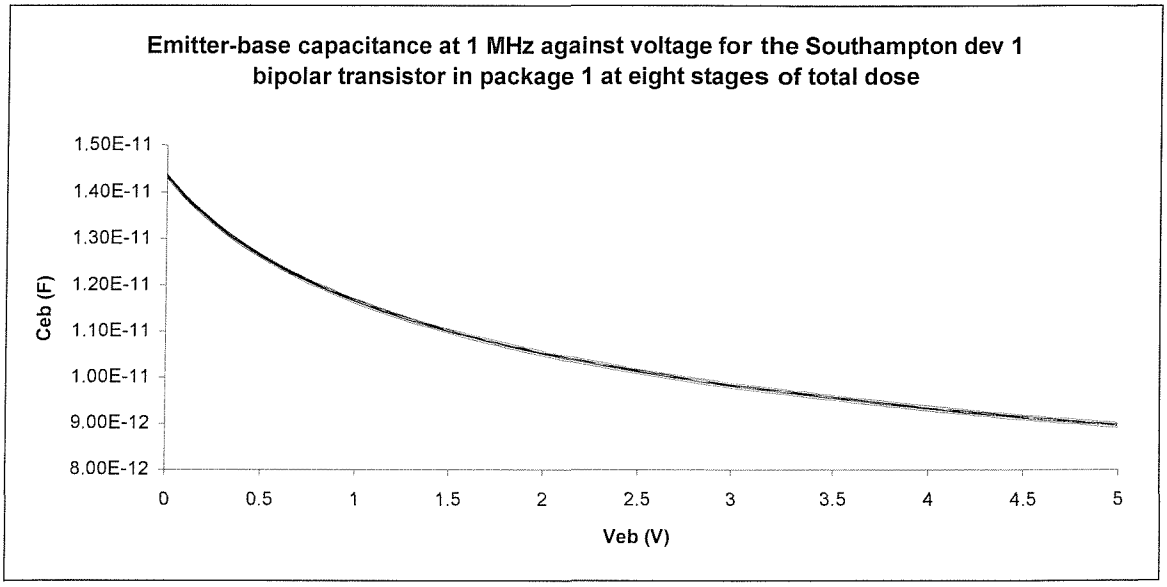

Figure 12.105: emitter-base C-V plot at 1 MHz for SU device 1 in package 1.

The two graphs for collector-base capacitance are very similar in shape, as are those for emitter-base capacitance. This indicates that both frequencies of 100 kHz and 1 MHz are high enough to be showing only the effects of traps in the bulk of the region of interest and that series resistance effects are minimal. Interface traps are believed to charge much more slowly than bulk traps and so do not have time to charge up in the duration of the applied high frequency test signal. An alternative explanation is that there is no significant concentration of interface traps in the collector-base region in

the pre-irradiation state. A change in the relative shape of the curves at the two different frequencies after irradiation would indicate both that significant numbers of interface traps had been created by the irradiation and were being activated by the lower frequency test signal.

The magnitude of the capacitance values measured lies between 10 and 15 picofarads. This is substantially greater than the estimated parasitic capacitance of 1 picofarad per contact pad and sot eh latter can be neglected.

The following figures show only the reverse bias region of interest identified above and provide examples of the change in C-V characteristics observed with total dose. In the majority of cases, the change was gradual and in a constant direction as the total dose increased. Figures 12.106 to 12.111 show the collector-base capacitance for several different devices, in different packages and at both measurement frequencies.

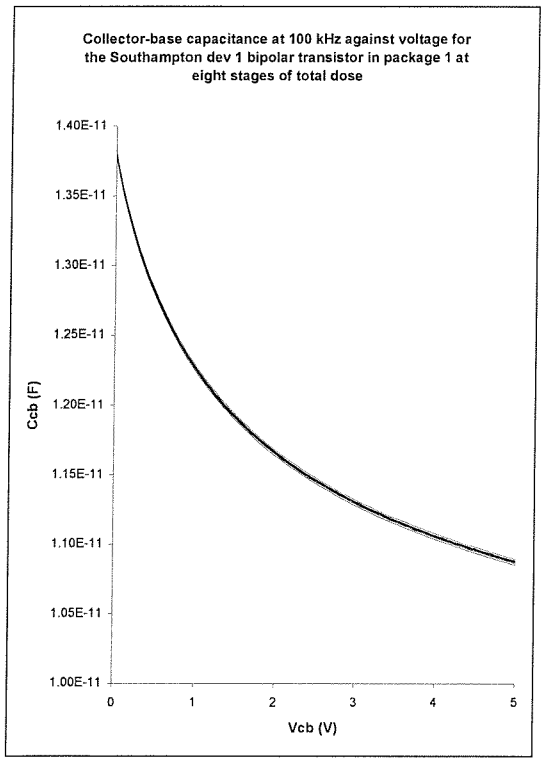

Figure 12.106: Collector-base C-V plot at 100 kHz for device 1 in package 1.

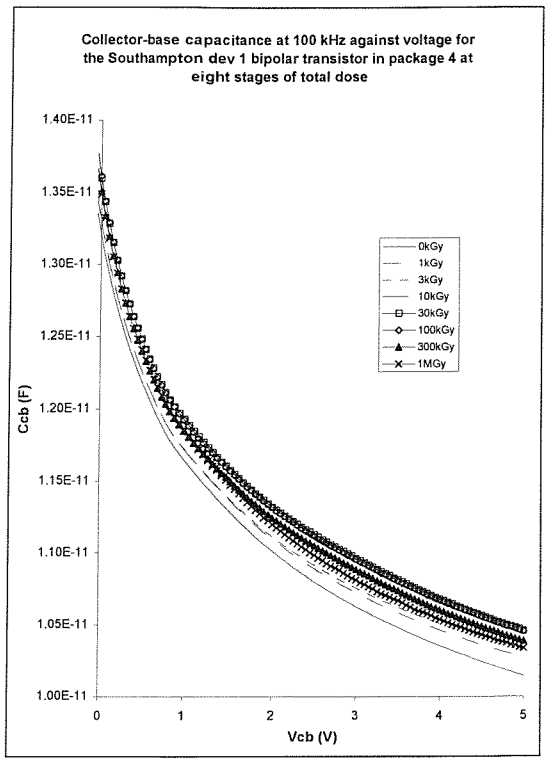

Figure 12.107: Collector-base C-V plot at 100 kHz for device 1 in package 4.

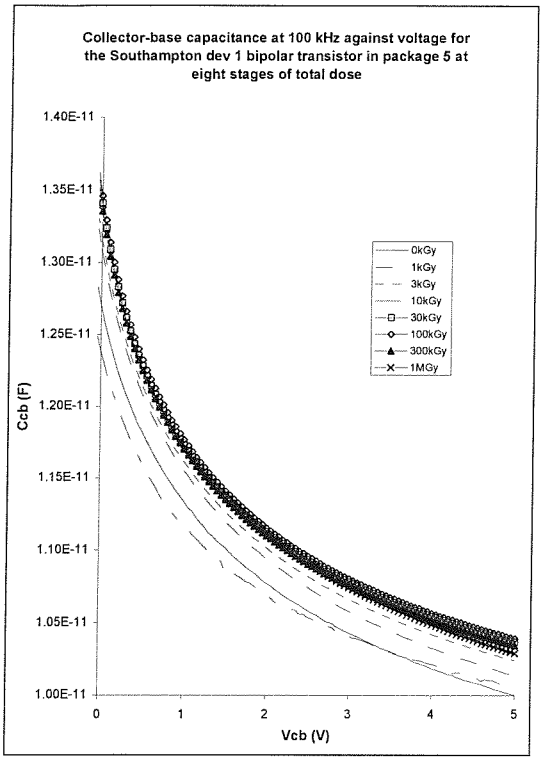

Figure 12.108: Collector-base C-V plot at 100 kHz for device 1 in package 5.

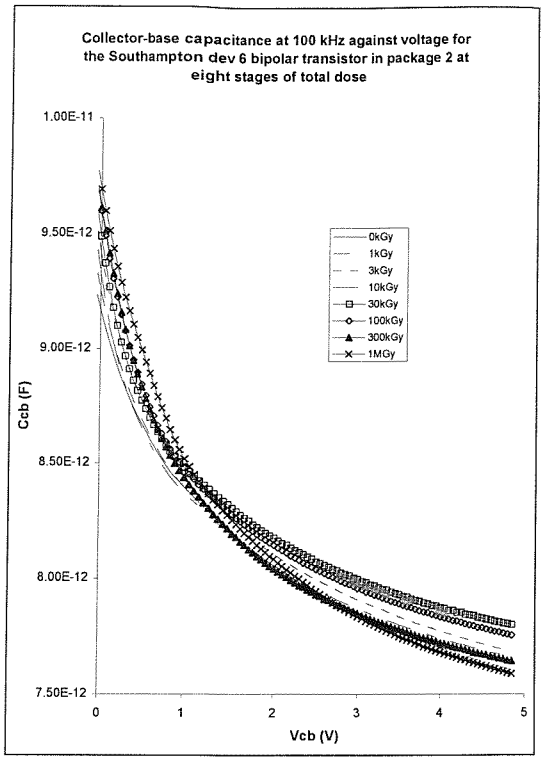

Figure 12.109: Collector-base C-V plot at 100 kHz for device 6 in package 2.

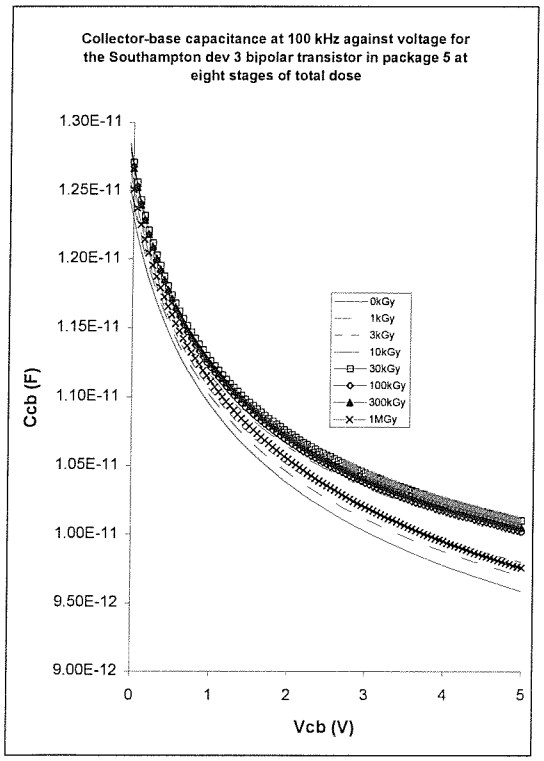

Figure 12.110: Collector-base C-V plot at 100 kHz for device 3 in package 5.

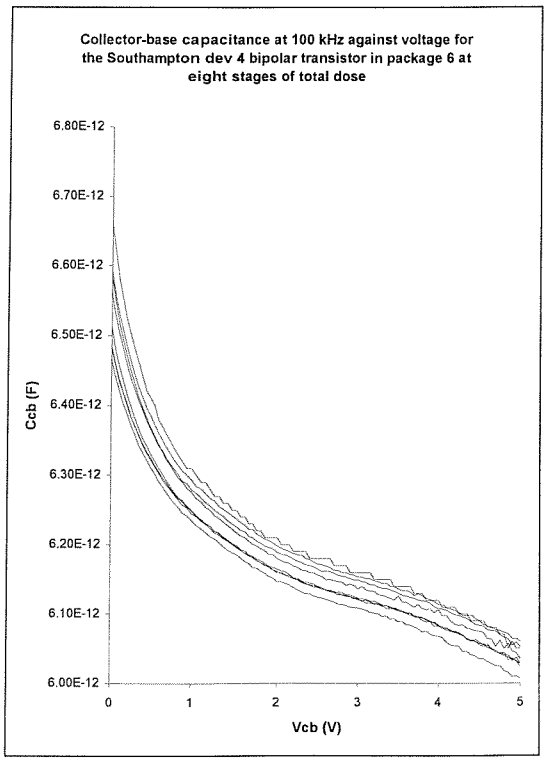

Figure 12.111: Collector-base C-V plot at 100 kHz for device 4 in package 6.

The collector-base capacitance data for the control devices are consistent, both in terms of repeated measurement at each stage and in terms of the measurement frequency. Most of the other devices showed an excellent degree of consistency between the two measurement frequencies, although there were one or two outliers in some cases. Overall, the curves showed an increasing trend with total dose, although the magnitude of the change was small at under 10% for the majority (increasing at higher reverse bias voltages) and therefore comparable with the limits of uncertainty associated with measurements.

The next set of figures, 12.112 to 12.117, shows the emitter-base capacitance.

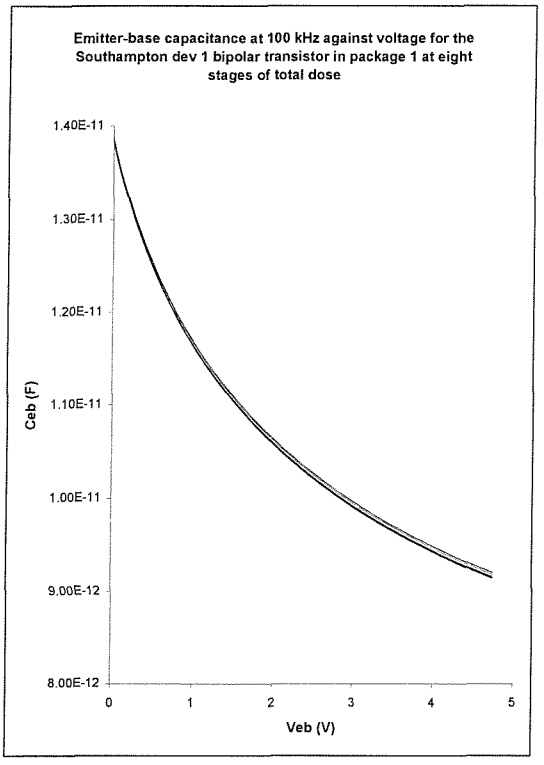

Figure 12.112: Emitter-base C-V plot at 100 kHz for device 1 in package 1.

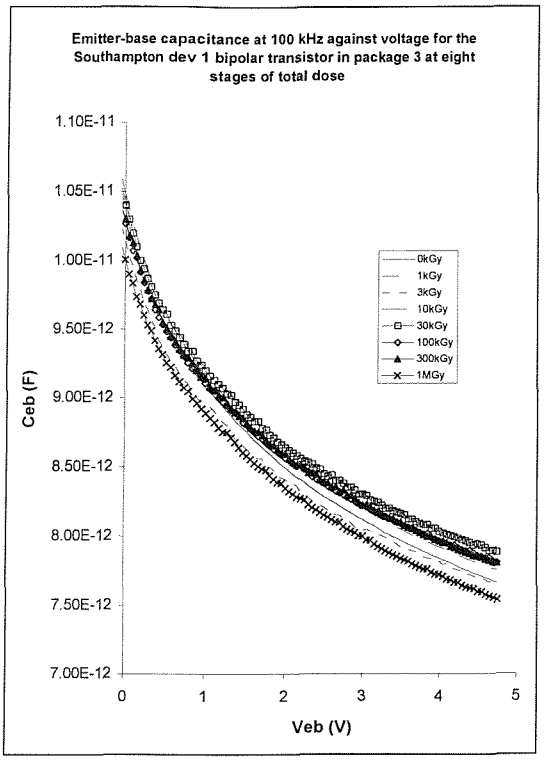

Figure 12.113: Emitter-base C-V plot at 100 kHz for device 1 in package 3.

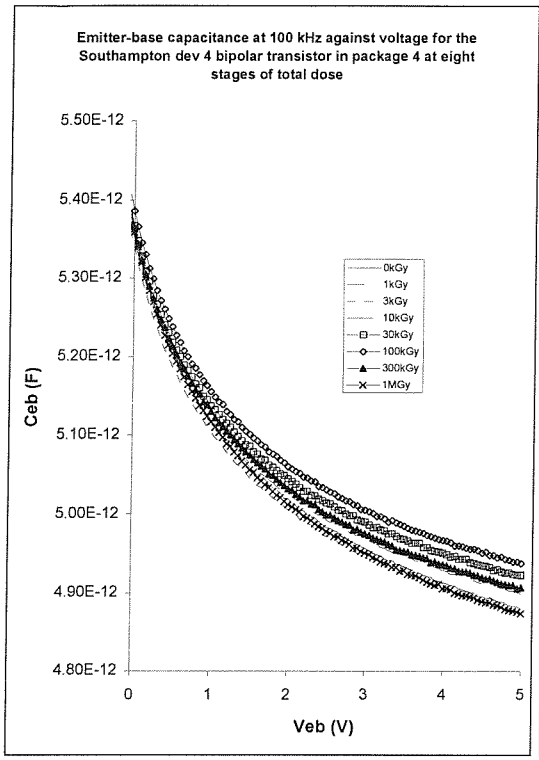

Figure 12.114: Emitter-base C-V plot at 100 kHz for device 4 in package 4.

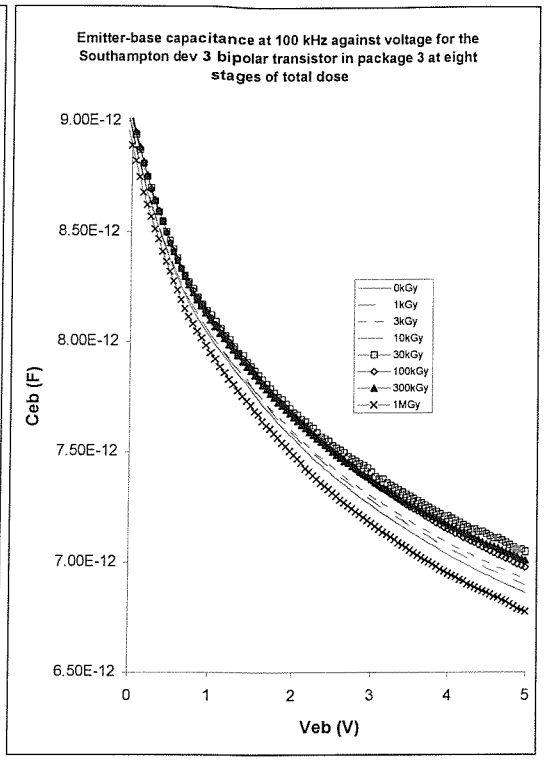

Figure 12.115: Emitter-base C-V plot at 100 kHz for device 3 in package 3.

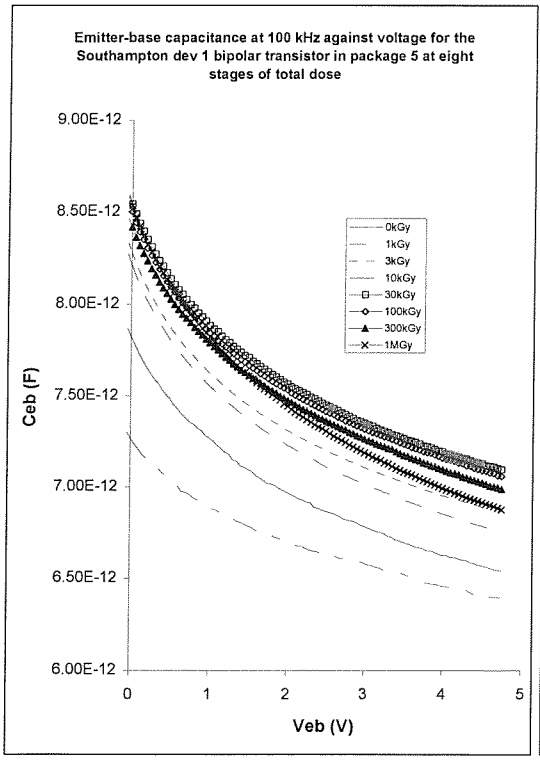

Figure 12.116: Emitter-base C-V plot at 100 kHz for device 1 in package 5.

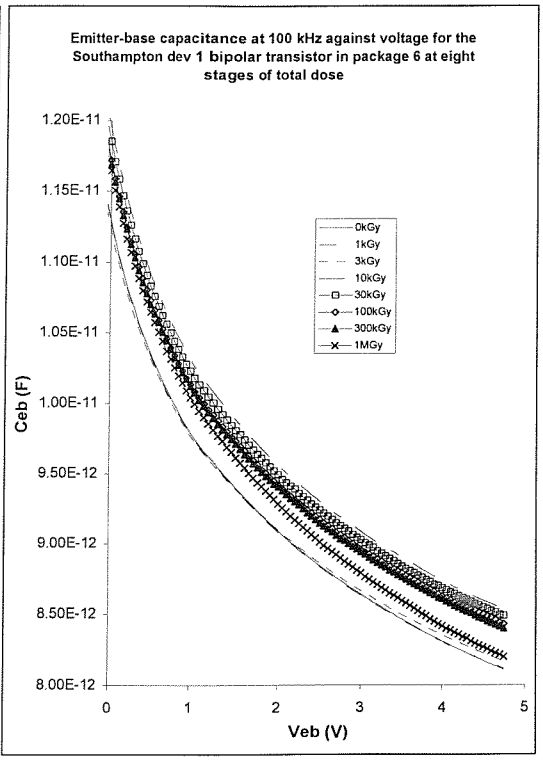

Figure 12.117: Emitter-base C-V plot at 100 kHz for device 1 in package 6.

The emitter-base capacitance data for both the control and irradiated devices are consistent, both in terms of repeated measurement at each stage at a given frequency and at both frequencies. The irradiated devices showed only small changes with total dose. One of the few exceptions to this trend is shown in figure 12.116, exhibiting a change of the order of 50% after 1 MGy. In most cases, the data are not monotonic, showing a rise in capacitance up to a total dose of 30 to 100 kGy and then a fall, back towards the pre-irradiation value. It may be concluded that there is some evidence for a rise in capacitance of typically 10% with total dose, although this was as high as 50% in one case. Hence, the concentration of either acceptor or donor-like defects has been affected to this extent by the irradiation.

12.6.2 The BC108 transistors

Results for the BC108 transistors were very consistent. The control device showed virtually identical traces at each stage at which it was tested. The other devices showed plots that were very similar to each other and so only one of each type is shown here. Once again, the plots at the two frequencies are similar for both collector-base and emitter-base capacitances and so only the data at 100 kHz is shown.

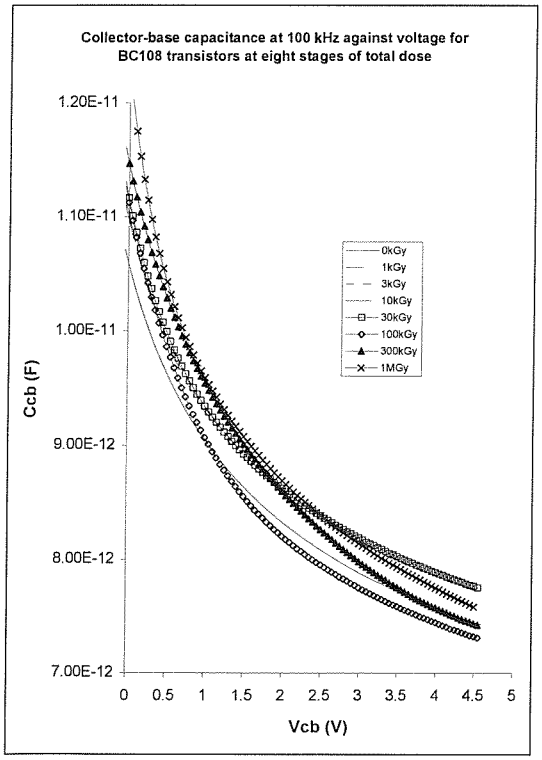

Figure 12.118: Collector-base C-V plot at 100 kHz for BC108 device number 95.

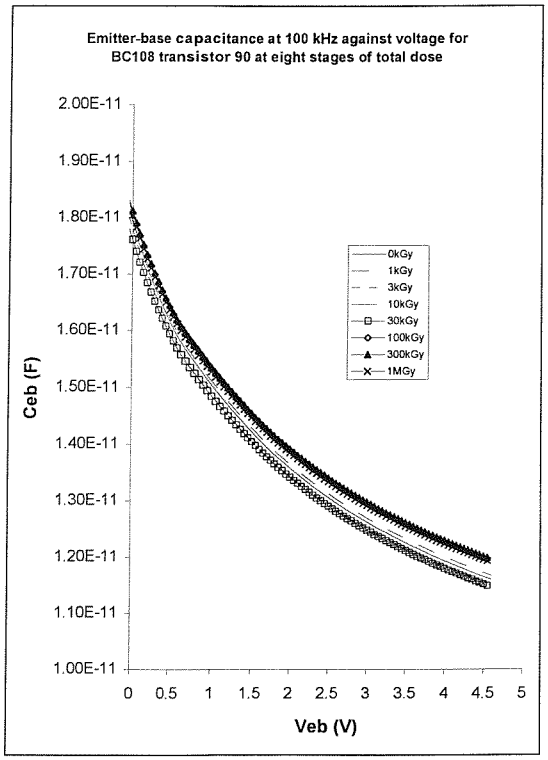

Figure 12.119: Emitter-base C-V plot at 100 kHz for BC108 device number 90.

The collector-base capacitance results (figure 12.118) show an increasing trend in capacitance but the magnitude of the increase is small and only just outside the limits of uncertainty of the measurements. The emitter-base capacitance results (figure 12.119) show curves that are very close together, implying very little change with total dose.

The conclusion that can be drawn from these results is that a total dose of 1 MGy had a small effect on the collector-base capacitance and a barely measureable effect on the emitter-base capacitance C-V traces for the BC108 transistors. This implies that, as for the SU devices, irradiation affected the concentration of acceptor or donor-like defects by around 10%.

12.7 LIFETIME MEASUREMENTS

Despite the problems encountered during the first phase of the work, direct lifetime measurements were included in the second phase because of their importance to understanding the effects of radiation on semiconductor devices. With the instrumentation available, coupled with the variation in the characteristics of the devices, it proved too difficult to make reliable and repeatable measurements on the SU devices. Consequently, a batch of BC108, COTS transistors was used, for which corresponding C-V, Gummel plot and dc point reading measurements were also made, as described above.

It did prove possible to make some measurements of transit time on the BC108 devices and the values obtained showed a steady decrease with irradiation, as expected. In fact, the measured values decreased sufficiently that, after 30 kGy and 100 kGy, it was possible to make only one measurement at most for each irradiated device and after 300 kGy, the readings became too small to measure at all (i.e. less than 0.5 microseconds). Figures 12.120 to 12.123 show the measured values of step recovery time against the first logarithmic term in equation 6.50. The decrease with total dose is clear from a comparison of the graphs, showing that the minority carrier lifetime has been significantly reduced by the irradiation.

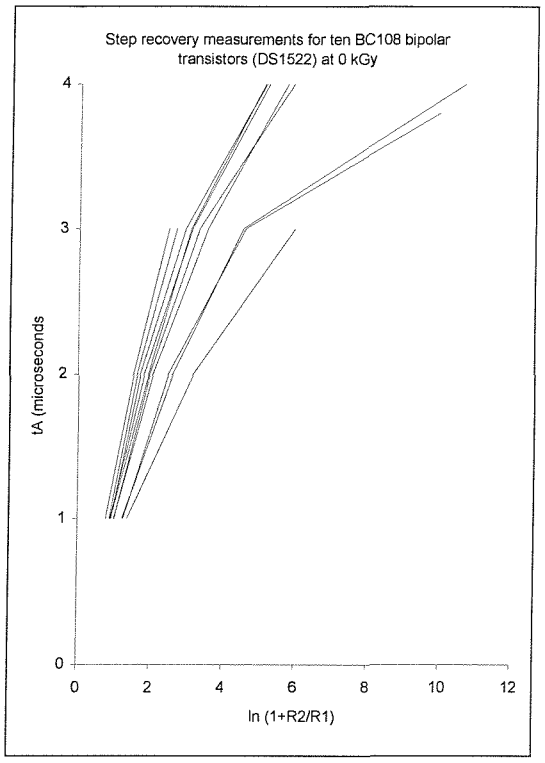

Figure 12.120: Step recovery time for the BC108 transistors at 0 kGy.

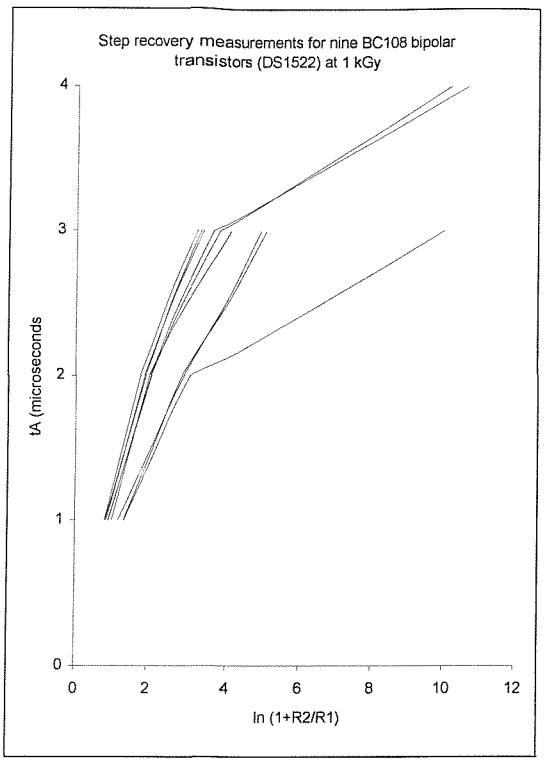

Figure 12.121: Step recovery time for the BC108 transistors after 1 kGy.

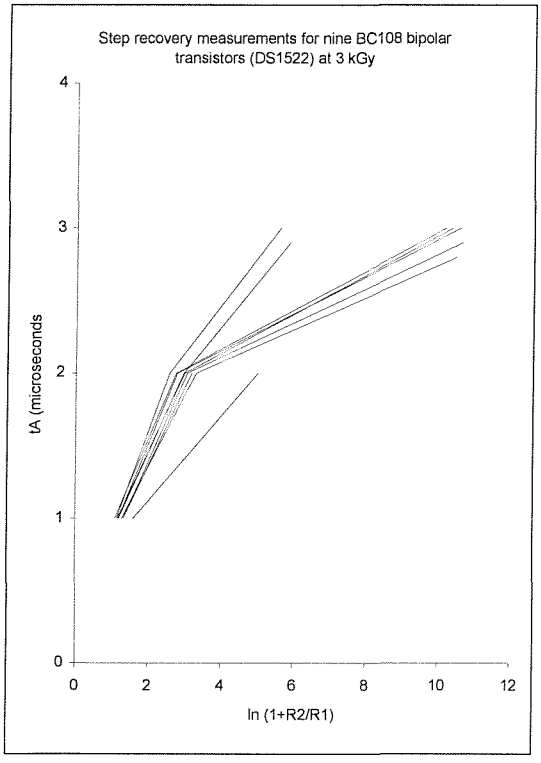

Figure 12.122: Step recovery time for the BC108 transistors after 3 kGy.

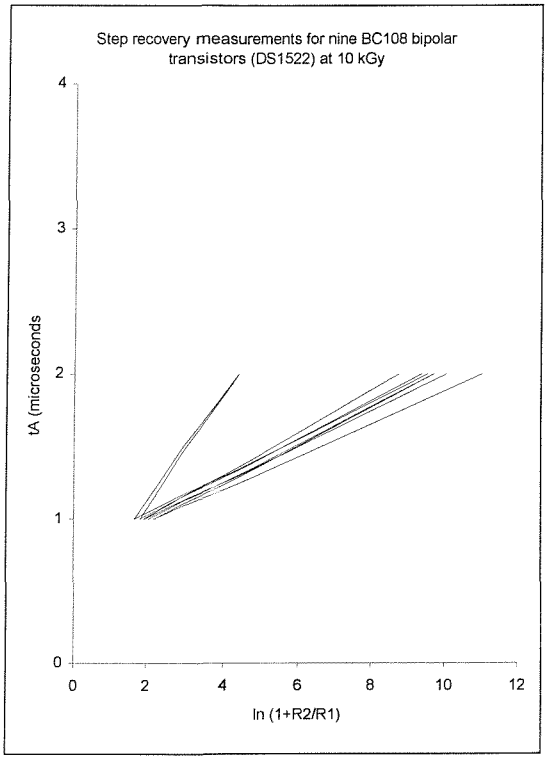

Figure 12.123: Step recovery time for the BC108 transistors after 10 kGy.

By measuring the slope and intercept of the curves in these charts, the values given in table 12.6 are obtained.

	0 kGy	1 kGy	3 kGy	10 kGy
Slope	0.60	0.29	0.19	0.13
Intercept	0.68	1.28	1.10	0.76

Table 12.6: measured values of slope and intercept for the curves in figures 12.120 to 12.123.

These data show again that the storage time has fallen significantly with increasing exposure to radiation. However, difficulties with setting the current to give reliable readings at such short storage times did introduce larger uncertainties to the measurements than was ideal.

Table 12.7 shows the calculated values of the lifetime, based on the data in table 12.6, the gain measured during the DC point measurements (again assuming that the forward and reverse gain have the same value) and using equations 6.45 to 6.47.

	0 kGy	1 kGy	3 kGy	10 kGy
Mean gain	145	59	21	8
Lifetime	8.3	9.9	18.8	36

Table 12.7: calculated values of lifetime for the curves in figures 12.120 to 12.123, assuming that forward and reverse gain are equal.

These results indicate that the lifetime has increased with total dose, clearly contradicting the picture illustrated in the figures. This shows that at least one of the assumptions made in deriving the value of lifetime from the storage time measurements is wrong for these devices. A key assumption is that $\tau_F << \tau_R$. If this remains correct then it is necessary that the forward and reverse values for gain are no longer equal. If the reverse gain is assumed to remain unchanged with irradiation then the results shown in table 12.8 are obtained instead.

	0 kGy	1 kGy	3 kGy	10 kGy
Forward gain	145	59	21	8
Reverse gain	145	145	145	145
Lifetime	8.3	6.9	10.4	17.3

Table 12.8: calculated values of lifetime for the curves in figures 12.120 to 12.123, assuming that reverse gain is unchanged with irradiation.

Whilst these results indicate that the lifetime begins by falling at the lowest total dose, it then increases again and proceeds to exceed the pre-irradiation value. This is clearly still incorrect. Hence, either the reverse gain has increased with total dose or the assumption that $\tau_F << \tau_R$ must be incorrect. We are measuring τ_F and showing that it is falling. If the assumption linking τ_F and τ_R is false then τ_R must be falling at a very much greater rate than is τ_F. This discussion is taken further in the next chapter.

13 Review of phase 2 results

13.1 SUITABILITY OF MEASUREMENT TECHNIQUES

Four measurement techniques were used in the second phase of the work: Gummel plots, DC point data, C-V plots and lifetime. The first two of these worked as effectively as during the first phase and yielded results of consistent reliability and quality. The data obtained for the BC108 transistors accorded with the values quoted in the manufacturers' datasheets, providing further confidence in the test routines and instrumentation. As during the first phase, some variations to the voltage and current at which individual parameters were measured were made to optimise the data obtained and ensure compliance with the recommendations made in the relevant datasheets.

No datasheets were available for the SU transistors and the results from these devices proved problematic. The measurement techniques were reliable but the consistency of the results from one device to another of the same type was poor. Repeated measurements on the same device gave very close results, indicating that the poor consistency was a real manifestation of differences between one device and another, despite their originating from the same source wafer.

C-V measurements were made on both the SU devices and on the BC108 transistors. The measurement technique proved reliable and repeatable, yielding stable results that were self-consistent. The initial definition of the test conditions, carried out with fixed value, calibrated capacitors, proved successful and enabled good confidence to be gained in the later data. Sensitivity to picofarad levels was obtained.

The same technique for the measurement of minority carrier lifetime was used in phase two as in the first phase. This continued to suffer from an inability to measure values below one microsecond, which limited the total dose at which readings could be taken. The BC108 transistors had a relatively low minority carrier lifetime before irradiation and the further reduction in lifetime effected by irradiation brought the value down to the limit of measurement after a total integrated dose of just 10 kGy. Improvement of the sensitivity of this technique would have required significant investment, which did not prove to be available.

13.2 REVIEW OF RESULTS

The irradiation procedures used during the second phase worked well, with results for the control devices again remaining constant within the limits of error. No devices appeared to have sustained damage due to in appropriate handling, electrostatic discharge or from the measurement process itself.

The SU devices were divided into two groups; one irradiated with bias applied and one with all the pins on each device shorted together. This was in an attempt to identify which condition led to greater damage and which was more relevant to in-service conditions. Unfortunately, the data were too scattered to enable any clear distinction to be drawn between the two bias conditions. Two of the three devices that had no bias applied did show a different response from that of the biased devices for some parameters but the third such device showed results much more like those for the biased devices. It is possible that tests on a larger sample of devices might have enabled a clearer picture to emerge, although the range of response of individual devices would have complicated this.

At first sight, the storage time measurements proved more satisfactory for the BC108 transistors than did those in the first phase of the work. The simplicity of the test equipment, with lifetimes of one microsecond or less not easily being measured, remained a limitation of the technique and this precluded measurements at total doses greater than about 10 kGy. Even so, the storage time measurements showed a rapidly falling trend, as expected. However, the calculations of lifetime based upon these measurements did not yield the expected results.

Making the assumptions used in the derivation of the equations in the literature, the lifetime appeared to have increased with irradiation, in contradiction of both the storage time and gain measurements. Removing the simplifying assumption that forward and reverse gain are equal before and after irradiation and assuming, instead, that reverse gain is unchanged by exposure to radiation, insufficient compensation appears. Neglecting the unlikely possibility that reverse gain has increased while forward gain has fallen (measurements on other devices showed that a fall in reverse gain occurred), leaves us with the assumption that the forward transit time is very much smaller than the reverse transit time. There is a considerable body of literature to back up this assumption in all but special cases, leaving a contradiction. The impression, therefore, is of a problem with the measurement technique or the

instrumentation. In the absence of more sophisticated equipment, it was regrettably not possible to investigate this further.
Lifetime measurements on the SU devices did not prove possible due to the limitations of the equipment and their specific characteristics in the region of interest.

The test routine and procedures for Gummel plot and dc point measurements worked extremely well again. The range of measurements made with the ATE was unchanged from that shown in table 11.1. The Gummel plots for the BC108 transistors showed well the changes in base current that occurred with increasing total dose, in line with the expectations from the first phase data. The pre-irradiation curves showed that the devices had useful gain over a wide range of current, from nanoamps to milliamps in terms of collector current. After 1 kGy, the curves crossed at around 1 nanoamp, showing that gain at the lower currents had been reduced. This trend continued and, by 100 kGy, little gain was left at any value of current as the curves crossed at around 1 microamp. This picture is confirmed by the gain measurements.
The plots show clearly that the changes in parameter values brought about by irradiation are caused by the base current curves moving, rather than those for the collector current. This is further support for the theory that a reduction in minority carrier lifetime is responsible for the degradation observed. This pattern is monotonic up to the final stage of irradiation, at 1 MGy. At this stage, the base current curve changes in a more complex manner. Whilst the shift continues at high values of base current, at moderate and low currents, the curve retreats slightly, back past the 300 kGy curve towards the 100 kGy position. This lower current is consistent with an increase in resistivity starting to become apparent, due to displacement damage in the silicon. It is also possible to infer such a change from the response of collector-emitter breakdown voltage with total dose, exhibiting an increase of some 25% after 1 MGy.

The Gummel plot measurements for the SU devices also gave reliable and repeatable results. In most cases, the plots for individual devices showed the same general trends as described above for the BC108 transistors. The collector current curves remained largely invariant, with just a few instances of increasing leakage current at low voltage. The base current curves showed a rising trend with total dose, again similar to that observed for the BC108 transistors. However, the plots for devices of the same type, simply housed in different packages, differed significantly in virtually all cases. The

shape of both the collector and base current curves covered a wide range, with some rather extreme cases. This made it difficult to compare the different types of device because the range of response overlapped so much.

It is interesting to note that there is some evidence of deterioration in the characteristics of one of the devices even without irradiation. Figure 12.24 shows the Gummel plots for the control device of type 3. Both the collector and base current curves can be seen to remain unchanged over much of the plot but to diverge at the higher currents. Whilst the ratio of the two stayed similar, the absolute value of the current that was available at a given base-emitter voltage increased with each successive set of measurements, tending more towards the theoretically ideal shape. This phenomenon was not observed for any of the other devices in the same package and so could be evidence of a process defect associated solely with this device.

The leakage current measurements showed rather good agreement between devices of the same type for the SU transistors. In most cases, leakage currents remained more of less stable under irradiation, although collector-base and base-emitter leakage currents did rise slightly, by around one order of magnitude. Given that all the leakage currents were small before irradiation (with the exception of a small number of rogue devices), this increase is unlikely to have any implications for use of the devices in-cell.

Collector-emitter leakage current showed a slightly different response, with a reduction during the first two stage of irradiation, followed by a slow increase up to a total dose of 300 kGy and a steeper rise after 1 MGy. This final rise brought values just above the pre-irradiation values. The same trends were observed for the BC108 devices, although the increases with total dose were somewhat larger at up to three orders of magnitude. Again, even these increases have little implication for circuits as the maximum value reached was just 10 nA.

Saturation voltage was expected to rise with total dose and this was observed for all the devices. The SU devices exhibited rather high values before irradiation, lying between 2 and 3 volts. An increase of about 20% was observed. The BC108 transistors started with a much lower saturation voltage, typically 50 mV, but saw a larger increase of some 200%. The curve increased in steepness with total dose, giving a final value around 140 mV.

As was seen during the first phase, gain fell for all the devices. The SU devices showed values before irradiation of between 50 and 100, with just a small number having

higher values. After a total dose of 1 MGy, these had fallen by several tens of per cent, reaching approximately 20 at the lower measurement currents and 50 at the higher currents. However, there are several interesting features associated with the shape of the curves between these end points. The rate of degradation was generally higher at low collector currents. This accords with the Gummel plots, showing larger shifts in the base current curves at low base-emitter voltage, i.e. lower current. At a collector current of 10 mA, the rate of degradation was noticeably lower and the final values of gain were higher. Again, this agrees with the Gummel plots, indicating that gain is less affected by irradiation at higher currents.

A second feature worth pointing out is a slight increase in gain after a total dose of around 100 kGy, followed by a reduction again after 1 MGy. This was observed for many of the devices and for all values of collector current. The magnitude of the increase was small, between 5 and 10 in absolute terms, although this represented up to 50% of the gain at that point. Brucker (1966) predicted that, due to the dependence of surface recombination velocity on surface potential and his experiments on the change in surface potential with irradiation, a reversal in the degradation of gain might be expected. He was unable to demonstrate this effect but it is clearly visible here in the case of the SU devices.

The BC108 transistors showed much higher pre-irradiation values of gain, at between 100 and 250. This was a relatively large spread for devices that otherwise showed very close agreement in parameter values. The pattern of degradation was similar to that for the SU devices, with more rapid loss at lower currents. Final values were in single figures at 0.01 mA and near 50 mA at 10 mA. The spread in results was much reduced by the higher stages of total dose. The decrease in gain was monotonic for the BC108 devices.

Emitter-base and base-emitter breakdown voltages remained largely unchanged with irradiation for both the SU and BC108 devices. There was a small number of exceptions, showing a reduction after the first stages of total dose. However, this reduction simply served to bring them into line with the other examples of the same type, indicating that it was the pre-irradiation readings that were suspect. Collector-base breakdown voltage showed small variations, with a slight fall in value up to 30 kGy, followed by an increase, leaving the final value close to that before irradiation. Collector-emitter breakdown voltage showed an increase with total dose. Initial value for the SU devices lay between 25 and 40V and an increase of around 30% after 1

MGy was typical. The BC108 transistors had pre-irradiation values of near 60V and these also rose by approximately one third.

C-V measurements were introduced to the work during the second phase. Both collector-base and emitter-base capacitance measurements were made over a six-volt range of junction bias, covering a small region of forward bias and 5 volts of reverse bias. The measurement technique and instrumentation proved reliable, shown by the readings for the control devices remaining constant and repeatable through the tests. The results for the BC108 transistors showed that the main response to irradiation for both parameters was an increase of around 10% in the measured value of capacitance. This was the same at both measurement frequencies but was not monotonic. The highest change in capacitance occurred at between 30 and 100 kGy, with the measured values then declining towards the pre-irradiation values.
The SU devices showed a very similar response to irradiation. Results at the two measurement frequencies were very similar. Both parameters showed a rise by about 10% with irradiation, again peaking at moderate total doses and then falling slightly as total dose rose further. One example is shown where the increase was much larger, reaching 50%. Further analysis of these data is given in chapter 14.

13.3 COMMENTS ON THE DEVICE TYPES

The BC108 transistors showed the benefits they were expected to exhibit, namely consistency across the batch, quality and reliability. The results of the measurements were in good agreement with the datasheet values and were repeatable. No further information on the processing, treatment or geometry of these devices was obtained from the manufacturers. The main purpose of including these devices in the testing was to provide a high quality reference for the more experimental SU devices. Although details of the geometry, etc. for the BC108s were not available, the type and magnitude of changes in parameter values due to irradiation were predicted on the basis of previous data, including those obtained during the first phase of the work. If the measured changes due to irradiation varied significantly from the predictions then that would have indicated a problem with either the measurement process or the irradiation conditions. The fact that no such variations were seen acted as confirmation of the front-line safeguards on the consistency of the approach.

The SU devices behaved better than the BC108 transistors in some respects but rather worse in others. Full information on the design layout, fabrication procedures and processing steps was available from the University. However, the devices showed large variability between nominally identical examples. The intention of using devices of different but known geometries was expected to be useful in linking measured radiation effects with features of the individual transistors. This was not achieved in practice because devices of nominally the same construction and processing proved to exhibit characteristics that differed widely. The range of characteristics for the different types of device overlapped to a large extent, preventing meaningful separation and complicating the data analysis.

14 Analysis and discussion

14.1 OVERVIEW

The first phase of the work yielded a considerable volume of data covering the effects of exposure to ionising radiation on a variety of semiconductor components. The gathering of these data enabled reliable measurement techniques to be developed for some of the parameters and unreliable methods to be discarded. The techniques that proved successful were put to good effect in the second phase, giving good confidence in the readings and permitting the tests to proceed without interruptions due to measurement problems. The techniques that were unreliable included some of the more useful methods for gathering data at the microscopic level and it is unfortunate that this ruled out the possibility of linking the changes in operating parameters to specific features of the devices or to defect theories.

Furthermore, the devices that were specially fabricated to enable the influence of geometry on radiation response to be quantified proved to exhibit such different characteristics from each other that no clear pattern could be drawn from the data. Fortunately, some useful data were derived from the BC108 transistors and these enabled a number of conclusions to be developed. Despite the lack of knowledge of the fabrication of these devices and their random selection with no traceability, they did prove of high quality, gave consistent results and were well-matched to each other.

The irradiation procedures worked smoothly in all the facilities used and high confidence is placed in the dose rate and total dose measurements, enabling results from different test runs reliably to be compared.

This chapter now examines the results, what information can be obtained from them and the influence on them of various factors.

14.2 BASIC EFFECTS OF IRRADIATION

The first phase of the work enabled a basic appreciation of the effects of irradiation on the operating parameters of semiconductor devices to be gained. This was important as it is these effects that have the greatest practical impact on the selection and manner of use of devices in real applications in radiation environments. Whilst an

understanding of the effects at a microscopic level is required for the development of any generalised predictive tools, it was felt to be necessary to appreciate the device-level phenomena as a first step.

The simplest devices studied were ordinary junction diodes. The effects of radiation on these devices proved to be small, with ionisation damage leading to very little change in any operating parameter. At higher values of total dose, displacement damage started to accumulate to significant levels and this did lead to shifts in, for example, reverse breakdown voltage. Rare cases of shifts in leakage current were observed but the magnitude of the shifts, whilst attaining a factor of ten, remained low compared with the magnitude of the current itself. In some cases, the leakage current actually reduced, i.e. improved, with increasing exposure to radiation. The degree of damage observed during these tests accorded with predictions in the literature of the likely effects of high total doses of ionising radiation, compared with the previously-studied effects of particle (especially neutron) radiation. A conclusion that can be drawn from these tests is that the majority of junction diodes are suitable for use in high radiation environments with little or no modification in their manner of use in an electronic circuit. There are a few cases where leakage current may increase considerably but, even in these cases, diodes used for basic voltage rectification purposes or in medium or high power circuitry will not unduly be affected. Low-noise detector circuits, as used on some in-cell sensor instrumentation, may be more sensitive to increasing leakage current and so would justify more careful selection of the diodes used.

The principal operating parameters of bipolar transistors were expected to be affected to a large degree by irradiation. However, in contrast to the case of devices such as MOSFETs, these changes were not expected to lead to functional failure of the transistors, rather to a gradual degradation of many parameters that eventually stabilised at moderate to high total doses. In essence, this was the picture obtained from the published data.

The results of the first phase showed that leakage currents generally increased, although some instances of a reduction were found. Breakdown voltages tended to remain steady, although slight increases were observed in a number of cases. Saturation voltage rose in most cases, sometimes by an order of magnitude. Gain always fell, often to single figures after a total dose of 1 MGy. The shape of the response curve to irradiation varied with the device type and manufacturer. It was not even constant for

different batches of the same device from the same fabrication facility, although the greatest variations were found between manufacturers of the same device type.

A commonly quoted view in the literature is that gamma radiation causes only ionisation damage. At low to moderate total doses, it is clear that the majority of the damage observed is, indeed, due to ionisation effects, i.e. the creation of electron-hole pairs along the track followed by a gamma ray as it progresses through the device structure. However, in a small number of cases, atoms in the lattice structure of silicon can be displaced by gamma rays or the more energetic secondary electrons, causing a small amount of dislocation damage to be suffered, more typical of particle irradiation. At high total doses, the degree of this dislocation damage can become sufficient to cause noticeable effects on the common operating parameters. This phenomenon was observed in the case, for example, of collector-emitter breakdown voltage, which was shown to increase by a few per cent after total doses of a few hundred kilogray in some cases. This increase is consistent with a low rate of dislocation damage, manifested as the creation of vacancies or vacancy complexes in the silicon lattice. As the concentration of these defects increases, the resistivity of the material is increased, enabling it to withstand a higher voltage before breakdown occurs. Successful DLTS measurements could have shown how the concentration of these defects varied with total dose, allowing this theory to be tested. Nevertheless, there are sufficient cases reported in the literature that defect concentration does rise significantly when high total doses of gamma radiation are imparted to, for example, silicon detectors and bulk silicon samples in order to be confident that this is the effect being observed in this instance.

The initial changes in gain and saturation voltage are consistent with a reduction in minority carrier lifetime. More current is required in the base in an attempt to compensate for this reduction, leading to the shifts in the base current curves shown in the Gummel plots. Consequently, the gain falls, by definition, and the saturation voltage rises (see, for example, Harris (1966)). The limited measurements that were made here of lifetime showed that there was a sharp reduction in this parameter, so sharp that it could no longer be measured after relatively low total doses. It is not unreasonable to assume that the lifetime continues to fall as total dose increases, although there will be a limit to how far this degradation can proceed. The reduction in minority carrier lifetime due to the effects of irradiation is now so well established that irradiation by high energy ions has become a standard technique for the

processing of IGBTs and fast recovery diodes, as a cleaner and more predictable alternative to doping with gold or other metals. Efficient switching of these devices is desirable because the high currents being handled can lead to substantial power losses for inefficient devices.

The change in carrier lifetime brought about by this irradiation is due to the introduction of elevated concentrations of defects. The defects are reported as being largely vacancies or vacancy complexes produced by the impact of high energy ions with silicon atoms. The silicon atoms are displaced from their positions in the lattice, leaving a vacancy. Hence, these radiation-induced defects cause a reduction in the carrier lifetime. The remaining questions in respect of this work relate to the relative efficiency of electromagnetic, i.e. gamma, radiation at producing defects with similar, lifetime reducing properties and whether such a reduction in lifetime leads to the changes in gain, etc, measured experimentally.

14.3 GUMMEL PLOT DATA

In many cases, the Gummel plots showed the trend expected from the literature. The data for the SU devices were rather scattered, showing poor consistency between devices of nominally the same type. However, the general trend was clear and showed collector current curves that changed little with irradiation, apart from a very few instances of increasing leakage current. This is a strong indication that carrier mobility is not being significantly affected by the irradiation. The base current curves showed a rising trend with total dose, especially at low base-emitter voltage. However, the final curve, at a total dose of 1 MGy, often moved in the opposite direction, back towards or even beyond that for 100 kGy. These features are illustrated in the two examples shown in figures 14.1 and 14.2.

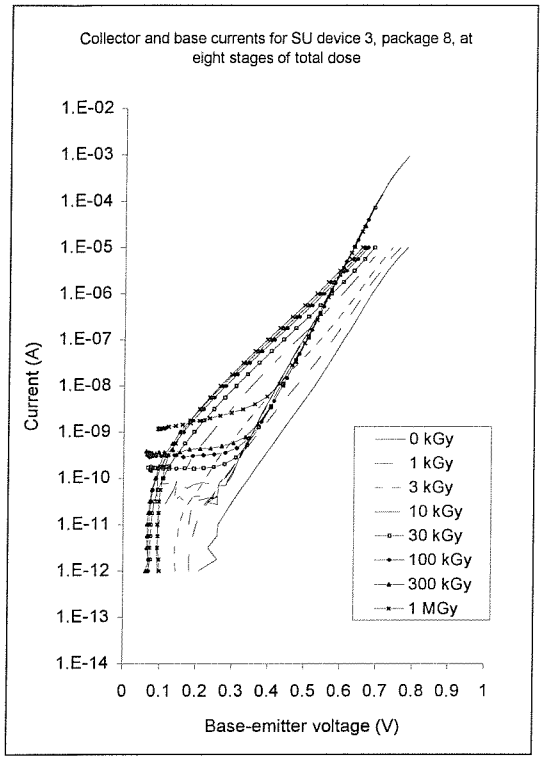

Figure 14.1: Gummel plot for device 3 in package 8.

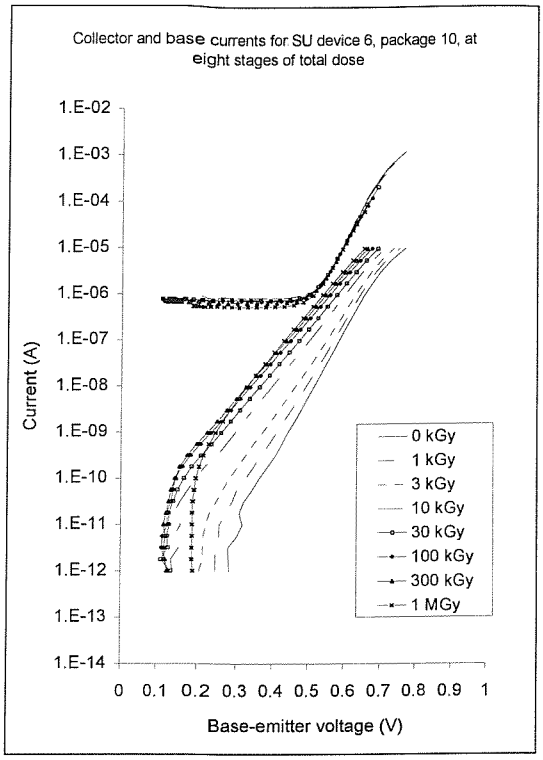

Figure 14.2: Gummel plot for device 6 in package 10.

Both figures show a sequence of rising base current curves as total dose increases. Both also show the curve for 1 MGy moving in the opposite direction at low base-emitter voltage, most obviously in figure 14.2. This region is shown at an expanded scale in figure 14.3 in order to illustrate the point more clearly.

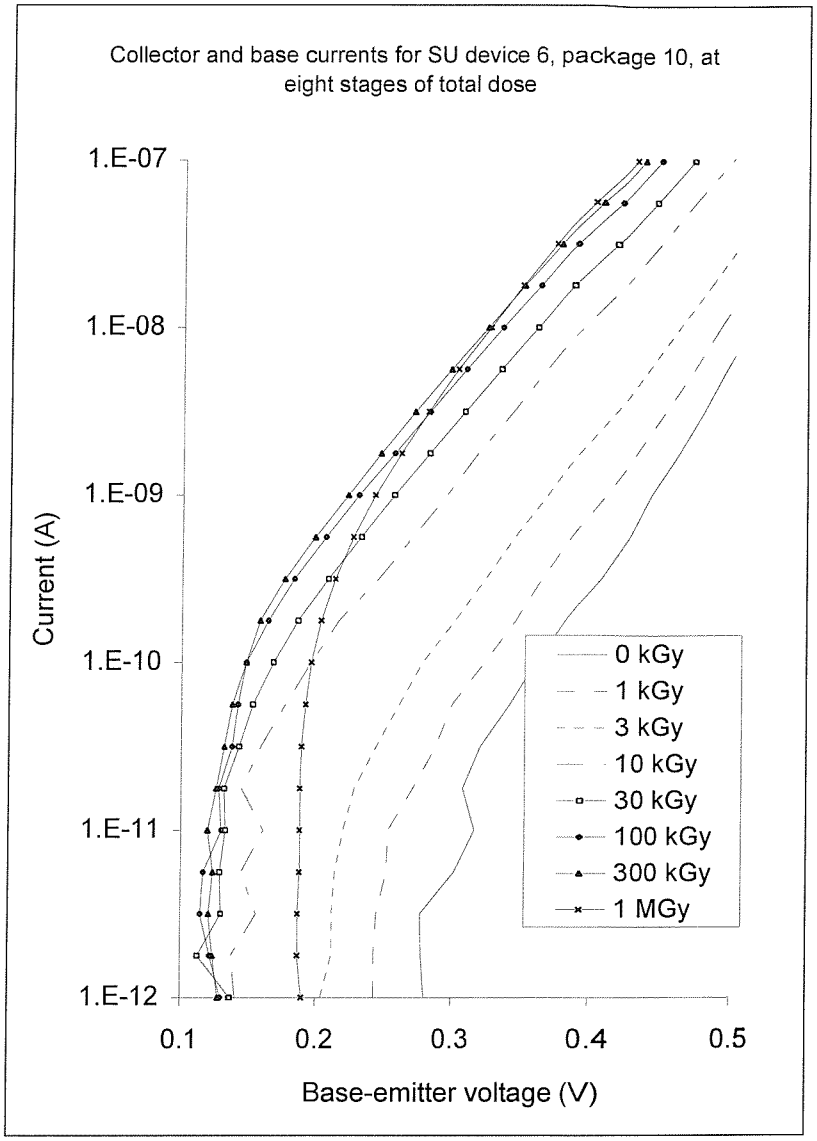

Figure 14.3: Expanded Gummel plot for device 6 in package 10.

At this scale, it can easily be seen that the 1 MGy curve crosses the 300 kGy curve at a current of around 20 nA. It can also be seen that the 300 kGy curve coincides with the 100 kGy curve at a current of 0.1 nA, crossing it at 10 pA and the 100 kGy curve itself crosses the 30 kGy curve at a few pA. The last two features may be at the level of sensitivity of the instrumentation but do indicate a trend in the opposite direction at low current at the higher levels of total dose. This could be partly due to a rising value of collector-base leakage current affecting the base current curve at 1 MGy. However, figure 12.62 shows that this leakage current rises only slightly with total dose (from 0.1 to 1.0 nanoamps between 10 kGy and 1 MGy) and certainly exhibits no substantial increase between the final two stages of irradiation.

Other features to point out include the change in slope of the base current curves as the total dose increases. This was a common feature, observed on most of the Gummel plots. This is indicative of the ideality factor, identified in chapter 6.2, changing as the device is exposed to radiation. The pre-irradiation data show that the ideality factor was close to unity over most of the range of base-emitter voltage. This shows that the amount of recombination in the emitter-base depletion region was small in the unirradiated devices. (In fact, two regions can just be discerned for the pre-irradiation and 1 kGy cases, with the less steep slope being at lower values of base-emitter voltage, and differing by about 15%. The section with the steeper slope was the more parallel to the collector current curve in all cases. Hence, a certain degree of recombination was detectable but this was small compared with the diffusion current contribution.) As the total dose increased, so did the ideality factor, as shown in figure 14.4, showing results taken from the measured slope of the base current curves at a current of 100 nanoamps.

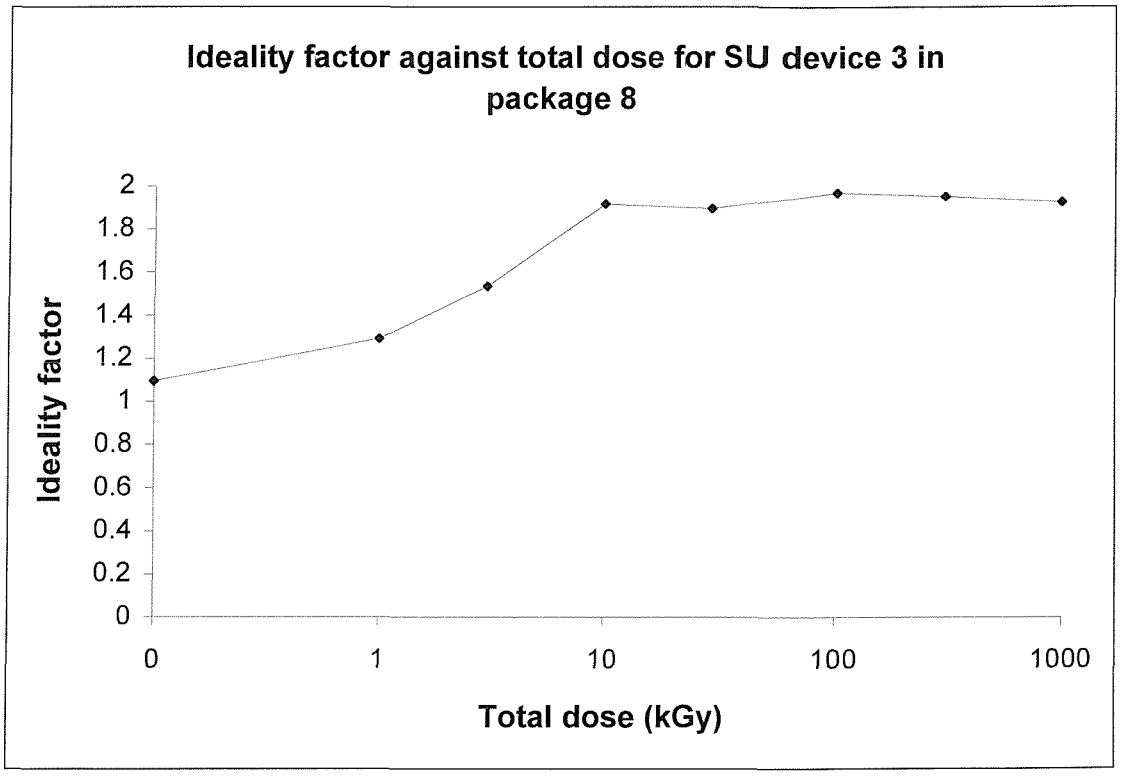

Figure 14.4: ideality factor against total dose for SU device 3 in package 8.

Clearly, the ideality factor rose rather rapidly at total doses up to 10 kGy but then remained essentially constant, as shown by the nearly parallel base current curves at

higher total doses on the Gummel plot. Recombination in the emitter-base depletion region has become of greater importance over the first few stages of irradiation, indicative of a significant increase in the density of defect states capable of enabling recombination to take place.

Hence, equation 6.36 can be seen to apply over the whole range of total dose:

$$I_B = I_1 e^{qV_{BE}/kT} + I_2 e^{qV_{BE}/mkT} \tag{14.1}$$

where I_1 dominates at low doses and I_2 becomes dominant at higher doses. To satisfy this, both coefficients must be functions of the total dose over the appropriate range. The collector current curves remained largely constant with irradiation. The curves in figure 14.1 show a rising collector-emitter leakage current at the higher values of total dose but very close agreement at all stages at currents above 3 nA. Figure 14.2 shows that, although the collector-emitter leakage current for this device was high even before irradiation, it did not change during the irradiations, with all the curves remaining together.

A similar analysis can be applied to the BC108 data. A typical graph of the ideality factor against total dose is shown in figure 14.5, for device number 87.

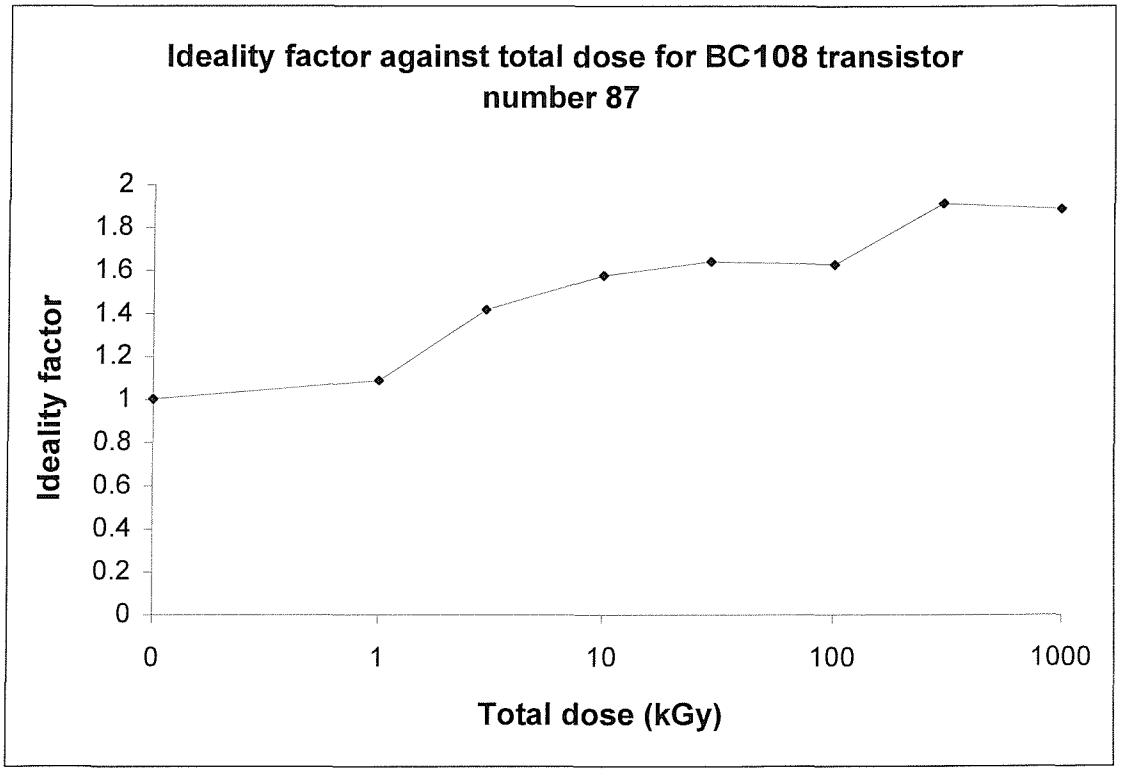

Figure 14.5: ideality factor against total dose for one BC108 device.

As before, measurements were taken at a current of 100 nanoamps. This figure shows that, whilst the ideality factor did not increase quite as rapidly for the BC108 transistors as it did for the SU device, it did reach a similar final value after a total dose of 1 MGy. This confirms that recombination in the emitter-base depletion region played as important a role in the high total dose region for these transistors as for the SU devices. The same model can be applied to these devices as to the SU devices before (equation 14.1).

As in the case of some of the SU devices, two distinct slopes can be seen on the Gummel plot for the BC108s (see figure 12.53) before irradiation. The difference in slope is small but is indicative of a small contribution to the total current from recombination, even in the unirradiated condition. The upper part of the pre-irradiation base current curve is very nearly parallel to the collector current curve, showing that the recombination contribution is negligible for currents higher than a few nanoamps. This indicates the presence of a non-zero defect concentration in the unirradiated condition. The break in slope is not visible for total doses higher than 1 kGy until 100 kGy is reached. Here, a further break in slope occurs, with the low current region again showing a less steep slope. This pattern is reversed at 1 MGy, when the curve becomes a nearly straight line again, albeit with a steeper slope, crossing the 300 kGy curve at a current of some 200 nA.

The collector curves for the BC108 transistors remained very close together over the majority of the range of base-emitter voltage. An increase in collector-emitter leakage current is visible, but this does not exceed a few hundred picoamps and, thus, is very unlikely to affect the type of circuitry used in-cell. There is no evidence of high-level injection effects over the range of current used here (noting that the maximum value of base current was limited to 10 microamps by the test software).

14.4 RADIATION-INDUCED CHANGE IN GAIN

The simple Messenger-Spratt equation (equation 6.60, repeated below at equation 14.2) indicates that the change in gain brought about by neutron irradiation is controlled by a simple term incorporating the total dose. The factor K is an energy dependent lifetime damage constant that is particular to each individual type of device and can only be determined empirically.

$$\frac{1}{\beta} = \frac{1}{\beta_0} + \frac{\Phi}{\omega_T K} \tag{14.2}$$

This equation can be modelled by assuming a value for the dose-dependence and continuing the assumptions made by Messenger, i.e. the gain is at least 3; surface effects are negligible; and the gain-bandwidth product does not change with irradiation. This gives an equation of the form:

$$\frac{1}{\beta} = \frac{1}{\beta_0} + \frac{\Phi}{K'} \tag{14.3}$$

where K' is a constant. This equation gives a basic relationship with dose that is shown in figure 14.6, using an initial value for gain of 100 and a value for K' of 1000.

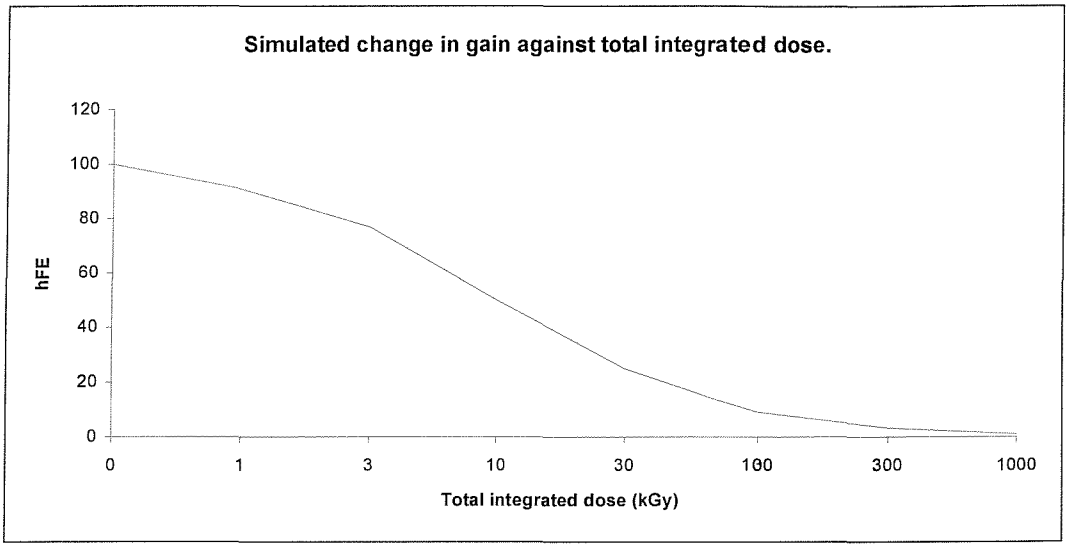

Figure 14.6: Change in gain with total dose according to equation 14.3.

It can be seen that the experimental results of this work do approximate to such a relationship at low to moderate total doses for the SU devices (figure 14.7), particularly for the two lower traces. The similarity is rather less obvious but extends over the whole total dose range for the BC108 transistors (figure 14.8).

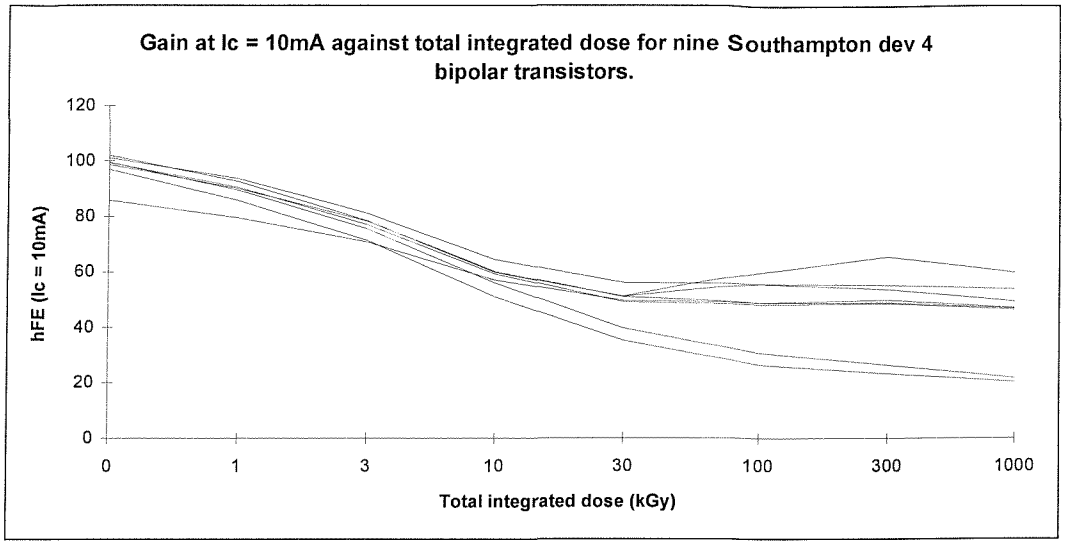

Figure 14.7: Change in gain (Ic = 10 mA) against total dose for SU device 4.

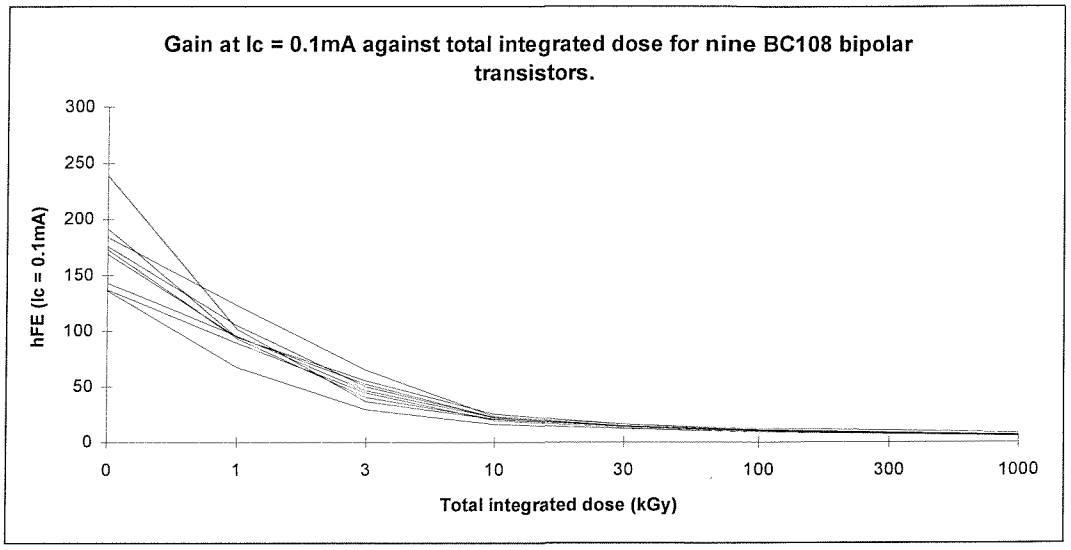

Figure 14.8: Change in gain (Ic = 0.1 mA) against total dose for BC108 (DS1522).

A difference in both cases between the measured and predicted data is that the magnitude of gain at high total dose remains higher than predicted by the Messenger-Spratt model. Therefore, the model appears to explain the changes observed at low to moderate total doses but does not accurately predict the behaviour at higher levels. One assumption made above is that the gain-bandwidth product remains constant. This is not true where the gain changes significantly. For a falling value of gain, and assuming that the bandwidth does not change, equation 14.2 shows a more rapid increase in the reciprocal gain at higher total doses, as shown the plot of gain against total dose in figure 14.9.

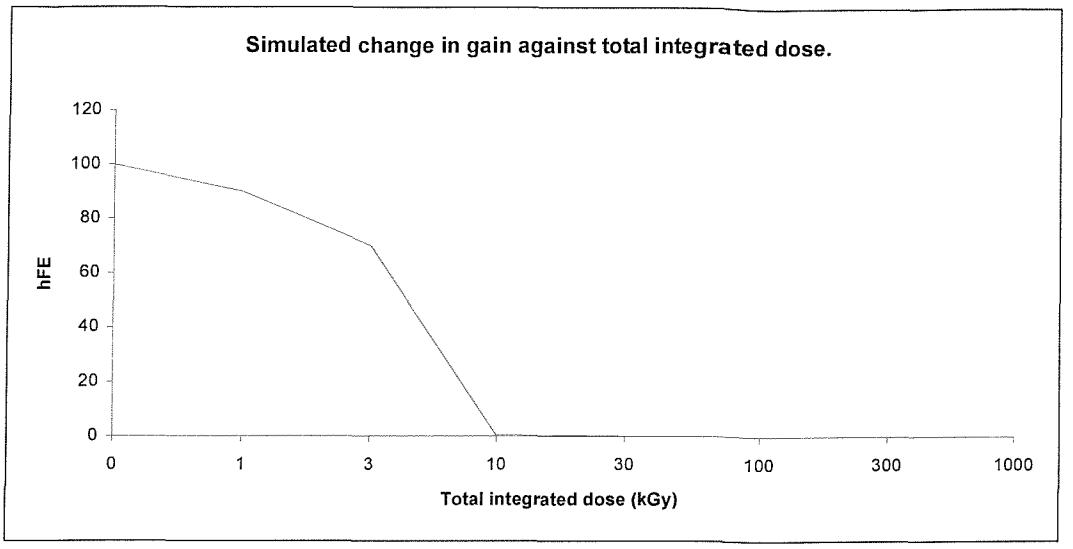

Figure 14.9: Change in gain with total dose according to equation 14.2.

Clearly, this does not match the experimental data as well as figure 14.6, confirming that the Messenger-Spratt model breaks down at higher total doses. The dose-dependent term requires modification in order to be applicable at total doses in the nuclear power industry regime.

A better model to the gain degradation curve at high total dose appears to be provided by a gain-independent factor for dose, as shown in figure 14.6, although the proportionate reduction in gain is too great. Using the results for the SU device 4 transistors shown in figure 14.7 and applying equation 14.3 to the measured gain data for the two lowest traces in the high total dose regime, values for K' can be extracted, as shown in figure 14.10.

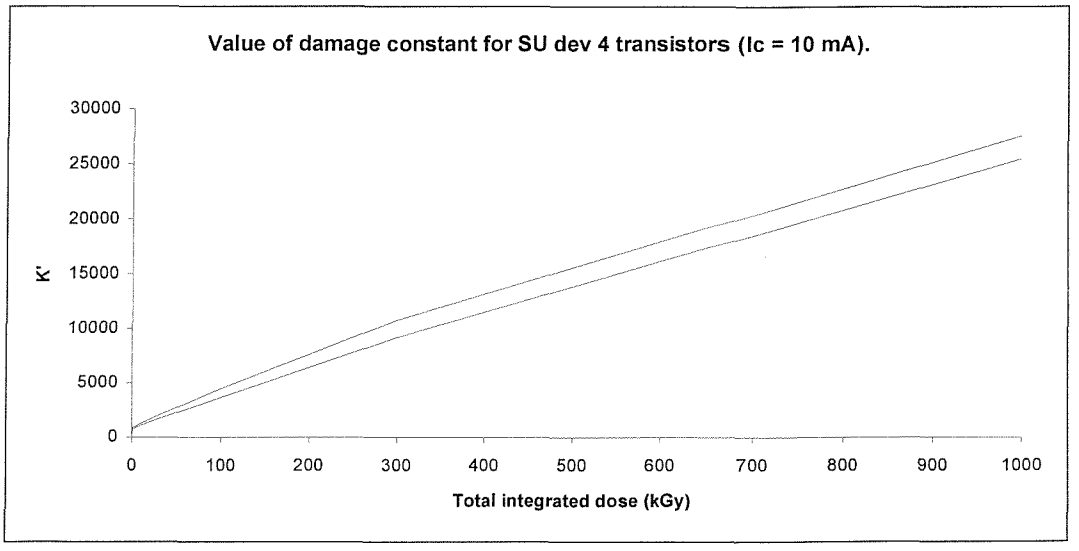

Figure 14.10: Damage constant against total dose for SU device 4.

Applying the same process to the results for the SU device 2 transistors, values for K' as shown in figure 14.11 are obtained.

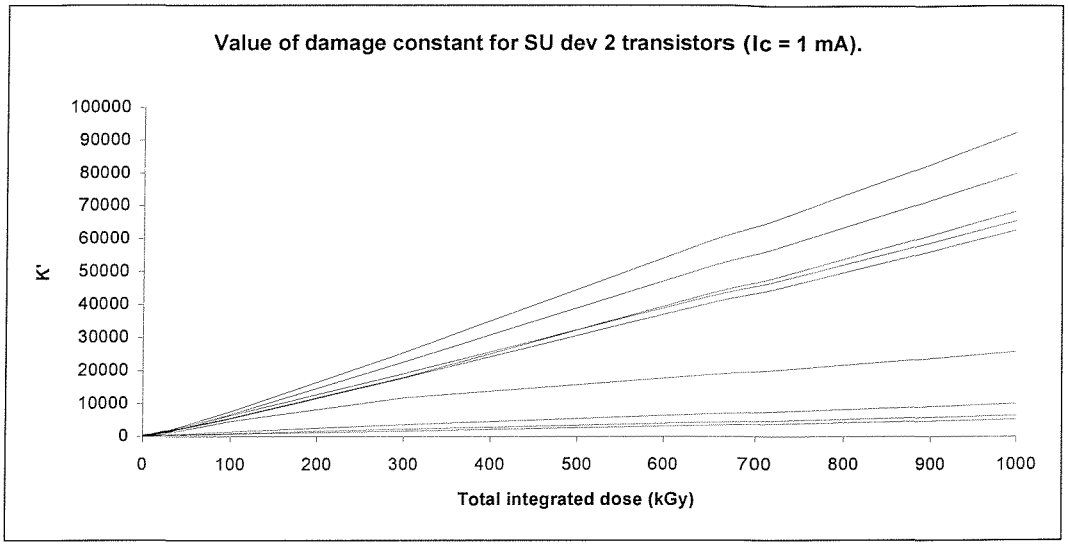

Figure 14.11: Damage constant against total dose for SU device 2.

Clearly, K' is not a constant and increases substantially and nearly linearly with total dose. Closer examination of the low dose region indicates that a quadratic expression better fits the data, although the coefficient of the square of the dose is very small. Hence, K' is nearly linearly dependent on total dose, especially at high values of total dose. The similarity of the traces in figure 14.10 reflects that of the measured gain data. The variation in the slope of the curves in figure 14.11 also reflects the measured data, showing that there was a greater range of results for these transistors.

Given that gain does not have a linear proportionality to total dose, a simple dependence of K' on gain is insufficient to explain the measured results. Higher values of total dose seem to have a proportionally lower effect on the reduction in gain. Consequently, the damage constant in the Messenger-Spratt equation does show a gain dependence at low total dose but this changes to a dose dependence at high total doses. Hence:

$$\frac{1}{\beta} = \frac{1}{\beta_0} + \frac{\Phi}{K'} \qquad (14.4)$$

does accord with the measured results, where

$$K' = f(\beta) \tag{14.5}$$

at low total doses and

$$K' = f(\Phi) \tag{14.6}$$

at high total doses.

Continuing the hypothesis that irradiation by gamma radiation reduces lifetime by the introduction of electrically active defects, we must now consider which lifetime(s) and how that affects gain. The three-term equation for gain derived in section 6.1 (equation 6.33) provides a convenient expression with which to probe this aspect. The first term in the equation is a reciprocal function of lifetime in the neutral base region. The second term is not directly dependent on any lifetime, until mobility effects become very significant. The third term is also a function of reciprocal lifetime, this time in the emitter-base region. It is useful to note that the second term is dependent on the ratio of the concentrations of donors and acceptors, including donor-like and acceptor-like defects, while the third term is dependent on the donor concentration. Thus,

$$\frac{1}{\beta} = f\left(\frac{1}{\tau_n}\right) + f\left(\frac{N_{AB}}{N_{DE}}\right) + f\left(\frac{N_{AB}}{\tau_0}\right) \tag{14.7}$$

and gain will fall as either of the lifetimes falls, as the donor concentration in the emitter falls and as the acceptor concentration in the base rises. Hence, one or more of these changes must occur as total dose increases in order for irradiation to cause a reduction in gain. In fact, for thin-base, small-signal transistors, such as those examined for this work, recombination in the bulk of the base is very small and unlikely to contribute significantly to the total base current, even after irradiation.

In the previous section, it was demonstrated that the ideality factor increases from almost exactly unity to nearly double that value over the range of total dose examined. This is indicative of recombination in the emitter-base region contributing increasingly to the base current as total dose rises. This can be interpreted as the third term in equation 14.7 becoming more dominant as total dose increases. This must be due either to the donor-like defect concentration rising or to the lifetime in that region falling or, alternatively, to a combination of both factors. Hence, we can modify this equation as follows:

$$\frac{1}{\beta} = f\left(\frac{1}{\tau_n(\Phi)}\right) + f\left(\frac{N_{AB}(\Phi)}{N_{DE}(\Phi)}\right) + f\left(\frac{N_{AB}(\Phi)}{\tau_0(\Phi)}\right) \qquad (14.8)$$

Sections 12.5.1 shows the change in emitter-base leakage current. Both of these parameters exhibited a small rise with total dose, indicating that the donor-like and acceptor-like defect concentrations have changed, albeit not dramatically. The C-V measurements provide more insight into defect concentration changes and these are covered in section 14.7 below, showing changes of between 5 and 10%. Thus, we may conclude that the increase in recombination in the emitter-base region is due mostly to a reduction in the carrier lifetime in this region. This demonstrates that the process of irradiation using gamma radiation produces defects with similar, lifetime altering properties as the electron and proton irradiation described previously.

Nevertheless, the changes in gain observed at higher total doses cannot be explained by a model based on falling minority carrier lifetime alone. In several cases, gain was observed to rise slightly after a total dose of 100 to 300 kilogray, although this did not occur for all of the device types. It was seen, for example, in many of the SU devices but not at all for the BC108 transistors. There are three candidates for this effect.
It has already been shown that the doping concentration can be affected by high doses of radiation by the radiation-induced introduction of acceptor and donor-like defect states. The effect is small and so would be expected to become visible only in the highest part of the total dose range. It is feasible that the relative concentration of minority and majority carrier-like defects might change under these conditions, leading to competition between the emitter injection and emitter-base recombination terms in equation 6.33 and therefore influencing the change in gain as lifetime falls. This could be examined by a technique such as DLTS to identify the defects and their relative concentrations. The C-V measurements indicate a maximum change of between 5 and 10% of the initial doping concentration (see section 14.7). This contributes but does not account for all the observed change in gain.
A second mechanism is the suggestion that the increase in gain at high total doses is due to the small degree of dislocation damage caused by the gamma radiation, as discussed above. This damage leads, via a reduction in the carrier concentration, to an increase in resistivity. For constant bias conditions, the current flowing is therefore reduced, reflected in a shift in the base current curve on the Gummel plot in the

opposite direction from that induced by falling carrier lifetime. By definition, the gain increases again when this happens. The increase in resistivity is small and so one would expect the increase in gain also to be small and this is the case in practice. However, the greatest effect is observed to take place at low base-emitter voltage, just where the impact of resistivity changes are at their lowest. The magnitude of the shift in the base current curve would hardly be visible, corresponding to a few millivolts, at most.

The effects of minority carrier lifetime reduction and resistivity increase are competing at high total doses and so it would be expected for some devices to show one effect dominating and other devices to reflect the opposite trend, depending on their design and fabrication. Hence, some devices would show gain continuing to fall, whilst others would show a slight increase with total dose. This accords with the pattern observed during this work. If the initial rate of decrease in minority carrier lifetime due to irradiation is low then the decrease could continue to higher values of total dose, masking the effect of any increase in resistivity. Conversely, if the minority carrier lifetime falls quickly at first, with the rate of change slowing down at moderate total doses, then the influence of a small rise in resistivity would be more readily apparent at high total doses.

The final candidate is surface effects. As described in section 6, surface effects have been shown to be an important aspect of radiation effects in some cases. Where the base depletion region reaches to the surface of the device and where this region has been extended due to charge imbalance, recombination of carriers at the surface can rise significantly. The build-up of charge at surface states that cannot exchange charge with the bulk can cause this effect. This effectively adds to the base recombination term of equation 6.33 and so, assuming that the surface potential and surface recombination velocity do not change, causes a reduction in gain. However, by definition, increased recombination means an increase in surface potential and Brucker (1966) showed that the surface potential does, indeed, increase with irradiation. This would act to reduce the applied base-emitter voltage and therefore lower the base current at a given value of base-emitter voltage, i.e. the gain would stop falling and then increase as the surface potential continued to rise. He was unable to find a case where the gain rose as he predicted but such a phenomenon has been measured here. Consequently, surface effects are also a potential cause of the anomalous rise and subsequent repeated fall in gain at high total doses. However, this aspect is beyond the scope of the current work and its influence remains speculative.

14.5 THE DETECTION OF SURFACE EFFECTS BY THE POCH METHOD

An assumption was made in the derivation of equations 6.30 and 6.32 that collector-base leakage current is negligible when compared with the emitter current likely to be used in a circuit. The post-irradiation measurements made here show that, whilst an increase in this leakage current was observed, it did not exceed a few nanoamps, even after a total dose of 1 MGy, and so the assumption remains valid after irradiation to high total doses. The implication of this is that the minority carrier lifetime must be affected by irradiation in a linear fashion relative to the changes in gain measured during the tests. Further assumptions were made, omitting surface and high-level injection effects. The latter have already been ruled out for the BC108 transistors and all but a very small number of the SU devices. Surface effects have been shown to play a role in radiation damage where gamma radiation is the principal contributor and so they might well have an influence on the link between gain and lifetime.

One method for detecting surface effects was suggested by Poch and is expressed in equation 6.67 as a development of the Messenger-Spratt equation. This equation says that the change in reciprocal gain is equivalent to the sum of two components, one related to surface damage (which would dominate in the low total dose regime) with a power dependence lying between 0.4 and 1 and the other component related to bulk damage (which would become more relevant as total dose increased), following a power law of unity. Plotting the change in reciprocal gain enables this theory to be tested. Figures 14.12 and 14.13 show this quantity for the BC108 transistors, plotted with a logarithmic total dose scale, measured at collector currents of 0.01 and 10 mA, respectively. Figures 14.14 and 14.15 show the same data with a linear total dose scale. The curves for collector currents of 0.1 and 1 mA lie between the examples shown. Figures 14.14 and 14.15 show that a power dependence of less than unity applies, certainly over the first part of the total dose scale. At higher total doses, the curves straighten out, particularly at the higher values of collector current, indicating that the power dependence has increased. Nevertheless, it can clearly be seen that a unity power dependence applies only for the very high total dose region. According to Poch, this indicates that surface damage dominates for low and moderate total doses, with bulk damage becoming important around 100 kGy and then dominating at higher total doses.

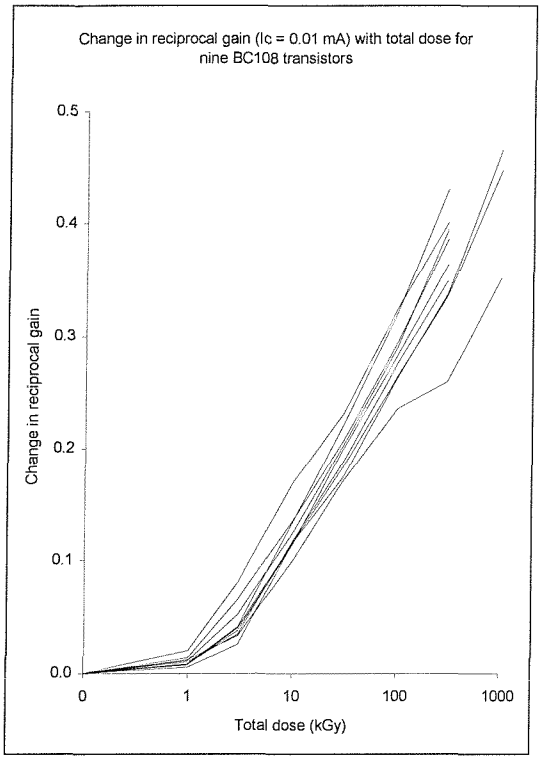

Figure 14.12: change in reciprocal gain (Ic = 0.01 mA) with total dose for the BC108 transistors.

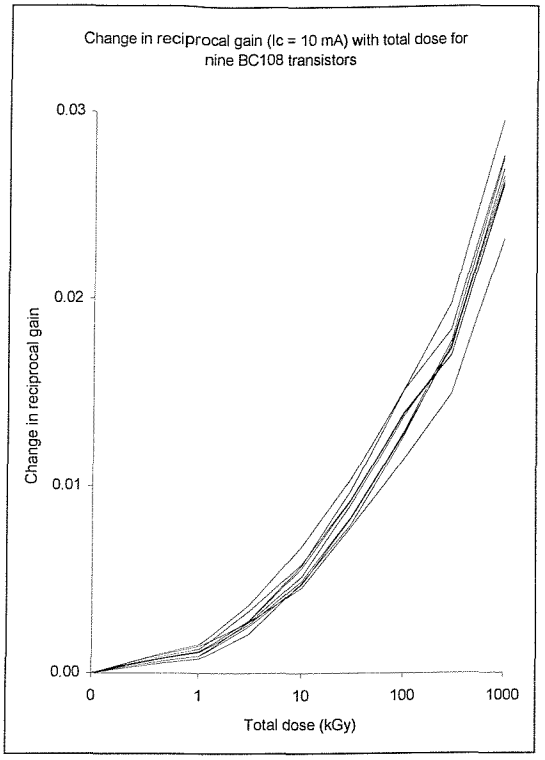

Figure 14.13: change in reciprocal gain (Ic = 10 mA) with total dose for the BC108 transistors.

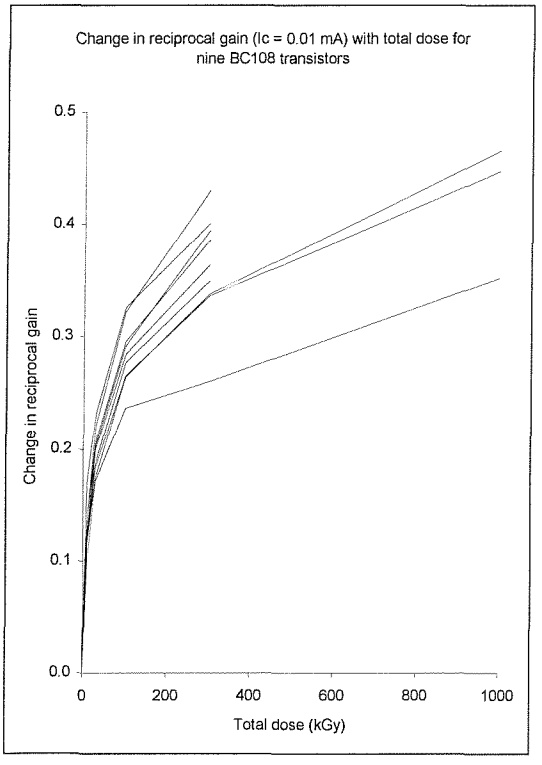

Figure 14.14: figure 14.12 with a linear total dose scale.

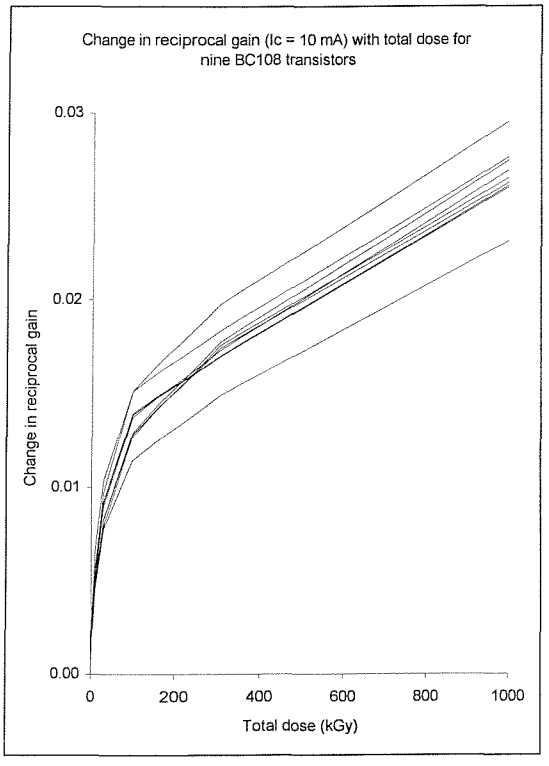

Figure 14.15: figure 14.13 with a linear total dose scale.

In the case of the SU devices, there are some similarities with the data for the BC108 transistors and some differences. Figures 14.16 and 14.17 show plots of the change in reciprocal gain for two of the device types, using a linear scale for total dose.

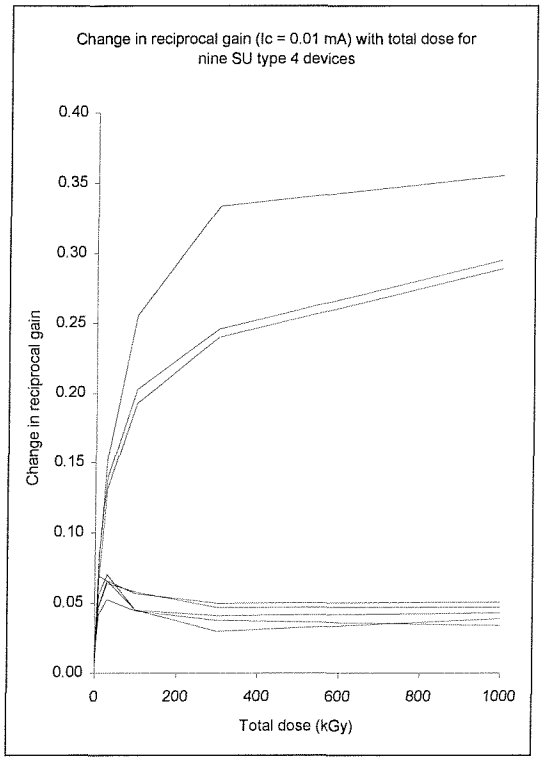

Figure 14.16: change in reciprocal gain (Ic = 0.01 mA) with total dose for the SU type 4 devices.

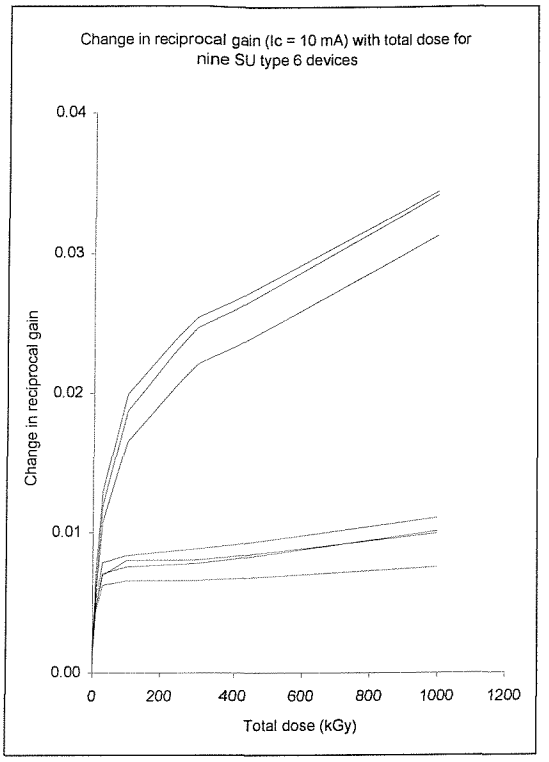

Figure 14.17: change in reciprocal gain (Ic = 10 mA) with total dose for the SU type 6 devices.

Both figures show two distinct groups of devices, corresponding to the biased (lower set of curves) and unbiased (upper set) conditions during irradiation. For the biased devices, the curves rise until a total dose of 100 kGy has been received, after which point they flatten out and either rise or fall only slightly. The curves for the unbiased devices, on the other hand, continue their rise without any break, maintaining the same power dependence over the whole total dose range. This has a significant implication for the type of damage occurring in the two cases. The biased devices appear to show a surface damage contribution at low and moderate total doses, with the bulk damage contribution becoming dominant around 30 kGy. The unbiased devices appear to show no contribution from the bulk damage factor, even after a total dose of 1 MGy. At the lowest total doses, the two groups of curves are very close

together, separating only after the first few stages of total dose have been accumulated. This fact is clearer on a plot with a logarithmic total dose scale, as can be seen by comparing figures 14.18 and 14.19 with figures 14.16 and 14.17.

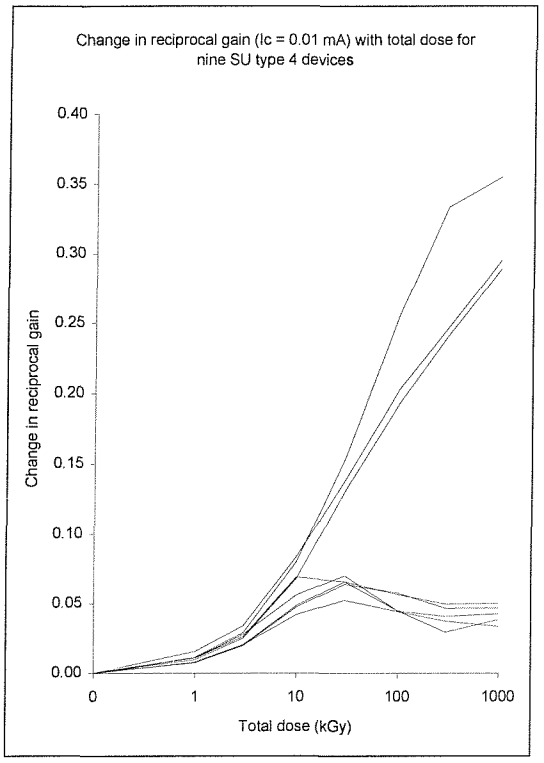

Figure 14.18: figure 14.16 with a logarithmic total dose scale.

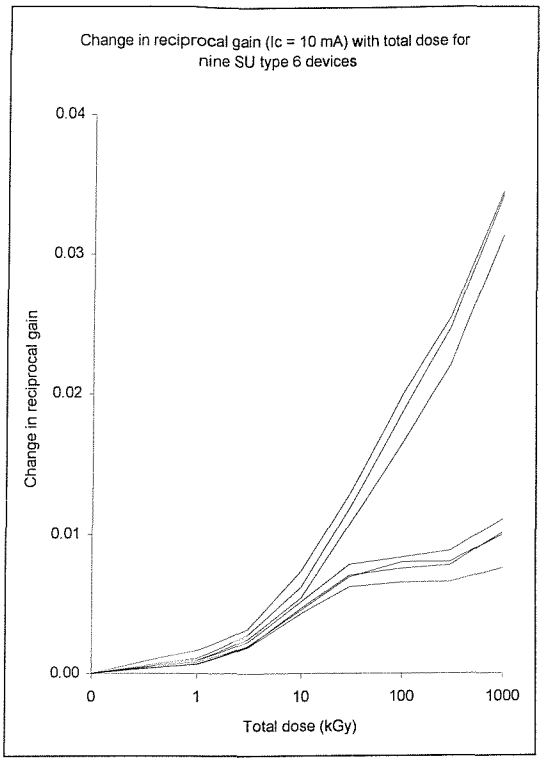

Figure 14.19: figure 14.17 with a logarithmic total dose scale.

Hence, it may be concluded that bias has a significant influence on the predominant form of damage that occurs in these devices. For biased devices, bulk or displacement damage appears to have a marked effect at high total doses. For unbiased devices, surface damage appears to remain the most important degradation mechanism, even at total doses as high as 1 MGy. Clearly, further investigation of the influence of bias on the degradation mechanisms is warranted. However, this is beyond the scope of this present work.

Another view on the gain data is to consider the change in reciprocal gain across a range of collector current at various total doses. If the damage constants show a logarithmic proportionality to collector current, as suggested by Poch, then a plot of the change in reciprocal gain against collector current on a logarithmic scale should show a series of parallel lines. Figure 14.20 illustrates this plot for one of the BC108 devices, showing how the curves form a series of parallel curves, shifting towards the

upper right region of the graph with increasing total dose. This demonstrates that, while the relationship between the damage constants and collector current is clearly far from linear, it is not exactly logarithmic either.

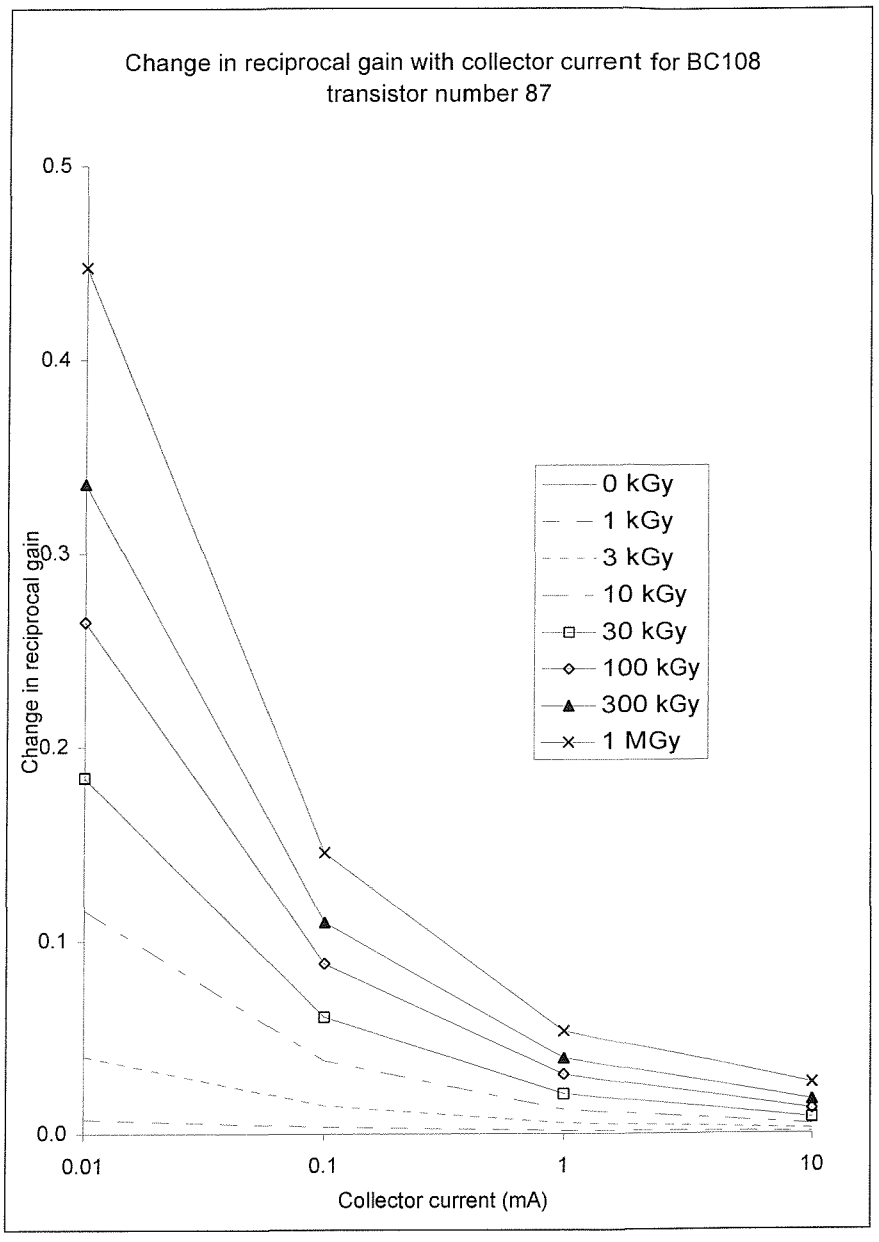

Figure 14.20: change in reciprocal gain against collector current for BC108 transistor number 87.

For completeness, two similar figures are presented for the SU devices, one for the case of an unbiased device (figure 14.21) and one for a biased device (figure 14.22).

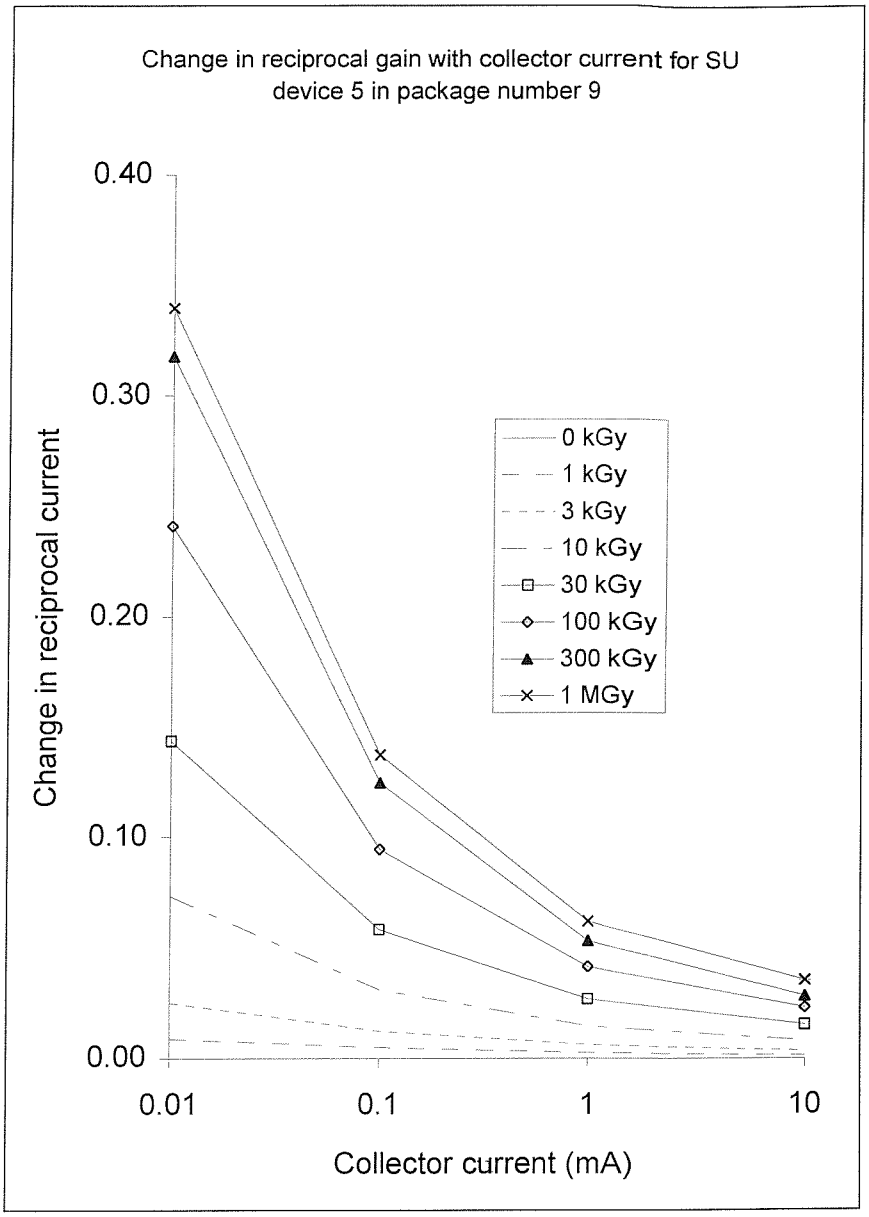

Figure 14.21: change in reciprocal gain against collector current for SU device number 5 in package number 9.

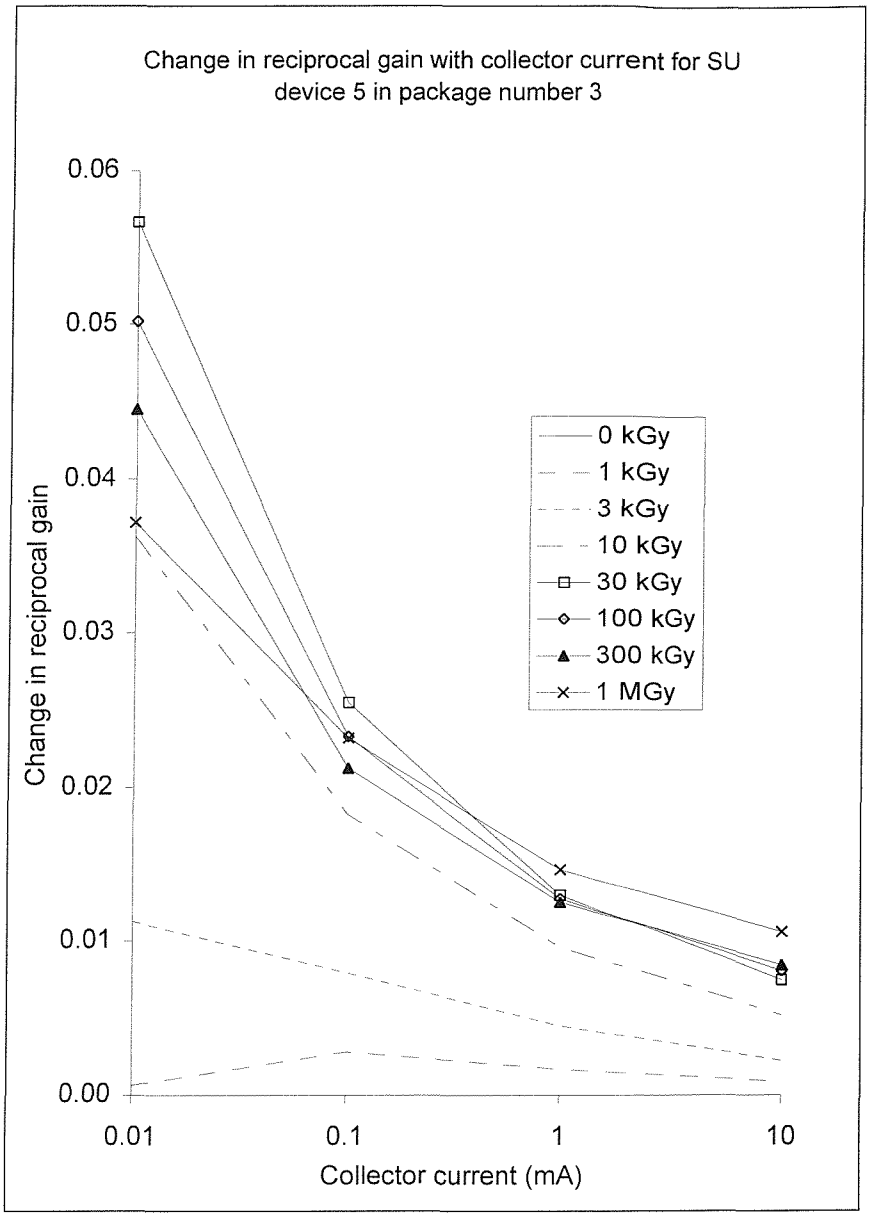

Figure 14.22: change in reciprocal gain against collector current for SU device number 5 in package number 3.

Both of these figures show a similar result: while the damage constants are related to collector current by a power law, it is not a simple relationship. It is also clear from these two figures that there is, again, a large difference between the unbiased and biased cases. The conclusions from this part of the analysis are unclear and indicate that the Poch approach adds little to the understanding of the radiation effects observed for these devices over the wide range of total dose examined. Poch's model may apply to low total doses but does not appear to work in the regime considered here.

14.6 LIFETIME DATA

At 1.1 eV, the bandgap in silicon is too large for thermally stimulated carriers to be able to cross it directly. Use of silicon as a semiconductor, therefore, requires donor and acceptor states to be introduced near the edges of the bandgap to enable conduction to take place. This is achieved by the introduction of dopants during fabrication. Irradiation also introduces states in the bandgap, the most damaging of which lie near its centre, by creating defects in the lattice structure through a range secondary phenomena.

It had been hoped that, in the absence of DLTS data, the minority carrier lifetime measurements would enable the defect creation process and distribution in the regions of interest to be probed. This information would have been a very useful aid towards understanding the effects of irradiation at a microscopic level. Unfortunately, the characteristics of the SU devices prevented such measurements. Some measurements were made on COTS transistors and these appeared, initially, to demonstrate that lifetime fell rapidly with total dose. Results for ZTX450 transistors, for example, showed a 50% reduction after a total dose of just 10 kGy. The storage time data obtained from the BC108 transistors also looked promising. Subsequent calculations based upon the data, however, showed that they indicated an increase in lifetime. This was in clear contradiction to the changes in other parameter values, most notably gain, that proved that lifetime was indeed falling.

The contradiction shown here could have been due to an assumption falsely having been made during the derivation of the equations or to a fault with the measurement technique or instrumentation used. It is possible, therefore, that the SU devices could have given acceptable results if the postulated fault with the set-up had been eliminated. However, in the absence of any other technique for measuring the lifetime directly on the packaged devices, the root of the problem could not be traced.

Whilst there are several proven methods for measuring minority carrier lifetime on bare die or test structures, the lack of a technique for packaged devices, without using complex and expensive test equipment, is a substantial impediment to understanding the processes at a microscopic level caused by exposure to irradiation.

14.7 C-V DATA

The C-V data for the SU devices showed very similar responses to irradiation, both across different device types and between the two measurement frequencies. Consequently, only a selection of plots is presented here and all show results taken at 100 kHz.

Equation 6.71 shows that by plotting $1/C^2$ against the applied bias voltage, a slope equivalent to the defect concentration is obtained The intercept of this plot gives the so-called built-in potential, equivalent to the difference between the barrier height of the junction and V_n, the difference between the Fermi level and the bottom of the conduction band (Sze (1985)). Taking two examples for collector-base capacitance, we can examine the implications of this in terms of the results obtained here. In the following diagrams, the first two plots show the capacitance-voltage curves and the next two show the respective $1/C^2$ curves. Figures 14.23 to 14.30 show collector-base capacitance data for four different SU devices.

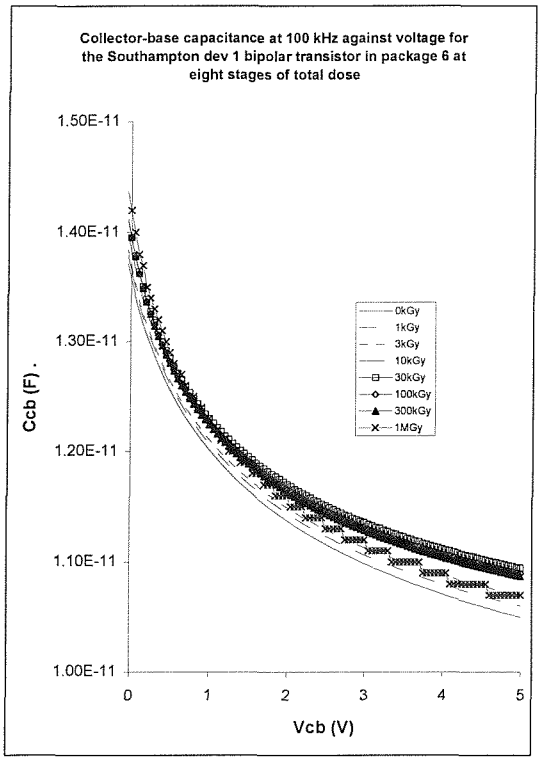

Figure 14.23: Collector-base C-V plot at 100 kHz for device 1 in package 6.

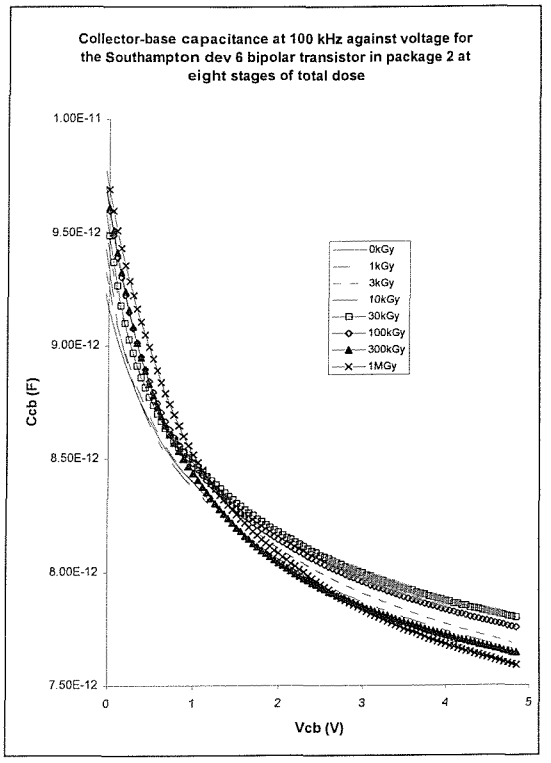

Figure 14.24: Collector-base C-V plot at 100 kHz for device 6 in package 2.

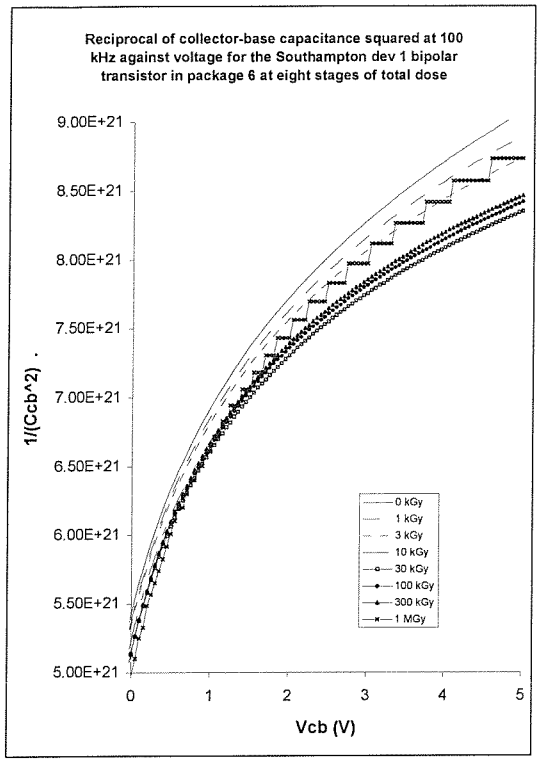

Figure 14.25: $1/C_{cb}^{2}$ plot at 100 kHz for device 1 in package 6.

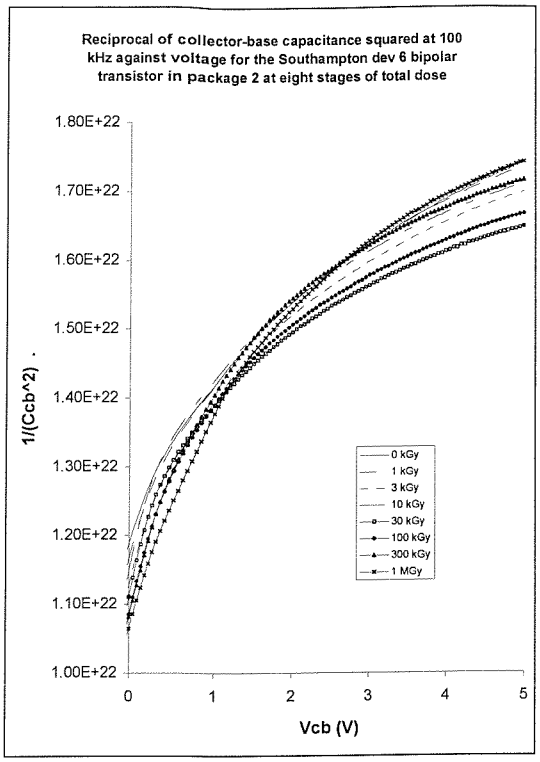

Figure 14.26: $1/C_{cb}^{2}$ plot at 100 kHz for device 6 in package 2.

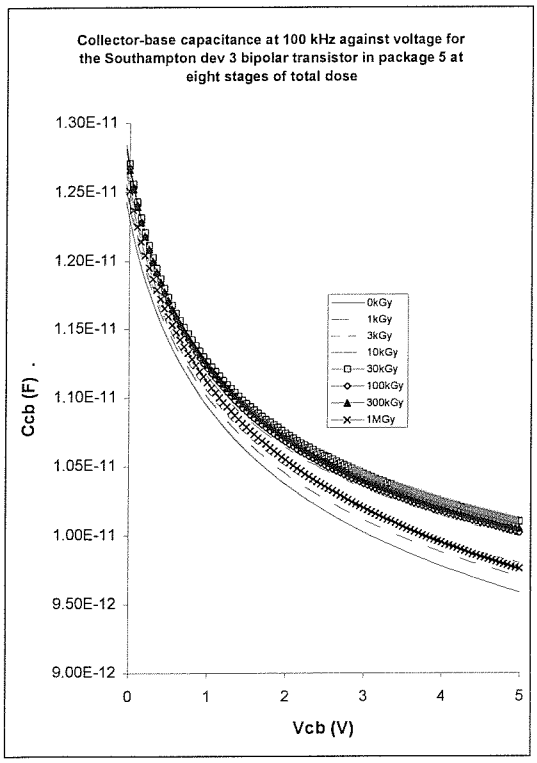

Figure 14.27: Collector-base C-V plot at 100 kHz for device 3 in package 5.

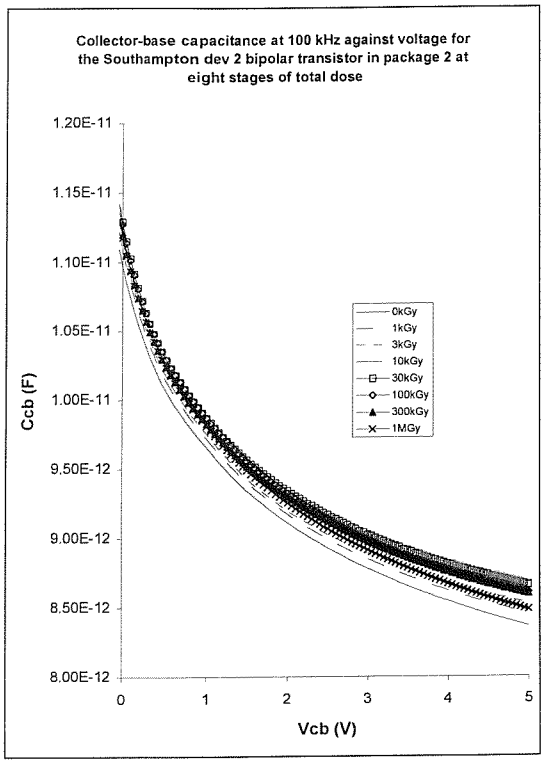

Figure 14.28: Collector-base C-V plot at 100 kHz for device 2 in package 2.

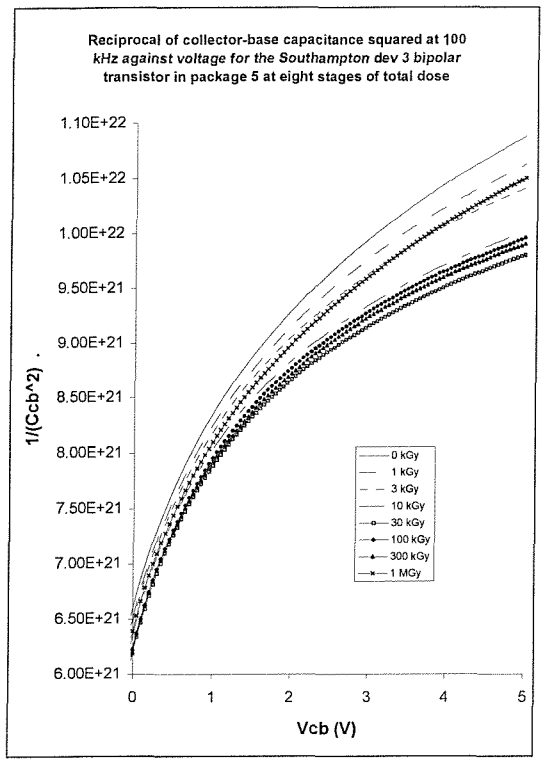

Figure 14.29: $1/C_{cb}^2$ plot at 100 kHz for device 3 in package 5.

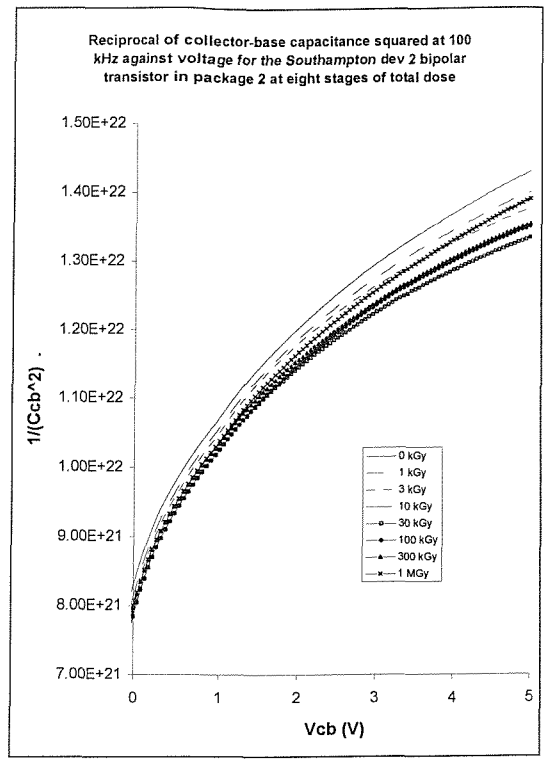

Figure 14.30: $1/C_{cb}^2$ plot at 100 kHz for device 2 in package 2.

The collector-base C-V curves all show the same pattern. The magnitude of capacitance increases with total dose up to 30 kGy and then falls back towards the pre-irradiation value as total dose rises further. This is mirrored in the $1/C^2$ plots, where the value at a given voltage falls to a minimum at 30 kGy and then rises again as total dose increases.

The one partial exception to this trend is device 6 in package 2, which shows a monotonic trend for capacitance changes with total dose at low values of reverse bias. At voltages above approximately 1 volt, it follows the same trend as the other devices. It can clearly be seen that none of the $1/C^2$ plots shows a straight line, as predicted by equation 6.71. This implies that these devices do not have simple, step junctions and that the doping concentration varies across the depletion region. The maximum change is between 5 and 10% of the pre-irradiation value.

The radiation-induced change is more clearly apparent in figures 14.31 to 14.34, showing the change in slope of the $1/C^2$ plots against total dose. Values are plotted for collector-base voltages of 2 and 4 volts, illustrating the difference in measured doping concentration with depth.

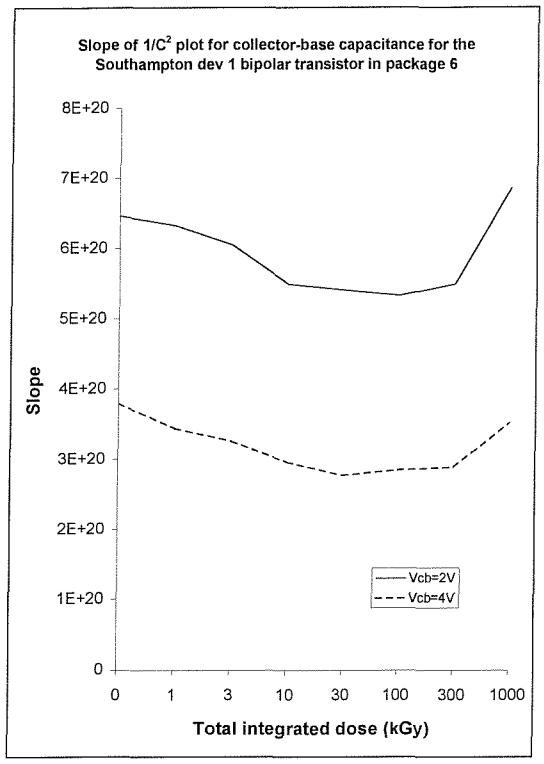

Figure 14.31: slope of $1/C_{cb}^{2}$ plot at 100 kHz for device 1 in package 6.

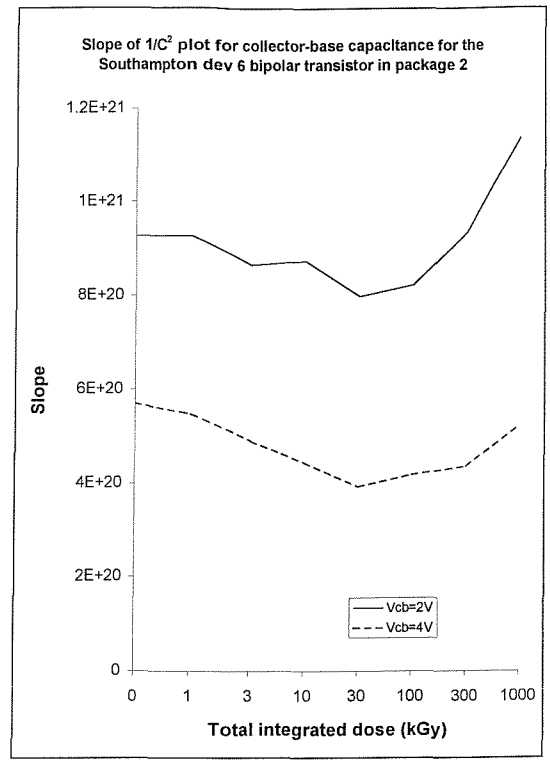

Figure 14.32: slope of $1/C_{cb}^{2}$ plot at 100 kHz for device 6 in package 2.

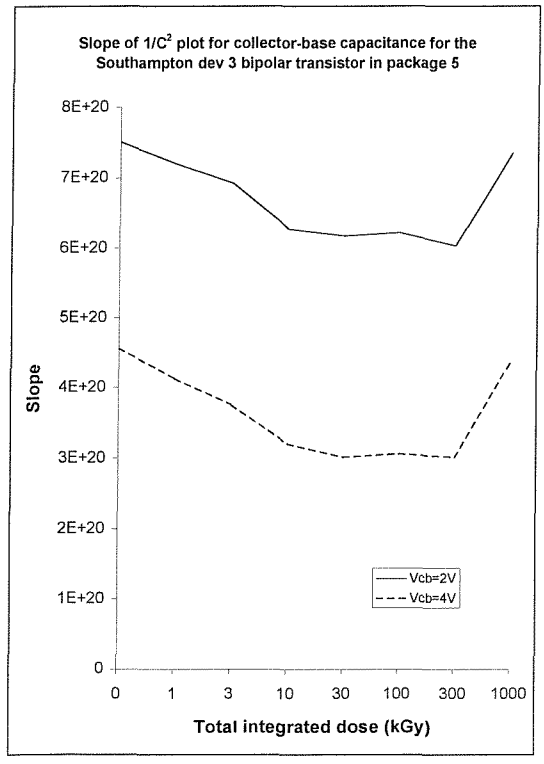

Figure 14.33: slope of $1/C_{cb}^{2}$ plot at 100 kHz for device 3 in package 5.

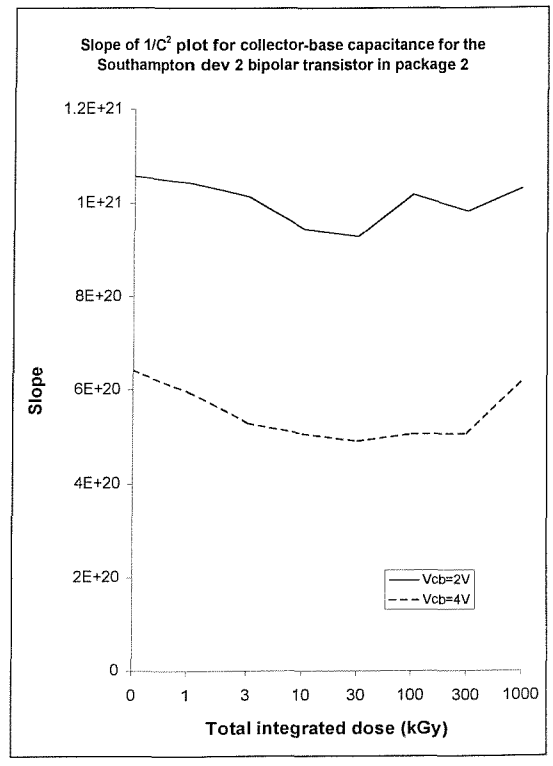

Figure 14.34: slope of $1/C_{cb}^{2}$ plot at 100 kHz for device 2 in package 2.

These figures show changes of between 5 and 20% in the slope of the $1/C^2$ plots, implying that irradiation has introduced defects to a concentration of between 5 and 20% of the initial doping concentration by a total dose of 30 kGy. These radiation-induced defects act so as to reduce the effective doping concentration. Hence, in the case of the collector-base C-V plots, acceptor-like defects are being created in the n-type, collector material. The majority of these radiation-induced defects has then been annihilated or compensated for as the total dose rises further to 1 MGy.

Figures 14.35 to 14.42 show the emitter-base capacitance results for the same four SU devices as above, also with the capacitance voltage plots followed by the $1/C^2$ curves and then plots of the slope of these curves against total dose.

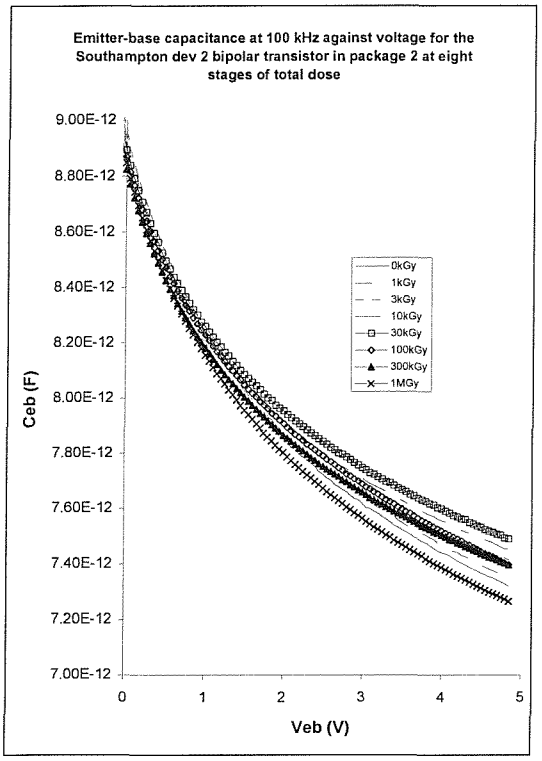

Figure 14.35: Emitter-base C-V plot at 100 kHz for device 1 in package 6.

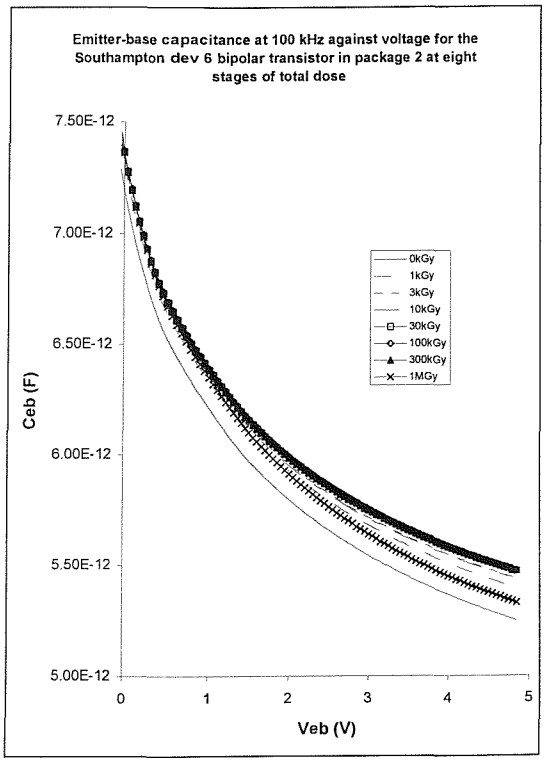

Figure 14.36: Emitter-base C-V plot at 100 kHz for device 6 in package 2.

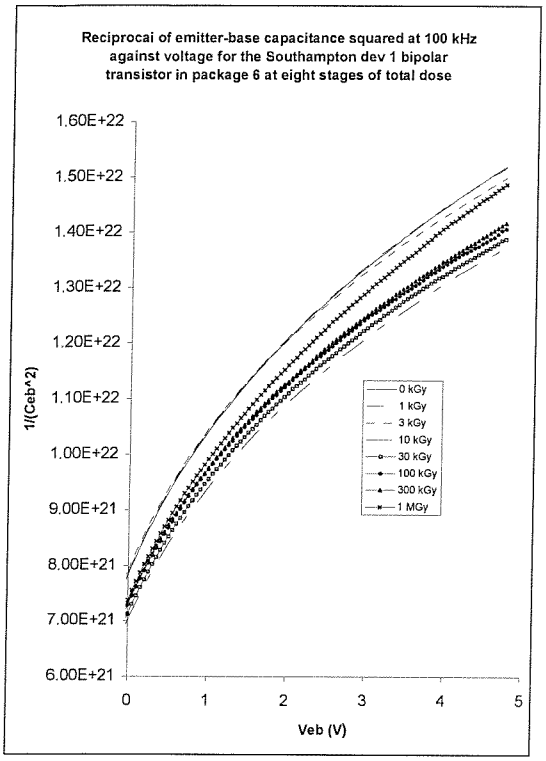

Figure 14.37: $1/C_{eb}^2$ plot at 100 kHz for device 1 in package 6.

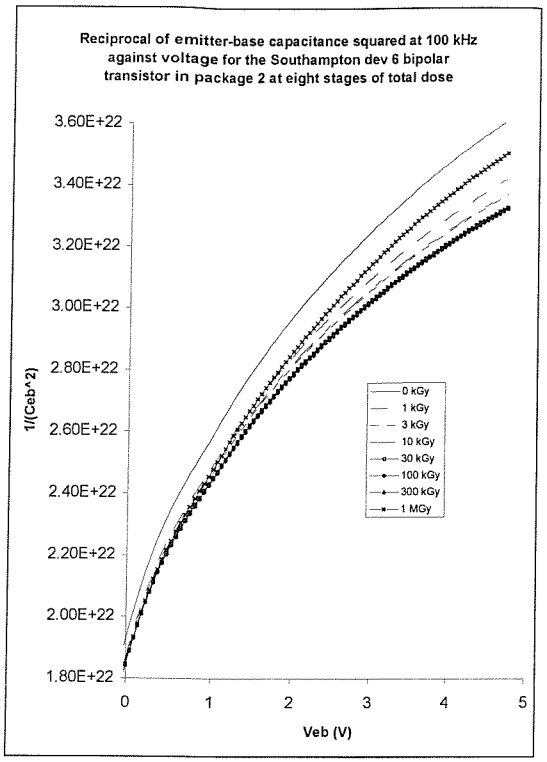

Figure 14.38: $1/C_{eb}^2$ plot at 100 kHz for device 6 in package 2.

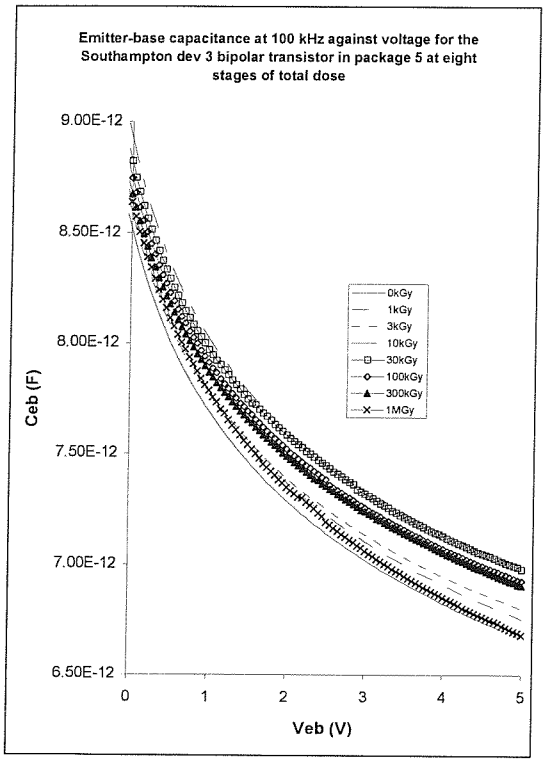

Figure 14.39: Emitter-base C-V plot at 100 kHz for device 3 in package 5.

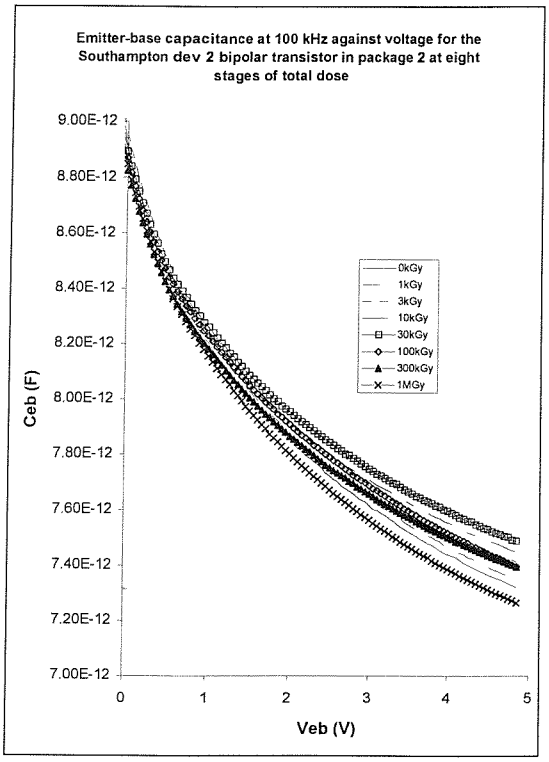

Figure 14.40: Emitter-base C-V plot at 100 kHz for device 2 in package 2.

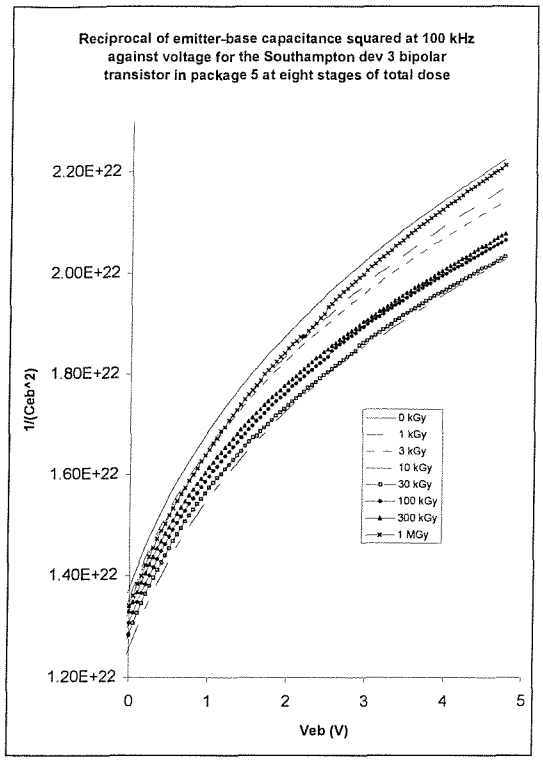

Figure 14.41: $1/C_{eb}^2$ plot at 100 kHz for device 3 in package 5.

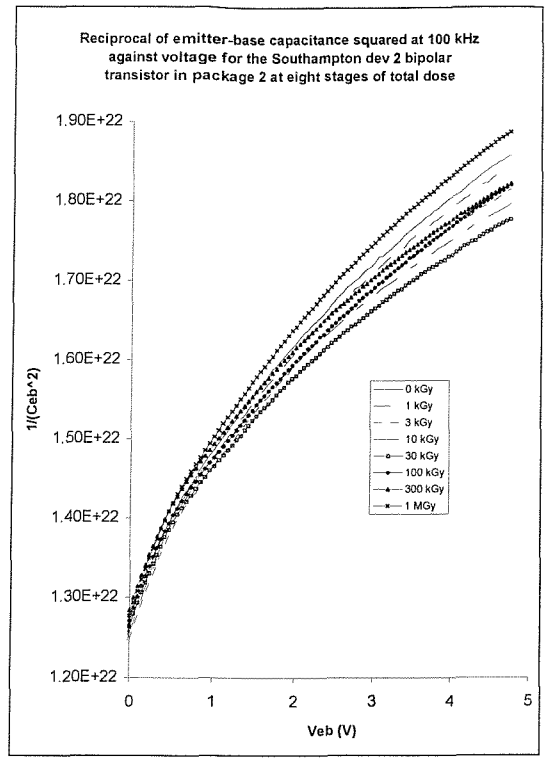

Figure 14.42: $1/C_{eb}^2$ plot at 100 kHz for device 2 in package 2.

The emitter-base data follow a very similar pattern to that described for the collector-base data above. The maximum value of capacitance is reached between 10 and 30 kGy and device 6 in package 2 shows a small difference at low voltage, although this is less clear than for the collector-base capacitance. The magnitude of the observed changes is again in the range from 5 to 10%. Again, the the $1/C^2$ plots show curves rather than straight lines.

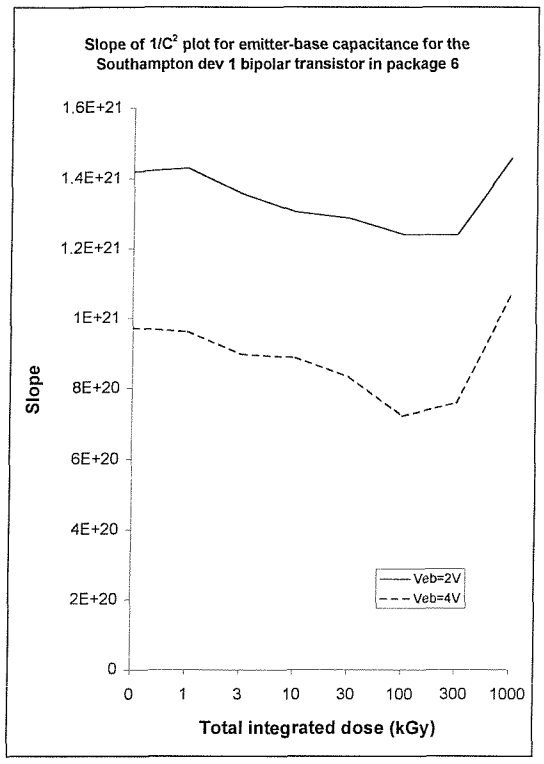

Figure 14.43: slope of $1/C_{eb}^{2}$ plot at 100 kHz for device 1 in package 6.

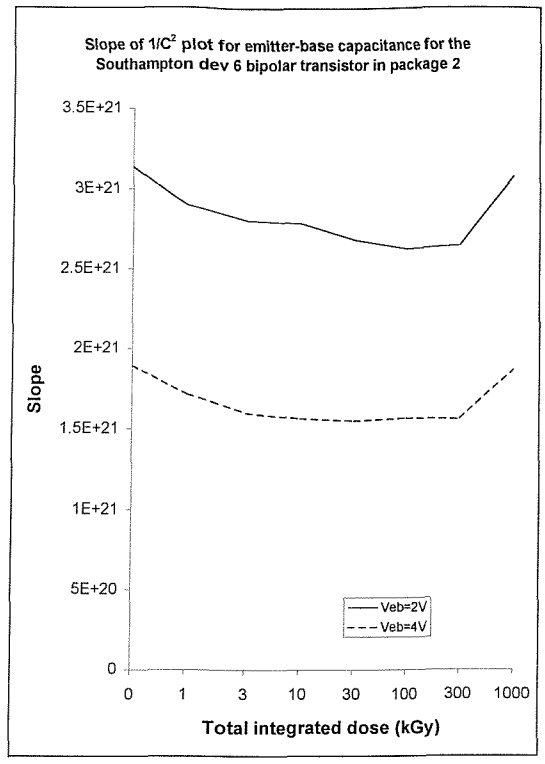

Figure 14.44: slope of $1/C_{eb}^{2}$ plot at 100 kHz for device 6 in package 2.

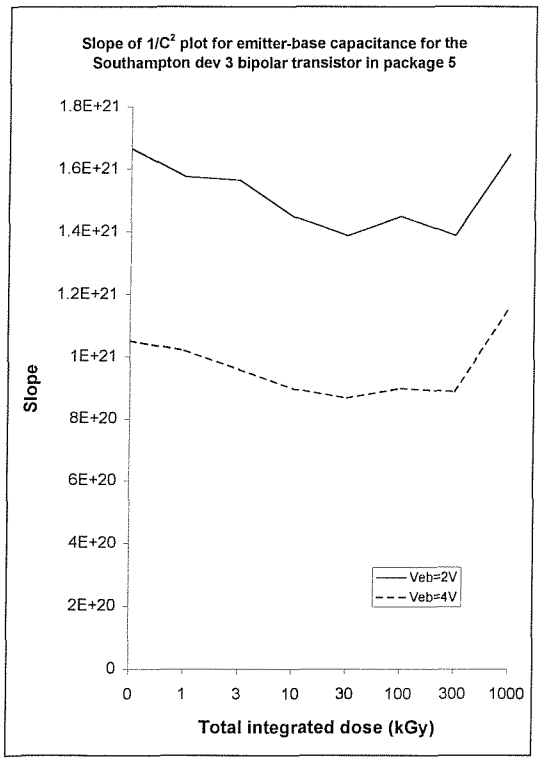

Figure 14.45: slope of $1/C_{eb}^{2}$ plot at 100 kHz for device 3 in package 5.

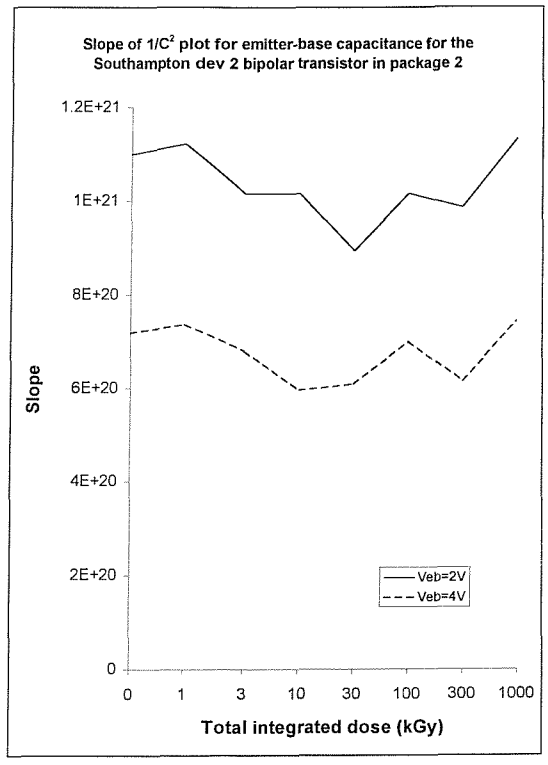

Figure 14.46: slope of $1/C_{eb}^{2}$ plot at 100 kHz for device 2 in package 2.

The slope plots for both collector-base and emitter-base capacitance show similar trends with total dose. The measured effective doping concentration is shown to reduce by between 5 and 20% with total dose for total doses of up to 30 to 300 kGy. For higher total doses, the measured value increases, either attaining the pre-irradiation value or even exceeding it in some cases. The overall pattern is very similar across the range of device types, packages, junction and depth into the depletion region, implying a very consistent effect.

As for the SU devices, the data for the BC108 transistors showed consistent results and so, again, data at only 100 kHz are presented. The collector-base capacitance data for the BC108 devices is illustrated in figures 14.47 to 14.52 for two devices.

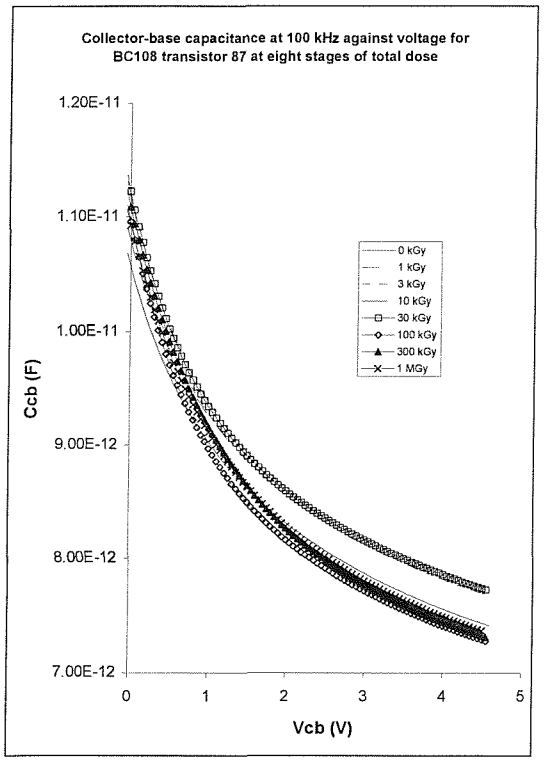

Figure 14.47: Collector-base C-V plot at 100 kHz for BC108 device number 87.

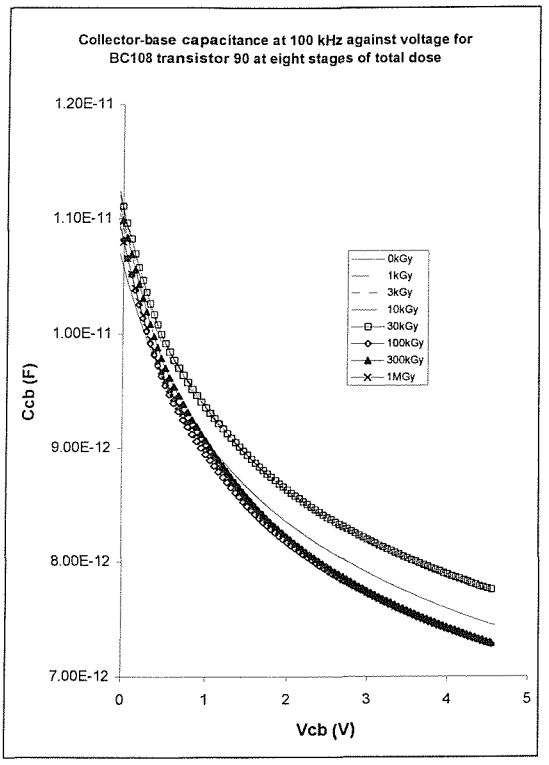

Figure 14.48: Collector-base C-V plot at 100 kHz for BC108 device number 90.

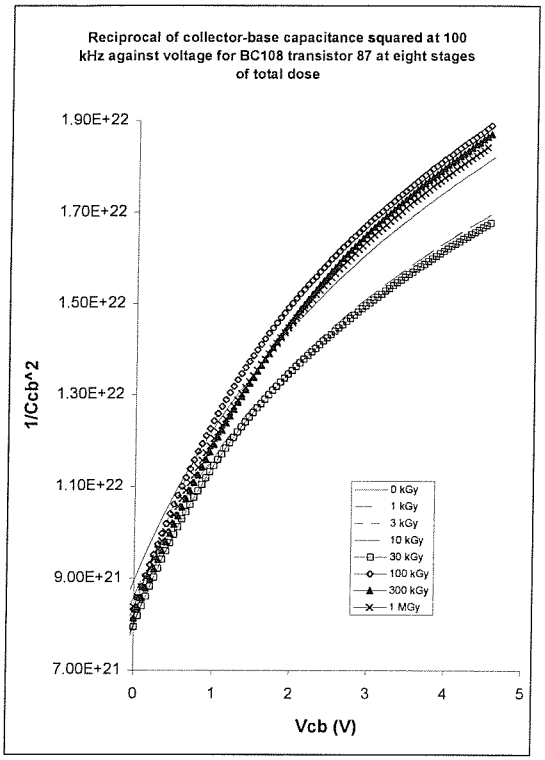

Figure 14.49: $1/C_{cb}^{2}$ plot at 100 kHz for BC108 device number 87.

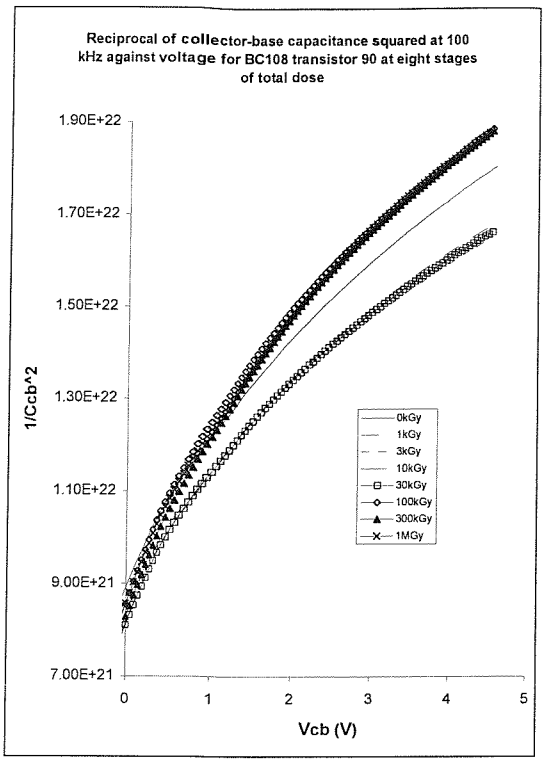

Figure 14.50: $1/C_{cb}^{2}$ plot at 100 kHz for BC108 device number 90.

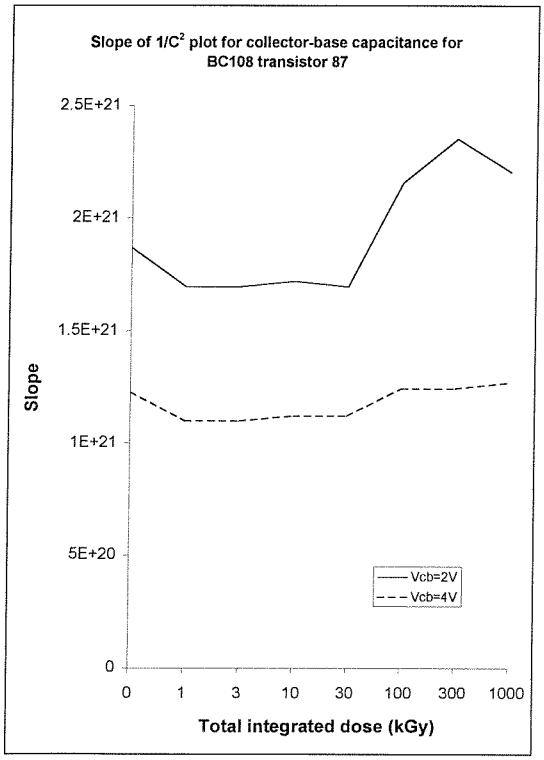

Figure 14.51: slope of $1/C_{cb}^{2}$ plot at 100 kHz for BC108 device number 87.

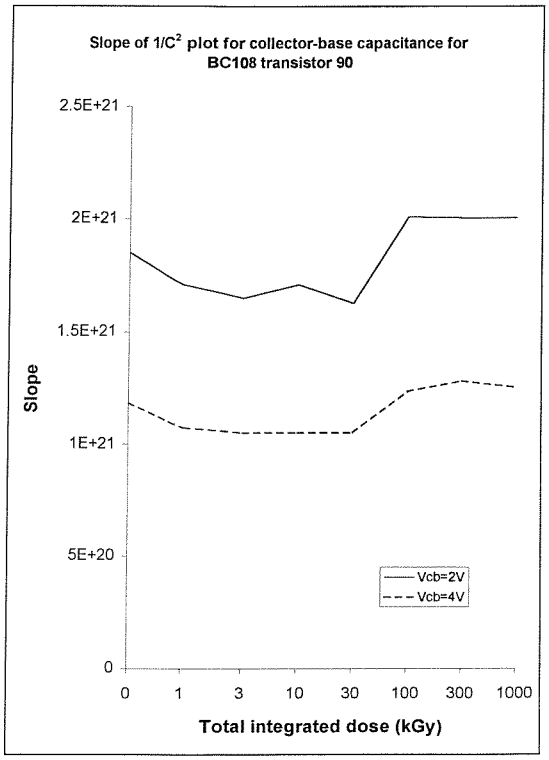

Figure 14.52: slope of $1/C_{cb}^{2}$ plot at 100 kHz for BC108 device number 90.

These devices showed a slightly different response to irradiation than did the SU devices. The measured value of capacitance rose after the first stage of irradiation, remained roughly constant up to 30 kGy and then fell sharply to below the pre-irradiation value for measurements at higher total doses. The magnitude of the maximum change was similar to that exhibited by the SU devices, i.e. between 5 and 10%. The slope of the $1/C^2$ plots show that the effective doping concentration in the region of the collector nearest the base was reduced by radiation-induced defects. The reduction was by approximately 10% after a total dose of 30 kGy. At higher total doses, the effective doping concentration increased, reaching a peak value of between 10 and 30% above the pre-irradiation value after a total dose of 1 MGy.

The emitter-base capacitance results are shown in figures 14.53 to 14.56.

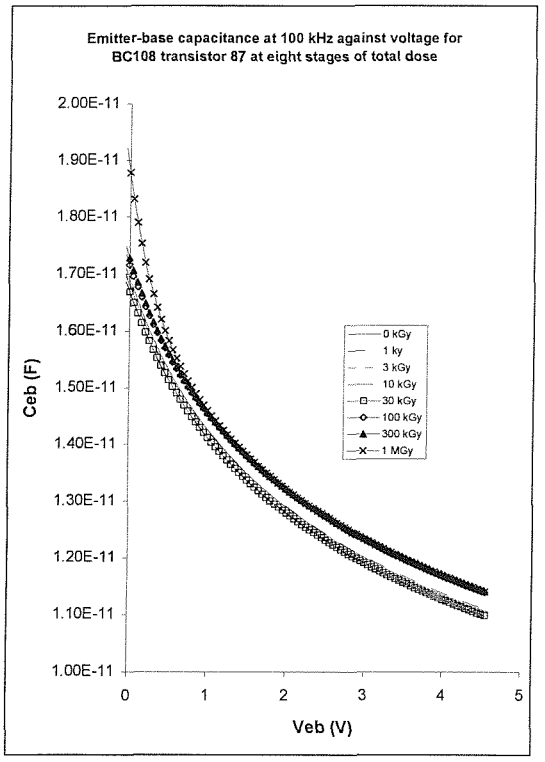

Figure 14.53: Emitter-base C-V plot at 100 kHz for BC108 device number 87.

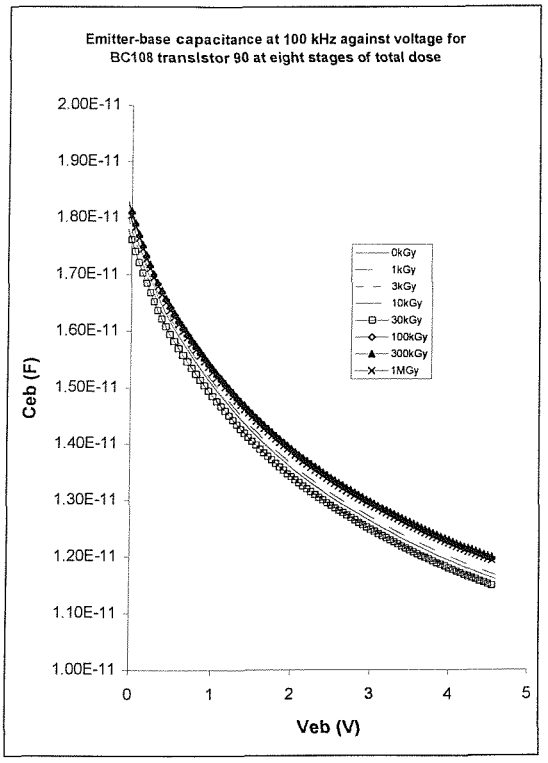

Figure 14.54: Emitter-base C-V plot at 100 kHz for BC108 device number 90.

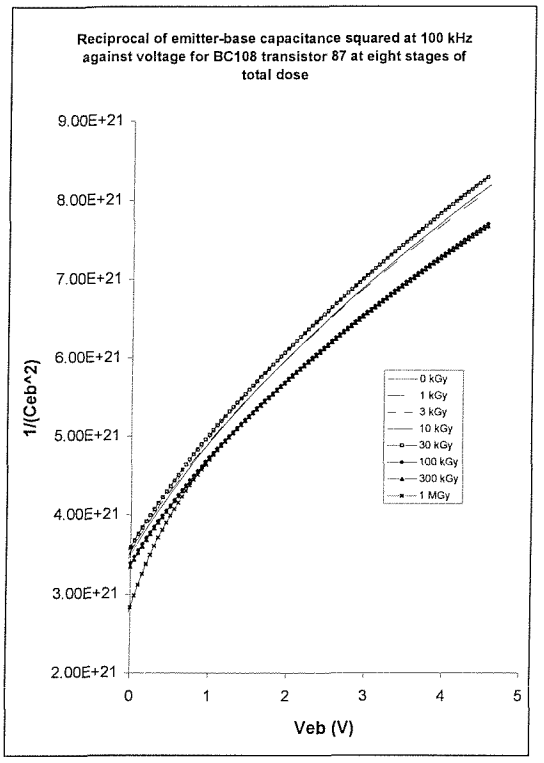

Figure 14.55: $1/C_{eb}^{2}$ plot at 100 kHz for BC108 device number 87.

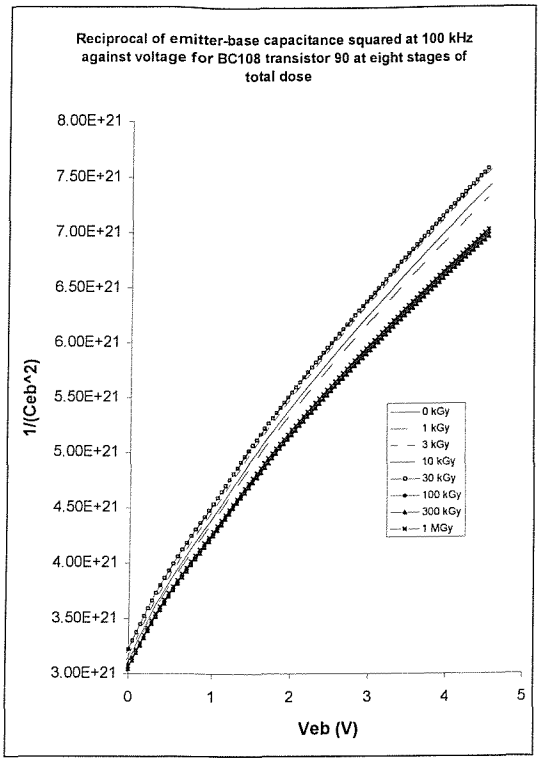

Figure 14.56: $1/C_{eb}^{2}$ plot at 100 kHz for BC108 device number 90.

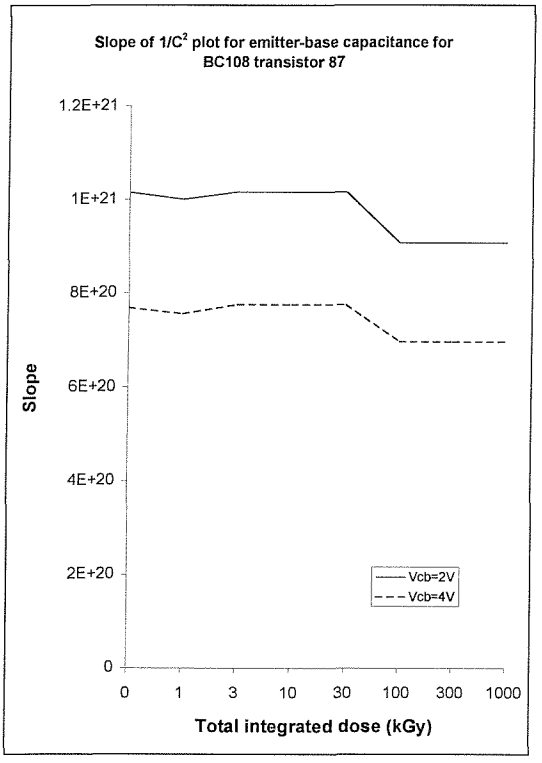

Figure 14.57: slope of $1/C_{eb}^{2}$ plot at 100 kHz for BC108 device number 87.

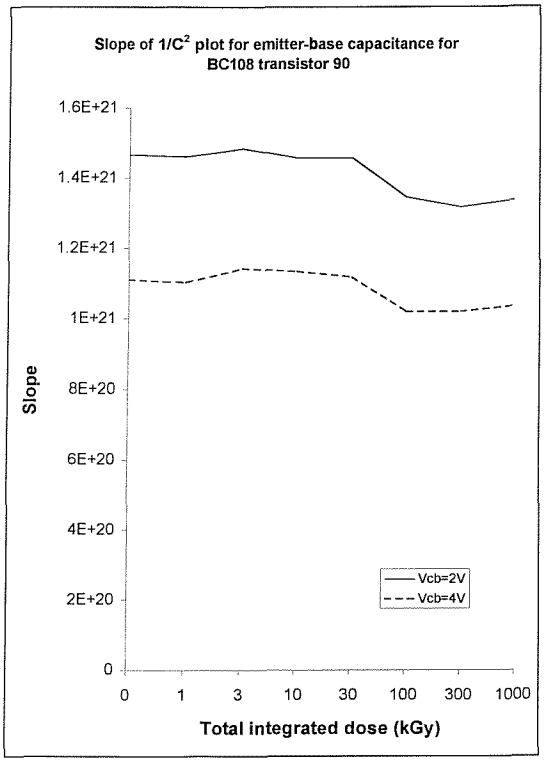

Figure 14.58: slope of $1/C_{eb}^{2}$ plot at 100 kHz for BC108 device number 90.

Again, the emitter-base capacitance data showed similar results to those for the collector-base junction. The magnitude of the observed changes is between 5 and 10% of the pre-irradiation values. It can be seen that these $1/C^2$ plots for the BC108 transistors are the closest to the straight line predicted by the theory. This implies that the emitter-base junction for these devices is the closest to a step junction of all those examined. The effective doping concentration is shown to reduce at low to moderate total doses, as for the previous measurements, although the subsequent increase observed to take place at the highest values of total dose is not apparent here. The measured values remain some 10% below the pre-irradiation values.

In summary, we can conclude that irradiation does introduce a measurable concentration of electrically-active defects that oppose the action of the intended doping. The effect of these defects reaches a peak at total doses around 30 kGy, reducing the effective doping concentration by between 5 and 20%, and then falls off as total dose increases further. At 1 MGy, the magnitude of the effect is either similar to that before irradiation or serves to increase the effective doping concentration. The effect is very similar for all the devices examined, across both measurement frequencies, for both junctions and at different depths, except for the emitter-base junction of the BC108 transistors.

14.8 INFLUENCE OF DOSE RATE

Although not a central part of this work, allied results (Wall (1998)) have shown that dose rate does play a role in determining the degree of radiation damage experienced by a device at a given total dose. This is particularly true over the range between the dose rates found in the naturally-occurring natural space environment and those commonly used for the accelerated testing of electronic components, as defined in the relevant international test standards. The dose rates found in typical nuclear power industry facilities lie very much at the upper end of this range and beyond. The inference of this is that the significant effects of dose rate will not be observed in nuclear facilities and so may be neglected here.

Very low dose rate nuclear applications do exist but they are characterised by relatively short or intermittent exposure times (e.g. manned-entry or maintenance activities) or situations where other physical effects will lead to removal, failure or destruction of

the electronic equipment before radiation damage has reached significant levels (e.g. decommissioning tasks).

The radiation dose rates used during much of the first phase of this work and throughout the second phase were considerably higher than those found to lead to variations in radiation-induced damage. Consequently, any influence of dose rate on the results obtained in this work has been discounted.

14.9 INFLUENCE OF PACKAGE STYLE

The influence of package style on the effects of irradiation was not studied as part of this work. However, the parallel work mentioned above (Wall (1998)) examined this aspect and concluded that hermetically-sealed devices showed a greater response to irradiation than did the same devices encapsulated in plastic packages.

The difference was noticeable at very low dose rates but became much smaller at the higher dose rates found in the nuclear industry. This phenomenon is tentatively thought to be due to the different thermal budget applied to the silicon die as it passes through the packaging process. Similar effects have been noted in some cases of devices to which an elevated temperature burn-in treatment has been applied. However, no explanation has so far been offered to explain why such a sensitivity might occur only at very low dose rates. This is a serious concern for users of devices in space but is not a cause for concern for users in the nuclear power industry.

14.10 INFLUENCE OF DEVICE GEOMETRY

Given the anticipated reduction in minority carrier lifetime as a result of exposure to radiation, it may be expected that the physical dimensions of the base might play a role in determining the extent of any degradation that occurs. One purpose of using the SU devices was to enable the influence of the geometry of a device on its response to irradiation to be quantified. To this end, the six devices in each package encompassed a variety of perimeter to area ratios for base, collector and emitter. The ideality factor has been measured at a base current of 100 nanoamps for each type of SU device in a selection of packages and these results are shown in figures 14.59 to 14.64.

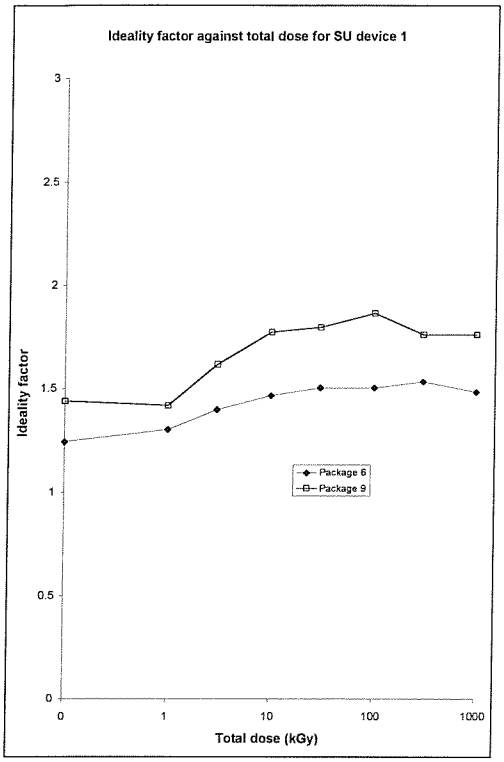

Figure 14.59: Ideality factor against total dose for SU device 1.

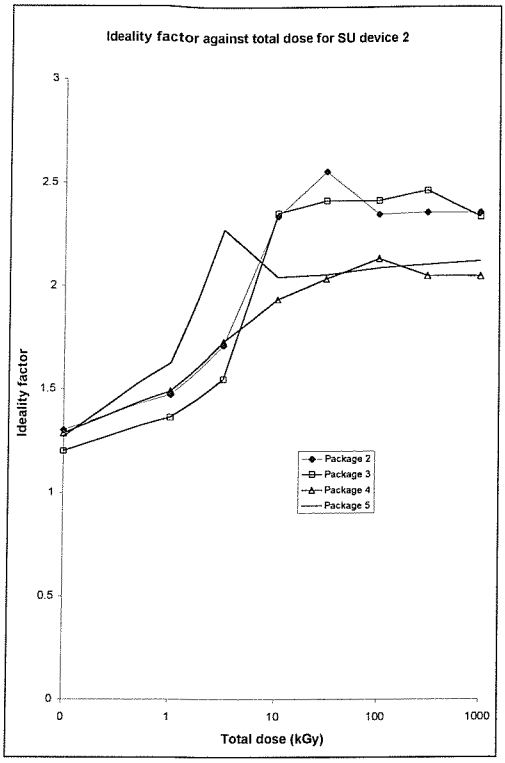

Figure 14.60: Ideality factor against total dose for SU device 2.

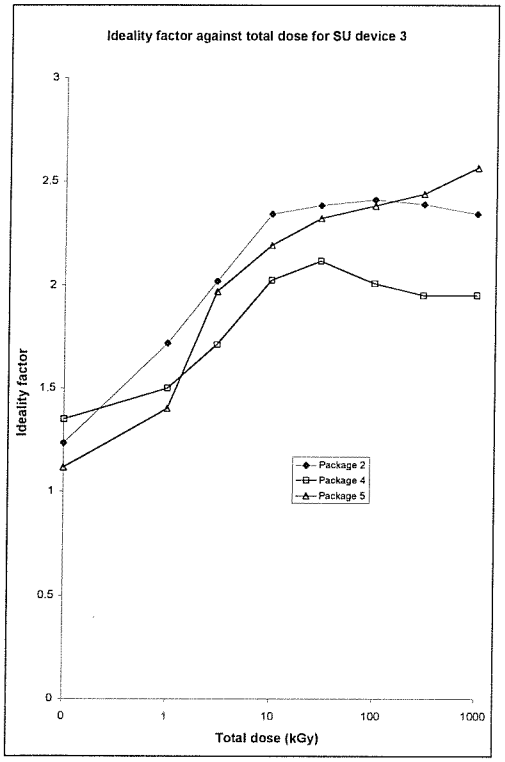

Figure 14.61: Ideality factor against total dose for SU device 3.

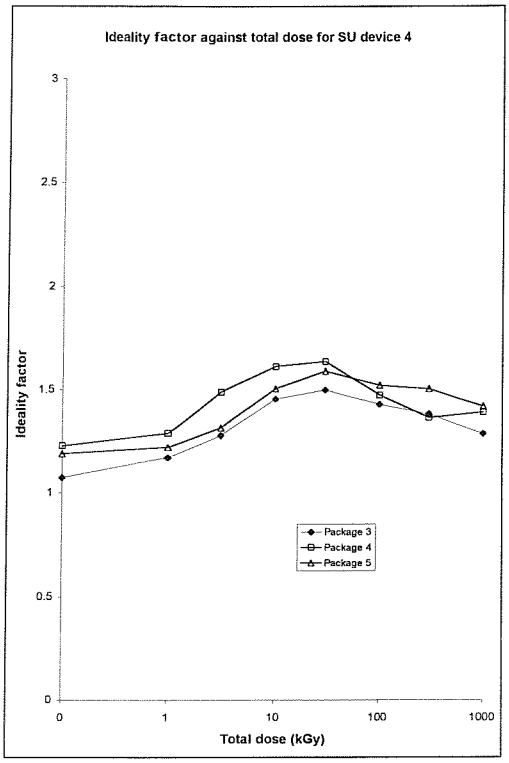

Figure 14.62: Ideality factor against total dose for SU device 4.

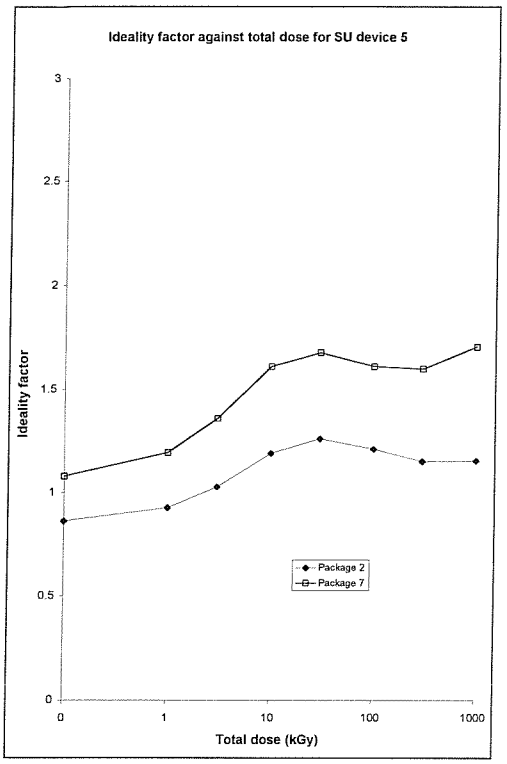

Figure 14.63: Ideality factor against total dose for SU device 5.

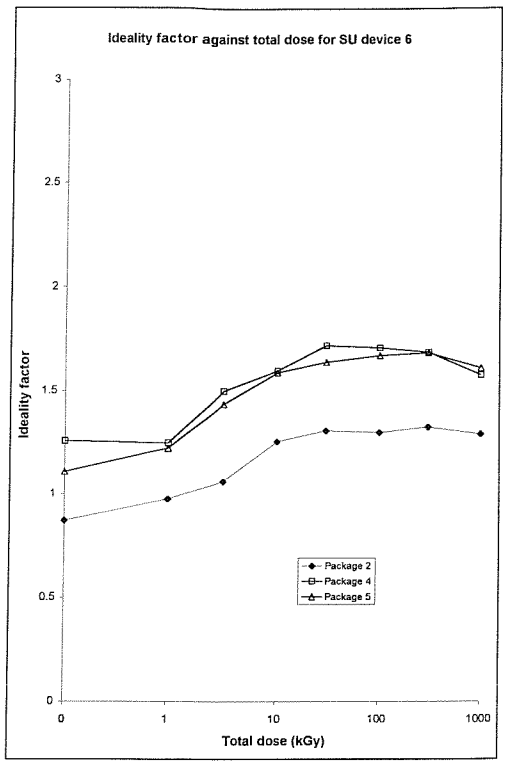

Figure 14.64: Ideality factor against total dose for SU device 6.

It is clear that these plots fall into two categories. SU device types 1, 4, 5 and 6 show increases in ideality factor of approximately 70%, peaking around 30 kGy and then remaining stable or falling slightly. SU device types 2 and 3 show a similar pattern of change but the magnitude of the change is more than 100%.

The base area, base perimeter, emitter area and emitter perimeter for devices of types 1, 2 and 3 are similar and very different from the corresponding values for devices of types 4, 5 and 6. The similarity of the ideality factor plots for device types 1, 4, 5 and 6, with quite different shape plots for types 2 and 3 does not correspond with the geometric data shown in table 12.1. Consequently, it is difficult to associate features of the change in ideality factor with geometric aspects of the devices.

14.11 INFLUENCE OF PRODUCTION BATCH

The main test vehicles of this work, the SU devices, were all fabricated on the same wafer. The BC108 transistors were not traceable to production batch level, merely to the date code marked on them. One date code can cover a number of production batches and is not a reliable guide to provenance. Thus, the influence of varying

production batch was deliberately excluded for the former and not controlled for the latter. No conclusions can therefore be drawn regarding this factor.

Results from other workers have indicated that differences may be observed between devices produced at different times in the same facility. However, these differences are usually small compared with those due to other factors, e.g. different manufacturers, and would almost certainly have been dwarfed by the wide range in characteristics of the SU devices even if had been possible to study devices from different batches.

In terms of recommendations for users of bipolar transistors in equipment for nuclear environments, no specific measures come out of this work. In general terms, it may be necessary to quantify the variation in radiation response across a number of different production lots, especially where the change in a particular parameter has been shown to approach the limit of acceptability. In this situation, a slightly higher rate of degradation in another batch may lead to failure of the equipment earlier than expected from a more limited round of development testing.

14.12 INFLUENCE OF APPLIED BIAS

Features to examine the influence of this factor were built into the bias board for the SU devices, with six packages being irradiated under bias and three with all the pins shorted together. Because of the large range of characteristics measured, it was not possible to discern difference between the biased and unbiased cases for most of the parameters measured. The devices in packages 9 and 10, both unbiased, did exhibit characteristics that were noticeably different from those of the devices in any of the other packages for some parameters. However, this pattern was not uniformly replicated for those in package 8, also unbiased, and was not seen for all parameters. Given the range of response seen across the batch of SU devices, it is quite possible that the differences between the results for packages 9 and 10 and all the others are simply a reflection of the variability of the device characteristics, rather than a systematic effect due to bias. In addition, the difference was sometimes in a direction indicating greater degradation and sometimes in the opposite direction. Consequently, it would be unsafe to draw any general conclusions regarding bias conditions from these data.

The one exception to the viewpoint given above is for gain. Here, systematic differences between the response of the biased and unbiased devices were noted. The

values of gain for the unbiased devices generally degraded more rapidly that did those for the biased transistors. This can be seen in the figures in chapter 12 but two examples are shown here to clarify the point. Figures 14.65 and 14.66 show gain readings for two different devices, one of type 4 and one of type 6. Each figure shows the results for all the irradiated devices of the given type.

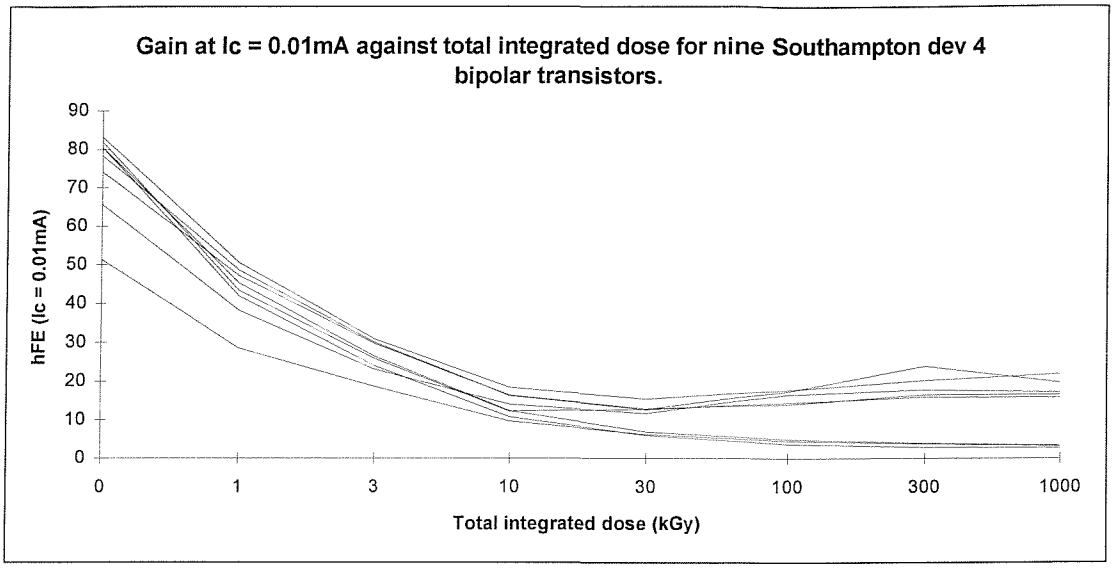

Figure 14.65: Change in gain (Ic = 0.01 mA) against total dose for SU device 4.

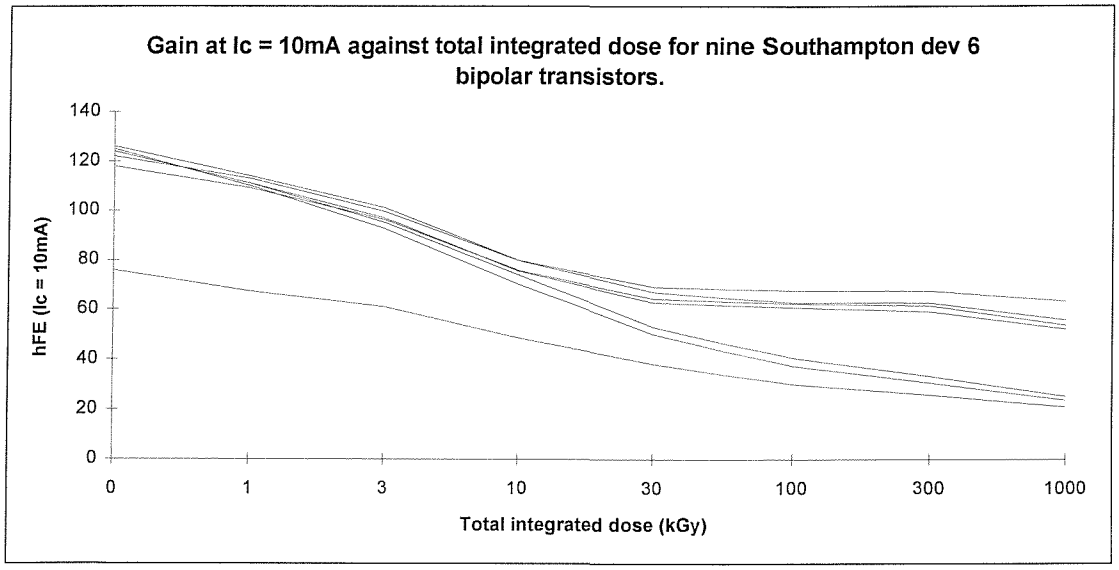

Figure 14.66: Change in gain (Ic = 10 mA) against total dose for SU device 6.

The set of devices can be seen to divide into two groups at the higher values of total dose, one groups continuing an unbroken, downward trend with irradiation. The second, larger group shows a different trend, with the degradation levelling off or even reversing, showing a small rise in gain between a few tens of kilogray and a few

hundred kilogray. The devices that form the first group are always the unbiased devices. Where the two groups are visible, the lower group always consists of all the unbiased devices and the upper group always contains all of the biased devices. This clear distinction on the basis of applied bias during irradiation was not unexpected but it was a surprise that it was so clear. Nevertheless, the effect is not apparent for all the device types nor at all values of collector current, so any general conclusions must be bear this in mind.

Other workers have also shown that differences in bias conditions can lead to significant differences in the measured radiation-induced changes. However, the majority of these results have been for integrated circuits, such as operational amplifiers, logic gates and digital memories, and so cannot easily be transferred to discrete, bipolar transistors.
All the BC108 devices were irradiated in the same bias condition and so cannot contribute in this instance. Most of the devices tested in phase one were irradiated with all their leads shorted together and so also do not allow any conclusions to be drawn related to this factor.

14.13 ANNEALING

Virtually all radiation damage has a thermal component, whereby storage at room temperature will enable the degree of damage to reduce as the radiation-induced defects created in the semiconductor are annealed out. The rate of annealing depends on the type of defect and its activation energy, i.e. the ambient temperature, and so is influenced by whether and how bias is applied to the device during this period. In fact, annealing starts at the same point as the device is first exposed to radiation. In other words, annealing of radiation damage takes place during the irradiation itself, as well as after the irradiation has ceased. This can be important for long duration exposures, for example at very low dose rate, and is one of the factors that must be compensated for when comparing results from tests at widely differing dose rates. Care was taken during the measurements for this work to take readings after as short an interval as possible after the end of the relevant irradiation, usually commencing within thirty minutes of the removal of the sources from the irradiation cell. This is in compliance with the requirements of the two international standards for radiation testing that are most closely aligned with the methods applied here. Furthermore, any

bias applied during irradiation was removed immediately the irradiation ceased and none was applied again until after the measurements had been completed. The temperature of the test laboratory was controlled and the currents flowing through a device during testing kept low or pulsed to minimise self-heating. The purpose of these measures was to ensure than any annealing that occurred was minimised and, ideally, was consistent from one set of tests to another.

14.14 SUMMARY

The measured data show that irradiation by gamma radiation has a dramatic and clear effect on many of the parameters measured, summarised by the changes visible on a Gummel plot. The governing equations are as follows.

Base current changes according to:

$$I_B = I_1 e^{qV_{BE}/kT} + I_2 e^{qV_{BE}/mkT} \tag{14.9}$$

where both the ideality factor, m, and the coefficients I_1 and I_2 are functions of the total dose. The first term is dominant at low doses and the second term becomes more important as total dose increases. The derivation of ideality factors from the Gummel plot data show that this dependence is demonstrated for all of the types of device tested, although the total dose at which the dependence changes over varies. Some devices showed a measurable contribution according to $m > 1$ even before irradiation and further work to examine the total dose at which the break in slope occurs would help identify the manufacturing features that influence this.

The Messenger-Spratt equation has been shown to explain the gain behaviour at low doses. However, it does not extend to the high dose regime, where gain falls much less rapidly than it predicts.

$$\frac{1}{\beta} = \frac{1}{\beta_0} + \frac{\Phi}{\omega_T K} \tag{14.10}$$

A better model of the change in gain is provided by a modified version:

$$\frac{1}{\beta} = \frac{1}{\beta_0} + \frac{\Phi}{K'} \tag{14.11}$$

where K' is a function of gain at low dose, changing to a function of total dose at high doses. This has been shown to match well to the measured data. K' is a quadratic function of the total dose, with the main contribution coming from the linear term.

The combination of these equations shows that recombination in the emitter-base depletion region is very likely to be the cause of the radiation-induced change in gain. This increased recombination is brought about either by a reduction in the carrier lifetime in this region or by a change in the effective carrier concentration, as a result of the introduction of defects, or by a combination of the two. This is shown in the following equation:

$$\frac{1}{\beta} = f\left(\frac{1}{\tau_A(\Phi)}\right) + f\left(\frac{N_D(\Phi)}{N_A(\Phi)}\right) + f\left(\frac{N_D(\Phi)}{\tau_C(\Phi)}\right) \qquad (14.12)$$

Leakage current measurements have shown that, while the concentrations of acceptor and donor-like defect states have increased, this is insufficient to explain the changes in gain observed. The C-V measurements provide further evidence of a small change in defect concentration, reaching a maximum of between 5 and 10% after a total dose of some 30 kGy, and then falling back towards the pre-irradiation value as total dose increases. Furthermore, the base width in the small-signal transistors used for this work is very small, limiting the influence of the first term. Hence, a reduction in the carrier lifetime in the base-emitter depletion region must be the primary cause of the fall in gain, i.e.

$$\frac{1}{\beta} \approx f\left(\frac{1}{\tau_A}\right) + f\left(\frac{N_D}{N_A}\right) + f\left(\frac{N_D}{\tau_C(\Phi)}\right) \qquad (14.13)$$

However, the changes in gain observed at higher total doses cannot be explained fully by a model based on falling minority carrier lifetime. In several cases, gain was observed to rise slightly after a total dose of a few hundred kilogray. This increase is explained by one of two mechanisms: a rise in resistivity or surface effects. The creation of bulk damage, i.e. dislocations, in the silicon lattice by high levels of gamma irradiation can lead to a rise in resistivity and consequently a reduction in base current. This would be manifested as a rise in gain. This effect is competing with minority carrier lifetime reduction, with a dependence on manufacturing properties and layout. Hence, some devices might be expected to show it, while others do not. Alternatively, an expansion of the area of the base-emitter depletion region at the surface of the device could lead to an increase in the surface potential in this region. This would act to reduce the applied base-emitter voltage and therefore lower the

base current at a given value of base-emitter voltage, i.e. the gain would stop falling and then increase as the surface potential continued to rise. Surface effects were identified as important by Poch, according to the equation:

$$\Delta \frac{1}{\beta} = K_B \Phi + K_S \Phi^n \tag{14.14}$$

where n takes a value between 0.4 and 1. The measured value of n from this work lies at the lower end of this range (figures 14.14 to 14.17), confirming the important contribution to the phenomenon by surface effects, especially at low total doses.

15 Conclusions

A number of important conclusions can be drawn from the analysis in the preceding section. The constancy of the collector current curves on the Gummel plots indicates that carrier mobility has not significantly been affected by irradiation. Whilst direct measurements of carrier lifetime proved unsuccessful, there is very good, indirect evidence of a reduction in lifetime. This evidence comes from measurements of leakage currents and gain and also from increases in collector-emitter saturation voltage.

Section 14 has shown that the radiation-induced change in gain follows a dependence at low and moderate total doses as predicted by Messenger and encapsulated in equation 14.2. At higher total doses, this dependency changes to that given in equation 14.3. The difference lies in a change in the damage constant (K') from a function of gain to a function of total dose as total dose rises. The reason for this change has been shown to lie in the effect of irradiation at reducing the minority carrier lifetime in the emitter-base region by the creation of electrically-active defects that enhance the probability of an individual carrier recombining. Hence, gamma radiation has been shown to be as effective in creating defects that reduce carrier lifetime as are electron and proton radiation, both of which are used commercially to generate this effect for the manufacture of fast-switching power devices. In some cases, subtle effects at high total doses lead to a slight increase and subsequent further fall in gain. This has been shown to result either from a change in resistivity due to strong bulk damage of the silicon lattice or from enhanced surface effects due to the surface potential changing with total dose. The more marked effect for the SU devices compared to the BC108 transistors indicates a more likely influence of surface effects in this case.

Capacitance-voltage measurements show that the effective doping concentration is reduced at low to moderate total doses by between 5 and 20%. At higher total doses, it increases and often exceeds the pre-irradiation value after a total dose of 1 MGy. The effect was observed across the range of device types, packages, junction and depth, with the sole exception of emitter-base capacitance for the BC108 transistors, where no increase was observed at the highest total doses. A more thorough examination of

the nature of the radiation-induced defects and their relative prominence in different types of device would be likely to provide more insight into this process, helping the development of a predictive methodology for this important feature of the use of transistor circuits in high total dose conditions.
The influence of bias during irradiation has been shown to be significant in some cases. This certainly warrants further investigation as a detailed consideration of its impact was beyond the scope of this work.

For many years, the nuclear power industry has dealt with its requirement for reliable, radiation tolerant, in-cell electronics by eliminating vulnerable components from the radioactive environment or accepting severely downgraded performance. This has restricted the ease with which electromechanical solutions have been implemented and reduced the benefits that have been gained therefrom. All other sectors of industry have been able to introduce more efficient and productive working methods by the use of electronic systems and the work described in this thesis has been aimed at enabling the adoption of some of these methods into nuclear facilities.
The main contribution of the work is the development of guidelines to aid designers to use bipolar transistors in such a manner that the lifetime of their equipment and instrumentation is extended to useful durations and is also predictable.
The results described above have a number of implications for the way bipolar transistors should be used for applications in the high radiation environments of the nuclear power industry and these will now be summarised.
Firstly, any circuit using the devices must be designed in such a manner that the post-irradiation values of the relevant parameters are taken account of at the beginning. For example, if the gain is predicted to fall by 80% at the total dose of interest then designing for the typical datasheet value will lead to failure of the circuit well before the required lifetime has been achieved. In order for this to be possible, the radiation-induced changes in the characteristics of the device must be known, at least approximately. Where the approximate post-irradiation values lead to uncertainty about the functionality of the circuit then radiation testing of the specific devices intended for use may be required in order to confirm the values likely to be encountered in service and to reduce the uncertainty associated with them.
This work has shown that the likely changes in leakage currents and breakdown voltages are not large and so can be allowed for with a reasonable degree of

confidence. The changes in saturation voltage are more varied but do appear to be larger in magnitude when the pre-irradiation value is large. Hence, an approximation to the in-service value at a given total dose may be made, based upon the datasheet information. The response of gain to radiation is more complex and, hence, more difficult to predict. The degraded value tends to be lower for low collector currents and is considerably affected by the bias applied while the component is exposed to radiation. A value can be given as a general rule, below which the gain for any transistor is unlikely to fall. However, this will be a very low value, probably in single figures at low currents, placing significant obstacles in the path of the circuit designer. This would increase the size and cost of circuits, and therefore equipment, but may still be feasible for some applications. With the information available to date, there is likely to remain a requirement to carry out radiation testing in order to characterise the response for a specific type of transistor.

Secondly, transistor pre-treatment may be considered. This could include burn-in, although the data indicate that this will have little practical impact at the dose rates typically found in-cell. It could also include pre-irradiation. This has been suggested as a method by which to stabilise the radiation-induced change in parameter values, especially at low currents, by moving the device into the moderate total dose regime before being deployed into an in-cell application. This technique was used for certain devices used on the Voyager satellite missions, for example. Pre-irradiation to a moderate total dose would degrade parameter values but the subsequent rate and degree of change would be reduced substantially when compared with untreated examples. This has the advantage of yielding a device that is more stable when exposed to radiation, at the expense of a reduction in lifetime of a few per cent. It is possible that this technique would ease the design process by reducing the range of, for example, gain over which a circuit should function.

Thirdly, the layout of the components on a circuit board can be considered. Thermal annealing will have a bearing on the degree of radiation-induced damage present at a given time and this may be taken advantage of by judicious positioning of components relative to heat-dissipating devices. This factor has not been quantified during the present work but there are indications in the literature that this may offer benefits in some cases.

Fourthly, packaging materials have a small impact on the radiation tolerance of a component. The effect is small at the dose rates found in-cell but may be worth taking

account of in some low dose rate applications. The reasons for the differences observed due to packaging materials and techniques are not yet fully understood and so further work is required before any useful practices can be defined.

Fifthly, redundancy and bias arrangements are important. Some in-cell equipment has made use of multiple components performing a given function, cycling around the sequence each time the equipment is powered up, for example. The justification for this is that the rate of damage is lower when the device is exposed to radiation in the unbiased condition, compared with that under bias. This work has shown that, for the SU devices, the radiation-induced loss of gain is considerably higher for an unbiased device, completely negating the benefit of this approach. Clearly, the relative rate of degradation between biased and unbiased devices could vary, depending on the device type, so this must be quantified for the devices of interest before knowing whether this technique will provide an operational advantage. Simple techniques, such as ensuring that adequate base current is available for both the pre-irradiation and post-irradiation cases, will contribute greatly to improved reliability.

If the biased condition leads to more rapid degradation then redundancy can offer benefits. If the converse is true then the lifetime of the equipment could be extended by ensuring that it is not switched off while in the radioactive environment, even when not in use. This function may be built into the circuitry or may form part of the operating instructions.

Sixthly, the position of the equipment in the cell will dictate the dose rate to which it is exposed. Reducing the dose rate is an important factor in extending the time between maintenance or replacement activities. Making use of in-cell features, such as structural items, large pieces of machinery and unused corners can all help to reduce the dose rate experienced by the equipment. Even the form of the equipment case itself can offer some shielding, although this is likely to be small for high energy gamma radiation.

Finally, the duty cycle of operation can have a bearing on the rate of degradation. Depending on the ratio of the rate of degradation in the biased and unbiased cases, there could be advantages in aiming for a certain duty cycle for periods during which the equipment is used and left idle. A series of short periods of operation, each followed by time for some of the damage to anneal out, is likely to lead to a longer lifetime than an intense campaign of use and a long period of inactivity.

There remain several areas that warrant further investigation. A better understanding of the relationship between minority carrier lifetime and irradiation by gamma rays may enable progress to be made in developing predictive tools based upon the known physical characteristics of a device. This would eliminate the need to carry out radiation testing, other than for confirmatory purposes, further reducing development costs and time. Designers would benefit from a set of standard building blocks or circuit elements that are known to function well in high radiation environments. There is a long history of such circuit elements for benign areas, many of which are used over and over again throughout industry. The establishment of a just a few of these for high total dose tolerance would improve the ability of equipment manufacturers to meet the needs of the nuclear sector.

In any case, the precise set of conditions by which best to prolong the lifetime of in-cell equipment based upon bipolar transistors can be determined only partly by the characteristics of the devices themselves. Features of the plant, the radiation environment within it and the operating practices associated with the tasks being undertaking also have a substantial influence on the rate of degradation. These must always be assessed on an individual basis in order to ensure that the optimum performance in achieved.

Appendix A

Example listing of software used for measurements made with the HP4142B test instrumentation:

```
10  ! ************************************************************
20  ! * This program will perform the following tests on       *
30  ! * NPN bipolar transistors:  Iebo, Icbo, Iceo, Ibeo,      *
40  ! * Vce(sat), hFE at 0.01, 0.1, 1 and 10 mA, V(br)ebo,     *
50  ! * V(br)cbo, V(br)ceo, V(br)beo and Gummel plot readings  *
60  ! ************************************************************
70  !
80  !
90  !
100 !
110 !  VERSION D          DATE: 11/06/96
120 !
130 !
140 !
150 !  Written by R.E. Sharp, based on NPN10GUM
160 !  Original program based on NPNPROG, written by Paul Scott.
170 !  hFE (100mA) test commented out, other tests added.
180 !
190 !
200 !"If this program needs to be altered follow the procedure detailed
210 ! in RTS Software Management Instruction DD/TSD/WI/3"
220 !
230 !
240 !"If the program is altered please update the Version Number and Date
250 ! above and LINE 530"
260 !
270 !
280 !       ****************
290 !       *INITIALISATION*
300 !       ****************
310 !
320 INTEGER B_ch,C_ch,Sn,Dn,Fn
330 DIM A$[31]          ! RESULTS
340 DIM C$[31]          ! Control device (1)
350 DIM C2$[31]         ! Control device (2)
360 DIM D$[31]          ! Temperature
370 DIM E$[31]          ! Q
380 DIM F$[31]          ! Filename
390 DIM G$[31]          !
400 DIM H$[31]          !
410 DIM J$[31]          ! Start test
420 DIM P$[31]          ! Tested by
430 DIM R$[31]          ! Radiation stage
440 DIM S$[31]          !
450 DIM T$[31]          ! Device type
460 DIM U$[31]          ! Electrical Conditions
470 DIM V$[31]          ! Time irradiation ended
480 DIM W$[31]          ! Date irradiation ended
```

```
490  DIM X$[23]          ! Error checking
500  DIM Z$[31]          ! Error results prompt
510  !
520  CLEAR SCREEN
530  PRINT "NPN Bipolar Transistor Test Program **"
540  PRINT " "
550  PRINT "VERSION D              DATE: 11/06/96"
560  PRINT " "
570  PRINT " "
580  PRINT " "
590  PRINT "This program requires a 10 kohm resistor to be inserted during the
V(br) tests."
600  PRINT " "
610  PRINT "If you wish to edit the test parameters, Press PAUSE followed by
F1."
620  !
630  !
640  !
**********************************************************************
**
650  ! *                EDIT PROGRAM                *
660  !
**********************************************************************
**
670  !
680  !
690  !
700  Vebo=3              ! Ve for Iebo test
710  Iebo_comp=.01       ! Ie compliance = 0.01A (max = 0.125)
720  Vcbo=20             ! Vc for Icbo test
730  Icbo_comp=.1        ! Ic compliance = 0.1A (max = 0.125)
740  Vceo=20             ! Vc for Iceo test
750  Iceo_comp=.1        ! Ic compliance = 0.1A (max = 0.125)
760  Vbeo=-.5            ! Vb for Ibeo test
770  Ibeo_comp=.1        ! Ib compliance = 0.1A (max = 0.125)
780  !
790  !
800  Ibsat=1.E-3         ! Electrical condition for Vce(sat), Ib(mA)
810  Icsat=1.0E-2        ! Electrical condition for Vce(sat), Ic(mA)
820  Vce_comp=10         ! Vce(sat) max=10V
830  Vbsat_comp=3        ! Pulsed I source, Vb_comp=3
840  !
850  Vb_start=0          ! Hfe Vb_start, (V)
860  Vb_stop=3           ! Hfe Vb_stop, (V)
870  Vb_rate=600         ! Hfe Vb_rate, (V)
880  Vchfe=5             ! Hfe Test, Vc (V)
890  Ic1_target=1.E-3    ! Hfe Test1, target of Ic=1mA
900  Ic2_target=1.E-2    ! Hfe Test2, target of Ic=10mA
```

```
910  Ic3_target=1.E-1      ! Hfe Test3, target of Ic=100mA
920  Ic4_target=1.E-4      ! Hfe Test4, target of Ic=0.1mA
930  Ic5_target=1.E-5      ! Hfe Test5, target of Ic=0.01mA
940  Ic1_comp=1.15E-3      ! Hfe Test1, compliance of Ic=1.15mA
950  Ic2_comp=1.15E-2      ! Hfe Test2, compliance of Ic=11.5mA
960  Ic3_comp=1.15E-1      ! Hfe Test3, compliance of Ic=115mA
970  Ic4_comp=1.15E-4      ! Hfe Test4, compliance of Ic=0.115mA
980  Ic5_comp=1.15E-5      ! Hfe Test5, compliance of Ic=0.0115mA
990  Ichigh=Ic3_target     ! Highest collector current, Ichigh
1000 Icerr=Ic3_target*.05  ! Error in highest collector current, Icerr
1010 Ib_comp=5.00E-4       ! Base current compliance, Ib_comp (hFE1)
1020 Ib2_comp=5.E-3        ! Base current compliance, Ib2_comp (hFE2)
1030 Ib3_comp=5.00E-2      ! Base current compliance, Ib3_comp (hFE3)
1040 Ib4_comp=5.E-5        ! Base current compliance, Ib4_comp (hFE4)
1050 Ib5_comp=5.E-6        ! Base current compliance, Ib5_comp (hFE5)
1060 !
1070 Iebbr=1.0E-5          ! Vbr(ebo), Ie
1080 Vebbr_comp=50         ! Vbr(ebo), V
1090 Icbbr=1.0E-5          ! Vbr(cbo), Ic
1100 Vcbbr_comp=200        ! Vbr(cbo), V
1110 Icebr=1.0E-2          ! Vbr(ceo), Ic
1120 Vcebr_comp=200        ! Vbr(ceo), V
1130 Ibebr=1.0E-5          ! Vbr(beo), Ie
1140 Vbebr_comp=50         ! Vbr(beo), V
1150 !
1160 !
1170 !
1180 !
**********************************************************************
1190 !*            END OF EDIT                    *
1200 !
**********************************************************************
1210 !
1220 !
1230 !
1240 INPUT "Please enter the save filename, ####X.XLH:",F$
1250 IF F$="" THEN
1260   GOTO 1240
1270 ELSE
1280 END IF
1290 CREATE F$,10
1300 ASSIGN @Path TO F$;FORMAT ON
1310 ASSIGN @Hp4142 TO 717
1320 CLEAR @Hp4142
1330 !
1340 B_ch=3                    !SMU2
1350 C_ch=2                    !SMU1
1360 !
```

```
1370 CLEAR SCREEN
1380 !
1390 !
1400 !    ********************************
1410 !    * Inputing Device Parameters *
1420 !    ********************************
1430 !
1440 !
1450 OUTPUT @Path;"Device category:";CHR$(9);"NPN Bipolar Transistor"
1460 !
1470 INPUT "Please enter Radiation Stage, (A-H):",R$
1480 IF R$="" THEN
1490   GOTO 1470
1500 ELSE
1510 END IF
1520 IF R$>"H" THEN
1530   GOTO 1470
1540 ELSE
1550 END IF
1560 OUTPUT @Path;"Radiation stage:";CHR$(9);R$[1,31]
1570 !
1580 !
1590 INPUT "Electrical conditions during irradiation: Unpowered",U$
1600 IF U$="" THEN
1610   OUTPUT @Path;"Electrical conditions:";CHR$(9);"Unpowered"
1620 ELSE
1630   OUTPUT @Path;"Electrical conditions:";CHR$(9);U$[1,31]
1640 END IF
1650 !
1660 !
1670 INPUT "Temperature during irradiation (DEGREES 'C): 20",D$
1680 IF D$="" THEN
1690   OUTPUT @Path;"Temperature:";CHR$(9);"20"
1700 ELSE
1710   OUTPUT @Path;"Temperature:";CHR$(9);D$[1,31]
1720 END IF
1730 !
1740 !
1750 OUTPUT @Path;"Highest collector current:";CHR$(9);Ichigh
1760 !
1770 OUTPUT @Path;"Error in highest collector current:";CHR$(9);Icerr
1780 !
1790 OUTPUT @Path;"Elec. Conditions for Iceo:";CHR$(9);Vceo
1800 !
1810 OUTPUT @Path;"Elec. Conditions for
Vce(sat):";CHR$(9);Ibsat;CHR$(9);Icsat
1820 !
```

```
1830 OUTPUT @Path;"Elec. Conditions for Hfe
(1mA):";CHR$(9);Vchfe;CHR$(9);Ic1_target
1840 !
1850 OUTPUT @Path;"Elec. Conditions for Hfe
(10mA):";CHR$(9);Vchfe;CHR$(9);Ic2_target
1860 !
1870 OUTPUT @Path;"Elec. Conditions for Hfe
(100mA):";CHR$(9);Vchfe;CHR$(9);Ic3_target
1880 !
1890 OUTPUT @Path;"Elec. Conditions for V(br)ceo:";CHR$(9);Icvbr
1900 !
1910 INPUT "Please enter device type:",T$
1920 IF T$="" THEN
1930   GOTO 1910
1940 ELSE
1950 END IF
1960 OUTPUT @Path;"Device type:";CHR$(9);T$[1,31]
1970 !
1980 !
1990 INPUT "Please enter device start number:",Sn
2000 IF Sn<1 THEN
2010   GOTO 1990
2020 ELSE
2030 END IF
2040 INPUT "Please enter device finish number:",Fn
2050 IF Fn<Sn THEN
2060   GOTO 1990
2070 ELSE
2080 END IF
2090 !
2100 !
2110 LINPUT "Please enter 1st control device number, (#):",C$
2120 IF C$="" THEN
2130   GOTO 2110
2140 ELSE
2150 END IF
2160 !
2170 LINPUT "Please enter 2nd control device number, (#):",C2$
2180 IF C2$="" THEN
2190   GOTO 2270
2200 ELSE
2210 END IF
2220 IF C$>C2$ THEN
2230   GOTO 2110
2240 ELSE
2250 END IF
2260 !
2270 OUTPUT @Path;"1st Control device:";CHR$(9);C$[1,31]
```

```
2280 OUTPUT @Path;"2nd Control device:";CHR$(9);C2$[1,31]
2290 !
2300 !
2310 LINPUT "Tested by:",P$
2320 IF P$="" THEN
2330  GOTO 2310
2340 ELSE
2350 END IF
2360 OUTPUT @Path;"Tested by:";CHR$(9);P$[1,31]
2370 !
2380 !
2390 Dd$=TRIM$(DATE$(TIMEDATE))
2400 !
2410 OUTPUT @Path;"Time:";CHR$(9);TIME$(TIMEDATE)
2420 OUTPUT @Path;"Date:";CHR$(9);Dd$
2430 !
2440 !
2450 LINPUT "Time irradiation ended, (hh:mm):",V$
2460 IF V$="" THEN
2470  GOTO 2450
2480 ELSE
2490 END IF
2500 OUTPUT @Path;"Time irradiation ended:";CHR$(9);V$[1,31]
2510 LINPUT "Date irradiation ended, (dd/mm/yy):",W$
2520 IF W$="" THEN
2530  GOTO 2510
2540 ELSE
2550 END IF
2560 OUTPUT @Path;"Date irradiation ended:";CHR$(9);W$[1,31]
2570 !
2580 !
2590 PRINT "Rad Stage: ",R$
2600 PRINT "Device TYPE: ",T$
2610 PRINT "Device START No: ",Sn
2620 PRINT "Device FINISH No: ",Fn
2630 PRINT "Control No.1: ",C$
2640 PRINT "Control No.2: ",C2$
2650 PRINT "Time Irrad. ended: ",V$
2660 PRINT "Date Irrad. ended: ",W$
2670 PRINT "  "
2680 !
2690 !
2700 INPUT "Is this information correct, Press ""Y"" to continue or PAUSE to
EXIT",E$
2710 IF E$="" THEN
2720  GOTO 2700
2730 ELSE
2740 END IF
```

```
2750 IF E$="Y" THEN
2760   GOTO 2820
2770 ELSE
2780   GOTO 2700
2790 END IF
2800 !
2810 !
2820 !  ******************************************
2830 !  *    BEGINNING OF MAIN TEST PROGRAM    *
2840 !  ******************************************
2850 !
2860 !
2870 FOR X=Sn TO Fn STEP 1
2880   J$=""
2890   PRINT "Ensure that the test box leads are inserted correctly"
2900   PRINT "NEXT DEVICE No. = ",X        ! X=Device No. Loop Counter
2910   PRINT " "
2920   PRINT "Press PAUSE to EXIT"
2930   INPUT "Press <ENTER> to start test, (or S to skip a test)",J$
2940   IF J$="" THEN
2950     GOTO 3070
2960   ELSE
2970   END IF
2980 !
2990 !
3000   IF J$="S" THEN
3010     FOR Y=1 TO 6 STEP 1
3020       OUTPUT @Path;X
3030     NEXT Y
3040     CLEAR SCREEN
3050     GOTO 10420
3060   END IF
3070   CLEAR SCREEN
3080 !
3090 !
3100 !      ******************
3110 !      * Iebo Pre-Test *
3120 !      ******************
3130 !
3140 !
3150   INPUT "Please swap test leads for base and emitter.",O$
3160   OUTPUT @Hp4142;"*RST"
3170   OUTPUT @Hp4142;"CN";B_ch,C_ch
3180   OUTPUT @Hp4142;"FL";0,C_ch            !Filter off
3190   OUTPUT @Hp4142;"PI";C_ch,0,0,1.0E-5,Vbsat_comp
3200   OUTPUT @Hp4142;"PT";0,1.E-3           !Hold time, pulse width
3210 ! OUTPUT @Hp4142;"DI";B_ch,0,Icsat,Vce_comp
3220   OUTPUT @Hp4142;"MM";3,B_ch
```

```
3230   OUTPUT @Hp4142;"XE"
3240   OUTPUT @Hp4142;"CL"
3250 !
3260 !
3270 !     ******************
3280 !     * Iebo Test  *
3290 !     ******************
3300 !
3310 !
3320   OUTPUT @Hp4142;"*RST"
3330   OUTPUT @Hp4142;"CN";B_ch
3340   OUTPUT @Hp4142;"DV";B_ch,0,Vebo,Iebo_comp
3350   OUTPUT @Hp4142;"MM";1,B_ch
3360   OUTPUT @Hp4142;"XE"
3370   OUTPUT @Hp4142;"CL"
3380   ENTER @Hp4142;A$
3390   Iebo_meas=VAL(A$[4,15])
3400 !
3410 !
3420 !     **********************
3430 !     * ERROR CHECKING *
3440 !     **********************
3450 !
3460 !
3470   GOSUB 12980
3480 !
3490   IF A$[1,1]<>"N" THEN
3500     BEEP
3510     PRINT "Iebo"
3520     GOSUB 12090
3530   ELSE
3540   END IF
3550 !
3560   IF Z$="*" THEN
3570     Z$="*"
3580   ELSE
3590     Z$=""
3600   END IF
3610   OUTPUT
@Path;X;CHR$(9);"Iebo";CHR$(9);ABS(DROUND(Iebo_meas,6));CHR$(9);Z
$
3620   PRINT X,"Iebo",ABS(DROUND(Iebo_meas,6))
3630 !
3640 !
3650 !     ******************
3660 !     * Icbo Pre-Test *
3670 !     ******************
3680 !
```

```
3690 !
3700   OUTPUT @Hp4142;"*RST"
3710 !
3720   OUTPUT @Hp4142;"CN";B_ch,C_ch
3730   OUTPUT @Hp4142;"FL";0,B_ch              !Filter off
3740   OUTPUT @Hp4142;"PI";B_ch,0,0,1.0E-5,Vbsat_comp
3750   OUTPUT @Hp4142;"PT";0,1.E-3             !Hold time, pulse width
3760 ! OUTPUT @Hp4142;"DI";C_ch,0,Icsat,Vce_comp
3770   OUTPUT @Hp4142;"MM";3,C_ch
3780   OUTPUT @Hp4142;"XE"
3790   OUTPUT @Hp4142;"CL"
3800 !
3810 !
3820 !     ******************
3830 !     *  Icbo TEST   *
3840 !     ******************
3850 !
3860 !
3870   OUTPUT @Hp4142;"*RST"
3880   OUTPUT @Hp4142;"CN";C_ch
3890   OUTPUT @Hp4142;"DV";C_ch,0,Vcbo,Icbo_comp
3900   OUTPUT @Hp4142;"MM";1,C_ch
3910   OUTPUT @Hp4142;"XE"
3920   OUTPUT @Hp4142;"CL"
3930   ENTER @Hp4142;A$
3940 ! PRINT A$
3950   Icbo_meas=VAL(A$[4,15])
3960 !
3970 !
3980 !     **********************
3990 !     * ERROR CHECKING *
4000 !     **********************
4010 !
4020 !
4030   GOSUB 12980
4040 !
4050   IF A$[1,1]<>"N" THEN
4060     BEEP
4070     PRINT "Icbo"
4080     GOSUB 12090
4090   ELSE
4100   END IF
4110 !
4120   IF Z$="*" THEN
4130     Z$="*"
4140   ELSE
4150     Z$=""
4160   END IF
```

```
4170   OUTPUT
@Path;X;CHR$(9);"Icbo";CHR$(9);ABS(DROUND(Icbo_meas,6));CHR$(9);Z
$
4180   PRINT X,"Icbo",ABS(DROUND(Icbo_meas,6))
4190 !
4200   INPUT "Please swap back test leads for base and emitter",O$
4210 !
4220 !
4230 !      ******************
4240 !      * Iceo Pre-Test *
4250 !      ******************
4260 !
4270 !
4280   OUTPUT @Hp4142;"*RST"
4290 !
4300   OUTPUT @Hp4142;"CN";B_ch,C_ch
4310   OUTPUT @Hp4142;"FL";0,B_ch              ! Filter OFF
4320   OUTPUT @Hp4142;"PI";B_ch,0,0,1.0E-5,Vbsat_comp
4330   OUTPUT @Hp4142;"PT";0,1.E-3          ! Hold Time, Pulse Width
(min=1mS)
4340 ! OUTPUT @Hp4142;"DI";C_ch,0,Icsat,Vce_comp
4350   OUTPUT @Hp4142;"MM";3,C_ch              ! Measurement Mode
4360   OUTPUT @Hp4142;"XE"
4370   OUTPUT @Hp4142;"CL"
4380 !
4390 !
4400 !      ******************
4410 !      *  Iceo TEST  *
4420 !      ******************
4430 !
4440 !
4450   OUTPUT @Hp4142;"*RST"
4460   OUTPUT @Hp4142;"CN";C_ch
4470   OUTPUT @Hp4142;"DV";C_ch,0,Vceo,Iceo_comp
4480   OUTPUT @Hp4142;"PA1"
4490   OUTPUT @Hp4142;"MM";1,C_ch
4500   OUTPUT @Hp4142;"XE"
4510   OUTPUT @Hp4142;"CL"
4520   ENTER @Hp4142;A$
4530   Iceo_meas=VAL(A$[4,15])
4540 !
4550 !
4560 !
4570 !      **********************
4580 !      *  ERROR CHECKING  *
4590 !      **********************
4600 !
4610 !
```

```
4620 !
4630   GOSUB 12980
4640 !
4650 !
4660   IF A$[1,1]<>"N" THEN
4670     BEEP
4680     PRINT "Iceo"
4690     GOSUB 12090
4700   ELSE
4710   END IF
4720 !
4730   IF Z$="*" THEN
4740     Z$="*"
4750   ELSE
4760     Z$=""
4770   END IF
4780   OUTPUT
@Path;X;CHR$(9);"Iceo";CHR$(9);ABS(DROUND(Iceo_meas,4));CHR$(9);Z
$
4790   PRINT X,"Iceo",ABS(DROUND(Iceo_meas,4))
4800 !
4810 !
4820 !      ******************
4830 !      * Ibeo Pre-test *
4840 !      ******************
4850 !
4860 !
4870   OUTPUT @Hp4142;"*RST"
4880 !
4890   OUTPUT @Hp4142;"CN";B_ch,C_ch
4900   OUTPUT @Hp4142;"FL",0,C_ch            ! Filter off
4910   OUTPUT @Hp4142;"PI";C_ch,0,0,1.0E-5,Vbsat_comp
4920   OUTPUT @Hp4142;"PT";0,1.0E-3          ! Hold time, pulse width
4930 ! OUTPUT @Hp4142;"DI";B_ch,0,Icsat,Vce_comp
4940   OUTPUT @Hp4142;"MM";3,B_ch
4950   OUTPUT @Hp4142;"XE"
4960   OUTPUT @Hp4142;"CL"
4970 !
4980 !
4990 !      ******************
5000 !      *  Ibeo Test  *
5010 !      ******************
5020 !
5030 !
5040   OUTPUT @Hp4142;"*RST"
5050   OUTPUT @Hp4142;"CN";B_ch
5060   OUTPUT @Hp4142;"DV";B_ch,0,Vbeo,Ibeo_comp
5070   OUTPUT @Hp4142;"MM";1,B_ch
```

```
5080   OUTPUT @Hp4142;"XE"
5090   OUTPUT @Hp4142;"CL"
5100   ENTER @Hp4142;A$
5110   Ibeo_meas=VAL(A$[4,15])
5120 !
5130 !
5140 !     **********
5150 !     * ERROR CHECKING *
5160 !     **********
5170 !
5180 !
5190   GOSUB 12980
5200 !
5210   IF A$[1,1]<>"N" THEN
5220     BEEP
5230     PRINT "Ibeo"
5240     GOSUB 12090
5250   ELSE
5260   END IF
5270 !
5280   IF Z$="*" THEN
5290     Z$="*"
5300   ELSE
5310     Z$=""
5320   END IF
5330   OUTPUT
@Path;X;CHR$(9);"Ibeo";CHR$(9);ABS(DROUND(Ibeo_meas,6));CHR$(9);Z
$
5340   PRINT X,"Ibeo",ABS(DROUND(Ibeo_meas,6))
5350 !
5360 !
5370 !     **********
5380 !     * Vce(sat) Measurement *
5390 !     **********
5400 !
5410 !
5420   OUTPUT @Hp4142;"*RST"
5430 !
5440   OUTPUT @Hp4142;"CN";B_ch,C_ch
5450   OUTPUT @Hp4142;"FL";0,B_ch          ! Filter OFF
5460   OUTPUT @Hp4142;"PI";B_ch,0,0,Ibsat,Vbsat_comp
5470   OUTPUT @Hp4142;"PT";0,1.E-3         ! Hold Time, Pulse Width
(min=1mS)
5480   OUTPUT @Hp4142;"DI";C_ch,0,Icsat,Vce_comp
5490   OUTPUT @Hp4142;"MM";3,C_ch          ! Measurement Mode
5500   OUTPUT @Hp4142;"XE"
5510   OUTPUT @Hp4142;"CL"
5520 !
```

```
5530   ENTER @Hp4142;A$
5540   Vce=VAL(A$[4,15])
5550 !
5560 !
5570 !**********************
5580 !* ERROR CHECKING   *
5590 !**********************
5600 !
5610 !
5620   GOSUB 12980
5630 !
5640   IF A$[1,1]<>"N" THEN
5650     BEEP
5660     PRINT "Vce(sat)"
5670     GOSUB 12090
5680   ELSE
5690   END IF
5700 !
5710   IF Z$="*" THEN
5720     Z$="*"
5730   ELSE
5740     Z$=""
5750   END IF
5760   OUTPUT
@Path;X;CHR$(9);"Vce(sat)";CHR$(9);ABS(DROUND(Vce,5));CHR$(9);Z$
5770 !
5780   PRINT X,"Vce(sat)",DROUND(Vce,5)
5790 !
5800 !
5810 !      ***************************
5820 !      * Hfe TEST * Ic = 0.01mA *
5830 !      ***************************
5840 !
5850 !
5860   OUTPUT @Hp4142;"*RST"
5870   Delay_time=1.E-4
5880   OUTPUT @Hp4142;"CN";B_ch,C_ch
5890   OUTPUT @Hp4142;"ASV";B_ch,Vb_start,Vb_stop,Vb_rate,Ib5_comp
5900   OUTPUT @Hp4142;"AVI";C_ch,Vchfe,Ic5_target,Ic5_comp
5910   OUTPUT @Hp4142;"ASM";1,4
5920   OUTPUT @Hp4142;"AT";0,Delay_time
5930   OUTPUT @Hp4142;"MM";6
5940   OUTPUT @Hp4142;"XE"
5950   OUTPUT @Hp4142;"CL"
5960 !
5970   ENTER @Hp4142;A$
5980 ! PRINT A$
```

```
5990   Ib=VAL(A$[4,15])
6000   Ic_meas=VAL(A$[20,31])
6010   Hfe=Ic_meas/Ib
6020 !
6030 !
6040 !      **********************
6050 !      * ERROR CHECKING *
6060 !      **********************
6070 !
6080 !
6090   GOSUB 12980
6100 !
6110   IF A$[1,1]<>"N" OR A$[17,17]<>"N" THEN
6120     BEEP
6130     PRINT "hFE 0.01mA"
6140     GOSUB 10690
6150   ELSE
6160   END IF
6170 !
6180   IF Z$="*" THEN
6190     Z$="*"
6200   ELSE
6210     Z$=""
6220   END IF
6230   OUTPUT
@Path;X;CHR$(9);"Hfe(0.01mA)";CHR$(9);DROUND(Hfe,3);CHR$(9);Z$
6240 !
6250   PRINT X,"hFE 0.01mA",DROUND(Hfe,3)
6260 !
6270 !
6280 !      ************************
6290 !      *Hfe TEST * Ic = 0.1mA *
6300 !      ************************
6310 !
6320 !
6330   OUTPUT @Hp4142;"*RST"
6340   Delay_time=1.E-4
6350   OUTPUT @Hp4142;"CN";B_ch,C_ch
6360   OUTPUT @Hp4142;"ASV";B_ch,Vb_start,Vb_stop,Vb_rate,Ib4_comp
6370   OUTPUT @Hp4142;"AVI";C_ch,Vchfe,Ic4_target,Ic4_comp
6380   OUTPUT @Hp4142;"ASM";1,4
6390   OUTPUT @Hp4142;"AT";0,Delay_time
6400   OUTPUT @Hp4142;"MM";6
6410   OUTPUT @Hp4142;"XE"
6420   OUTPUT @Hp4142;"CL"
6430 !
6440   ENTER @Hp4142;A$
6450 ! PRINT A$
```

```
6460   Ib=VAL(A$[4,15])
6470   Ic_meas=VAL(A$[20,31])
6480   Hfe=Ic_meas/Ib
6490 !
6500 !
6510 !     **********************
6520 !     * ERROR CHECKING *
6530 !     **********************
6540 !
6550 !
6560   GOSUB 12980
6570 !
6580   IF A$[1,1]<>"N" OR A$[17,17]<>"N" THEN
6590     BEEP
6600     PRINT "hFE 0.1mA"
6610     GOSUB 10690
6620   ELSE
6630   END IF
6640 !
6650   IF Z$="*" THEN
6660     Z$="*"
6670   ELSE
6680     Z$=""
6690   END IF
6700   OUTPUT
@Path;X;CHR$(9);"Hfe(0.1mA)";CHR$(9);DROUND(Hfe,3);CHR$(9);Z$
6710   PRINT X,"hFE 0.1mA",DROUND(Hfe,3)
6720 !
6730 !
6740 !     **********************
6750 !     *Hfe TEST * Ic = 1mA *
6760 !     **********************
6770 !
6780 !
6790   OUTPUT @Hp4142;"*RST"
6800   Delay_time=1.E-4
6810   OUTPUT @Hp4142;"CN";B_ch,C_ch
6820   OUTPUT @Hp4142;"ASV";B_ch,Vb_start,Vb_stop,Vb_rate,Ib_comp
6830   OUTPUT @Hp4142;"AVI";C_ch,Vchfe,Ic1_target,Ic1_comp
6840 !
6850   OUTPUT @Hp4142;"ASM";1,4          ! Op.mode, Meas. mode
6860   OUTPUT @Hp4142;"AT";0,Delay_time     ! Hold Time, Delay Time
6870   OUTPUT @Hp4142;"MM";6
6880   OUTPUT @Hp4142;"XE"
6890   OUTPUT @Hp4142;"CL"
6900 !
6910   ENTER @Hp4142;A$
6920 ! PRINT A$
```

```
6930   Ib=VAL(A$[4,15])
6940   Ic_meas=VAL(A$[20,31])
6950   Hfe=Ic_meas/Ib
6960 !
6970 !
6980 !       ************************
6990 !       * ERROR CHECKING   *
7000 !       ************************
7010 !
7020 !
7030   GOSUB 12980
7040 !
7050 !
7060   IF A$[1,1]<>"N" OR A$[17,17]<>"N" THEN
7070     BEEP
7080     PRINT "hFE 1mA"
7090     GOSUB 10690
7100   ELSE
7110   END IF
7120 !
7130   IF Z$="*" THEN
7140     Z$="*"
7150   ELSE
7160     Z$=""
7170   END IF
7180   OUTPUT
@Path;X;CHR$(9);"Hfe(1mA)";CHR$(9);DROUND(Hfe,3);CHR$(9);Z$
7190 !
7200   PRINT X,"hFE 1mA",DROUND(Hfe,3)
7210 !
7220 !
7230 !    ************************
7240 !    *Hfe TEST * Ic = 10mA *
7250 !    ************************
7260 !
7270 !
7280   Delay_time=1.E-4
7290 !
7300   OUTPUT @Hp4142;"CN";B_ch,C_ch
7310   OUTPUT @Hp4142;"ASV";B_ch,Vb_start,Vb_stop,Vb_rate,Ib2_comp
7320   OUTPUT @Hp4142;"AVI";C_ch,Vchfe,Ic2_target,Ic2_comp
7330   OUTPUT @Hp4142;"ASM";1,4
7340   OUTPUT @Hp4142;"AT";0,Delay_time
7350   OUTPUT @Hp4142;"MM";6
7360   OUTPUT @Hp4142;"XE"
7370   OUTPUT @Hp4142;"CL"
7380 !
7390   ENTER @Hp4142;A$
```

```
7400 ! PRINT A$
7410   Ib=VAL(A$[4,15])
7420   Ic_meas=VAL(A$[20,31])
7430   Hfe=Ic_meas/Ib
7440 !
7450 !
7460 !       ************************
7470 !       * ERROR CHECKING   *
7480 !       ************************
7490 !
7500 !
7510   GOSUB 12980
7520 !
7530 !
7540   IF A$[1,1]<>"N" OR A$[17,17]<>"N" THEN
7550     BEEP
7560     PRINT "hFE 10mA"
7570     GOSUB 10690
7580   ELSE
7590   END IF
7600 !
7610   IF Z$="*" THEN
7620     Z$="*"
7630   ELSE
7640     Z$=""
7650   END IF
7660   OUTPUT
@Path;X;CHR$(9);"Hfe(10mA)";CHR$(9);DROUND(Hfe,3);CHR$(9);Z$
7670 !
7680   PRINT X,"hFE 10mA",DROUND(Hfe,3)
7690 !
7700 !
7710 !     ************************
7720 !     *Hfe TEST * Ic = 100mA *
7730 !     ************************
7740 !
7750 !
7760 ! Delay_time=1.E-4
7770 !
7780 ! OUTPUT @Hp4142;"CN";B_ch,C_ch
7790 ! OUTPUT @Hp4142;"ASV";B_ch,Vb_start,Vb_stop,Vb_rate,Ib3_comp
7800 ! OUTPUT @Hp4142;"AVI";C_ch,Vchfe,Ic3_target,Ic3_comp
7810 ! OUTPUT @Hp4142;"ASM";1,4
7820 ! OUTPUT @Hp4142;"AT";0,Delay_time
7830 ! OUTPUT @Hp4142;"MM";6
7840 ! OUTPUT @Hp4142;"XE"
7850 ! OUTPUT @Hp4142;"CL"
7860 !
```

```
7870 ! ENTER @Hp4142;A$
7880 !
7890 ! Ib=VAL(A$[4,15])
7900 ! Ic_meas=VAL(A$[20,31])
7910 ! Hfe=Ic_meas/Ib
7920 ! PRINT A$
7930 !
7940 !
7950 !       ************************
7960 !       * ERROR CHECKING   *
7970 !       ************************
7980 !
7990 !
8000 ! GOSUB 8850
8010 !
8020 ! IF A$[1,1]<>"N" OR A$[17,17]<>"N" THEN
8030 !  BEEP
8040 !  PRINT "hFE 100mA"
8050 !  GOSUB 6560
8060 ! ELSE
8070 ! END IF
8080 !
8090 ! IF Z$="*" THEN
8100 !  Z$="*"
8110 ! ELSE
8120 !  Z$=""
8130 ! END IF
8140 ! OUTPUT
@Path;X;CHR$(9);"Hfe(100mA)";CHR$(9);DROUND(Hfe,3);CHR$(9);Z$
8150 ! PRINT X,"hFE 100mA",DROUND(Hfe,3)
8160 !
8170 !
8180 !      **********************
8190 !      * GUMMEL PLOT TEST *
8200 !      **********************
8210 !
8220 !
 8230  Ibgp=1.E-12
 8240  OUTPUT @Hp4142;"*RST"
 8250  OUTPUT @Hp4142;"CN";B_ch,C_ch
 8260  OUTPUT @Hp4142;"DI";B_ch,0,Ibgp,10
 8270  OUTPUT @Hp4142;"DV";C_ch,0,5,.2
 8280  OUTPUT @Hp4142;"MM";1,C_ch
 8290  OUTPUT @Hp4142;"XE"
 8300  ENTER @Hp4142;A$
 8310  !
 8320  OUTPUT @Hp4142;"MM";1,B_ch
 8330  OUTPUT @Hp4142;"XE"
```

```
8340   OUTPUT @Hp4142;"CL"
8350   ENTER @Hp4142;B$
8360   Icgp_meas=VAL(A$[4,15])
8370   Vbe_meas=VAL(B$[4,15])
8380 !
8390 !
8400 !     **********************
8410 !     * ERROR CHECKING   *
8420 !     **********************
8430 !
8440 !
8450   GOSUB 12980
8460 !
8470   IF A$[1,1]<>"N" THEN
8480     BEEP
8490     PRINT "Igp"
8500     GOSUB 12090
8510   ELSE
8520   END IF
8530 !
8540   IF Z$="*" THEN
8550     Z$="*"
8560   ELSE
8570     Z$=""
8580   END IF
8590   OUTPUT
@Path;X;CHR$(9);"Ibgp";CHR$(9);DROUND(Ibgp,3);CHR$(9);"Icgp";CHR$
(9);DROUND(Icgp_meas,3);CHR$(9);"Vbe";CHR$(9);DROUND(Vbe_meas,3)
;CHR$(9);Z$
8600   PRINT
X,"Ibgp",DROUND(Ibgp,3),"Icgp",DROUND(Icgp_meas,3),"Vbe",DROUND
(Vbe_meas,3)
8610 !
8620 !
8630   Ibgp=Ibgp*SQRT(SQRT(10))
8640   IF Ibgp>1.E-5 THEN
8650     GOTO 8700
8660   ELSE
8670     GOTO 8240
8680   END IF
8690 !
8700 !
8710 !     ******************
8720 !     * V(BR)ebo TEST *
8730 !     ******************
8740 !
8750 !
```

```
8760   INPUT "Please swap test leads for base & emitter and insert 10 kohm
SMU2 resistor.",O$
8770 !
8780   OUTPUT @Hp4142;"*RST"
8790   OUTPUT @Hp4142;"CN";B_ch
8800   OUTPUT @Hp4142;"DI";B_ch,0,Iebbr,Vebbr_comp
8810   OUTPUT @Hp4142;"MM";1,B_ch
8820   OUTPUT @Hp4142;"XE"
8830   OUTPUT @Hp4142;"CL"
8840   ENTER @Hp4142;A$
8850   Vbr_meas=VAL(A$[4,15])
8860   Result=Iebbr*10000
8870   Vbr_meas=Vbr_meas-Result
8880 !
8890 !
8900 !     ********************
8910 !     * ERROR CHECKING *
8920 !     ********************
8930 !
8940 !
8950   GOSUB 12980
8960 !
8970   IF A$[1,1]<>"N" THEN
8980     BEEP
8990     PRINT "VBR(ebo)"
9000     GOSUB 12090
9010   ELSE
9020   END IF
9030 !
9040   IF Z$="*" THEN
9050     Z$="*"
9060   ELSE
9070     Z$=""
9080   END IF
9090   OUTPUT
@Path;X;CHR$(9);"V(BR)ebo";CHR$(9);DROUND(Vbr_meas,3);CHR$(9);Z$
9100   PRINT X,"V(BR)ebo",DROUND(Vbr_meas,3)
9110 !
9120 !
9130 !     ******************
9140 !     * V(BR)cbo TEST *
9150 !     ******************
9160 !
9170 !
9180   INPUT "Please move resistor to SMU1 test lead.",O$
9190 !
9200   OUTPUT @Hp4142;"*RST"
9210   OUTPUT @Hp4142;"CN";C_ch
```

```
9220   OUTPUT @Hp4142;"DI";C_ch,0,Icbbr,Vcbbr_comp
9230   OUTPUT @Hp4142;"MM";1,C_ch
9240   OUTPUT @Hp4142;"XE"
9250   OUTPUT @Hp4142;"CL"
9260   ENTER @Hp4142;A$
9270   Vbr_meas=VAL(A$[4,15])
9280   Result=Icbbr*10000
9290   Vbr_meas=Vbr_meas-Result
9300 !
9310 !
9320 !      **********************
9330 !      * ERROR CHECKING *
9340 !      **********************
9350 !
9360 !
9370   GOSUB 12980
9380 !
9390 !
9400   IF A$[1,1]<>"N" THEN
9410     BEEP
9420     PRINT "VBR(cbo)"
9430     GOSUB 12090
9440   ELSE
9450   END IF
9460 !
9470   IF Z$="*" THEN
9480     Z$="*"
9490   ELSE
9500     Z$=""
9510   END IF
9520   OUTPUT
@Path;X;CHR$(9);"V(BR)cbo";CHR$(9);DROUND(Vbr_meas,3);CHR$(9);Z$
9530   PRINT X,"V(BR)cbo",DROUND(Vbr_meas,3)
9540 !
9550 !
9560 !      ******************
9570 !      * V(BR)ceo TEST *
9580 !      ******************
9590 !
9600 !
9610   INPUT "Please swap back base and emitter leads, leaving SMU1 resistor in
place.",O$
9620 !
9630   OUTPUT @Hp4142;"*RST"
9640   OUTPUT @Hp4142;"CN";C_ch
9650   OUTPUT @Hp4142;"DI";C_ch,0,Icebr,Vcebr_comp
9660   OUTPUT @Hp4142;"MM";1,C_ch
9670   OUTPUT @Hp4142;"XE"
```

```
9680   OUTPUT @Hp4142;"CL"
9690   ENTER @Hp4142;A$
9700   Vbr_meas=VAL(A$[4,15])
9710   Result=Icebr*10000
9720   Vbr_meas=Vbr_meas-Result
9730 !
9740 !
9750 !      **********************
9760 !      * ERROR CHECKING   *
9770 !      **********************
9780 !
9790 !
9800   GOSUB 12980
9810 !
9820 !
9830   IF A$[1,1]<>"N" THEN
9840     BEEP
9850     PRINT "VBR(CEO)"
9860     GOSUB 12090
9870   ELSE
9880   END IF
9890 !
9900   IF Z$="*" THEN
9910     Z$="*"
9920   ELSE
9930     Z$=""
9940   END IF
9950   OUTPUT
@Path;X;CHR$(9);"V(BR)ceo";CHR$(9);DROUND(Vbr_meas,3);CHR$(9);Z$
9960   PRINT X,"V(BR)ceo",DROUND(Vbr_meas,3)
9970 !
9980 !
9990 !      ******************
10000 !      * V(BR)beo TEST *
10010 !      ******************
10020 !
10030 !
10040   INPUT "Please remove SMU1 resistor and insert into SMU2 test lead.",O$
10050 !
10060   OUTPUT @Hp4142;"*RST"
10070   OUTPUT @Hp4142;"CN";B_ch
10080   OUTPUT @Hp4142;"DI";B_ch,0,Ibebr,Vbebr_comp
10090   OUTPUT @Hp4142;"MM";1,B_ch
10100   OUTPUT @Hp4142;"XE"
10110   OUTPUT @Hp4142;"CL"
10120   ENTER @Hp4142;A$
10130   Vbr_meas=VAL(A$[4,15])
10140   Result=Ibebr*10000
```

```
10150  Vbr_meas=Vbr_meas-Result
10160 !
10170 !
10180 !     **********
10190 !     * ERROR CHECKING *
10200 !     **********
10210 !
10220 !
10230  GOSUB 12980
10240 !
10250  IF A$[1,1]<>"N" THEN
10260   BEEP
10270   PRINT "V(BR)beo"
10280   GOSUB 12090
10290  ELSE
10300  END IF
10310 !
10320  IF Z$="*" THEN
10330   Z$="*"
10340  ELSE
10350   Z$=""
10360  END IF
10370  OUTPUT
@Path;X;CHR$(9);"V(BR)beo";CHR$(9);DROUND(Vbr_meas,3);CHR$(9);Z$
10380  PRINT X,"V(BR)beo",DROUND(Vbr_meas,3)
10390 !
10400  PRINT " "
10410  INPUT "Please remove SMU2 resistor.",O$
10420 NEXT X
10430 GOTO 13200
10440 !
10450 !
10460 !
10470 !
10480 !
10490 !
10500 !
10510 !          **********
10520 !          **********
10530 !               SUBROUTINES
10540 !          **********
10550 !          **********
10560 !
10570 !
10580 !
10590 !
10600 !
```

```
10610
!*****************************************************************
10620 !*  GOSUB ROUTINE -- ERROR CHECKING ROUTINE FOR hFE TESTS  *
10630
!*****************************************************************
10640 !
10650 !
10660 !
10670 !
10680 !
10690 IF A$[1,1]="G" THEN
10700   PRINT "ERROR G: Target value not reached, (Collector)"
10710   PRINT " "
10720   INPUT "Press ENTER to continue or PAUSE to exit",O$
10730 ELSE
10740 END IF
10750 !
10760 IF A$[17,17]="G" THEN
10770   PRINT "ERROR G: Target value not reached, (Base)"
10780   PRINT " "
10790   INPUT "Press ENTER to continue or PAUSE to exit",O$
10800 ELSE
10810 END IF
10820 !
10830 !
10840 ! ***********************************************
10850 !
10860 !
10870 IF A$[1,1]="S" THEN
10880   PRINT "ERROR S: Measurement is made before the feedback search is complete (Collector)"
10890   PRINT " "
10900   INPUT "Press ENTER to continue or PAUSE to exit",O$
10910 ELSE
10920 END IF
10930 !
10940 IF A$[17,17]="S" THEN
10950   PRINT "ERROR S: Measurement is made before the feedback search is complete, (Base)"
10960   PRINT " "
10970   INPUT "Press ENTER to continue or PAUSE to exit",O$
10980 ELSE
10990 END IF
11000 !
11010 !
11020 ! ************************************************
11030 !
```

```
11040 !
11050 IF A$[1,1]="T" THEN
11060   PRINT "ERROR T: Another channel(s) reach V compliance, power compliance, or the current limit of VS, (Collector)"
11070   PRINT " "
11080   INPUT "Press ENTER to continue or PAUSE to exit",O$
11090 ELSE
11100 END IF
11110 !
11120 IF A$[17,17]="T" THEN
11130   PRINT "ERROR T: Another channel(s) reach V compliance, power compliance, or the current limit of VS, (Base)"
11140   PRINT " "
11150   INPUT "Press ENTER to continue or PAUSE to exit",O$
11160 ELSE
11170 END IF
11180 !
11190 !
11200 ! ************************************************
11210 !
11220 !
11230 IF A$[1,1]="C" THEN
11240   PRINT "ERROR C: This measurement channel reaches V compliance, i compliance, power compliance or current limit of VS, (Collector)"
11250   PRINT " "
11260   INPUT "Press ENTER to continue or PAUSE to exit",O$
11270 ELSE
11280 END IF
11290 !
11300 IF A$[17,17]="C" THEN
11310   PRINT "ERROR C: This measurement channel reaches V compliance, i compliance, power compliance or current limit of VS, (Base)"
11320   PRINT " "
11330   INPUT "Press ENTER to continue or PAUSE to exit",O$
11340 ELSE
11350 END IF
11360 !
11370 !
11380 ! ************************************************
11390 !
11400 !
11410 IF A$[1,1]="V" THEN
11420   PRINT "ERROR V: This channel output exceeds the measurement range, (Collector)."
11430   PRINT " "
11440   INPUT "Press ENTER to continue or PAUSE to exit",O$
11450 ELSE
11460 END IF
```

```
11470 !
11480 IF A$[17,17]="V" THEN
11490   PRINT "ERROR V: This channel output exceeds the measurement
range, (Base)."
11500   PRINT " "
11510   INPUT "Press ENTER to continue or PAUSE to exit",O$
11520 ELSE
11530 END IF
11540 !
11550 !
11560 ! ******************************************************
11570 !
11580 !
11590 IF A$[1,1]="X" THEN
11600   PRINT "ERROR X: One or more SMU/HVU(s) is oscillating,
(Collector)."
11610   PRINT " "
11620   INPUT "Press ENTER to continue or PAUSE to exit",O$
11630 ELSE
11640 END IF
11650 !
11660 IF A$[17,17]="X" THEN
11670   PRINT "ERROR X: One or more SMU/HVU(s) is oscillating, (Base)."
11680   PRINT " "
11690   INPUT "Press ENTER to continue or PAUSE to exit",O$
11700 ELSE
11710 END IF
11720 !
11730 !
11740 ! ******************************************************
11750 !
11760 !
11770 IF A$[1,1]="F" THEN
11780   PRINT "ERROR F: One or more HVU output(s) does not settle before
measurement, (Collector)."
11790   PRINT " "
11800   INPUT "Press ENTER to continue or PAUSE to exit",O$
11810 ELSE
11820 END IF
11830 !
11840 IF A$[17,17]="F" THEN
11850   PRINT "ERROR F: One or more HVU output(s) does not settle before
measurement, (Base)."
11860   PRINT " "
11870   INPUT "Press ENTER to continue or PAUSE to exit",O$
11880 ELSE
11890 END IF
11900 Z$="*"
```

```
11910 !
11920 RETURN
11930 !
11940 !
11950 !
11960 !          ************************************
11970 !          ************************************
11980 !
11990 !
12000 !
12010 !
*****************************************************************
12020 ! * GOSUB -- ERROR CHECKING ROUTINE FOR
Iceo,Vce(sat),Vbrceo *
12030 !
*****************************************************************
12040 !
12050 !
12060 !
12070 !
12080 !
12090 IF A$[1,1]="G" THEN
12100   PRINT "ERROR G: Target value not reached, (Collector)"
12110   PRINT " "
12120   INPUT "Press ENTER to continue or PAUSE to exit",O$
12130 ELSE
12140 END IF
12150 !
12160 !
12170 ! ***********************************************
12180 !
12190 !
12200 IF A$[1,1]="S" THEN
12210   PRINT "ERROR S: Measurement is made before the feedback search is
complete "
12220   PRINT " "
12230   INPUT "Press ENTER to continue or PAUSE to exit",O$
12240 ELSE
12250 END IF
12260 !
12270 !
12280 ! ***************************************************
12290 !
12300 !
12310 IF A$[1,1]="T" THEN
12320   PRINT "ERROR T: Another channel(s) reach V compliance, power
compliance, or the current limit of VS"
12330   PRINT " "
```

```
12340   INPUT "Press ENTER to continue or PAUSE to exit",O$
12350 ELSE
12360 END IF
12370 !
12380 !
12390 ! ************************************************
12400 !
12410 !
12420 IF A$[1,1]="C" THEN
12430   PRINT "ERROR C: This measurement channel reaches V compliance, i
compliance, power compliance or current limit of VS"
12440   PRINT " "
12450   INPUT "Press ENTER to continue or PAUSE to exit",O$
12460 ELSE
12470 END IF
12480 !
12490 !
12500 ! ************************************************
12510 !
12520 !
12530 IF A$[1,1]="V" THEN
12540   PRINT "ERROR V: This channel output exceeds the measurement
range"
12550   PRINT " "
12560   INPUT "Press ENTER to continue or PAUSE to exit",O$
12570 ELSE
12580 END IF
12590 !
12600 !
12610 ! ************************************************
12620 !
12630 !
12640 IF A$[1,1]="X" THEN
12650   PRINT "ERROR X: One or more SMU/HVU(s) is oscillating"
12660   PRINT " "
12670   INPUT "Press ENTER to continue or PAUSE to exit",O$
12680 ELSE
12690 END IF
12700 !
12710 !
12720 ! ************************************************
12730 !
12740 !
12750 IF A$[1,1]="F" THEN
12760   PRINT "ERROR F: One or more HVU output(s) does not settle before
measurement"
12770   PRINT " "
12780   INPUT "Press ENTER to continue or PAUSE to exit",O$
```

```
12790 ELSE
12800 END IF
12810 !
12820 Z$="*"
12830 RETURN
12840 !
12850 !
12860 !
12870 !
12880 !       ******************************************
12890 !       ******************************************
12900 !
12910 !
12920 !
12930 !
12940 !   ************************************************
12950 !   * GOSUB--ERROR  CHECKING--RUN 4142 ERROR PROG *
12960 !   ************************************************
12970 !
12980 Z$=""
12990 !
13000 !
13010 OUTPUT 717;"ERR?"
13020 ENTER 717;X$
13030 IF X$="0,0,0,0" THEN
13040   RETURN
13050 ELSE
13060   BEEP
13070   PRINT "ERROR",X$
13080   Z$="*"
13090 END IF
13100 !
13110 RETURN
13120 !
13130 !
13140 !
13150 !
13160 !         ******************************************
13170 !
13180 !
13190 !
13200 BEEP
13210 INPUT "TESTS COMPLETE, Press <ENTER> to Exit.",O$
13220 END
```

16 List of references

Anon (1991), "Ionizing radiation (total dose) test procedure, method 1019.4 in "Test method standard. Microcircuits", Mil-Std-883E, published by the Department of Defense, USA.

Anon (1995), "Total dose steady-state irradiation test method", ESA /SCC Basic Specification no. 22900, published by the European Space Agency, Noordwijk, The Netherlands.

Anon (2001), "The nuclear fuel cycle", from the corporate website of Framatome ANP GmbH.

Ashburn, P. (1988), "Design and realization of bipolar transistors", published by John Wiley & Sons, New York.

Bardeen, J. and Brattain, W.H. (1948), "The transistor, a semiconductor triode", Phys. Rev., vol. 24, p. 230.

Barnes, C., Johnston, A., Lee, C., Swift, G. and Rax, B. (1997), "Recent radiation effects activities at JPL: coping with COTS", ESA SP-395, third ESA Electronic Components Conference, ESTEC, Noordwijk, The Netherlands, 22 – 25 April 1997.

Blair, R.R. (1963), "Surface effects of radiation on transistors", IEEE Trans. Nuc. Sci., NS-10.

Blood, P. and Orton, J.W. (1992), "The electrical characterisation of semiconductors: majority carriers and electron states", published by Academic Press, London.

Brucker, G.J., Dennehy, W.J. and Holmes-Siedle (1966), "Ionization and displacement damage in silicon transistors", IEEE Trans. Nuc. Sci., NS-13, no. 6, p. 188.

Clark, S.D., Bings, J.P., Maher, M.C., Williams, M.K., Alexander, D.R. and Pease, R.L. (1995), "Plastic packaging and burn-in effects on ionising dose response in CMOS microcircuits", IEEE Trans. Nuc. Sci., vol. 42, no. 6, p. 1607.

Corbett, J.W. (1966), "Electron radiation damage in semiconductors and metals", published by Academic Press, London.

Fleetwood, D. (1995), "A first-principles approach to hardness assurance", section III of the 1995 NSREC short course, entitled "Advanced qualification

techniques; a practical guide for radiation testing of electronics", published by IEEE in "Archive of radiation effects short course notebooks 1980 – 1998".

Grove, A.S. (1967), "Physics and technology of semiconductor devices", published by John Wiley & Sons, New York.

Hall, R.N. (1956) "Power rectifiers and transistors", Proc. IRE, vol. 44, p. 72.

Harris, J.N., Gray, P.E. and Searle, C.L. (1966), "Digital transistor circuits", published by John Wiley & Sons, New York.

Hart, A.R., Smyth, J.B. Jr., van Lint, V.A.J., Snowden, D.P. and Leadon, R.E. (1978), "Hardness assurance considerations for long-term ionizing radiation effects on bipolar structures", IEEE Trans. Nuc. Sci., NS-25, no. 6.

Holmes-Siedle, A. and Adams, L. (1993), "Handbook of radiation effects", published by Oxford University Press, Oxford.

Kahn, J. (1959), J. Appl. Phys., vol. 30, p. 1310.

Kaye, G.W.C. and Laby, T.H. (1986), "Tables of physical and chemical constants", published by Longman, London and New York, 15th edition.

Kuno, H.J. (1964), "Analysis and characterization on P-N junction diode switching", IEEE Trans. Elec. Dev., ED-11, p. 8.

Lang, D.V. (1974), "Deep-level transient spectroscopy: a new method to characterize traps in semiconductors", J. Appl. Phys., vol. 45, p. 3023.

Ma, T.P. and Dressendorfer, P.V. (1989), "Ionizing radiation effects in MOS devices and circuits", published by John Wiley & Sons, New York.

Messenger, G.C. and Spratt, J.P. (1958), "The effects of neutron irradiation on germanium and silicon", Proc. IRE, June 1958, p. 1038.

Messenger, G.C. (1965(1)), "Displacement damage in silicon and germanium transistors", IEEE Trans. Nuc. Sci., NS-12.

Messenger, G.C., *et al* (1965(2)), "Displacement damage in MOS transistors", IEEE Nuclear Science Group Meeting, July 1965.

Messenger, G.C. (1973), "A general proof of the β degradation equation for bulk displacement damage", IEEE Trans. Nuc. Sci., NS-20(1), p. 809.

Messenger, G.C. and Ash, M.S. (1986), "The effects of radiation on electronic systems", published by Van Nostrand Reinhold, New York.

Miller, S.L. (1955), "Ionisation rates for electrons and holes in silicon", Phys. Rev., vol. 99, p. 1234.

Moll, M. (2000), "Microscopic defects in silicon", published by CERN, Switzerland.

Olesen, H.L. (1966), "Radiation effects on electronic systems", published by Plenum Press, New York.

Pater, S.L. and Sharp, R.E. (1995), "Gamma radiation effects on bipolar transistors. A comparison of surface mount and standard packages", proceedings of the third European conference on radiation and its effects on components and systems, RADECS'95, Arcachon, France.

Pater, L. (1996 (1)), "Irradiation of samples in a cobalt-60 cell", AEAT/GWI/26/4/4, issue 1, AEA Technology internal QA work instruction, June 1996.

Pater, L. (1996 (2)), "Testing of bipolar transistors using the HP4142B system", AEAT/GWI/26/4/8, issue 1, AEA Technology internal QA work instruction, June 1996.

Poch, W.J. and Holmes-Siedle, A.G. (1968), "A prediction and selection system for radiation effects in planar transistors", IEEE Trans. Nuc. Sci., NS-15, no. 6, p. 213.

Rappaport, P. and Loferski, J. (1955), "Thresholds for electron bombardment induced lattice displacements in Si and Ge", Phys. Rev., vol. 100, no. 4, p. 1261.

Reddi, V.G.K. (1967), "Influence of surface conditions on silicon planar transistor current gain", Solid-State Electronics, vol. 10, p. 305.

Sah, C.T., Noyce, R.N. and Shockley, W. (1957), "Carrier generation and recombination in *pn* junctions and *pn* junction characteristics", Proc. IRE, vol. 45, p. 1228.

Schönbacher, H. and Tavlet, M. (1989), "Compilation of radiation damage test data, Part 1, 2nd edition: halogen-free cable-insulating materials", published by CERN, Geneva, CERN 89-12.

Shaneyfelt, M.R., Fleetwood, D.M., Schwank, J.R., Meisenheimer, T.L. and Winokur, P.S. (1994), "Effects of burn-in on radiation hardness", IEEE Trans. Nuc. Sci., vol. 41, pp. 2550 – 2559, December 1994.

Sharp, R.E. and Scheiwiller, P. (1993), "Simulation of radiation effects on closed-circuit TV cameras", proceedings of the INE International conference on modelling and simulation for the nuclear industry, Edinburgh.

Sharp, R.E. and Pater, S.L. (1993(2)), "A comparison of the effects of gamma radiation from spent fuel and cobalt-60 on electronic components",

proceedings of the second European conference on radiation and its effects on components and systems, RADECS'93, St. Malo, France.

Sharp, R.E. and Garlick, D.R. (1994), "Radiation effects on electronic equipment. A designers'/users' guide for the nuclear power industry", published by AEA Technology, Harwell.

Sharp, R.E., Pater, S.L. and Garlick, D.R. (1995), "Radiation tolerance of current CCD-based CCTV cameras", proceedings of the third European conference on radiation and its effects on components and systems, RADECS'95, Arcachon, France.

Sharp, R.E., Dawson, J. and Pater, S.L. (2000), "A new radiation testing facility for the nuclear power industry", proceedings of the INE international conference on Control & Instrumentation in nuclear installations, Bristol, United Kingdom.

Shockley, W. (1949), "The theory of p-n junction in semiconductors and p-n junction transistor", Bell Syst. Tech. J., vol. 28, p. 435.

Smith, J.W. (1996), "Radiation Testing Service Procedures", AEAT/GP/26/4/17, issue 1, AEA Technology internal QA procedure, May 1996.

Sze, S.M. (1981), "Physics of semiconductor devices", published by John Wiley & Sons, New York.

Sze, S.M. (1985), "Semiconductor devices physics and technology", published by John Wiley & Sons, New York.

Vavilov, V.S. (1965), "Effects of radiation on semiconductors", published by Consultants Bureau, New York.

Wall, J.J., Sharp, R.E. and Pater, S.L. (1998), "The effects of space radiation and burn-in on plastic encapsulated semiconductors", Proceedings of the RADECS'98 conference, Oxford, United Kingdom.

Wall, J.J., Sharp, R.E. and Pater, L. (1999), "The effects of space radiation and burn-in on plastic encapsulated semiconductors", Data Workshop of the IEEE Nuclear, Space and Radiation Effects Conference (NSREC), Norfolk, Virginia, USA.

17 Bibliography

Other works not listed in the previous section but found to provide useful material include the following.

Getreu, I. (1976), "Modeling the bipolar transistor", published by Tektronix Inc, Beaverton, Oregon, USA.

IEEE Transactions on Nuclear Science, especially volume 6, a selection of papers from the annual Nuclear and Space Radiation Effects Conference (NSREC), run by the Nuclear and Plasma Sciences Society.

Kircher, J.F. and Bowman, R.E. (1964), "Effects of radiation on materials and components", published by Reinhold Publishing Corporation, New York.

Schroeder, D.K. (1990), "Semiconductor material and device characterization", published by John Wiley and Sons, New York.

Snowden, C.M. (1989), "Semiconductor device modelling", published by Springer-Verlag, Berlin.

18 Index